2D- Hexagonal Boron Nitride Heterostructures based Triboelectric Nanogenerator for Mechanical Energy Harvesting and Tactile Sensing Applications

By

Bhavya A. S.

Registration No: 10CC18A39012

A thesis submitted to the

Academy of Scientific & Innovative Research

for the award of the degree of

DOCTOR OF PHILOSOPHY

in

SCIENCE

Under the supervision of

Dr. K. P. Surendran

CSIR-National Institute for Interdisciplinary Science and technology (CSIR-NIIST) Thiruvananthapuram - 695 019

Academy of Scientific and Innovative Research
AcSIR Headquarters, CSIR-HRDC campus
Sector 19, Kamla Nehru Nagar,
Ghaziabad, U.P. – 201 002, India

January 2024

Dedicated to . . . . .

My Father

CERTIFICATE

This is to certify that the work incorporated in this Ph.D. thesis entitled, **"2D- Hexagonal Boron Nitride Heterostructures based Triboelectric Nanogenerator for Mechanical Energy Harvesting and Tactile Sensing Applications"** submitted by **Ms. Bhavya A. S.,** to the Academy of Scientific and Innovative Research (AcSIR), in fulfilment of the requirements for the award of the Degree of **Doctor of Philosophy in Science,** embodies original research work carried out by the student. We, further certify that this work has not been submitted to any other University or Institution in part or full for the award of any degree or diploma. Research materials obtained from other sources and used in this research work have been duly acknowledged in the thesis. Images, illustrations, figures, tables etc., used in the thesis from other sources, have also been duly cited and acknowledged.

Bhavya A. S.

(Student)

Dr. K. P. Surendran

(Thesis Supervisor)

January, 2024

Thiruvananthapuram

STATEMENTS OF ACADEMIC INTEGRITY

I, **Bhavya A.S.**, a Ph.D. student of the Academy of Scientific and Innovative Research (AcSIR) with Registration No. 10CC18A39012 hereby undertake that, the thesis entitled *"2D- Hexagonal Boron Nitride Heterostructures based Triboelectric Nanogenerator for Mechanical Energy Harvesting and Tactile Sensing Applications"* has been prepared by me and that the document reports original work carried out by me and is free of any plagiarism in compliance with the UGC Regulations on "Promotion of Academic Integrity and Prevention of Plagiarism in Higher Educational Institutions (2018)" and the CSIR Guidelines for "Ethics in Research and in Governance (2020)".

Bhavya A. S.

January, 2024

Thiruvananthapuram

It is hereby certified, that the work done by the student, under my supervision, is plagiarism free in accordance with the UGC Regulations on "Promotion of Academic Integrity and Prevention of Plagiarism in Higher Educational Institutions (2018)" and the CSIR Guidelines for "Ethics in Research and in Governance (2020)".

05/01/2024
Dr. K. P. Surendran

January, 2024

Thiruvananthapuram

DECLARATION

I, Bhavya A. S., bearing AcSIR Registration No. 10CC18A39012 declare that my thesis entitled, *"2D- Hexagonal Boron Nitride Heterostructures based Triboelectric Nanogenerator for Mechanical Energy Harvesting and Tactile Sensing Applications"* is plagiarism free in accordance with the UGC Regulations on "Promotion of Academic Integrity and Prevention of Plagiarism in Higher Educational Institutions (2018)" and the CSIR Guidelines for "Ethics in Research and in Governance (2020)".

I would be solely held responsible if any plagiarised content in my thesis is detected, which is violative of the UGC regulations 2018.

Bhavya A. S.

January, 2024

Thiruvananthapuram

ACKNOWLEDGEMENTS

Bhavya A. S.

x

CONTENTS

LIST OF ABBREVIATIONS

1D	One dimensional
2D	Two dimensional
3D	Three dimensional
AgNWs	Silver nano wires
$BaTiO_3$	Barium titanate
BNNSs	Boron nitride nanosheets
BN-PC	BNNSs-polycarbonate composite
BN-PVP	BNNSs- polyvinyl pyrrolidone composite
BoPET	Biaxially oriented polyethylene terephthalate
CNT	Carbon nanotube
CS	Contact-separation
DI	Deionized water
DMF	Dimethylformamide
EC	Ethyl cellulose
EDX	Energy Dispersive X-ray
ES-CA	Electrospun cellulose acetate
FEP	Fluorinated ethylene propylene
FFT	Fast Fourier transformation
FS	Freestanding
FS-TENG	Flexible screen-printed TENG
FT-IR	Fourier transform infrared
h-BN	Hexagonal boron nitride
HR-TEM	High-resolution transmission electron microscopy
IoT	Internet of Things
ITO	Indium tin oxide

LIG	Laser-induced graphene
LS	Lateral sliding
MoS_2	Molybdenum disulfide
O-BN	Oxidised h-BN
P-BN	Functionalized porous aerogel
PDMS	Polydimethylsiloxane
PENG	Piezoelectric nanogenerator
PET	Polyethylene terephthalate
PMMA	polymethyl methacrylate
PTFE	Polytetrafluoroethylene
PU	Polyurethane
PVA	Polyvinyl alcohol
PVB	polyvinyl butyral
PVDF	Polyvinyldine fluoride
P(VDF-TrFE)	Poly(vinylidenefluoridetrifluoroethylene)
PVP	Polyvinyl pyrrolidone
Ra	Average surface roughness
Rq	Root mean square roughness
SE	Single electrode
TENG	Triboelectric Nanogenerator
TGA	Thermogravimetric analysis
TMDs	Transition-metal dichalcogenides
VdW	Van der Waals
WAXD	Wide-angle X-ray diffraction
XPS	X-ray photoelectron spectroscopy

PREFACE

Over the years, the market demand for flexible and wearable electronic devices is mind blowing that poses new challenges to global energy crisis. Low-power electronic gadgets such as wearable sensors, wireless devices, actuators, and health monitoring devices require microwatts to milliwatts of power for their operation. The conventional method of using batteries as a power supply is an obstacle to the miniaturisation of gadgets, since their periodic replacement and recycling are operational hazards. Scavenging different forms of available energy from our day-to-day activities is considered as the best alternative to overcome the future energy crisis. The search for new energy harvesting techniques from clean and sustainable sources has brought rapid progress in the development of nanogenerators. Among various energy harvesters, triboelectric nanogenerators (TENGs) are designed to convert low-frequency, high-entropy mechanical vibrations into electrical energy. These devices, which act as potential candidates for self-powered operation, have received immense global attention by virtue of their simple operation, higher efficiency, enhanced stability, and cost-effectiveness. Thus, TENG based power solution is proven to be useful for applications like the Internet of Things (IoT) and energy autonomous sensor networks. Incorporation of new materials through innovative designs is actively pursued in TENGs, with the central aim of enhancing their output performance. Layered two dimensional (2D) materials are an ideal choice for this purpose, thanks to their higher lateral size and atomic level thickness. This is because the high specific surface area and capacity for charge trapping of such materials help to supplement the triboelectric charge density and thereby improve the power output. Additionally, the newly reported 2D TENGs have high transparency and flexibility, for usage in foldable and wearable electronic devices. In short, 2D materials present new opportunities in energy autonomous wearable electronics.

The present doctoral investigation is focused on creating various structural designs for TENGs, employing hexagonal boron nitride nanosheets (h-BNNSs). These devices are beneficial for applications that harvest energy, and thereby power small-scale electronic gadgets. The whole thesis has been organized into six chapters.

In chapter 1, we discuss the theory, mechanism and significance of TENG. Further, we covered recent advancements in 2D layered materials acting as triboactive layers for

TENG's improved output performance. The rationale behind the choice of the materials and methods were also elaborated.

Chapter 2 discusses the fabrication of a contact separation mode glass supported rigid TENG using a liquid-phase exfoliated 2D material, BNNSs. Bulk material was transformed into 2D BNNSs using a liquid-phase exfoliation process supported by ultrasonication in a suitable solvent, di-methylformamide (DMF). The exfoliated BNNSs were spin-coated onto the BoPET (biaxially oriented polyethylene terephthalate) surface, with polyvinyl butyral (PVB) serving as the film's binder. Here the 2D material could act as the triboelectric negative material against paper that acts as the counter-positive material. This innovative design yielded excellent results. The fabricated device could provide an output voltage of ~200 V and a current density of ~0.48 mA/m^2 under moderate finger tapping. The TENG device has a maximum power density of 0.14 W/m^2. Handheld electronic gadgets such as LCD clocks and digital thermometers, could be successfully powered using BNNSs/BoPET-paper TENG.

Chapter 3 reveals an ink-based printing technique used to fabricate a high-performance flexible TENG that has benefits such as facile fabrication and scalability. In order to prepare a triboelectric contact layer, BNNSs were formulated as a composite ink (BN-PC ink) with a suitable viscosity that was adequate for printing. Remarkably, the flexible screen-printed TENG which was made with BNNSs-based ink as the tribo-negative material and printed positive polyvinyl pyrrolidone (PVP) on BoPET as the tribo-positive material, demonstrated an incredibly high voltage of ~800 V and a short-circuit current density of ~0.78 mA/m^2 under an external force of 10 N with 5 Hz frequency. The maximum power density for TENG is ~1.36 W/m^2. Our research results suggest that these devices are useful for transforming portable electronic devices and LED's into energy autonomous.

Chapter 4 deals with the working of TENG as a self- powered tactile sensor designed for touch sensing. Electrospun cellulose acetate nanofibers (ES-CANF) and screen-printed BNNSs composite ink (BN-PVP) on BoPET substrate were used as the trioactive materials. This improvised design yielded impressive results of ~1200 V as open-circuit voltage and 1.33 mA/m^2 as short-circuit current density. The peak power density could go upto 1.4 W/m^2 for a 3 cm x 3 cm area device. Further, this BNPVP-ES-CA flexible TENG design was modified to act as a touch sensor for detecting input forces of very low magnitude (0.05 N). Remarkably, the sensitivity of the fabricated touch sensor for very

small forces (2 N) was 3.98 V/N, whereas for comparably higher forces within the range of (2–10 N), it was found to be 1.843 V/N.

In chapter 5, our focus was on employing high surface area porous h-BN based 3D structure to improve TENG's output. In this study, oxygen functionalized h-BN was cross-linked covalently using glutaraldehyde-resorcinol chemistry, resulting in the formation of a porous monolithic solid with a 3D interconnected network. To demonstrate the output performance of porous material based TENG (P-TENG), spin-coated ethyl cellulose film on the surface of ITO PET (indium tin oxide-coated polyethylene terephthalate) was paired with h-BN based aerogel as two trioactive materials. The developed aerogel-based TENG exhibited an open circuit voltage of ~720 V and a short-circuit current density of ~10 mA/m^2 for a 2 cm x 2 cm device, under 10 N external force with 5 Hz frequency. Power density reached the highest ever value of this doctoral investigation (~1.7 W/m^2). A successful demonstration of powering a series of commercial LEDs suggests its suitability for future potential applications.

Chapter 6 gives an overall summary of the significant findings drawn from this doctoral investigation and the future scopes of the present work.

Chapter I

2D-Nanomaterials-based Triboelectric Nanogenerators (2D-TENGs)
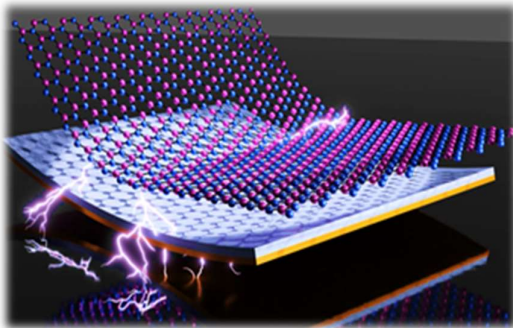
TENGs, are a cutting-edge innovation developed to serve for self-powered operation. These devices have attracted enormous global attention since they present as a solution to energy autonomous handheld devices. This chapter outlines the mechanism, theory, and relevance of TENGs. Further, we also discusses the emerging innovations in the domain of 2D materials functioning as triboelectric layers for the enhanced output performance of TENGs

1.1 Introduction

Internet of Things (IoT) is the new mantra of digital world, where billions of sensors and smart devices are interconnected using internet and manage their operations wirelessly. In this way, IoT creates an ecosystem of interconnected devices, which is going to be the lifeline of smart healthcare systems in future.[1] A significant challenge in this journey is the massive power demand for these devices. The depletion of fossil-fuel sources such as coal and natural gas and their imminent environmental pollution enunciate the need for alternate sustainable solutions for future energy needs.[2]

Power management has two essential parts; (i) power production and (ii) storage. Conventionally, batteries are the most popular energy storage devices that cumulate the power to be used at a later time. However, they have a number of drawbacks, including (i) limited functioning life that necessitates replacement regularly, (ii) limitations on device miniaturization due to their large size, and (iii) environmental contamination due to their poisonous lead-based components.[3] Hence, the inefficient power configurations of the present must be modified drastically for future electronics. Thus, developing innovative self-powered technologies employing alternative sustainable energy sources may be the key to addressing the problem of rising energy consumption in low and high-power applications. Handheld devices need only low-power solutions, whereas biomedical devices demand that power sources should be perpetual and maintenance-free.[4]

In the era of nanotechnology, energy harvesting from natural resources *via* eco-friendly protocols has drawn prominent attention.[5] Sufficient knowledge is now available to tap energy from resources like vibrations, mechanical load, temperature gradients, solar light, etc. High entropy mechanical energy can be conveniently harnessed from resources like human movement[6], flowing water[7], wind[8], vehicle movement[9] etc. These resources have the advantage of providing energy continuously and sustainably.

In the past few decades, alternative energy harvesting technologies have met with dramatic transformations. An interesting concept is the nanogenerator (NG) which is ideally designed to address the energy consumption associated with portable electronic gadgets. They were developed to transform the energy present in the ambient environment into useful electrical signals, by using the mechanism of energy transfer such as the electrostatic effect, piezoelectric effect, and thermoelectric effect.[10] NGs have

incredible advantages in the booming era of IoT, since they are sustainable, lightweight, easily producible, and care-free systems.

1.2 Nanogenerators (NGs)

The fundamental idea behind nanogenerators, which was initially materialized in Georgia Tech, USA in the year 2006, is to transform mechanical or thermal energy generated *via* physical changes into an electrical signal.[11] The term 'nanogenerator' was derived from the fact that the first reported work used a single vertically grown ZnO nanowire for producing electric power by using an AFM tip, its deformation aided minute mechanical energy converted into electric power. The practical working of nanogenerators are mainly based on three aspects.[12]

- Piezoelectric effect
- Triboelectric effect
- Pyroelectric effect

In the piezoelectric and triboelectric approaches, mechanical energy is harvested, whereas in pyroelectric technique, nanogenerators use thermal energy to produce power. The development of nanogenerators for the small-scale functioning of nanosystems, can use the exceptional capabilities of nanomaterials to address the current energy constraint.[4] In IoT technology, there are scores of electronic devices that need to be sustainably powered which can constantly process and transmit loads of data.[13] In other words, the future requirement is that portable devices should be made energy-autonomous. These lightweight devices with variant energy-efficient applications are found promising in IoT-based applications including sensing, environmental monitoring, personal electronics, and defense technology etc.[14] Triboelectric nanogenerator is the youngest among the several types of nanogenerators, which has received the most attention of late, due to its versatility and many advantages.

1.3 Triboelectric nanogenerator (TENG)

The first TENG for harvesting mechanical energy was developed in 2012 by Z. L. Wang's group[15] in Georgia Tech, USA. Since then, one of the most emerging option for the modern era, due to various reasons including high instantaneous power output, cheap fabrication process, and broad choice of available materials, eco-friendliness, and

customizable working modes for target applications. Compared to piezoelectric nanogenerators (PENGs), TENGs generate more electricity from the abundant mechanical energy present in the immediate surroundings (see the illustration in Figure 1.1).[16,17]

The physics of triboelectric phenomenon lies in the principles of static electricity which will be elaborated in the subsequent sections. In simplest terms, the process of press and release between two contact materials with opposite triboelectric nature results in a combined effect of static electrification and also another electrostatic induction effect too. More specifically, contact-induced electrification generates polarized charges on the material surfaces of contact. Then, electrostatic induction initiates the conversion from its mechanical form of energy to electricity via the electrical potential difference developed by the mechanically mediated separation process.[18,19] Let us have a close look at the triboelectric phenomenon.

Figure 1.1: A representation of the transformation of mechanical energy into an electric signal

1.3.1 Triboelectric effect

In the contact electrification process (which is the heart of TENGs), two dissimilar materials become electrically activated when they are separated that were previously in contact, this is called triboelectric charging. Here, generated charges have variable strengths and polarities according to the material's properties including surface roughness, strain, and other factors. During the separation stage, charge transfer occurs between the contact materials surface to preserve an electrochemical potential equality. Ions or molecules can make up these transferred charges which creates electric potential.[20,21]

Interestingly, triboelectrification is a commonly occurring phenomenon in nature. It can generate electrostatic charges in industrial components that cause fire, dust explosions, electronic damage, dielectric breakdown, and other problems. For this reason,

the triboelectric effect has been condemned as a negative effect that is primarily mitigated by suitable technology design methods.[22] On the contrary from an energy perspective, when these developed electrostatic charged surfaces are viewed as part of a capacitive energy device (in the separation stage), they open new windows to the horizon of electrostatic nanogenerators.[23]

1.3.2 Triboelectric series

A galaxy of materials we come across in daily life shows triboelectric phenomena, but their standard quantification is not yet available. Almost all materials like metals, semiconductors, polymers (both natural and artificial), ceramics, glass, etc., exhibit this phenomenon and are used as potential candidates for TENG.[24] The relative polarity of a material with respect to its opposite contact material indicates the sign of charge carried by the material. Based on the polarities of different available materials, a ranking system called the triboelectric series was developed as shown in Figure 1.2.[25] The first triboelectric series was developed in 1757 by Johan Carl Wilcke[26], whose series was dominated by some metals and polymers.
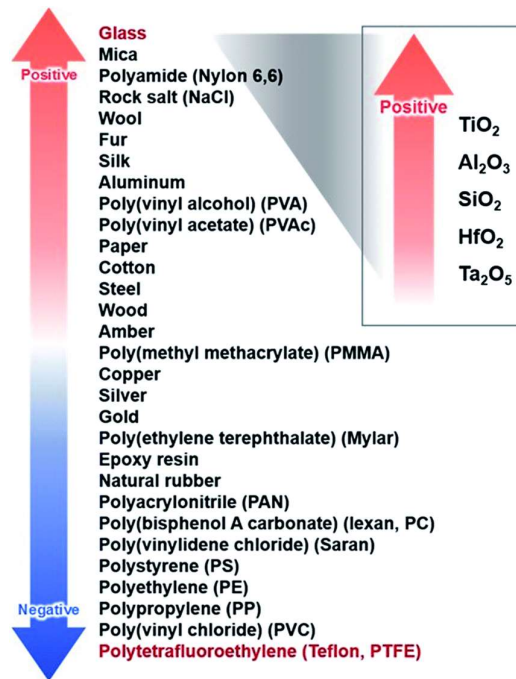
Figure 1.2: *A standard triboelectric series of some common materials. [Reproduced from ref. 25 with permission, copyright 2017, John RSC publishers]*

Triboelectric series is very useful for selecting materials in TENG fabrication. In this series, the frictional materials are arranged according to their ability to gain or lose electrons.[27] Later, it was again modified using charge affinity values. Over the years, an updated quantified series was proposed by Zou *et al.*, by including a number of non-metallic inorganic materials with their triboelectric charge densities.[25]

1.3.3 Fundamental theory

To explain the theoretical origin of TENGs, a physical model based on the electromagnetic theory was developed. Maxwell's displacement current is the main driving force internally for the TENGs energy conversion.[28] Here, non-electric field created polarization term in addition to the medium polarization due to electric field, modifies Maxwell's equation of displacement current. The power generation of TENG accounts for the induced surface electrostatic charges produced from the contact electrification process; hence, an additional 'Wang term' (**Ps**) was added to the displacement vector **D**. Thus, Maxwell's original equations were expanded by Z. L. Wang in 2017, as given below:[29]

$$\boldsymbol{D} = \varepsilon_0 \mathbf{E} + \mathbf{P} + \boldsymbol{P_S} \qquad (1.1)$$

where vacuum permittivity is represented by ε_0 and **P** is the polarization vector related to the externally available electric field **E**. The Wang term, represented by **Ps** mainly stands for the developed charges on surface that are completely field independent. By substituting the above equation (1.1) into original Maxwell's equations, we could obtain

$$\boldsymbol{D}' = \varepsilon_0 \boldsymbol{E} + \boldsymbol{P} \qquad (1.2)$$

Maxwell's equations for stationary conditions were reformulated for their applicability to mechano-driven moving media like TENG. From the four self-consistent physics laws, Wang has developed the differential form of modified Maxwell's equations are given below.

$$\nabla \cdot \boldsymbol{D}' = \rho' \qquad (1.3)$$

$$\nabla \cdot \boldsymbol{B} = 0 \qquad (1.4)$$

$$\nabla \times \boldsymbol{E} = -\partial \boldsymbol{B}/\partial t \qquad (1.5)$$

$$\nabla \times \boldsymbol{H} = \boldsymbol{J}' + \partial \boldsymbol{D}'/\partial t \qquad (1.6)$$

The volume charge density is given by the equation

$$\rho' = \rho - \nabla \cdot \boldsymbol{P_S} \qquad\qquad (1.7)$$

The current density is defined by,

$$J' = J + \nabla \cdot \partial \boldsymbol{P_S} / \partial t \qquad\qquad (1.8)$$

Maxwell's displacement current, revised by using Equations (1.1) and (1.3),

$$\boldsymbol{J_D} = \partial \boldsymbol{D} / \partial t = \varepsilon\, \partial \boldsymbol{E} / \partial t + \partial \boldsymbol{P_S} / \partial t \qquad\qquad (1.9)$$

In the above equation (1.9), the term $\varepsilon \partial \boldsymbol{E}/\partial t$ represents the displacement current as a result of a time-varying electric field and the induced medium polarization due to that electric field. The other term $\partial \boldsymbol{Ps}/\partial t$, called the 'Wang derivative', indicates displacement current that are developed due to surface charges under a mechanical strain field, which does not rely on the electric field. Wang's modification of displacement current which is the main internal driving force of TENGs, acts as a guide towards the development of innovative nanogenerators. In an ideal condition of no leakage current, the conduction current observed at electrodes and the displacement current are equal.[30]

1.3.4 Modes of operation

TENGs can operate in four distinct ways depending on the electrode configuration and the change in polarisation orientation. We briefly discuss here the four fundamental modes of operation and their mechanisms.[31,32]

- Vertical contact-separation (CS) mode
- Lateral sliding (LS) mode
- Single-electrode (SE) mode
- Free-standing (FS) triboelectric-layer mode

1.3.4.1 Vertical contact-separation

This mode was suggested by Zhu *et al*. in 2012[33] and is the most frequently used and earliest documented working mode in TENG. In this method of operation, electrodes are positioned on the top and bottom parts of the material surface wherein two distinct materials are aligned vertically face-to-face, as shown in Figure 1.3. Under the influence of a stimulus, the two triboelectric contact layers undergo a continuous contact separation

process in the vertical direction, generating opposite charges on their surfaces. During its releasing stage, the developed potential drop drives the electron flow between the electrodes *via* electrostatic induction, until a charge equilibrium condition is achieved (see Figure 1.3 (a)).

1.3.4.2 Lateral sliding

In LS mode, the TENG structure is almost similar to the CS mode described above. In contrast to contact separation mode, where the mechanical force is applied in a perpendicular direction to the layer top, the mechanical force operating in a parallel direction in this device construction is considerably different. Parallel sliding of contact layers over one another under a mechanical stimulus, will start a periodic contact and separation that might produce surface triboelectric charges. As a result, the external circuit experiences an electron flow to maintain electrostatic equilibrium (see Figure 1.3 (b)). In short, contact layers periodically closing and sliding provide an AC output signal.[17]

1.3.4.3 Single-electrode

From the described two TENG working modes above, two interconnected electrodes form a closed loop with an external load for the flow of electrons. However, these kinds of device structures limit their applicability in situations where they harvest energy from freely moving mobile objects. For example, in situations like moving vehicles, animals walking, and people using touch displays to type, electron exchange takes place between the bottom electrode and ground. There, single-electrode TENG with the ground as the reference electrode has been developed (see Figure 1.3 (c)). This mode produces electricity by periodic contact separation or sliding between one triboelectric layer with a back electrode and the grounded complementary layer.[34]

1.3.4.4 Free-standing triboelectric-layer

In this mode (which is also made to work with moving objects), a pair of linked, identical electrodes attached to a FS layer shift positions in response to the movement of moving objects (see Figure 1.3 (d)). Further, this will generate an asymmetric charge distribution that drives the electron flow between the electrodes also produces electric current.[35]
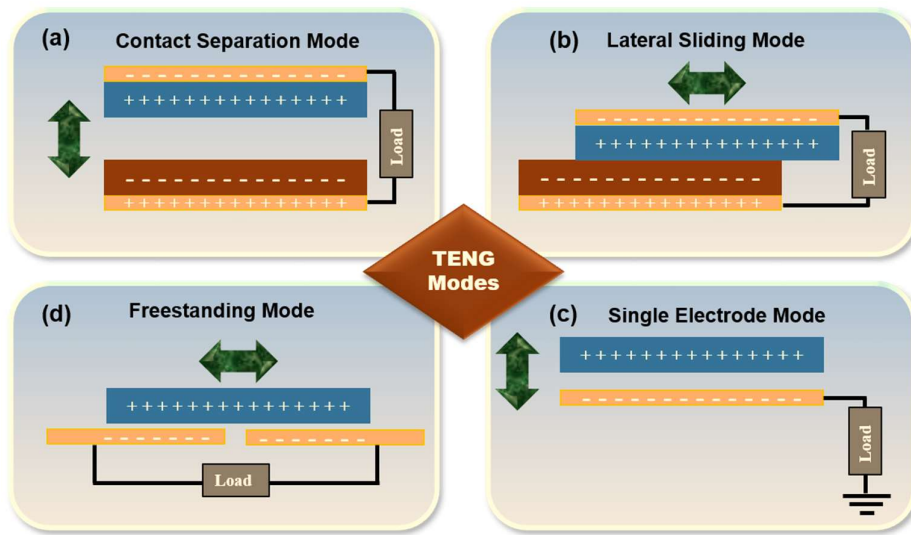
Figure 1.3: *Four basic working modes of TENG operation (a) CS mode, (b) LS mode, (c) FS mode, and (d) SE mode*

1.3.5 Choice of materials for TENG beyond triboelectric series

Metals and dielectric polymers predominate among the several materials used in the traditional triboelectric series. Theoretically, the pair of preferred materials should have a significant variation in their charge affinities to provide a greater TENG output. When these two materials come into physical contact, electron transfer is triggered, and their direction depends on the electron affinity. Materials known as electron acceptors have a propensity to draw electrons from other materials. The opposing one acts as an electron donor and loses its electrons. Identification of the acceptor and donor behavior of materials may be done using the order of arrangement in triboelectric series. For the fabrication of TENGs, material selection, and their triboelectric effects are crucial. A good TENG design means it should qualify the basic quality control parameters for any nanogenerator which include (i) operating stability, (ii) power density, (iii) sustainability, and (iv) adaptability.[36]

In practice, compared to the increased difference in charge affinities and chemical composition, various physical properties of contact materials, such as friction, elasticity, and surface morphological structure, are also superior. Polymers, including PDMS, PTFE, FEP, kapton, PET, and silicone, are among the most widely used materials for electron acceptors. There have been several discoveries of donor materials such as aluminium, copper, nylon, polymethyl methacrylate (PMMA), polyurethane (PU), and indium tin

oxide (ITO). Metal films such as silver, copper, aluminium, etc., can also serve as both electrodes and triboelectric layers.[37]

Recently, a lot of green materials, as well as some inorganic materials with improved performance, have attracted more attention, in addition to the above-mentioned polymer materials. A significant improvement in TENG output has been achieved using cellulose-based green materials, which are both sustainable in nature and mass-producible. A strong triboelectric effect is displayed by highly positive cellulose materials with improved performance. In addition to cellulose, high-performance TENGs also employ naturally occurring biopolymers such as chitosan, lignin, fish gelatin, etc.[16]

One of the future research directions may be on tailoring surface triboelectricity of materials by doping or chemically altering their surfaces with nanostructures, which will undoubtedly improve TENG output performance by modifying contact properties. However, the actual mechanism of charge production in these modified polymers remains unclear, necessitating further research. Compared to polymers, the mechanism of electron transfer is more predictable in inorganic two-dimensional (2D) materials, but only limited studies are available because of the difficulty of making large-area crystalline films. However, these materials are more resistant to surface oxidation than pure polymers, and hence they can tolerate harsh pressure and temperature conditions.

Against this background, 2D materials are a good choice since they can serve as both electrodes and contact materials. It is believed that the creation of composite structures that combine the benefits of currently used triboelectric components may greatly increase the device's lifetime and mechanical qualities. Embedded nanoparticles in composite structures will modify the surface electrification effect and the permittivity of the matrix, making them best suited for improving electrostatic induction. Against this background, the present thesis work is ideally designed to give more focus to the fabrication of 2D material-based composite structures for mechanically strong and durable TENGs.[38]

1.3.6 Factors affecting the output of TENGs

Surface charge density, contact material surface roughness, and environmental conditions like temperature and humidity are the primary variables that have a significant impact on TENGs' electrical output power. In certain triboelectrically active material pairs, their performances are mostly related to their surface charge density, which in turn

relates to the polarity and efficiency of contact between the two materials. Recently, several suitable techniques have been implemented to modify the area of contact and surface charge density. These protocols include surface engineering, adding more storage layers, chemical modification, nanocomposite formation, etc. The key elements affecting contact electrification are triboelectric polarity, contact efficiency, ability to store charge, environmental factors, etc. Let us discuss them one by one.

1.3.6.1 Triboelectric polarity

Triboelectric polarity is the material's innate ability to lose or acquire electrons during the process of contact electrification. In an observed triboelectric phenomenon, this polarity is directly proportional to the generated charges. Numerous studies led to the systematic arrangement of various materials in a "triboelectric series," ranging from strongly tribonegative to strongly tribopositive. Combining the appropriate elements from this series' top and bottom is expected to result in greater power output.[39]

Chemical functional groups on a material's surface have a significant impact on a triboelectric material's polarity. Due to their enhanced propensity to acquire electrons, highly electronegative functional groups like fluorine in a material's chemical structure, lead to the creation of additional charges. As a result, fluoropolymers often function as tribonegative polymers. The most commonly used fluoropolymers are polyvinyldine fluoride (PVDF), PTFE, and FEP. On the contrary, some amino-group polymers with nitrogen are naturally tribopositive. Chemical modification of the material surface through the introduction of suitable functional groups provides an efficient method for polarity control, which broadens its applicability to multiple domains.

1.3.6.2 Materials' effective area of contact

If one could increase the volume of surface charges in a triboelectric pair, more charge transfer will take place. Surface modification is one of the most efficient methods used for improving the contact area between frictional materials. PMMA and PDMS surfaces were used to create nanopatterns using the photolithographic process, which showed a higher output voltage than the unaltered structure. A hexagonal pattern with a narrower pillar width produces more voltage than a pattern with a wider pillar width. The effect of contact force on the surface of the materials in contact will alter their output efficiency. When the force acting on the material is higher, physicochemical properties of the surface induce more charge transfer.[40]

1.3.6.3 Charge-storage ability

Another viable strategy used for obtaining higher TENG output is to control the loss of generated charges on the material's surface due to friction. The ability of the tribolayer to store charges effectively retains the generated charges on material surface, that will definitely improves the charge density also contributes to a higher output. To do this, materials with high dielectric constants are mixed with frictional materials to create functional composite structures having abundant charge-trapping centers. A typical example is the addition of high dielectric constant barium titanate ($BaTiO_3$) nanoparticles to a ferroelectric matrix like P(VDF-TrFE) to improve the output of a nanocomposite based TENG.[41]

It is believed that, atomically thin 2D materials having a lamellar kind of structure are the best choice as charge trapping sites in their composite structure, and their ultra-high capacitance also improves the storage performance.[42] The multi-layered device construction with an extra storage layer between the frictional tribolayer and the electrode in a composite three-layer structure also stimulated attention towards the development of trioactive materials with efficient storage capabilities.[43] This composite three-layer construction greatly increased the surface charge density compared to the single-layer structure.[44]

1.3.6.4 Environmental factors

The electrical output of TENGs is greatly affected by external environmental conditions like temperature, humidity, and atmospheric pressure.[45] The triboelectric charges developed between the frictional materials increased nearly to 20%, with a considerable decrease in their relative humidity values. Studies have shown that humidity will adversely affect the charge generation between these trioactive materials.[46] Water-reluctant materials with improved hydrophobic properties can be converted into an anti-humidity TENG that will provide stable output without causing any significant changes even in humid conditions.

From extensive studies, it has been noticed that the effect of temperature could also produce a strong impact on the TENGs output.[47] The trends of output variation observed at different temperature ranges are quite different from one another. The gradually rising temperature from -20 to 20 °C causes decreased output performance, whereas between the temperature range of 20 and 100 °C output remains stable. A

further increase in temperature causes a rapid decline in output. At higher temperatures, surface oxidation generates surface defects, and material permittivity changes severely affect the device's output performance. In some kinds of insulating oxides like SiO_2 or Al_2O_3, the charge trapping ability of the material is significantly reduced at higher temperatures which also causes lower output.[48] The effect of atmospheric pressure on TENG can be identified by analysing the output performance of the device under vacuum conditions, which exhibits improved triboelectric charge density.

1.3.7 2D Material-based TENGs (2D-TENGs)

Atomically thin crystalline solids with layer thicknesses of a few nanometers or less are broadly classified as free-standing 2D materials. These types of materials allow for the unrestricted movement of electrons in a two-dimensional plane. However, they are unable to move in the third direction because of the laws of quantum physics. In 2004, Geim and Novoselov isolated the most popular 2D material reported so far, graphene.[49] 2D graphene separated from its bulk graphite powder by using a simple scotch tape micromechanical cleavage method. This invention heralded the beginning of a new era of research on 2D materials and a richness of associated properties.[50]

In the new millennium, the field of electronics saw revolutionary advancements that are contributed by many factors, and one of them is the advancements in the domain of atomically thin 2D materials. Several 2D layered materials including MXenes, boron nitride, TMDs, silicenes, black phosphorous, and bismuthenes were extensively investigated, even since the emergence of graphene. Compared to its bulk counterparts, 2D graphene has higher carrier mobility at room temperature, superior thermal conductivity, and extremely high mechanical strength. These single-layered substances display a variety of electrical behaviors. The mechanical, electrical, and optical performances of the few or single-layered materials are completely vary from their bulk material, and this motivates researchers to focus more on the development of ultra-thin layered materials.[51]

2D nanomaterials with astonishing physicochemical and optoelectronic properties integrated with TENGs can bring about 2D TENGs with enhanced output performance. The newly endowed 2D TENGs support the use of foldable electrical and optoelectronic devices. These nanomaterials have better flexibility, optical transparency, mechanical robustness, and a high surface-to-volume ratio, making them an appropriate

candidate for implementing 2D TENGs.[52] The unique structure of 2D nanomaterials empowers them with several peculiar properties that possess different functions in nanogenerators. The various roles performed by 2D material in TENGs are as follows:

- Electrode materials
- Triboelectric materials
- Both electrode and triboelectric materials

For TENGs with thin device structures, stacking structures can be created from 2D materials with very low atomic unit thickness. The incorporation of these tiny devices into wearables and bodily implants is realized through straightforward processes.[16] Recently, a few works have been proposed related to 2D TENGs, even though the triboelectric properties of 2D materials are still not clearly understood and their triboelectric mechanisms are poorly studied.[53] By investigating the TENG output from various combinations of 2D materials with known materials in triboelectric series, the charge polarities of all 2D materials could be identified.[54] Based on the investigations made by Seol *et al.*,[55] most of the analysed 2D materials show the tendency to accept electrons in TENG design and are located mostly at the negative side of the triboelectric series. Charge polarity of these materials are completely independent of their layer thickness and the adopted synthesis methods. Now let us discuss the commonly adopted protocols to improve the output performance in 2D TENGs.

1.3.7.1 Output enhancement in 2D TENGs

1.3.7.1.1 Ultra-high surface area

High surface contact area in 2D nanomaterials with similarly larger lateral sizes and atomic-level thickness contributes to a rise in triboelectric charge density and output improvement. Incorporation of high surface area materials in the triboelectric layer can improve the contact area of TENG operation.

1.3.7.1.2 Charge trapping sites

2D materials with interlayer voids can easily capture the charge carriers and store them. These materials also act as charge-trapping sites in the polymer matrix that will reduce the loss of electrons by transferring them to the interior of the layer from the surface. Otherwise, electron recombination with air particles or positively charged ions

causes a loss of electrons and decreases output to a great extent.

1.3.7.1.3 Triboelectric polarity

Theoretically, the effective charge transfer between a pair of triboelectric materials strongly depends on their difference in tribopolarity. If the selected materials are in a triboelectric pair located at the two ends of the triboelectric series, they can produce enhanced output performance due to more charge transfer. As we have seen before, 2D atomically thin materials are located near the negative end of the conventional series. Hence, the combination of 2D materials with higher positive triboelectric materials in a device-forming pair can produce more charge transfer and higher output.

1.3.7.1.4 Adaptability for further improvement

As hinted before, 2D materials have extended lateral dimensions which can bring about high power output by surface modification. Engineering of highly exposed surface atoms of 2D materials by external means can tailor the features and functions of the material and broaden its applicability. Along with all the above properties, 2D materials in the frictional layer provide better durability in high temperature and humid environmental conditions. The majority of TENGs' works solely use certain 2D materials, like graphene and MoS_2. The efforts taken for a thorough investigation of other 2D material-based TENGs and their working mechanisms have received increased attention now for their improved performance and future applicability. We focus our attention on h-BN, a 2D material, due to its exotic electronic properties in comparison with graphene.

1.3.7.2 Applications of 2D TENGs

Rapidly growing need for intelligent electronics in communication, environmental monitoring and healthcare systems, directs the focus toward the creation of devices that are responsive to environmental stimuli.[56] Recently, 2D TENG-like devices have major emphasis on energy harvesting in biomechanical field and also active in self-powered sensing like touch, motion, chemical and acceleration sensing. By the versatility of layered materials, 2D-TENGs can be integrated into biomedical devices so that human body movements can be converted into energy.[57,58] A graphene-based TENG in a single electrode configuration could go down to thickness up to less than 2.4 μm. This 2D TENG is conformally integrated into human skin for powering wearable gadgets without the need for charging. Such devices have also found application as a power source for

agricultural sensor networks.[59] Some unfavorable environmental circumstances, such as geology and weather may alter the TENG performance. To counteract the effects of these unfavorable factors, new nanogenerator designs have been recently developed with self-cleaning and humidity-resistant properties.[60] Furthermore, a fiber-based 2D TENG integrated agro textiles for an intelligent agricultural greenhouse net technology was also deployed.[61] This technology has the potential to minimise the negative consequences of persistent rain on agricultural productivity. The fiber-based 2D TENG utilized MXene ink and silver nanoparticles as raw materials. A flexible mixed dimensional (1D/2D) composite structure comprising of 1D silver nano wires (AgNWs) wrapped with 2D molybdenum disulfide (MoS_2) nanosheets, was reported where the so-developed strain sensor may be worn on the skin.[62]
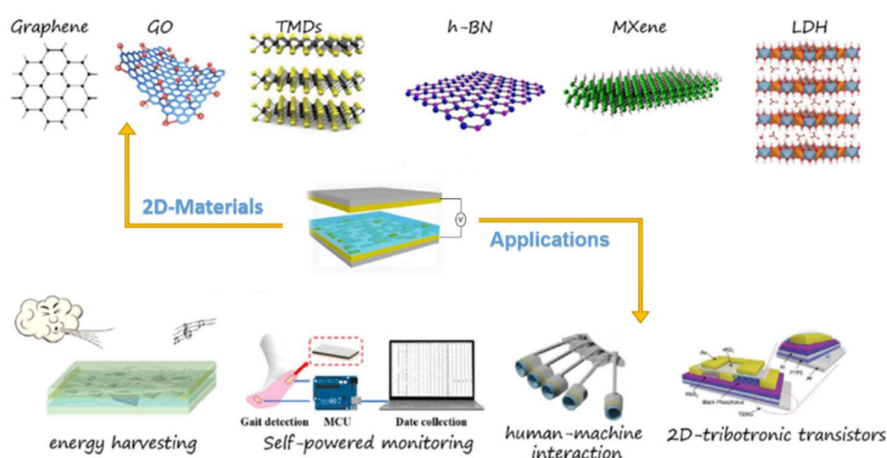
Figure 1.4: *2D materials in TENGs and their practical applications*

In 2D material-based potential active sensors, specific information regarding the external stimuli and environment will reflect the output signals *via* their amplitude or frequency. A self-powered handwriting recognition sensor array was reported by C. Jiang, *et al.* constructed of polydimethylsiloxane and MXene (PDMS/MXene) composite film over the laser-induced graphene (LIG) electrode. This sensor is designed to accomplish real-time trajectory detection.[63] Using a mixture of MoS_2/graphite glue, Karmakar *et al.* created a self-charging flexible power cell for detecting weight and temperature.[64] Commercially available glue (FEVI®GUM lime Fragrance) was employed as a medium of electron transport and also it used as a material for binding. Temperature sensing from ambient to 323 K and weight measurement of up to 72 kg was demonstrated. 2D TENGs

also act as an external power source to regulate the electron transport properties of semiconductor channels in 2D transistors.[65] Given below (Figure 1.4) are some examples of TENGs integrated with 2D materials and their real-world uses.

1.4 Hexagonal boron nitride (h-BN)

Well-known is the fact that h-BN is a structural analog of graphite having a very similar layered structure as seen in Figure 1.5. In this material, the individual layers are joined by weak vdW type bonding, and each layer has an equal amount of sp^2-hybridized boron and nitrogen atoms that are covalently placed in hexagonal planar configuration. These bonds are highly polarized. The polarity arises from the interlayer stacking pattern of h-BN in which each B atom in one layer is situated exactly above or below the adjacent layer N atoms. Exotic optoelectrical nature together with mechanical robustness, chemical inertness, and thermal stability, are some of the promising features exhibited by this material that make it suitable for various stream of applications in nanoelectronics, anti-corrosion, photonics, energy storage, and catalysis.[66]
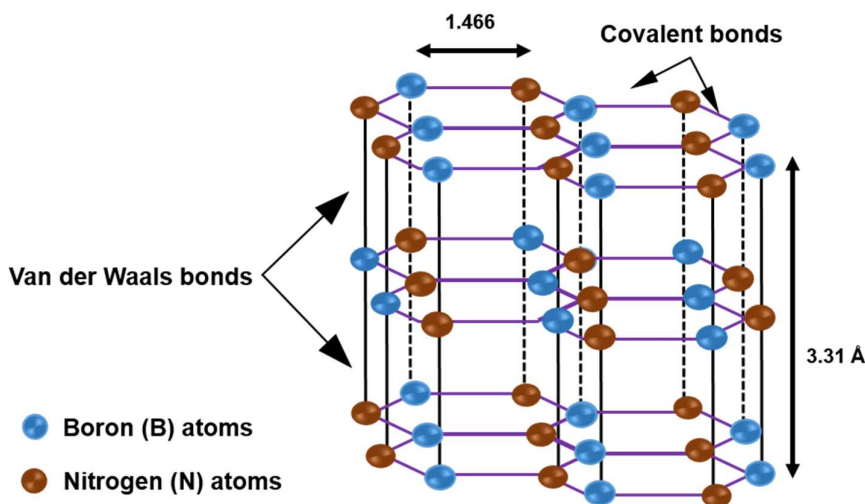
Figure 1.5: *Hexagonal boron nitride structure*

1.4.1 Synthesis of 2D boron nitride nanosheets (BNNSs)

Free-standing 2D materials that are created using both top-down and bottom-up techniques have recently received a lot of scientific attention. There have been numerous research efforts undertaken to develop 2D BNNSs.[67,68] Exfoliation is one of the popular top-down approaches for producing 2D BNNSs, in which the weak vdW force of attraction between the layers in the bulk material is allowed to cleave.[69] Liquid phase exfoliation is

the best-known low-cost and scalable method for the synthesis of 2D nanosheets, where the layered material is allowed to sonicate continuously in presence of a suitable solvent. In the ultrasonic-assisted delamination process, consequent to the pressure fluctuations created in the sonication bath, pressure bubbles are generated and collapse within the liquid medium, which is called acoustic cavitation effect. The cavitation effect, in combination with solvent polarity effect, renders the complete delamination of pristine h-BN in a suitable solvent (say, DMF). The mechanism of liquid phase exfoliation in DMF solvent is briefly illustrated in Figure 1.6.
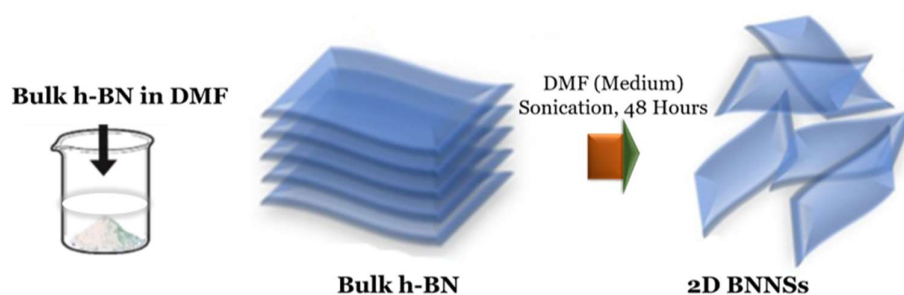
Figure 1.6: *Schematic representation of liquid phase exfoliation*

The process of ultrasonic delamination solicits a profound understanding of the colloidal dispersion of individual layers and the nature of the interaction between BN and the solvent of exfoliation. The selected solvent should be able to supply external energy for weakening the binding between layers, thereby intercalation of solvent takes place which in turn promotes the process of exfoliation.[70] The stability of the solvent to hold the exfoliated nanosheets in colloidal dispersion is of utmost importance since it can prevent the reverse recombination of exfoliated layers. Coleman *et al.*[71] proposed that the solvents selected for exfoliation should have a comparable surface tension similar to BN nanosheets, thereby minimising the enthalpy of mixing. The best solvents used for exfoliation are briefed in Table 1.1:

Table 1.1: Different solvents for exfoliation summarized (Solvents for exfoliation, Sample quality, Specific Remarks and Reference included)

Sl. No	Solvent for exfoliation	Sample quality	Remarks	Ref.
1	DMF	This method produces BNNSs of thickness around 1.2 nm (only one or two layers)	These nanosheets have in-plane micrometer-level lateral dimensions	72
2	IPA	Sheet thickness varies between 10–20 nm	Ultrasonication done vigorously in the solvent was used for both dispersion and exfoliation	73
3	NMP	Product yield was higher	This method utilized shear forces for exfoliating bulk flakes	74
4	Ethanol/water mixtures	Nanosheets of thickness 3–4 nm	Two poor solvents for exfoliation can be combined into one good solvent, which is based on the HSP (Hansen Solubility Parameter) theory	75
5	Methane-sulfonic acid	Obtained samples consisted of less than 10 layers ($\leq$ 3 nm)	The resultant BNNSs have good dispersibility in polar solvents	76
6	IPA:DI water (3 : 7)	3–4 layers of nanosheets, having a thickness of the order ~1.2 nm	Working principle is the Lewis acid-base mechanism of interaction	77

1.5 Methods for film formation

1.5.1 Spin coating

Spin coating is one of the most commonly employed techniques for depositing uniform thin coatings on substrate surfaces. The thickness of the coating developed on the substrate surface is in the order of micrometres and nanometers. In a typical spin coater, the substrate used for thin film formation is clamped using vacuum on a rotatable fixture, on the surface of which the coating solution is dispensed. The coating solution is driven radially outward by the high speed rotational accelerations during the spin coating process, leaving a very thin, uniform coating of the material on the substrate surface.[78] A schematic depicts the spin-coating method is given in Figure 1.7. The solution's viscous flow balances the high-speed acceleration and keeps the substrate's film structure in place. This flow concept was first introduced by Emslie, Bonner, and Peck.[79] Later, Meyerhofer[80] introduced the concept of controlled solvent evaporation by splitting the spin coating process into two stages. The first stage predominantly deals with viscous flow, and the second stage is for solvent evaporation. Based on this concept, the final coating thickness (h) is predicted as

$$h = x \, (e/2(1-x) \, K)^{1/3} \qquad\qquad (1.10)$$

where 'e' stands for the evaporation constant and 'K' is the flow constant, and 'x' is the total solid content of the solution.

Most often, polymeric materials in their solution form are applied for coating. This technique has been extensively utilized in the manufacturing process of optical mirrors, circuit boards, data storage magnetic discs and also in television screens etc.[81]
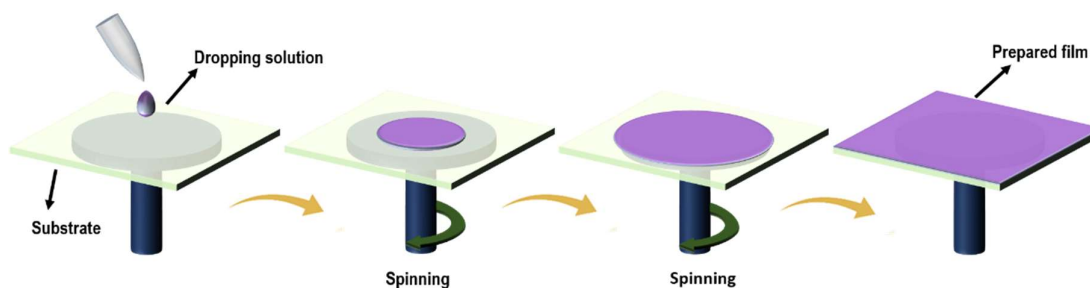
Figure 1.7: *Schematic representation involves various stages of the spin coating process*

1.5.2 Screen printing

Unlike a spin coating, screen printing is designed for transferring desired patterns onto a flat substrate surface. The most commonly used substrates for screen printing are paper, fabric, and some polymer films. This method of screen printing transfers dye or ink using a woven mesh screen with a stencil design that is impervious to ink. The forceful motion of a squeegee wetting the substrate surface fills the open holes of the mesh with ink. After the squeegee stroke, the screen springs back from the substrate surface, creating a pattern with sharp edges as shown in Figure 1.8.[82] Screen printing meshes are made up of materials like polyester, nylon, and stainless steel. In addition to being utilised for printing on fabric, this method is also recognised as a scalable production process for printed electronics, including the manufacture of sensors, multilayer circuits on thin ceramic substrates, wearable device components, etc.

The primary components of screen-printable inks are a formulated mixture of vehicles and functional particles. Dispersant solvents are commonly referred to as vehicles. Fillers, binders, and various additives are all included in functional powders. There are many different types of screen-printable inks available depending on the printing requirements. For high-quality printing, the rheological properties of the inks play a vital role. These characteristics of the inks include paste fluidity, viscoelastic behaviour and thixotropy, which are supposed to have a significant impact on the printing quality of the inks. Surface active agents, for example, are some additives that are used to obtain improved rheological properties.[83]
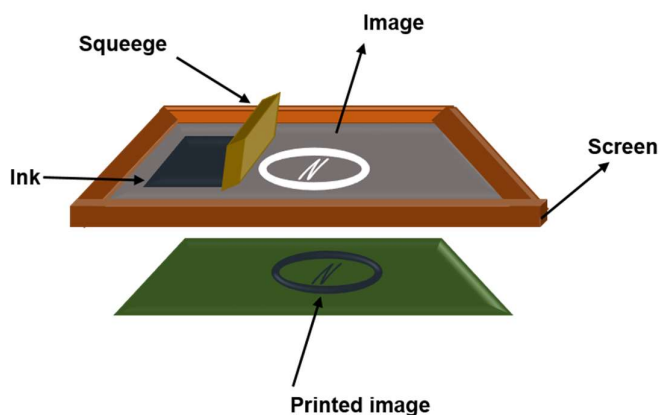
Figure 1.8: *Schematic representing the screen printing process*

1.5.3 Electrospinning

Electrospinning is a voltage-driven process for generating ultrafine, continuous fibers. The nanofibers produced from polymer solutions have a diameter in the range of nanometers to several hundred nanometers. In this method, an electrified liquid drop in the form of a jet is converted to a fiber by stretching and elongation process. An electrospinning setup consists of a reservoir of polymer solution, most commonly a syringe with a needle, a high voltage source, a grounded collector and a pump.[84] Different geometrical configurations of collectors like rotating drums or discs, mandrels, and flat plates are used for the electrospinning process. Figure 1.9 shows an electrospinning process experimental setup. The basic principle underlying the electrospinning process is that the higher voltage applied converts the liquid droplet at the needle tip to a conical shape called a "Taylor cone". This elongation happens when the electrostatic repulsion force overcomes its surface tension value. As a result, the charged liquid jet moved towards the collector. Electrospun nanofibers have comparably higher surface area and porosity than regular nanofibers. By controlling the composition of nanofibers, better functionalities and morphological structures could be achieved. Polymer nanofibers with attractive properties find many applications in diverse areas like tissue engineering, energy storage and conversion, wound dressing, sensors etc.[85]
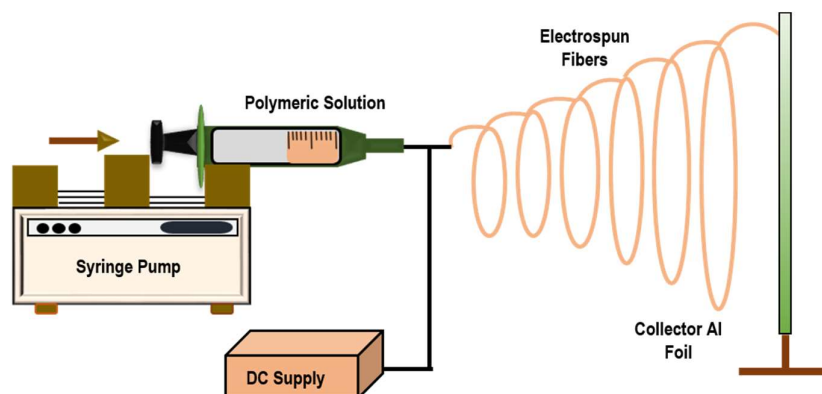
Figure 1.9: Schematic view of electrospinning experimental setup

1.6. Techniques for measuring TENG's output

Regardless of the TENG's structural design, certain crucial parameters are involved in the evaluation of its output performance. Measurement of output voltage (V_{OC}) (which may be performed in both open circuit and external load conditions), short-circuit current density (J_{SC}), and capacitor charging. These can be experimentally investigated using laboratory tools and another derived quantity called power density, also involved in this study is the power recorded in the unit area (P). These parameters are important for assessing how well a TENG performs.

1.6.1 Source measuring unit (Keithley 2450)

The characteristic techniques mainly used for measuring the output voltage include either a voltage module arrangement in a multifunctional setup of an electrometer that can directly measure the voltage produced. In another way, using a series arrangement of an ammeter and resistor setup provides voltage from Ohm's law calculations.[86] Here in our work, the above-listed electrical performances of the fabricated TENG device were studied using a source meter set up by Keithley 2450 (Figure 1.10). The two conductive electrodes connected to the TENG device were attached to the source meter directly to quantify the charges transferred between them. The produced voltage will vary relative to a number of factors like the kind of triboelectric materials used, force exerted, frequency, device configuration environmental factors, etc. All the experiments were conducted under the ambient room temperature conditions. The produced output voltages may vary from volts to thousand volts. A home-made force providing system was developed by altering a sewing machine used for imparting the mechanical forces of ∼ 10N and the developed voltage is measured. The power density of the developed TENG was also identified from observed voltages generated using various load resistors, ranging from 1 Ω to 1000 MΩ. Power can be calculated from the voltage using the given equation.

$$P = \frac{V^2}{R} \tag{1.11}$$

where 'V' stands for voltage and 'R' is the resistance

Figure 1.10: *Photograph of Keithley 2450 Source measuring unit*

1.6.2 Low noise current preamplifier (SR570)

A current preamplifier is required for measuring the low amplitude output currents generated within TENGs. The SR570 low-noise current preamplifier may provide up to 1 pA/V in current gains (Figure 1.11). The whole bandwidth of the TENG's current signal was relatively on time and possibly measured by the SR570 preamplifier. A lab-scale TENG of the active area of few cm^2 or less is intrinsically low in output current, its values are frequently measured in the nA to µA range.[87] These current measurements are complicated by TENG's high inherent impedance because the device is loaded by the input from a voltmeter. As a result a substantial percentage of the TENGs output current normally sinks. It makes it difficult to monitor the TENG output current with minimal interruption hence a pre-amplifier setup is useful for measuring a small current from a high-impedance source.

Figure 1.11: *Low noise current preamplifier (SR570)*

1.6.3 Motorised force impactor with digital force gauge (Mark-10)

A force gauge is an instrument mainly designed for measuring forces in compression, coefficient of friction, tension, etc. Nowadays, both the mechanical and digital force gauges are readily available. Mark 10 force gauges with motorized test stand seen in Figure 1.12 can record the generated peak force in a compression and tension process. These force gauges are available either as handheld type or in combination with a test stand and a supporting gripping fixture to establish a full testing solution. One of the fundamental parts of a force gauge is a load cell, which can translate force into an electric signal. In addition, a software and electronics part converts the voltage value from the load cell to a displayed force. Most often, pound or newton are the most popular test units for measuring force.

Figure 1.12: Mark-10 motorised force impactor with digital force gauge

1.7 Scope of the present research

As discussed before, the rising surge of non-renewable energy sources in our everyday lives and industrial activity has sparked concerns about an impending energy crisis. To reduce the dependence on conventional energy sources like fossil fuels, researchers are working to develop renewable energy harvesting methods. For several decades, intense search has been going on exploring renewable methods such as solar, tidal power, wind, etc. But tapping energy from these resources is limited by several constraints including weather, space and time. Interestingly, mechanical energy is regarded as the most wasted energy form.

This doctoral research is stemmed from the idea of harvesting mechanical energy in the surrounding environment. Energy scavenging from mechanical motion supplements the concept of sustainable, renewable and eco-friendly energy harvesting for future energy needs. Among mechanical scavengers, TENGs have received increased attention since they are way ahead of PENGs in terms of energy conversion efficiency. In the present investigation, different forms of triboelectric energy nanogenerators and tactile sensors are realized using a unique ultrathin 2D layered material, h-BN. The innovative material combinations chosen, synthetic protocols used and the device concepts realized, can be heralded as the novelties of the thesis. In this way, this investigation was designed to push the knowledge horizon in the domain of non-conventional energy harvesting, which will ease the fabrication of miniaturized, energy-autonomous and flexible devices for applications in biomedical and consumer electronics.

The thesis is framed based on the following objectives:

- Design and fabrication of glass supported rigid TENG, in contact separation mode employing exfoliated BNNSs.

- Demonstration of flexible screen-printed TENG (FS-TENG) for powering electronic devices utilizing composite ink based on BNNSs on a polymer substrate.

- Development of self-powered flexible triboelectric tactile sensor made of electrospun cellulose nanofibers and BNNS-based composite ink.

- Realization of a flexible TENG with triboelectric layer made of functionalized hexagonal boron nitride porous 3D structure and ethyl cellulose on ITO PET substrate.

1.8 References

(1) Chen, B.; Wang, Z. L. Toward a New Era of Sustainable Energy: Advanced Triboelectric Nanogenerator for Harvesting High Entropy Energy. *Small* **2022**, *18* (43), 2107034.

(2) Rathore, S.; Sharma, S.; Swain, B. P.; Ghadai, R. K. A Critical Review on Triboelectric Nanogenerator. *IOP Conf. Ser. Mater. Sci. Eng.* **2018**, *377* (1), 012186.

(3) Mohanty, A.; Parida, S.; Behera, R. K.; Roy, T. Vibration Energy Harvesting: A Review. *J. Adv. Dielectr.* **2019**, *9* (4), 1–17.

(4) Zhu, G.; Chen, J.; Jing, Q.; Wang, Z. L. Triboelectric Nanogenerators as a New Energy

Technology : From Fundamentals , Devices , to Applications. *Nano Energy* **2015**, *14*, 126–138.

(5) Delgado-Alvarado, E.; Elvira-Hernandez, E. A.; Hernandez-Hernandez, J.; Huerta-Chua, J.; Vazquez-Leal, H.; Martinez-Castillo, J.; Garcia-Ramirez, P. J.; Herrera-May, A. L. Recent Progress of Nanogenerators for Green Energy Harvesting: Performance, Applications, and Challenges. *Nanomaterials* **2022**, *12* (15), 2549.

(6) Bai, P.; Zhu, G.; Lin, Z.; Jing, Q.; Chen, J.; Zhang, G.; Ma, J.; Wang, Z. L. Integrated Multilayered Triboelectric Nanogenerator for Harvesting Biomechanical Energy from Human Motions. ACS nano **2013**, *7* (4), 3713–3719.

(7) Nanogenerator, T.; Cheng, G.; Lin, Z.; Du, Z.; Wang, Z. L. Electrostatic and Mechanical Energies from Flowing Water by a Hybridized.ACS nano **2014**, *8* (2), 1932–1939.

(8) Xie, Y.; Wang, S.; Lin, L.; Jing, Q.; Lin, Z.; Niu, S.; Wu, Z. Rotary Triboelectric Nanogenerator Based on a Hybridized Mechanism for Harvesting Wind Energy. ACS nano **2013**, *7* (8), 7119–7125.

(9) Zhang, H.; Yang, Y.; Zhong, X.; Su, Y.; Zhou, Y.; Hu, C.; Wang, Z. L. Single-Electrode-Based Rotating Triboelectric Nanogenerator for Harvesting Energy from Tires. ACS nano **2014**, *8* (1), 680–689.

(10) Guo, X.; Liu, L.; Zhang, Z.; Gao, S.; He, T.; Shi, Q.; Lee, C. Technology Evolution from Micro-Scale Energy Harvesters to Nanogenerators. *J. Micromechanics Microengineering* **2021**, *31* (9), 093002.

(11) Nguyen, V.; Zhu, R.; Yang, R. Environmental Effects on Nanogenerators. *Nano Energy* **2014**, *14*, 49–61.

(12) Wang, Z. L.; Zhu, G.; Yang, Y.; Wang, S.; Pan, C. Progress in Nanogenerators for Portable Electronics. *Mater. Today* **2012**, *15* (12), 532–543.

(13) Zhu, G.; Chen, J.; Jing, Q.; Wang, Z. L. Triboelectric Nanogenerators as a New Energy Technology : From Fundamentals , Devices , to Applications. *Nano Energy* **2015**, *14*, 126-138.

(13) Indira, S. S.; Vaithilingam, C. A.; Oruganti, K. S. P.; Mohd, F.; Rahman, S. Nanogenerators as a Sustainable Power Source: State of Art, Applications, and Challenges. *Nanomaterials* **2019**, *9* (5), 773.

(14) Basset, P.; Beeby, S. P.; Bowen, C.; Chew, Z. J.; Delbani, A.; Dharmasena, R. D. I. G.; Dudem, B.; Fan, F. R.; Galayko, D.; Guo, H.; Hao, J.; Hou, Y.; Hu, C.; Jing, Q.; Jung, Y. H.; Karan, S. K.; Kar-Narayan, S.; Kim, M.; Kim, S. W.; Kuang, Y.; Lee, K. J.; Li, J.; Li, Z.; Long, Y.; Priya,

S.; Pu, X.; Ruan, T.; Silva, S. R. P.; Wang, H. S.; Wang, K.; Wang, X.; Wang, Z. L.; Wu, W.; Xu, W.; Zhang, H.; Zhang, Y.; Zhu, M. Roadmap on Nanogenerators and Piezotronics. *APL Mater.* **2022**, *10* (10), 0085850.

(15) Lin, Z. Wang, Fan, F.; Tian, Z. Flexible Triboelectric Generator ! *Nano Energy* **2012**, *1* (2), 328–334.

(16) Khandelwal, G.; Maria Joseph Raj, N. P.; Kim, S. J. Materials Beyond Conventional Triboelectric Series for Fabrication and Applications of Triboelectric Nanogenerators. *Adv. Energy Mater.* **2021**, *11* (33), 1–32.

(17) Wu, C.; Wang, A. C.; Ding, W.; Guo, H.; Wang, Z. L. Triboelectric Nanogenerator : A Foundation of the Energy for the New Era. *Adv. Energy Mater.* **2019**, *1802906*, 1–25.

(18) Wang, Z. L. Triboelectric Nanogenerators as New Energy Technology and Self-Powered Sensors - Principles, Problems and Perspectives. *Faraday Discuss.* **2014**, *176* (11), 447–458.

(19) Cheng, T.; Gao, Q.; Wang, Z. L. The Current Development and Future Outlook of Triboelectric Nanogenerators: A Survey of Literature. *Adv. Mater. Technol.* **2019**, *4* (3), 1800588.

(20) Zhang, X.; Chen, L.; Jiang, Y.; Lim, W.; Soh, S. Rationalizing the Triboelectric Series of Polymers. *Chem. Mater.* **2019**, *31* (5), 1473–1478.

(21) Kim, W.; Kim, D.; Tcho, I.; Kim, J.; Kim, M.; Choi, Y. Triboelectric Nanogenerator: Structure, Mechanism, and Applications. *ACS nano* **2021**, *15* (1), 258-287.

(22) Furfari, F. A. A History of the Van de Graaff Generator. *IEEE Ind. Appl. Mag.* **1930**, *11*, 10–14.

(23) Wu, C.; Wang, A. C.; Ding, W.; Guo, H.; Wang, Z. L. Triboelectric Nanogenerator: A Foundation of the Energy for the New Era. *Adv. Energy Mater.* **2019**, *9* (1), 1–25.

(24) Gooding, D. M.; Kaufman, G. K. Tribocharging and the Triboelectric Series. *Encyclopedia of Inorganic and Bioinorganic Chemistry*, **2011**, *15,* 1-14.

(25) Zou, H.; Zhang, Y.; Guo, L.; Wang, P.; He, X.; Dai, G.; Zheng, H.; Chen, C.; Wang, A. C.; Xu, C.; Wang, Z. L. Quantifying the Triboelectric Series. *Nat. Commun.* **2019**, *10* (1), 1–9.

(26) Wang, Z. L. Triboelectric Nanogenerator (TENG)— Sparking an Energy and Sensor Revolution. *Adv. Energy Mater***. 2020**, *10* (17), 1–6.

(27) Kim, Y. J.; Lee, J.; Park, S.; Park, C.; Park, C. Effect of the Relative Permittivity of Oxides on the Performance of Triboelectric Nanogenerators. *RSC Adv.* **2017**, *7*, 49368–49373.

(28) Luo, J.; Wang, Z. L. Recent Progress of Triboelectric Nanogenerators: From

Fundamental Theory to Practical Applications. *EcoMat* **2020**, *2* (4), 1–22.

(29) Wang, Z. L. On Maxwell's Displacement Current for Energy and Sensors: The Origin of Nanogenerators. *Mater. Today* **2017**, *20* (2), 74–82.

(30) Elsanadidy, E.; Mosa, I. M.; Luo, D.; Xiao, X.; Chen, J.; Wang, Z. L.; Rusling, J. F. Advances in Triboelectric Nanogenerators for Self-Powered Neuromodulation. *Adv. Funct. Mater.* **2023**, *33* (8), 2211177.

(31) Haroun, A.; Tarek, M.; Mosleh, M.; Ismail, F. Recent Progress on Triboelectric Nanogenerators for Vibration Energy Harvesting and Vibration Sensing. *Nanomater.* **2022**. *12* (17), 2960.

(32) Luo, J.; Gao, W.; Wang, Z. L. The Triboelectric Nanogenerator as an Innovative Technology toward Intelligent Sports. *Adv. Mater.* **2021**, *2004178*, 1–8.

(33) Zhu, G.; Pan, C.; Guo, W.; Chen, C.-Y.; Zhou, Y.; Yu, R.; Wang, Z. L. Triboelectric-Generator-Driven Pulse Electrodeposition for Micropatterning. *Nano Lett.* **2012**, *12* (9), 4960–4965.

(34) Khan, U.; Hinchet, R.; Ryu, H.; Kim, S.; Khan, U.; Hinchet, R.; Ryu, H.; Kim, S. Research Update : Nanogenerators for Self-Powered Autonomous Wireless Sensors Research Update : Nanogenerators for Self-Powered Autonomous Wireless Sensors. *APL materials* **2017**, *5* (7), *073803*.

(35) Kao, F.; Ho, H.; Chiu, P.; Hsieh, M.; Liao, J.; Lai, P. Self-Assisted Wound Healing Using Piezoelectric and Triboelectric Nanogenerators. *Sci. Technol. Adv. Mater.* **2022**, *23* (1), 1–16.

(36) Zhang, R.; Olin, H. Material Choices for Triboelectric Nanogenerators : A Critical Review. *EcoMat* **2020**, *2*(4), 1–13.

(37) Zou, Y.; Xu, J.; Chen, K.; Chen, J. Advances in Nanostructures for High-Performance Triboelectric Nanogenerators. *Adv. Mater. Technol.* **2021**, *6* (3), 1–16.

(38) Bera, B. Literature Review on Triboelectric Nanogenerator. *Imp. J. Interdiscip. Res.* **2016**, *2* (10), 1263–1271.

(39) Liu, Y.; Mo, J.; Fu, Q.; Lu, Y.; Zhang, N.; Wang, S.; Nie, S. Enhancement of Triboelectric Charge Density by Chemical Functionalization. *Adv. Funct. Mater.* **2020**, *30* (50), 1–33.

(40) Wang, N.; Liu, Y.; Ye, E.; Li, Z.; Wang, D. Control Methods and Applications of Interface Contact Electrification of Triboelectric Nanogenerators: A Review. *Mater. Res. Lett.* **2022**, *10* (3), 97–123.

(41) Seung, W.; Yoon, H.; Kim, T. Y.; Ryu, H.; Kim, J.; Lee, J.; Lee, J. H.; Kim, S.; Park, Y. K.;

Park, Y. J.; Kim, S. Boosting Power-Generating Performance of Triboelectric Nanogenerators *via* Artificial Control of Ferroelectric Polarization and Dielectric Properties. *Adv. Energy Mater.* **2017**, 7(2), 1600988.

(42) Wu, C.; Kim, T. W.; Choi, H. Y. Reduced Graphene-Oxide Acting as Electron-Trapping Sites in the Friction Layer for Giant Triboelectric Enhancement. *Nano Energy* **2017**, *32*, 542–550.

(43) Li, Z.; Zhu, M.; Qiu, Q.; Yu, J.; Ding, B. Multilayered Fi Ber-Based Triboelectric Nanogenerator with High Performance for Biomechanical Energy Harvesting. *Nano Energy* **2018**, *53*, 726–733.

(44) Wang, N.; Liu, Y.; Ye, E.; Li, Z.; Wang, D. Control Methods and Applications of Interface Contact Electrification of Triboelectric Nanogenerators : A Review. *Mater. Res. Lett.* **2022**, *10* (3), 97-123.

(45) Rathore, S.; Sharma, S.; Swain, B. P.; Ghadai, R. K. A Critical Review on Triboelectric Nanogenerator A Critical Review on Triboelectric Nanogenerator. *Mater. Sci. Eng.* **2018**, *377* (1), 012186.

(46) Lee, K. Y.; Chun, J.; Lee, J.; Kim, K. N.; Kang, N.; Kim, J.; Kim, M. H.; Shin, K.; Gupta, M. K.; Baik, J. M.; Kim, S. Hydrophobic Sponge Structure-Based Triboelectric Nanogenerator. **2014**, 5037–5042. https://doi.org/10.1002/adma.201401184.

(47) Lu, C. X.; Han, C. B.; Gu, G. Q.; Chen, J.; Yang, Z. W.; Jiang, T.; He, C.; Wang, Z. L. Temperature Effect on Performance of Triboelectric Nanogenerator. **2017**, *1700275*, 1–8. https://doi.org/10.1002/adem.201700275.

(48) Xu, C.; Zi, Y.; Wang, A. C.; Zou, H.; Dai, Y.; He, X.; Wang, P.; Wang, Y.; Feng, P.; Li, D.; Wang, Z. L. On the Electron-Transfer Mechanism in the Contact- Electrification Effect. **2018**, *1706790*, 1–9. https://doi.org/10.1002/adma.201706790.

(49) Novoselov, K. S.; Geim, A. K.; Morozov, S. V.; Jiang, D.; Zhang, Y.; Dubonos, S. V.; Grigorieva, I. V.; Firsov, A. A. Electric Field Effect in Atomically Thin Carbon Films. *Science* **2004**, *306* (5696), 666–669.

(50) Novoselov, K. S.; Jiang, D.; Schedin, F.; Booth, T. J.; Khotkevich, V. V.; Morozov, S. V.; Geim, A. K. Two-Dimensional Atomic Crystals. *Proc. Natl. Acad. Sci.* **2005**, *102* (30), 10451–10453.

(51) Bonaccorso, F.; Colombo, L.; Yu, G.; Stoller, M.; Tozzini, V.; Ferrari, A. C.; Ruoff, R. S.; Pellegrini, V. Graphene, Related Two-Dimensional Crystals, and Hybrid Systems for Energy Conversion and Storage. *Science* **2015**, *347* (6217), 1246501.

(52) Triboelectric, P.; Based, N.; Han, S. A.; Lee, J.; Lin, J.; Kim, J. H. Piezo/triboelectric nanogenerators based on 2-dimensional layered structure materials. *Nano Energy* **2019,** *57***,** 680-691

(53) Kim, S.; Gupta, M. K.; Lee, K. Y.; Sohn, A.; Kim, T. Y.; Shin, K.; Kim, D.; Kim, S. K.; Lee, K. H.; Shin, H. Transparent Flexible Graphene Triboelectric Nanogenerators. *Adv. Mater.* **2014**, *26* (23), 3918–3925.

(54) Liu, Y.; Ping, J.; Ying, Y. Recent Progress in 2D-Nanomaterial-Based Triboelectric Nanogenerators. *Adv. Funct. Mater.***2021**, *31(17), 2009994.*

(55) Seol, M.; Kim, S.; Cho, Y.; Byun, K.; Kim, H.; Kim, J.; Kim, S. K.; Kim, S.; Shin, H.; Park, S. Triboelectric Series of 2D Layered Materials. *Adv. Mater.* **2018**, *1801210*, 1–8.

(56) Zhang, P.; Wang, F.; Yu, M.; Zhuang, X.; Feng, X. Two-Dimensional Materials for Miniaturized Energy Storage Devices : From Individual Devices to Smart Integrated Systems. *Chem Soc Rev* **2018**,47 (19), 7426–7451.

(57) Kang, Z.; Beijing, T.; Zhao, X.; Beijing, T.; Zhang, Z.; Beijing, T. Development , Applications , and Future Directions of Triboelectric Nanogenerators. *Nano Research* **2018**, *11*. 2951-2969.

(58) Lee, E.; Yoo, H. Self-Powered Sensors: New Opportunities and Challenges from Two-Dimensional Nanomaterials. *Molecules* **2021**, *26* (16), 1–24.

(59) Chu, H.; Jang, H.; Lee, Y.; Chae, Y.; Ahn, J. Conformal, Graphene-Based Triboelectric Nanogenerator for Self-powered Wearable Electronics. *Nano Energy* **2016**, *27*, 298–305.

(60) Li, X.; Jiang, C.; Zhao, F.; Shao, Y.; Ying, Y.; Ping, J. A Self-Charging Device with Bionic Self-Cleaning Interface for Energy Harvesting. *Nano Energy* **2020**, *73*, 104738.

(61) Jiang, C.; Li, X.; Ying, Y.; Ping, J. A Multifunctional TENG Yarn Integrated into Agrotextile for Building Intelligent Agriculture. *Nano Energy* **2020**, *74*, 104863.

(62) Lan, L.; Yin, T.; Jiang, C.; Li, X.; Yao, Y.; Wang, Z.; Qu, S.; Ye, Z.; Ping, J.; Ying, Y. Highly Conductive 1D-2D Composite Film for Skin-Mountable Strain Sensor and Stretchable Triboelectric Nanogenerator. *Nano Energy* **2019**, *62*, 319–328.

(63) Jiang, C.; Li, X.; Yao, Y.; Lan, L.; Shao, Y.; Zhao, F.; Ying, Y. A Multifunctional and Highly Flexible Triboelectric Nanogenerator Based on MXene-Enabled Porous Film Integrated with Laser-Induced Graphene Electrode. *Nano Energy* **2019**, *66*, 104121.

(64) Karmakar, S.; Kumbhakar, P.; Maity, K.; Mandal, D. Development of Flexible Self-Charging Triboelectric Power Cell on Paper for Temperature and Weight Sensing. *Nano Energy* **2019**, *63*, 103831.

(65) Zhou, Y.; Zhang, J.; Li, S.; Qiu, H.; Shi, Y.; Pan, L. Triboelectric Nanogenerators Based on 2D Materials : From Materials and Devices to Applications. *Micromachines*, **2023**, 14 (5),1043.

(66) Zhang, K.; Feng, Y.; Wang, F.; Yang, Z.; Wang, J. Two Dimensional Hexagonal Boron Nitride (2D-HBN): Synthesis, Properties and Applications. *J. Mater. Chem. C* **2017**, *5* (46), 11992–12022.

(67) Lin, Yi.; Tiffany, V.; Williams, and J. W. C. Soluble, Exfoliated Hexagonal Boron Nitride Nanosheets. *J. Phys. Chem. Lett.* **2010**, *2*, 277–283.

(68) Cao, Li,; Emami, S.; and Lafdi, K.; Large-Scale Exfoliation of Hexagonal Boron Nitride Nanosheets in Liquid Phase. *Mater. Express* **2014**, *4*, 165–171.

(69) Ismach, A.; Chou, H.; Ferrer, D. A.; Wu, Y.; McDonnell, S.; Floresca, H. C.; Covacevich, A.; Pope, C.; Piner, R.; Kim, M. J.; Wallace, R. M.; Colombo, L.; Ruoff, R. S. Toward the Controlled Synthesis of Hexagonal Boron Nitride Films. *ACS Nano* **2012**, *6* (7), 6378–6385.

(70) Suslick, K. S.; Eddingsaas, N. C.; Flannigan, D. J.; Hopkins, S. D.; Xu, H. Extreme Conditions during Multibubble Cavitation: Sonoluminescence as a Spectroscopic Probe. *Ultrason. Sonochem.* **2011**, *18* (4), 842–846.

(71) Coleman, J. N. Liquid-Phase Exfoliation of Nanotubes and Graphene. *Adv. Funct. Mater.* **2009**, *19* (23), 3680–3695.

(72) Pullanchiyodan, A.; Nair, K. S.; Surendran, K. P. Silver-Decorated Boron Nitride Nanosheets as an Effective Hybrid Filler in PMMA for High-Thermal-Conductivity Electronic Substrates. *ACS omega* **2017**, 2 (12), 8825-8835.

(73) Chen, X.; Boulos, R. A.; Dobson, J. F.; Raston, C. L. Shear Induced Formation of Carbon and Boron Nitride Nano-Scrolls. *Nanoscale* **2013,** *5* (2), 498-502.

(74) Wang, H.; Su, X.; Song, T.; Li, Z.; Zhao, Y.; Lou, H.; Wang, J. Applied Surface Science Scalable Exfoliation and Dispersion of Few-Layer Hexagonal Boron Nitride Nanosheets in NMP-Salt Solutions. *Appl. Surf. Sci.* **2019**, *488*, 656–661.

(75) Zhou, K. G.; Mao, N. N.; Wang, H. X.; Peng, Y.; Zhang, H. L. A Mixed-Solvent Strategy for Efficient Exfoliation of Inorganic Graphene Analogues. *Angew. Chemie - Int. Ed.* **2011**, *50* (46), 10839–10842.

(76) Wang, Y.; Shi, Z.; Yin, J. Boron Nitride Nanosheets: Large-Scale Exfoliation in Methanesulfonic Acid and Their Composites with Polybenzimidazole. *J. Mater. Chem.* **2011**, *21* (30), 11371–11377.

(77) Mittal, N.; Kedawat, G.; Kanika; Gupta, S.; Gupta, B. K. An Innovative Method for Large-

Scale Synthesis of Hexagonal Boron Nitride Nanosheets by Liquid Phase Exfoliation. *ChemistrySelect* **2020**, *5* (40), 12564–12569.

(78) Birnie, D. P.; Spin Coating Technique. *Sol-gel technologies for glass producers and users* **2004**.49-55.

(79) Emslie, A. G.; Bonner, F. T.; Peck, L. G. Flow of a Viscous Liquid on a Rotating Disk. *J. Appl. Phys.* **1958**, *29, 858*.

(80) Meyerhofer, D. Characteristics of Resist Films Produced by Spinning Characteristics of Resist Films Produced by Spinning. *J. Appl. Phys.* **1978**, *49*, *3993*.

(81) Parija, B.; Panigrahi, S. Fundamental Understanding and Modeling of Spin Coating Process : A Review. **2009**, *83*, 493–502.

(82) Pillai, A. S.; Chandran, A.; Peethambharan, S. K. MWCNT Ink with PEDOT: PSS as a Multifunctional Additive for Energy Efficient Flexible Heating Applications. *Appl. Mater. Today* **2021**, *23*, 100987.

(83) Sauer, M.; Kalleder, A.; Mennig, M.; Schmidt, H. Screen Printing. *Springer US.* **2004**, 117-122

(84) Kurecic, M.; Smole M. S.; Electrospinning : Nanofibre Production Method Electrospinning : *Tekstilec* **2016**, 56 (1), 3–12.

(85) Xue, J.; Wu, T.; Dai, Y.; Xia, Y. Electrospinning and Electrospun Nano Fibers : Methods ,Materials , and Applications. *Chem. Rev.* **2018**, 119 (8), 5298-5415.

(86) Zhang, W.; Gu, G.; Qin, H.; Li, S.; Shang, W.; Wang, T.; Zhang, B.; Cui, P.; Guo, J.; Yang, F.; Cheng, G.; Du, Z. Measuring the Actual Voltage of a Triboelectric Nanogenerator Using the Non-Grounded Method. *Nano Energy* **2020**, *77*, 105108.

(87) Sunil, S.; Mallineni, K.; Behlow, H.; Podila, R.; Rao, A. M. A Low-Cost Approach for Measuring Electrical Load Currents in Triboelectric Nanogenerators. *Nanotechnology Reviews* **2018**, *7* (2), 149–156.

Chapter 2

Design and fabrication of glass supported rigid TENG, employing exfoliated BNNSs

In the current world of IoT technology and sensor networks, there is an enormous demand for sustainable energy harvesting methods. In this chapter, we have demonstrated a CS mode TENG using liquid-phase exfoliated 2D-BNNSs, coated on the surface of BoPET as one of the triboelectric material and paper as counter one. The new device system is capable for powering handheld electronic devices also showed an impressive power output, 70 times higher than simple BoPET-paper TENG assembly

2.1 Introduction

Smart cities of future demand power generation from multiple sustainable sources which can efficiently power up various energy-autonomous Internet of Things (IoT) based sensors. Within the past decade, intense research has been done in this domain to develop sustainable techniques that can harness mechanical motion into useful electrical energy.[1] TENG is suggested as the most promising among green energy harvesters, since it can immediately transform mechanical form of energy into power, without leaving any carbon footprint. Physical movements[2], mechanical vibrations[3], water waves[4], and wind power are the various forms of mechanical energy sources.[5] TENGs can harvest electrical energy from these abundant mechanical energy sources where the energy generation relies on the coupling effect of two phenomena; triboelectric effect and electrostatic induction.[6] In a CS mode TENG operation, the simultaneous contact and subsequent separation of two different material surfaces initiates the continuous flow of electrons. To improve the TENGs working efficiency, numerous strategies have been used such as the ideal selection of triboelectric materials and their suitable combinations.[7] Alteration of the materials surface by nanoparticles doping or chemical treatments,[8] developing novel configuration devices,[9] and also polarization method or corona charging which can inject charge into the triboelectric materials.[10] Small-scale electronic equipment's such as sensors, wireless transmitters and actuators need micro-to milli-watts range of power for their operation.[11] Making use of batteries for this purpose has to address challenges such as limited life span, recycling, and other environmental-related issues.[12]

2D layered materials, due to their rich spectrum of properties and atomic level thickness, offer an ocean of properties like transparency, flexibility, and together with bandgap engineering, it opens up new horizons of applications in wearable electronics, photonics, and healthcare sector.[13,14,15] Such materials are attractive candidates for TENGs, since they have a high transverse area with the maximum amount of surface atoms, which qualify them suitable for applications in the fields of wearable and body insertable electronic devices.[16] However, the triboelectrification mechanism of 2D materials is not profoundly understood. In 2014, Kim *et al*. reported the first graphene-based transparent, flexible TENG in which large-scale graphene was grown through CVD layer-by-layer transfer technique on copper and nickel foils.[17] Recently, Seol *et al*.

revealed the triboelectric charging behaviour of a series of 2D materials, including TMDs. They exfoliated 2D materials chemically from bulk in the liquid medium which was subsequently used for the fabrication of various materials combinations in TENGs. Finally, a modified triboelectric series was developed after including these 2D materials, by systematically analysing the output signals from various TENGs combinations. Later, Dong *et al.* reported MXene based high-performance TENG capable of generating power from simple muscle movements.[18]

Hexagonal boron nitride (h-BN), a popular 2D material isostructural to graphene, has individual layers made up of covalently bonded boron and nitrogen atoms held together by weak van der Waals force of attraction.[19] For applications in the field of microelectronics, it is possible to integrate 2D h-BN effectively with other materials, such as graphene, TMDs, and various polymers. Its exotic optoelectrical properties qualify them as suitable materials for future electronic device applications.[20,21] In short, the research on single-layered materials for TENG energy harvesting is still in its rudimentary stage, with the need for improved fabrication techniques and a better understanding of electrostatic phenomenon happening in 2D materials during triboelectrification.

Against this background, we developed a BNNS based TENG in which the mechanically exfoliated BNNSs in a liquid medium of comparable surface energy, which was spin-coated onto BoPET substrate, after adding polyvinyl butyral (butvar) as a binder. This BNNSs/BoPET assembly was used as negative triboelectric material paired with counter positive paper material for the fabricated TENG. In this device combination, the copper foil was used as electrodes, which are supported on the glass substrate. The fabricated BNNSs/BoPET-paper TENG device showed impressive electrical output performance with an open circuit voltage of ~200 V, a current density of ~0.48 mA/m^2, and a peak power of 0.14 W/m^2, which is ~70 times higher than simple BoPET-paper TENG.

Improving the working ability and output enhancement of the energy harvesting TENG is desirable for its real-world applications. Suitable material combinations and optimized conditions are the vital elements for improved performance and mechanical stability of the device. Here, we obtained a tremendous power enhancement in the BoPET-paper TENG by adding 2D BNNSs into the negative frictional contact layer. Our research

revealed that the introduction of 2D BNNSs not only enhanced the output of the triboelectric device massively but also supplemented the flexibility, lightweightness, and superior mechanical strength, which qualifies this material as a suitable candidate in wearable, flexible energy harvesting and storage devices.

2.2 Experimental

2.2.1 Materials

BN powder, 98% purity (Sigma Aldrich, USA). Dimethylformamide (DMF) was used as the solvent for exfoliation while polyvinyl butyral (Butvar-B-98) was used as binder for spin coating (Sigma Aldrich, USA). The substrate used here is the commercially available biaxially oriented polyethylene terephthalate (BoPET, Mylar®) and a copper tape with double side conduction as electrodes (3M Co.) was used. Glass slides of proper dimension act as mechanical support for the device.

2.2.2 Exfoliation of bulk h-BN

For the sonication assisted liquid phase exfoliation process, bulk h-BN powder of about 1g was added to 100 ml of DMF solvent contained in a 250 mL beaker, and the resulting solution was subjected to a temperature-controlled ultrasonication process for 48 hours at a controlled temperature of 50℃, with the aid of low power bath sonicator. The unexfoliated layers were allowed to settle, by keeping the solution undisturbed overnight. The supernatant solution containing the exfoliated nanosheets was separated by using a centrifugation process operating at higher rpm (10,000) rotation speed for 10 min and the top 20 mL solution of the exfoliated nanosheets was collected. The exfoliation process is pictorially represented in Figure 2.1 (a). The exfoliated BNNSs solution in DMF was mixed with 0.1g of polyvinyl butyral (PVB) as a binder for making good dispersion. Then the mixture was again sonicated for 3 hours using an ultrasonic bath for making a well-dispersed solution of BNNSs. The resultant milky white-colored dispersion of exfoliated nanosheets was used for thin-film fabrication.

2.2.3 Preparation of thin-film BNNSs

A well-dispersed solution of exfoliated BNNSs in DMF was then cast as thin films using the spin coating technique. The spin coating (using SpinNXG-P1, Apex Instruments,

India) was done on BoPET substrate in tailor-made dimensions of area (2.5 cm x 2.5 cm). The rotation speed was set at 100 rpm, which was optimized to have a thickness < 25 μm, where better adhesion to the substrate was provided by the binder. The spin coating process continued for 10 minutes at 100 rpm speed, forming a uniform film of BNNSs dispersion on the BoPET substrate. Finally, the films were dried at a previously set temperature of 80 °C for 12 hours for complete solvent evaporation. The thin-film formulation process is pictorially represented as step 4 in figure 2.1(b).
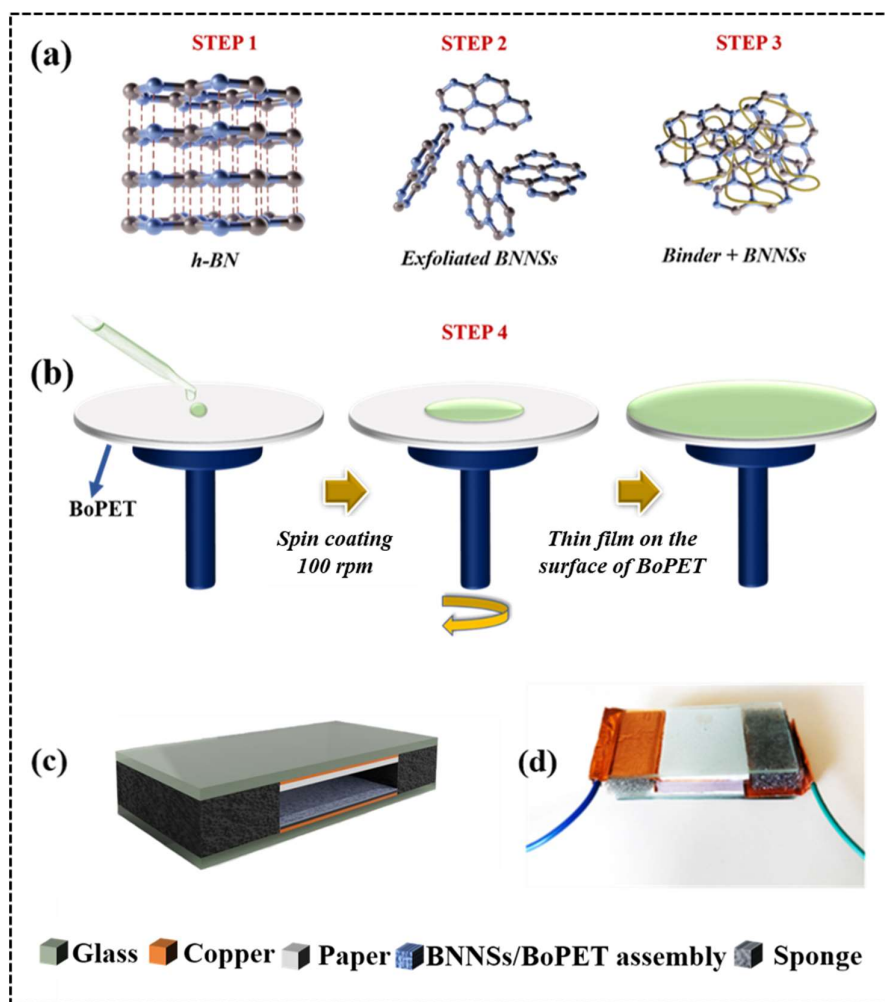
Figure 2.1: (a) and (b) Schematic illustration of the liquid-phase exfoliation process and thin-film formation of BNNSs dispersion on BoPET substrate through various process steps. (c) 3D model of the BNNSs/BoPET-paper TENG rendered using blender software. (d) Photographic image of an actual device

2.2.4 Fabrication of TENG device

The BNNSs based TENG fabrication process is in the following manner. Initially, two glass slides of 5 cm x 2.5 cm dimension, as supporting substrates, were chosen. A rigid support such as glass which allows the force to be evenly distributed throughout the material surface. In all devices, double side conductive copper foils (3M) were pasted over glass support as electrodes, using adhesive tapes. The active area of the copper electrode was set to be 6.25 cm^2 (2.5 cm × 2.5 cm). On top of the adhesive side of the first copper electrode, BoPET which is having the BNNSs thin films was placed. Thereafter, for the second glass slide with copper, a piece of paper with proper dimension (2.5 cm × 2.5 cm) was pasted as the counter triboelectric material. Subsequently, two sponges were docked between the substrates in the vacant spaces to enable a separation gap of .3 cm between the tribo-layers and to provide the recoiling force. The overall device structure is schematically represented in the Figure 2.1(c). Finally, two conductive leads of copper were connected to the back electrodes of the device for connecting them to the measuring instruments. The photograph of the final BNNSs/BoPET-paper TENG is also depicted in Figure 2.1(d).

2.2.5 Characterization methods

AFM in tapping mode (Bruker, Germany) was used to investigate the morphology and related information regarding the layered structure of the exfoliated BNNSs sample. The sample preparation was done by drop-casting the diluted sample solution of BNNSs on a thin mica sheet. In addition, the surface roughness of the thin coating over the BoPET was also analyzed by this technique. The translucent, but layered structure of the nanosheets was further confirmed using HRTEM technique (FEI Tecnai G2 30S-TWIN, FEI Co., USA), by drop-casting the diluted BNNSs sample solution sonicated in a suitable solvent onto a copper carbon-coated grid. The phase purity of the BNNSs was analysed by XRD (Cu-Kα radiation, PANalytical X'Pert PRO diffractometer, the Netherlands). Raman spectra of the exfoliated nanosheets and the material without exfoliation were examined using Raman Spectrometer equipped with 532 nm DPSS laser (Horiba Scientific Lab, Tokyo, Japan). The surface morphological analysis and thickness of the prepared BNNSs thin film were carried out using SEM analysis (Zeiss EVO 50, Oberkochen, Germany). The

optical micrographic images of the sample were analysed using a polarizing optical microscope (Leica DM2700P, Germany) fitted with a charge-coupled device (CCD) camera. To study the characteristic bonds in BNNSs and to compare the chemical structure with and without the incorporation of 2D materials onto the substrate, the FTIR analysis of the samples was carried out, using Nicolet Magna 560 FTIR (Thermo Scientific, Massachusetts, USA). The dielectric spectroscopic studies of the thin film structure BNNSs were performed using the impedance analyser (Solartron Impedance/Gain-Phase Analyser 1260A, USA). The electrical output characteristics of TENG devices were recorded using a source measuring unit (Keithley 2450) and a current preamplifier (SR570, Stanford Research) integrated with a digital phosphor oscilloscope (Tektronix DPO2004B, USA). By moderate finger tapping, a periodic mechanical impulse of ($\sim$3 N) was applied to the TENG device systematically and the generated output of the device was recorded. The load-dependent power density and capacitor charging profiles of the TENG were obtained with the help of different values of resistors and capacitors. To assess the versatility, the variation of the TENG results was tested at various biomechanical forces like single finger tapping, simultaneous multiple finger tapping, and palm tapping, which all differ in the magnitude of force exertion. Further, the same TENG was tested under various frequencies of the applied load and also up to 10000 continuous operation cycles, to assess its durability.

2.3 Results and discussions

2.3.1. Structural and morphological characteristics of exfoliated BNNSs

Ultrasonication-assisted solvent exfoliation is one of the simplest and efficient ways for the exfoliation of layered materials, wherein the solvent should possess surface energy compared to the layered materials energy per unit area. Here, DMF was proved to be ideal to exfoliate the bulk material effectively, which was confirmed with the help of the following techniques.[12]

Atomic force microscopy (AFM) is traditionally used for collecting surface information of the layered materials along with their lateral (edge-to-edge) analysis and thickness also. The AFM images in the tapping mode (see Figures (2.2 (a) and (b)) confirm the exfoliation of h-BN which were recorded after drop-casting them onto a clean mica

sheet. The height profile as an inset of Figure 2.2(b) clearly shows that the typical lateral size of the nanosheet is around 130 nm which indicates the reduction of the lateral dimension of the exfoliated material compared to its bulk counterpart of 1 μm size common in the liquid phase exfoliation process.[22] The height from the same holder substrate (mica) to the exfoliated layer provides the sheet thickness value, which is of the order of 1.05 nm. This recorded value is in close agreement with the reported values of 0.85 nm for one or two layers. These results indicate that effective delamination of the bulk material down to one or two layers, which is an indirect testimony to the efficiency of the exfoliation method used.[23,24]
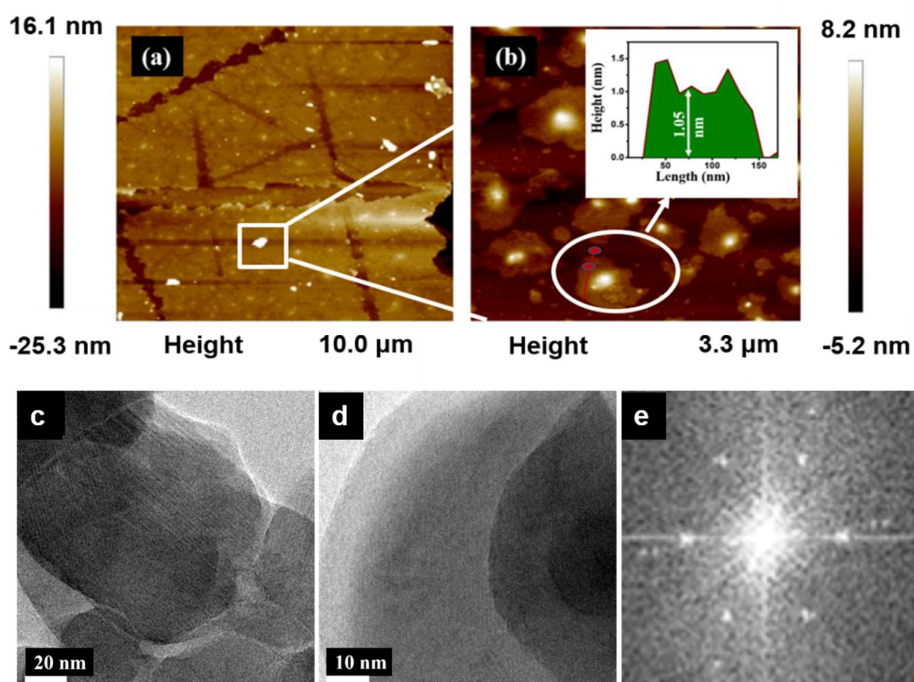
Figure 2.2: *(a) & (b) 2D AFM images in the tapping mode of the exfoliated BNNSs. Inset to (b) height profile of the exfoliated nanosheets. (c) and (d) TEM images of exfoliated BNNSs with a well-separated layered structure. (e) FFT pattern provides the typical six-fold symmetry and hexagonal view of the BNNSs*

Figures 2.2(c) & (d) represents the TEM images of the exfoliated BNNSs. The continuous solvent-assisted ultrasonication gives rise to continuous dense and sparse waves, forming an enormous number of microbubbles that implode violently, thereby creating high-speed liquid jets with high pressure and temperature.[25] These instantaneous high-pressure fronts of cavitation render constant but high pressure on

bulk h-BN, forcing them to slide apart, after releasing an enormous amount of energy to break the interlayer vdW force.[26,27] The ideal choice of solvent supplements this process by providing the necessary shear force to delaminate the individual h-BN layers. The so derived exfoliated sheets have lateral dimensions in the nanometer range, compared to the bulk material (~1 μm), indicating a reduction in size.[28] The seemingly translucent nature of the sheets in the present research indicates that the exfoliated sheets are thin and well-separated. The typical six-fold symmetry or honeycomb-like hexagonal planar structure is revealed from the fast fourier transformation (FFT) pattern, which is included as Figure 2.2(e). Further, the TEM micrographs indicate that there is no damage to the sheets during the synthesis and the formed thin sheets are well crystallized in nature without any defects or dislocations.[29]

The crystal phase structure of the as-prepared BNNSs sample and its delamination from h-BN can be identified by analyzing the powder XRD patterns. From Figure 2.3(a), it is evident that BNNSs are completely phase-pure which is indexed based on JCPDS file card no (00-034-0421), belonging to $P6_3/mmc$ space group. The observed diffraction peaks correspond to (002), (100), (101), (102), (004), (110), and (112) are the crystallographic planes of the hexagonal phase of BN. The efficient separation of pristine h-BN is confirmed from the increased intensity of the XRD peak for the crystal plane (002) in BNNSs. The increased intensity value suggests that the more exposed nature of the (002) crystal planes of BNNSs and the exfoliation takes place along this plane without any crystalline structure destruction.[30]
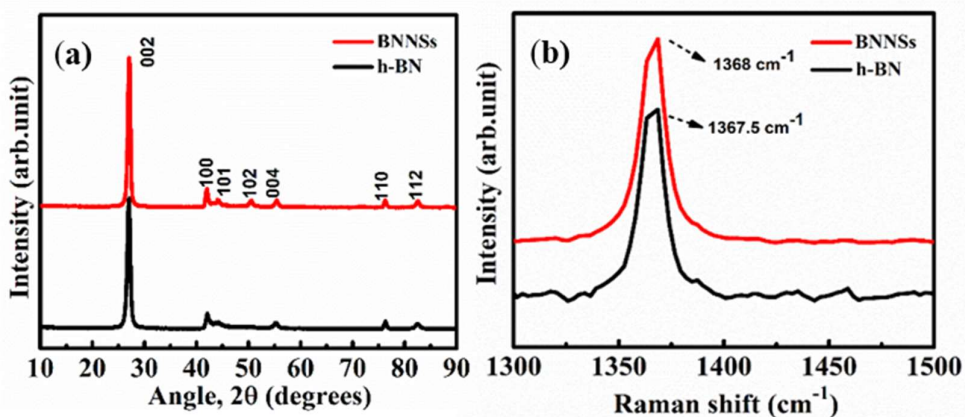
Figure 2.3: *(a) XRD pattern of h-BN & BNNSs. (b) Raman analysis of h-BN & BNNSs*

Figure 2.3(b) illustrates Raman spectra of the BNNSs along with their bulk counterpart. The observed Raman peak of BNNSs occurs at 1368 cm^{-1}, which arises as a result of E$_{2g}$ phonon vibration mode. After exfoliation, the E$_{2g}$ phonon mode is slightly blue-shifted compared to the bulk h-BN, even though this shift is within the experimental error limit. The blue-shift can be explained by phonons softening phenomena by the interlayer interactions. This interaction between layers causes the elongation of B–N bonds in bulk h-BN.[31,32]

2.3.2. Properties of thin film BNNSs on BoPET substrate

The presence of BNNSs in the thin film structure of BNNSs/BoPET was examined by FTIR spectra (see Figure 2.4(a)). Two core peaks of the material h-BN were identified at 786 cm^{-1} and 1342 cm^{-1}, which are the broad B–N–B out-of-plane vibrations as well as in-plane B–N stretching vibrations respectively.[33,34] The observed peak at 1730 cm^{-1} is due to the presence of C=O stretching of the ester groups present in the polymer BoPET. The peak centered at 1409 cm^{-1} is attributed to the presence of an aromatic ring in the polymeric structure. Characteristic peak around 1235.6 cm^{-1} due to the aliphatic C-H bending vibrations. The band observed at 1143 cm^{-1} attributed to the stretching vibrations of C-O and C-H skeletons. The peak at 730 cm^{-1} can be assigned to the out-of-plane C-H bending vibration of the polymer BoPET. Some of these characteristic peaks of the polymer BoPET are also observable in the BNNSs incorporated polymer film with the characteristic peaks of h-BN.[35,36] A typical AFM micrograph of the thin film, after spin coating on the surface of BoPET, is depicted in Figure 2.4(b). A more apparent microstructure of the developed thin film on the substrate surface is clear from the three-dimensional AFM images. The average surface roughness (Ra) of the spin-coated BNNSs layer is about 7.9 nm and the root mean square roughness (Rq) value is nearly 10.2 nm which represents the standard deviation in surface heights. The extent of surface height variations can be available from these parameter values. Skewness indicates the measure of surface asymmetry or variation of the sample surface. For ideal planar surfaces, the skewness value should be zero. The lower positive value for skewness (0.55) indicates the smoothness of the thin film on the substrate. The kurtosis of the topography height distribution is the distribution of spikes from the mean position, where a normal distribution planar surface is having a kurtosis value of 3 nm. The spin-coated thin film

on the BoPET substrate has a kurtosis value of 3.88 nm hence its surface is leptokurtoic.[37,38]

From profilometric technique, the coating thickness was further measured (included in Figure 2.4(c)). The approximate thickness of BoPET is 106 μm and 125 μm for BNNSs spin-coated on the surface of BoPET. This difference in thickness value is nearly identical to the thickness obtained from cross-sectional SEM micrographs. The frequency-dependent dielectric variation of the thin film triboelectric friction material BNNSs/BoPET and BoPET only in the range of frequency 10^2–10^6 Hz is shown in Figure 2.4(d).
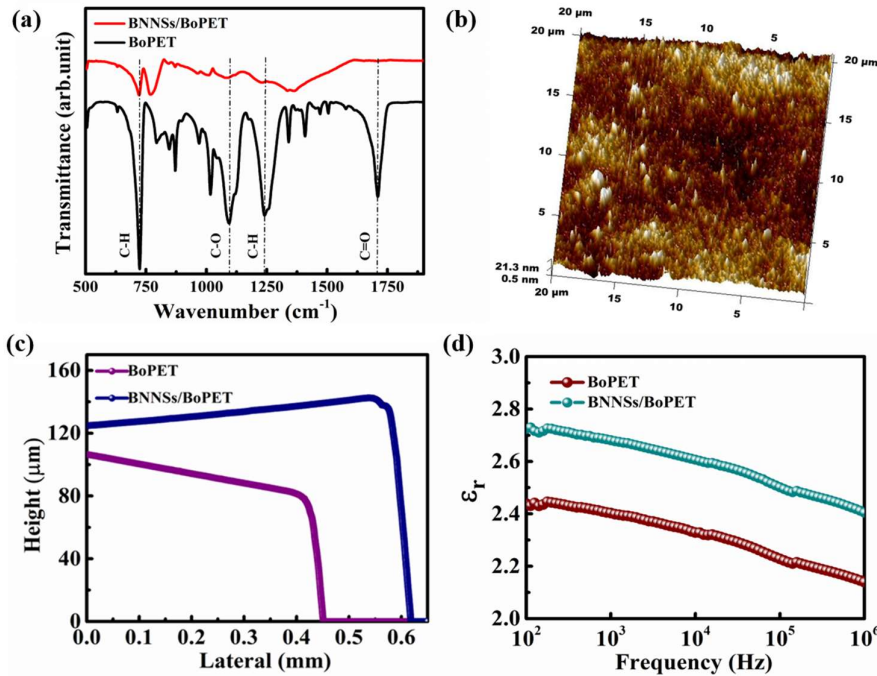
Figure 2.4: *(a) FTIR analysis of uncoated BoPET film and BoPET film with BNNSs. (b) Atomic force micrographic 3D image of BNNSs/BoPET thin-film structure. (c) The profilometric thickness of BoPET and BNNSs/BoPET films. (d) Dielectric dispersion spectrum of BoPET and BNNSs/BoPET*

The incorporation of BNNSs results in a distinct dielectric permittivity increase of the normal BoPET substrate. The dielectric permittivity reaches 2.7 at 10^3 Hz for BNNSs/BoPET, whereas this parameter is nearly 2.4 only for the pure BoPET film. The dielectric properties of the triboelectric friction materials are closely related to the electric output performance of a TENG. The enhancement in the value of dielectric

permittivity can also improve the charge trapping capability of the system[39], which further decreases the surface charge dissipation rate and also creates a visible enhancement in the surface charge density of the BNNSs/BoPET. The cumulative effect of these phenomena is expected to result in a better performance of the TENG.[40]

The representative photographic images and magnified surface and cross-sectional SEM images of the BNNSs thin-film on BoPET are given in Figure 2.5. Characteristics like morphology, thickness, film packing, etc. of the thin-film structure viewed in the sectional image (Figure 2.5(a)), reveal the quality of films. The flexibility of the spin-coated film could be seen in Figure 2.5(b). Further, the SEM surface morphology in Figure 2.5(c) confirms the homogeneous distribution of polymer blends
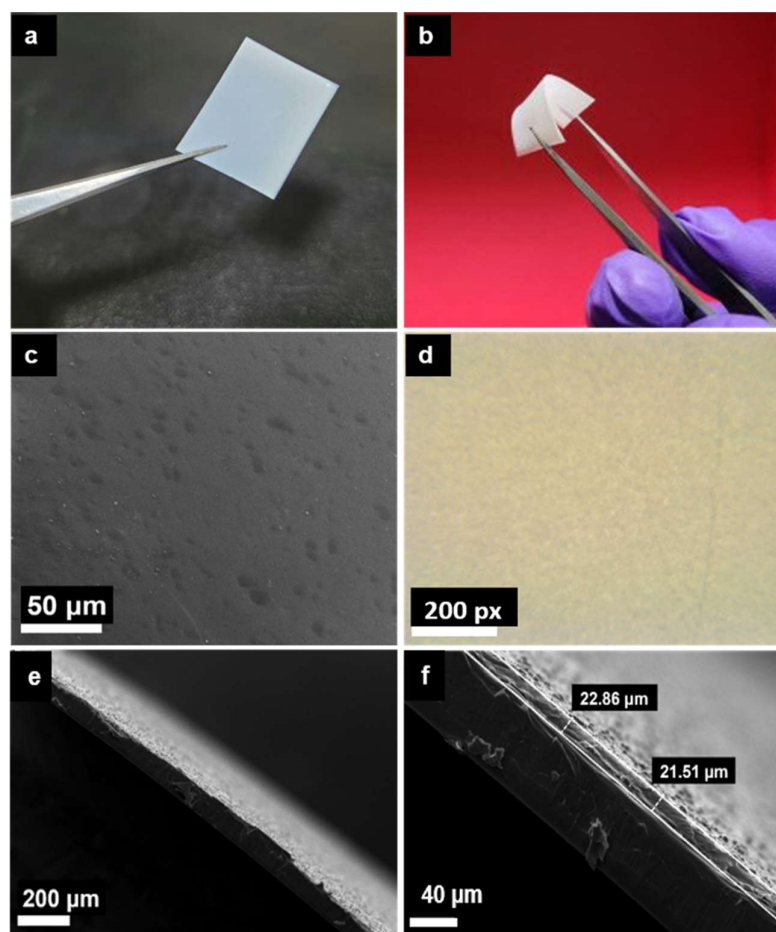
Figure 2.5: *(a) Photographic image of exfoliated BNNSs spin-coated on the surface of BoPET substrate and (b) the film in flexed form. (c) & (d) Optical images of BNNSs/ BoPET film surface. (e) & (f) Magnified cross-sectional SEM micrographs showing the thickness of the BNNSs thin film on BoPET*

The thin-film structure of BNNSs spin-coated on the surface of BoPET supports the claim that the thin-film surface is uniform, and the presence of macropores is not visibly observed. But on a closer look, some minor pores are visible, which is expected in the first place as a consequence of the solvent evaporation, and secondly, no post-printing sintering procedures were employed in the present protocol. From this observation, we can conclude that the presently adopted strategy is adequate to develop films with minimal aggregation of particles, discontinuity, and cracks when coated on BoPET substrate.[41] Normally, h-BN needs functionalization to improve its interfacial adhesion. However, we used a simple sonication-assisted mixing of BNNSs directly, which provides better blending with polymer.[42] Moreover, the optical micrographs of the BNNSs film (Figure 2.5 (d)) represent a uniform distribution over the substrate. From the cross-sectional SEM images, shown in Figure 2.5 (e) & (f) the coated film's thickness is estimated to be approximately 20 μm.

2.3.3. Properties of BNNSs/BoPET triboelectric nanogenerator

A vertical CS mode TENG (CS-TENG)[43] arrangement with BNNSs/BoPET assembly with paper as counter contact electrification material, is shown in Figure 2.6(a). The popularity of CS-TENG is due to its simple structural design, high instantaneous power density, and great device robustness compared with the other three fundamental working modes of the TENG.[44] This configuration is widely used to convert mechanical energy from finger typing[45], human walking[46], engine vibration[47], and also in biomedical systems.[48] As hinted before, spin-coating and subsequent heat treatment were employed for the BNNSs film development, which yielded thin and uniform BNNSs layers on the surface of BoPET, suitable for the fabrication of the TENG device. To assess the role of BNNSs on the output performance of the nanogenerator, a TENG device with bare BoPET was also fabricated with paper as the counter material. Both the devices bear the same positive contact layer (paper). The bottom stacked layer of BNNSs/BoPET in the friction layer acts as the negative friction material that can capture electrons from the top friction layer during the process of triboelectrification.[7,49]

In CS mode, the fundamental mechanism of electricity generation depends on the contact electrification and electrostatic induction process occurring in the triboelectric materials, which should ideally lie far apart in the triboelectric series.[50] Under an external

force, physical contact is initiated between the two materials, having different electron affinity values, thereby generating opposite charges on surfaces, as schematically represented in Figure 2.6 (b).
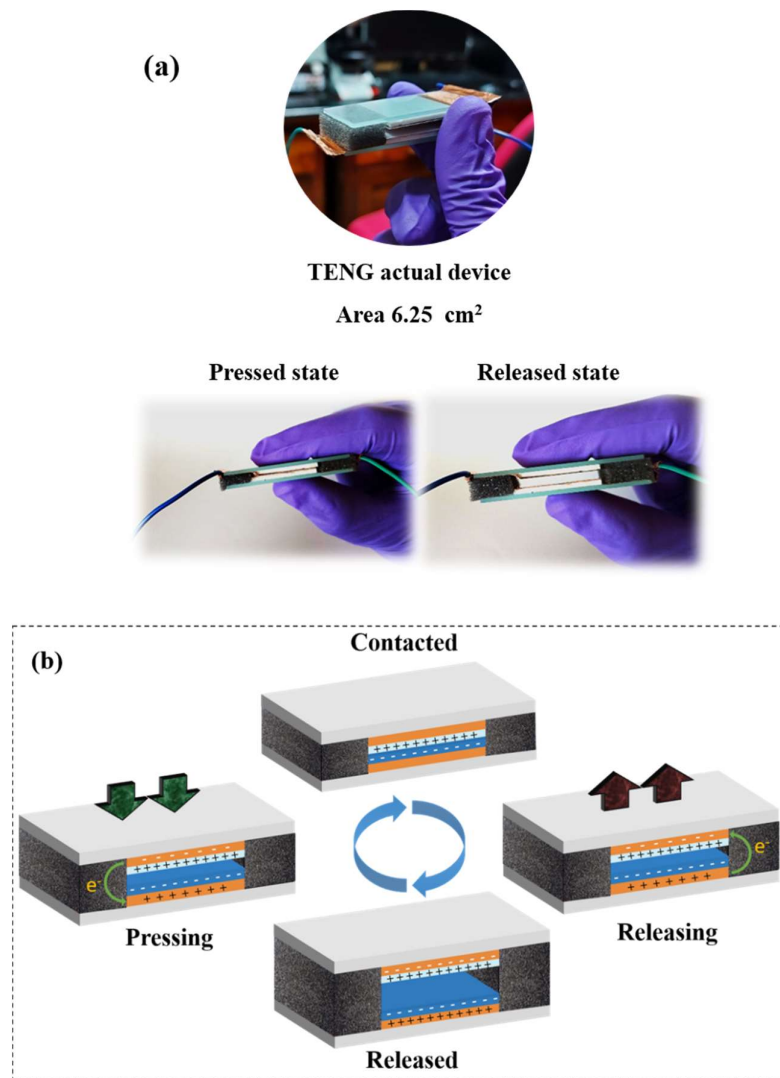
Figure 2.6: (a) Image of actual device pressed and released state also included. (b) Working mechanism of BNNSs/BoPET-paper TENG

Once the contact is lost by releasing the external force, the generated triboelectric charges are separated, which induces charges on the electrodes. These free electrons will flow from one electrode to the other to maintain the electrostatic charge balance. As a result, an electrical potential difference is created between the two planar electrodes placed on the top and bottom sides. On subsequent contact pressing, the electrostatic potential difference generated by the triboelectric charges diminishes, and the induced

electrons will pump back.[43,51] The entire working mechanism is schematically represented in Figure 2.6(b). Therefore, continuous pressing and releasing of the triboelectrically active structures drive the electrons to flow through the external circuit periodically.[40] In the present BNNSs incorporated TENG, the external force was provided by a moderate finger tapping (~3N). The BNNSs/BoPET layer acts as an electron acceptor because the embedded BNNSs having the ability to trap electrons and behave as more triboelectrically negative similar to other 2D materials.[7]

The observed voltage and current density of the fabricated TENG device with and without BNNSs are shown in Figures 2.7(a) and 2.7(b) respectively. The open-circuit voltage (V_{oc}) of the BoPET against paper TENG (without BNNSs film) is about 36 V whereas the V_{oc} value of the TENG with BNNSs film is as high as 200 V. Furthermore, it is seen from Figure 2.7(b) that, the short-circuit current density (J_{sc}) of the TENG with BNNSs (~0.48 mA/m^2) is comparably higher than that of the TENG without BNNSs (~0.016 mA/m^2). The output of the TENG devices was analysed under resistive loads ranging from 1 Ω to 1 GΩ. These experiments were carried out under ambient environmental conditions of relative humidity ~50 %, and temperature ~ 27 °C.

As depicted in Figures 2.7(c) and 2.7(d), the value of output voltage increases to 200 V with loading for BNNSs incorporated TENG as compared to the 36 V increment in TENG without BNNSs with the increase in load resistance. In addition, the electric power density (P_d) generated by the TENG can be calculated using the equation,

$$P_d = V^2/_{R.\,A} \qquad\qquad (2.1)$$

where V is the voltage and R is the load resistance and A is the area of contact. From Figures 2.7(c) and (d), it can be seen that the observed output power density initially increases to a sufficiently high value as resistance increases, and then it decreases as the resistance become too high. As per equation (2.1), the specific resistance at which maximum output power is delivered to the load is governed by the 'matching resistance' or 'impedance matching' phenomenon.[52] Here both the fabricated devices show impedance matching around a resistance value of ~200 MΩ. BoPET-paper TENG and BNNSs/BoPET-paper TENG devices exhibit a peak power density of 0.002 and 0.14 W/m^2 respectively, which shows a whopping 70 times power enhancement for the TENG, after the incorporation of an exfoliated BNNSs material.
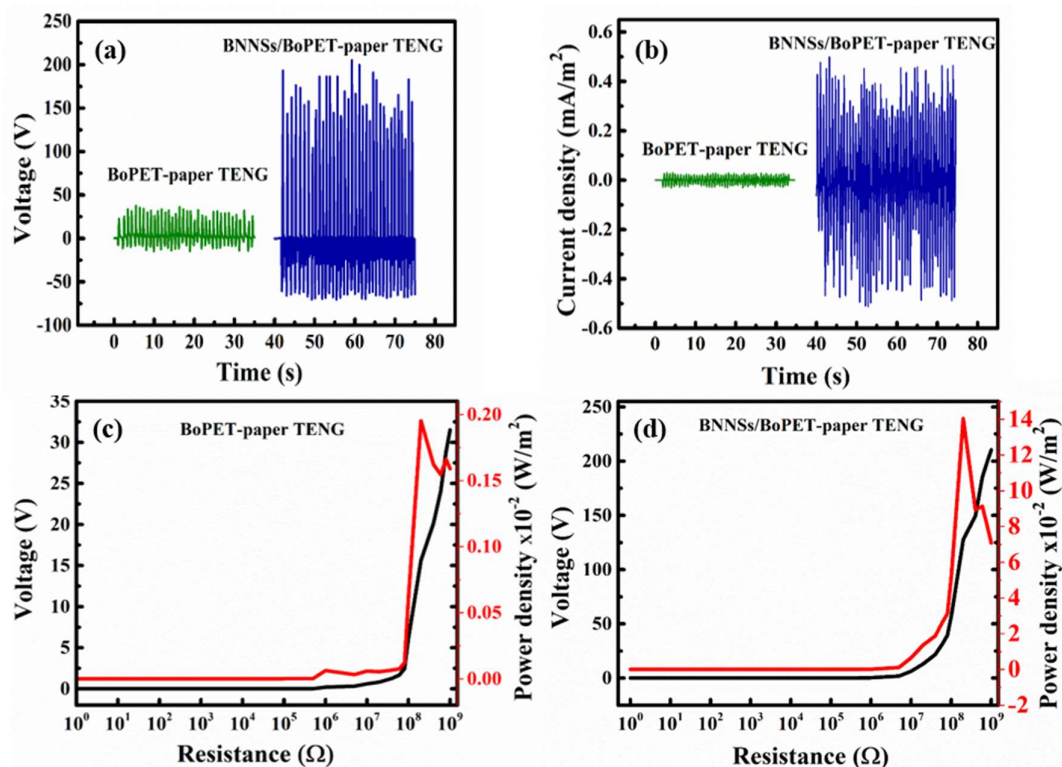
Figure 2.7: *(a) V_{oc} & (b) J_{sc} generated from the BoPET-paper & BNNSs/BoPET-paper TENG respectively under single finger tapping force of ~3 N. (c) & (d) Output power density of the BoPET-paper TENG & BNNSs/BoPET-paper TENG respectively under resistive load testing*

To analyze the force-dependent performance of the fabricated CS-TENG, different kinds of biomechanical forces such as single finger tapping (1.5-2 N), simultaneous tapping with multiple fingers (four, usually) (7-9 N), and tapping using palm (18-20 N), were carried out on the device and the corresponding current density and voltage generated were systematically analyzed, as shown in Figures 2.8(a) and (b). It should be noted that the average force exerted during single finger tapping is slightly inferior to moderate finger tapping (~3N). The current density and voltage generated by the BNNSs /BoPET-paper TENG under various biomechanical forces mentioned above show that the palm tapping can generate an appreciable current density of ~1.0 mA/m^2 which is much higher than the other motions like single finger tapping (~0.25 mA/m^2) and simultaneous multiple finger tapping (~0.7 mA/m^2). The voltage curves under various forces (measured using a voltage divider) follow the same trend as the current density curve, with a maximum value of voltage for palm tapping, which proportionately decreases with

decreasing biomechanical force. Frequency-dependent current density is also depicted in Figure 2.8(c), wherein the device was tested at 1.5 Hz, 2.0 Hz, 2.5 Hz, and 3.5 Hz. The BNNSs/BoPET-paper TENG shows almost the same output in the lower frequency ranges and as the frequency increases the output starts to decrease. The frequency dependency analysis showed that the BNNSs/BoPET-paper TENG is highly suitable for scavenging low-frequency biomechanical motions. Similarly, the apparent degradation of output power for long-term practical application was carried out with the help of an in-house developed force impactor that can deliver a constant force of 3N per impact. Here, BNNSs/BoPET-paper TENG was evaluated up to 10000 cycles. This investigation showed that the J_{sc} of (~0.5 mA/m^2) has no considerable fluctuations even after the 10000 press-release cycles, indirectly certifies the practical stability of the present design of BNNSs/BoPET-paper TENG.[53]
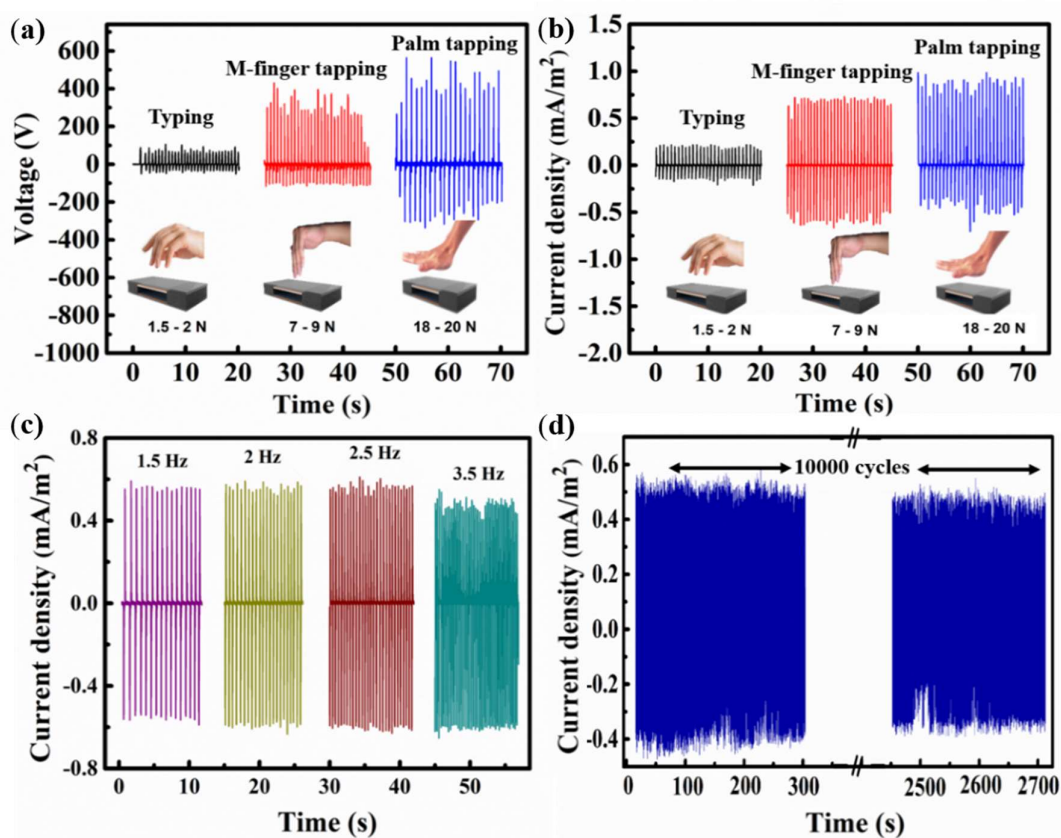
Figure 2.8: *(a) & (b) V_{oc} & J_{sc} generated from BNNSs/BoPET-paper TENG under various biomechanical forces such as single finger pressing, tapping with multiple fingers & pressing using palm. (c) Frequency dependence of generated current (d) Durability test of the device BNNSs/BoPET-paper TENG over 10000 cycles*

As seen before, the BNNSs based TENG generates electricity as alternating current signals. However, most small-scale electronic gadgets require a DC power supply rather than an AC source which would make the devices dysfunctional.[54] Hence the generated signals of the prepared BNNSs/BoPET-paper TENG were rectified by introducing a full-wave bridge rectifier circuit (see Figure 2.9(a)). These rectified output signals during the contact and non-contact movement of the TENG can charge a capacitor. Figure 2.9(b) shows the capacitor charging behaviour of BNNSs/BoPET-paper TENG, evaluated using various capacitors of capacitance values (0.47, 1.0, and 10.0 µF) for charging. The saturation voltage of 0.47 µF capacitor could reach up to 12 V within a couple of minutes. As expected, the saturation voltage decreases with the capacitance values increase.
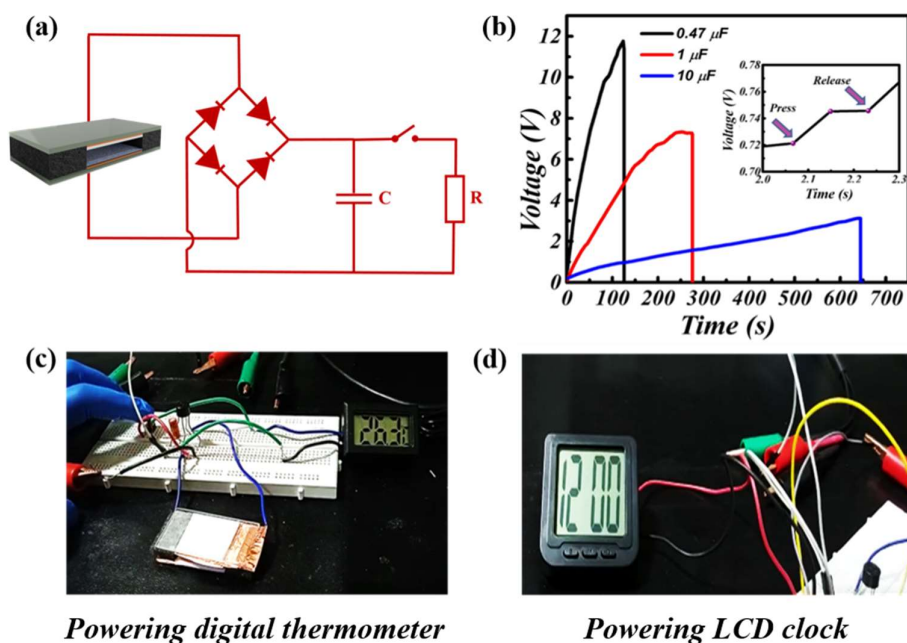
Figure 2.9: (a) Pictorial representation of the circuit diagram for capacitor charging. (b) Capacitor charging process showing the voltage profile of different capacitors 0.47 µF, 1 µF, and 10 µF by using the BNNSs/BoPET-paper TENG. The Inset of figure 2.9(b) shows the enlarged detailed view of the capacitor charging event. The photographic image shows the circuit diagram for powering (c) a digital thermometer and (d) an LCD clock using the BNNSs/BoPET-paper TENG.

The inset of Figure 2.9(b) shows the enlarged view of the capacitor charging process, which portrays the voltage increase during the pressing and releasing of the capacitor by the TENG. The utilization of electrical energy from BNNSs/BoPET-paper TENG could be used to power small electronic devices attached parallel to the capacitor, as shown in photographic images 2.9(c) and (d). Accordingly, with the help of a suitable rectifier circuit, the BNNSs based TENG was able to power a digital thermometer and an LCD clock.

2.4 Conclusions

Cost-effectiveness, light-weight, and sustainability are the vital driving elements for the materials chosen as power sources for small-scale electronics. In this first working chapter, we have reported the liquid-phase exfoliated BNNSs can act as an efficient triboelectric electron acceptors in the lab-scale demonstration of a TENG device. Sonication-assisted liquid-phase exfoliation method in a suitable solvent is used for the exfoliation. Subsequently, an energy-efficient CS-TENG prototype was fabricated using exfoliated BNNSs, employing a sponge to provide the recoiling force between electrode pairs and, glass as the structural support that allows the force to be evenly distributed throughout the material surface. For the film development, PVB was used as a binder while BoPET was used as the substrate. The new BNNSs based CS-TENG device, paired with ordinary paper as counter material, yielded excellent results. Under finger tapping force, the TENG could produce a voltage of $\sim$200 V and a current density of $\sim$0.48 mA/m^2. The power density of the TENG reached 0.14 W/m^2, which is 70 times better after the incorporation of BNNSs to the system. Small-scale electronic devices like LCD clocks, and digital thermometers were successfully demonstrated to power, using the newly designed BNNSs/BoPET-paper TENG. Further, the versatility and durability of the TENG was tested under various frequencies of the applied load and also up to 10000 continuous operation cycles. In this way, the present protocol of harvesting mechanical energy using exfoliated BNNSs incorporated BoPET-paper TENG is proven to be advantageous, due to its simplicity in fabrication and efficiency to power energy-autonomous electronic systems and portable low-power devices.

2.5 References

(1) Han, S. A.; Lee, J.; Lin, J.; Kim, S.-W.; Kim, J. H. Piezo/Triboelectric Nanogenerators Based on 2-Dimensional Layered Structure Materials. *Nano Energy* **2019**, *57*, 680–691.

(2) Zhou, H.; Li, D.; He, X.; Hui, X.; Guo, H.; Hu, C.; Mu, X.; Wang, Z. L. Bionic Ultra Sensitive Self-Powered Electromechanical Sensor for Muscle-Triggered Communication Application. *Adv. Sci.* **2021**, *8* (15), 2101020.

(3) Wu, C.; Liu, R.; Wang, J.; Zi, Y.; Lin, L.; Wang, Z. L. A Spring-Based Resonance Coupling for Hugely Enhancing the Performance of Triboelectric Nanogenerators for Harvesting Low-Frequency Vibration Energy. *Nano Energy* **2017**, *32*, 287–293.

(4) Ma, M.; Kang, Z.; Liao, Q.; Zhang, Q.; Gao, F.; Zhao, X.; Zhang, Z.; Zhang, Y. Development, Applications, and Future Directions of Triboelectric Nanogenerators. *Nano Res.* **2018**, *11* (6), 2951–2969.

(5) Long, L.; Liu, W.; Wang, Z.; He, W.; Li, G.; Tang, Q.; Guo, H.; Pu, X.; Liu, Y.; Hu, C. High Performance Floating Self-Excited Sliding Triboelectric Nanogenerator for Micro Mechanical Energy Harvesting. *Nat. Commun.* **2021**, *12* (1), 1–10.

(6) Wang, Z. L. Triboelectric Nanogenerators as New Energy Technology for Self-Powered Systems and as Active Mechanical and Chemical Sensors. *ACS Nano* **2013**, *7* (11), 9533–9557.

(7) Kuang, H.; Li, Y.; Huang, S.; Shi, L.; Zhou, Z.; Gao, C.; Zeng, X.; Pandey, R.; Wang, X.; Dong, S. Piezoelectric Boron Nitride Nanosheets for High Performance Energy Harvesting Devices. *Nano Energy* **2021**, *80*, 105561.

(8) Chen, B. D.; Tang, W.; Zhang, C.; Xu, L.; Zhu, L. P.; Yang, L. J.; He, C.; Chen, J.; Liu, L.; Zhou, T.; Wang, Z. L. Au Nanocomposite Enhanced Electret Film for Triboelectric Nanogenerator. *Nano Res.* **2018**, *11* (6), 3096–3105.

(9) Hu, Y.; Zheng, Z. Progress in Textile-Based Triboelectric Nanogenerators for Smart Fabrics. *Nano Energy* **2019**, *56*, 16–24.

(10) Wang, S.; Zi, Y.; Zhou, Y. S.; Li, S.; Fan, F.; Lin, L.; Wang, Z. L. Molecular Surface Functionalization to Enhance the Power Output of Triboelectric Nanogenerators. *J. Mater. Chem. A* **2016**, *4* (10), 3728–3734.

(11) Wang, Z. L. Self-Powered Nanotech. *Sci. Am.* **2008**, *298*, 82–87.

(12) Cheng, T.; Gao, Q.; Wang, Z. L. The Current Development and Future Outlook of Triboelectric Nanogenerators: A Survey of Literature. *Adv. Mater. Technol.* **2019**, *4* (3), 1800588.

(13) Seol, M.; Kim, S.; Cho, Y.; Byun, K.; Kim, H.; Kim, J.; Kim, S. K.; Kim, S.; Shin, H.; Park, S. Triboelectric Series of 2D Layered Materials. *Adv. Mater.* **2018**, *30* (39), 1801210.

(14) Radisavljevic, B.; Radenovic, A.; Brivio, J.; Giacometti, V.; Kis, A. Single-Layer MoS$_2$ Transistors. *Nat. Nanotechnol.* **2011**, *6* (3), 147–150.

(15) Bonaccorso, F.; Colombo, L.; Yu, G.; Stoller, M.; Tozzini, V.; Ferrari, A. C.; Ruoff, R. S.; Pellegrini, V. Graphene, Related Two-Dimensional Crystals, and Hybrid Systems for Energy Conversion and Storage. *Science.* **2015**, *347* (6217).

(16) Hasan, M. A. M.; Wang, Y.; Bowen, C. R.; Yang, Y. 2D Nanomaterials for Effective Energy Scavenging. *Nano-Micro Lett.* **2021**, *13* (1), 1–41.

(17) Kim, S.; Gupta, M. K.; Lee, K. Y.; Sohn, A.; Kim, T. Y.; Shin, K.; Kim, D.; Kim, S. K.; Lee, K. H.; Shin, H. Transparent Flexible Graphene Triboelectric Nanogenerators. *Adv. Mater.* **2014**, *26* (23), 3918–3925.

(18) Dong, Y.; Mallineni, S. S. K.; Maleski, K.; Behlow, H.; Mochalin, V. N.; Rao, A. M.; Gogotsi, Y.; Podila, R. Metallic MXenes: A New Family of Materials for Flexible Triboelectric Nanogenerators. *Nano Energy* **2018**, *44*, 103–110.

(19) Sreeprasad, T. S.; Berry, V. How Do the Electrical Properties of Graphene Change with Its Functionalization? *Small* **2013**, *9* (3), 341–350.

(20) Zhang, K.; Feng, Y.; Wang, F.; Yang, Z.; Wang, J. Two Dimensional Hexagonal Boron Nitride (2D-HBN): Synthesis, Properties and Applications. *J. Mater. Chem. C* **2017**, *5* (46), 11992–12022.

(21) Weng, Q.; Wang, X.; Wang, X.; Bando, Y.; Golberg, D. Functionalized Hexagonal Boron Nitride Nanomaterials: Emerging Properties and Applications. *Chem. Soc. Rev.* **2016**, *45* (14), 3989–4012.

(22) Lin, Y.; Williams, T. V.; Xu, T. B.; Cao, W.; Elsayed-Ali, H. E.; Connell, J. W. Aqueous Dispersions of Few-Layered and Monolayered Hexagonal Boron Nitride Nanosheets from Sonication-Assisted Hydrolysis: Critical Role of Water. *J. Phys. Chem. C* **2011**, *115* (6), 2679–2685.

(23) Joseph, A. M.; Nagendra, B.; Bhoje Gowd, E.; Surendran, K. P. Screen-Printable

Electronic Ink of Ultrathin Boron Nitride Nanosheets. *ACS Omega* **2016**, *1* (6), 1220–1228.

(24) Du, M.; Wu, Y.; Hao, X. A Facile Chemical Exfoliation Method to Obtain Large Size Boron Nitride Nanosheets. *CrystEngComm* **2013**, *15* (9), 1782–1786.

(25) Gu, X.; Zhao, Y.; Sun, K.; Vieira, C. L. Z.; Jia, Z.; Cui, C.; Wang, Z.; Walsh, A.; Huang, S. Method of Ultrasound-Assisted Liquid-Phase Exfoliation to Prepare Graphene. *Ultrason. Sonochem.* **2019**, *58*, 104630.

(26) Cunningham, G.; Lotya, M.; Cucinotta, C. S.; Sanvito, S.; Bergin, S. D.; Menzel, R.; Shaffer, M. S. P.; Coleman, J. N. Solvent Exfoliation of Transition Metal Dichalcogenides: Dispersibility of Exfoliated Nanosheets Varies Only Weakly between Compounds. *ACS Nano* **2012**, *6* (4), 3468–3480.

(27) Nicolosi, V.; Chhowalla, M.; Kanatzidis, M. G.; Strano, M. S.; Coleman, J. N. Liquid Exfoliation of Layered Materials. *Science.* **2013**, *340* (6139).

(28) Zhi, C.; Bando, Y.; Tang, C.; Kuwahara, H.; Golberg, D. Large-scale Fabrication of Boron Nitride Nanosheets and Their Utilization in Polymeric Composites with Improved Thermal and Mechanical Properties. *Adv. Mater.* **2009**, *21* (28), 2889–2893.

(29) Ci, L.; Song, L.; Jin, C.; Jariwala, D.; Wu, D.; Li, Y.; Srivastava, A.; Wang, Z. F.; Storr, K.; Balicas, L. Atomic Layers of Hybridized Boron Nitride and Graphene Domains. *Nat. Mater.* **2010**, *9* (5), 430–435.

(30) Kuang, Z.; Chen, Y.; Lu, Y.; Liu, L.; Hu, S.; Wen, S.; Mao, Y.; Zhang, L. Fabrication of Highly Oriented Hexagonal Boron Nitride Nanosheet/Elastomer Nanocomposites with High Thermal Conductivity. *Small* **2015**, *11* (14), 1655–1659.

(31) Lee, D.; Song, S. H. Ultra-Thin Ultraviolet Cathodoluminescent Device Based on Exfoliated Hexagonal Boron Nitride. *RSC Adv.* **2017**, *7* (13), 7831–7835.

(32) Ba, K.; Jiang, W.; Cheng, J.; Bao, J.; Xuan, N.; Sun, Y.; Liu, B.; Xie, A.; Wu, S.; Sun, Z. Chemical and Bandgap Engineering in Monolayer Hexagonal Boron Nitride. *Sci. Rep.* **2017**, *7* (1), 1–8.

(33) Ikram, M.; Hassan, J.; Imran, M.; Haider, J.; Ul-Hamid, A.; Shahzadi, I.; Ikram, M.; Raza, A.; Qumar, U.; Ali, S. 2D Chemically Exfoliated Hexagonal Boron Nitride (HBN) Nanosheets Doped with Ni: Synthesis, Properties and Catalytic Application for the Treatment of Industrial Wastewater. *Appl. Nanosci.* **2020**, *10*, 3525–3528.

(34) Radhakrishnan, S.; Das, D.; Samanta, A.; Carlos, A.; Deng, L.; Alemany, L. B.;

Weldeghiorghis, T. K.; Khabashesku, V. N.; Kochat, V.; Jin, Z. Fluorinated H-BN as a Magnetic Semiconductor. *Sci. Adv.* **2017**, *3* (7), e1700842.

(35) Akpınar Borazan, A.; Gökdai, D. Pine Cone And Boron Compounds Effect As Reinforcement On Mechanical And Flammability Properties Of Polyester Composites. **2018**.

(36) Cammarano, A.; Luca, G.; Amendola, E. Surface Modification and Adhesion Improvement of Polyester Films. *Open Chem.* **2013**, *11* (1), 35–45.

(37) Pullanchiyodan, A.; Surendran, K. P. Formulation of Sol–Gel Derived Bismuth Silicate Dielectric Ink for Flexible Electronics Applications. *Ind. Eng. Chem. Res.* **2016**, *55* (26), 7108–7115.

(38) Varghese, J.; Surendran, K. P.; Sebastian, M. T. Room Temperature Curable Silica Ink. *RSC Adv.* **2014**, *4* (88), 47701–47707.

(39) Lee, J. W.; Cho, H. J.; Chun, J.; Kim, K. N.; Kim, S.; Ahn, C. W.; Kim, I. W.; Kim, J.-Y.; Kim, S.-W.; Yang, C. Robust Nanogenerators Based on Graft Copolymers via Control of Dielectrics for Remarkable Output Power Enhancement. *Sci. Adv.* **2017**, *3* (5), e1602902.

(40) Shi, K.; Zou, H.; Sun, B.; Jiang, P.; He, J.; Huang, X. Dielectric Modulated Cellulose Paper/PDMS-based Triboelectric Nanogenerators for Wireless Transmission and Electropolymerization Applications. *Adv. Funct. Mater.* **2020**, *30* (4), 1904536.

(41) Pillai, A. S.; Chandran, A.; Peethambharan, S. K. MWCNT Ink with PEDOT: PSS as a Multifunctional Additive for Energy Efficient Flexible Heating Applications. *Appl. Mater. Today* **2021**, *23*, 100987.

(42) Tutgun, M. S.; Sinirlioglu, D.; Celik, S. U.; Bozkurt, A. Preparation and Characterization of Hexagonal Boron Nitride and PAMPS-NMPA-Based Thin Composite Films and Investigation of Their Membrane Properties. *Ionics.* **2015**, *21* (10), 2871–2878.

(43) Wang, Z. L.; Chen, J.; Lin, L. Progress in Triboelectric Nanogenerators as a New Energy Technology and Self-Powered Sensors. *Energy Environ. Sci.* **2015**, *8* (8), 2250–2282.

(44) Zhu, G.; Pan, C.; Guo, W.; Chen, C.-Y.; Zhou, Y.; Yu, R.; Wang, Z. L. Triboelectric-Generator-Driven Pulse Electrodeposition for Micropatterning. *Nano Lett.* **2012**, *12* (9), 4960–4965.

(45) Zhong, J.; Zhong, Q.; Fan, F.; Zhang, Y.; Wang, S.; Hu, B.; Wang, Z. L.; Zhou, J. Finger Typing Driven Triboelectric Nanogenerator and Its Use for Instantaneously Lighting up

LEDs. *Nano Energy* **2013**, *2* (4), 491–497.

(46) Zhu, G.; Bai, P.; Chen, J.; Lin Wang, Z. Power-Generating Shoe Insole Based on Triboelectric Nanogenerators for Self-Powered Consumer Electronics. *Nano Energy* **2013**, *2* (5), 688–692.

(47) Chen, J.; Zhu, G.; Yang, W.; Jing, Q.; Bai, P.; Yang, Y.; Hou, T.; Wang, Z. L. Harmonic-resonator-based Triboelectric Nanogenerator as a Sustainable Power Source and a Self-powered Active Vibration Sensor. *Adv. Mater.* **2013**, *25* (42), 6094–6099.

(48) Zhang, X.-S.; Han, M.-D.; Wang, R.-X.; Zhu, F.-Y.; Li, Z.-H.; Wang, W.; Zhang, H.-X. Frequency-Multiplication High-Output Triboelectric Nanogenerator for Sustainably Powering Biomedical Microsystems. *Nano Lett.* **2013**, *13* (3), 1168–1172.

(49) Wu, C.; Kim, T. W.; Park, J. H.; An, H.; Shao, J.; Chen, X.; Wang, Z. L. Enhanced Triboelectric Nanogenerators Based on MoS_2 Monolayer Nanocomposites Acting as Electron-Acceptor Layers. *ACS Nano* **2017**, *11* (8), 8356–8363.

(50) Zou, H.; Zhang, Y.; Guo, L.; Wang, P.; He, X.; Dai, G.; Zheng, H.; Chen, C.; Wang, A. C.; Xu, C.; Wang, Z. L. Quantifying the Triboelectric Series. *Nat. Commun.* **2019**, *10* (1), 1–9.

(51) Fan, F.-R.; Lin, L.; Zhu, G.; Wu, W.; Zhang, R.; Wang, Z. L. Transparent Triboelectric Nanogenerators and Self-Powered Pressure Sensors Based on Micropatterned Plastic Films. *Nano Lett.* **2012**, *12* (6), 3109–3114.

(52) Park, S.; Park, J.; Kim, Y.; Bae, S.; Kim, T.-W.; Park, K.-I.; Hong, B. H.; Jeong, C. K.; Lee, S.-K. Laser-Directed Synthesis of Strain-Induced Crumpled MoS_2 Structure for Enhanced Triboelectrification toward Haptic Sensors. *Nano Energy* **2020**, *78*, 105266.

(53) Varghese, H.; Chandran, A. A Facile Mechanical Energy Harvester Based on Spring Assisted Triboelectric Nanogenerators. *Sustain. Energy Fuels* **2021**.

(54) Wang, D.; Zhang, D.; Yang, Y.; Mi, Q.; Zhang, J.; Yu, L. Multifunctional Latex/Polytetrafluoroethylene-Based Triboelectric Nanogenerator for Self-Powered Organ-like MXene/Metal–Organic Framework-Derived CuO Nanohybrid Ammonia Sensor. *ACS Nano* **2021**, *15* (2), 2911–2919.

Chapter 3

Flexible screen-printed TENG for powering electronic devices utilizing composite ink based on BNNSs
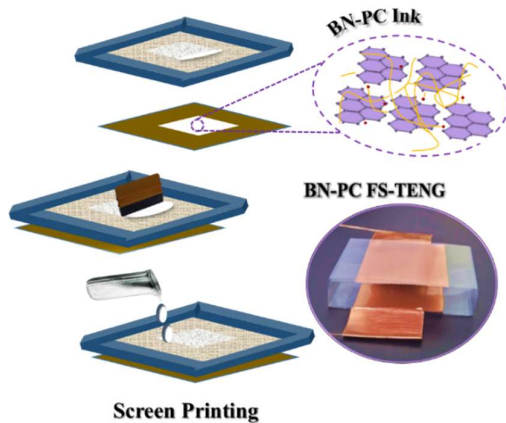
Printing, a revolutionary technique used to fabricate large area high-performance wearable devices, has many benefits such as facile fabrication and scalability. In this chapter, a high-performance flexible TENG was developed based on 2D- BNNSs ink printed on Mylar substrate as a triboelectric negative contact layer paired with the printed polyvinyl pyrrolidone (PVP) on Mylar as tribo-positive material

3.1 Introduction

The future of mankind is going to be anchored on innovations like the IoT which is a critical concept in creating an elite class of autonomous and mobile gadgets that need to operate for longer duration without any battery changes.[1,2] For this to happen, imperative efforts have to be made to harvest energy from ambient green resources for powering a multitude of portable devices. That is, energy harvesting is a key element in IoT-enabled systems that brings man's intelligence to the edge. As stated in previous chapters, vibrational energy harvesting techniques including TENGs can harness energy from human motions such as dancing, walking, computer key tapping, etc., to drive portable sensors, mobile gadgets, or even in high-voltage applications.[3] As long as there is friction between triboelectrically different materials by any means, there exists a finite amount of power that can be tapped using TENG by virtue of contact electrification and electrostatic induction.[4] An intuitive approach to enhance the process of triboelectrification is the improvement of contact charges developed between the surfaces of triboelectrically dissimilar materials, where it can be done by several means.[5] To enhance the TENG output, either the choice of materials should lie far from each other in the triboelectric series or the modification of the active surface layer to increase the contact area, which may eventually improve the surface charge density. In addition, the contact electrification property of the triboelectric materials is strongly influenced by the charge trapping capability of the contact materials. It is seen that the incorporation of nanomaterials with lamellar structure- enhances the charge trapping ability of frictional layers.[6]

Nowadays, developing cost-effective and scalable TENGs are given preeminence. Modern printing technology promises rapid advances in terms of its manufacturing efficiency and applicability in various fields. On the other hand, power sources of modern times should possess features like ultra-thinness, cost-effectiveness, flexibility and sustainability. Printed electronics can meet these goals and are considered an emerging revolutionary technology, aiming at relatively large-area electronic devices and components. In conventional flexible electronics, printed inks are used for various applications such as energy harvesting, smart packaging, radiofrequency (RF) communication, and flexible display applications.[7] Even though printing is a popular scalable additive manufacturing tool, it is not much explored for fabricating flexible TENG.[8,9] Seol *et al.* developed an all-printed TENG in which the core-shell structural frame

was fabricated by using a 3D printing method, in which the printing material was polylactic acid. 2D printing was also performed to form the functional contact layer poly (methyl methacrylate) (PMMA) with a grating pattern on nanocellulose substrate.[10] Salauddin *et al.* designed an MXene/Ecoflex nanocomposite-based flexible fabric TENG, which utilizes a 3D printing method for its contact material fabrications.[11]

Of the available printing methods, screen printing is an inexpensive method capable of rapid mass production and also provides good control over the printing area over a wide choice of substrates like polymers, papers, fabrics, etc.[12] In this technique, specific patterns are deposited on various substrates using screen masks for creating large-area high-resolution 2D patterns having thicknesses down to a few microns.[13,14] There are several available reports in connection with screen-printed TENGs. Cao *et al.* reported a screen printable carbon nanotube (CNT) ink-based flexible washable electronic textile, that serves as a touch or gesture sensor for intelligent human–machine interactions.[15] Similarly, Wen *et al.* proposed a silk fibroin-based printed TENG for wearable multi-functional sensing, which utilizes a screen-printing process to prepare the graphite interdigital electrodes on top of a soft PDMS substrate.[16] A 2D material-based TENG-directed flexible and self-powered humidity sensor was proposed by Zhang *et al.*, in which nanoflowers of tin disulphide/reduced graphene oxide nanohybrid has been used. This hybrid film was fabricated using the screen-printing method.[17]

h-BN is useful for a variety of stretchable and flexible applications. Exfoliated 2D materials are attractive for future energy harvesting technology as potential materials.[18,19] Traditionally, liquid phase exfoliation is a scalable method for the production of layered 2D nanostructures. The well-exfoliated nanosheet dispersion combined with suitable solvents and stabilizing polymers is ideal for printing applications.[20] In uniform printed films, the deposited BNNSs form a porous structure compromising their mechanical integrity, susceptibility to moisture, and also substrate adhesion. A solution-processable h-BN ink specially formulated for screen printing can yield thermally and chemically stable printed components for device applications.[21] There are several reports on h-BN nanosheet ink for use in printed electronic devices and components.[22] In 2007, Carey *et al.* demonstrated inkjet printed h-BN-based ink as a gate dielectric layer in an all-printed field effect transistor.[23] Similarly, highly viscous screen-printed polymer-based BNNSs inks were also developed for wearable and flexible

electronics.[24] A printed 2D BNNSs-based flexible triboelectric nanogenerator is a novel concept for power generation.

Herein, a successful demonstration of a CS mode flexible screen printed (FS-TENG) using BNNSs ink printed on a polymer substrate for powering electronic devices is presented. The formulated viscosity tunable ink, for screen printing purposes, incorporates ultra-thin BNNSs as a filler material, with polycarbonate as a polymer binder and other organic additives suitable for printing and rheology adjustments. A printed flexible TENG device is developed with the formulated screen-printed ink as negative material against printed PVP as the positive tribomaterial. Notably, the embedded layered 2D material boosts the output by ~7 times. The FS-TENG was further able to power handheld electronic devices, such as thermometers calculators and LED's.

3.2 Experimental

3.2.1 Materials

BN powder (1μm size), as well as the polymers polyvinyl pyrrolidone (PVP), and polycarbonate (PC) were procured from Sigma Aldrich, USA. The dispersant solvent DMF is purchased from HPLC lab reagents in India. Commercially available Mylar® (BoPET), (DuPont, USA), with 80 μm thickness was used as the substrate for screen printing, as well as the structural framework for FS-TENG. Ethanol (Merck Chemicals) was used for printing purposes as a substrate cleaning agent. A conducting copper tape (3M Co.) with adhesive on both sides was used as electrodes for the FS-TENG. All chemicals were used without any further modification or purification.

3.2.2 Formulation of BN-PC ink

BNNSs-polycarbonate composite (BN-PC) ink was formulated by simple solution mixing followed by sonication and magnetic stirring as shown in Figure 3.1. Initially, exfoliated BNNSs for screen-printable ink were produced by liquid-phase assisted exfoliation method (detailed characterization is shown in Chapter 2). Thereafter, polycarbonate and BNNSs in the weight ratio of 1:1 (0.5 g) were added to 1 ml of DMF solvent in a culture tube, followed by the addition of 50 μL Triton X100 as a thixotropy-controlling additive. The so-derived ink suspension was mechanically stirred vigorously for 12 hours at 700 rpm speed to ensure homogeneous mixing for stable dispersion. The

entire process was repeated without using BNNSs for printing pure polymer PC film.
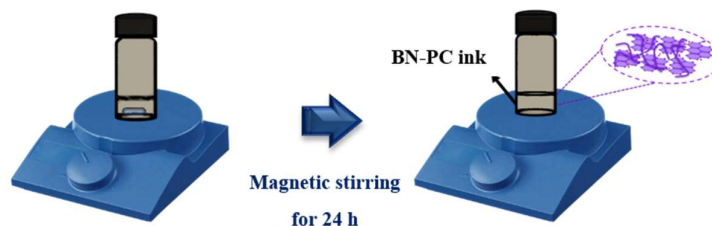
Figure 3.1: *Schematic depicting formulation of BN-PC ink*

3.2.3 Preparation of printed triboelectric layer

The rheology-optimized screen printable ink of exfoliated BNNSs was made into a flexible composite film using the screen printing technique. Here, a custom-made silk screen with a desired square pattern of active area of 9 cm² (3 cm x 3 cm), was fabricated by photoresistive masking. It was used as the screen for the printing of BN-PC ink on BoPET substrate. The screen printing process using BN-PC ink is schematically represented in Figure 3.2. Initially, the prepared viscous ink was placed over the screen with the substrate under it at a fixed snap-off distance. Then, with the help of a rubber squeegee, the ink was cast as films onto the substrate through the screen in the desired pattern. With repeated printing strokes, the thickness and quality of the film can be controlled. Here, the inter-particle cohesion and adhesion of the BNNSs on the BoPET substrate were made possible by the polycarbonate binder. Finally, it was dried in an oven at 60 °C to obtain polycarbonate BNNSs film on BoPET. Similarly, 20 wt% PVP in DMF was screen printed on BoPET and dried in the oven for use as the counter contact layer for the FS-TENG device.
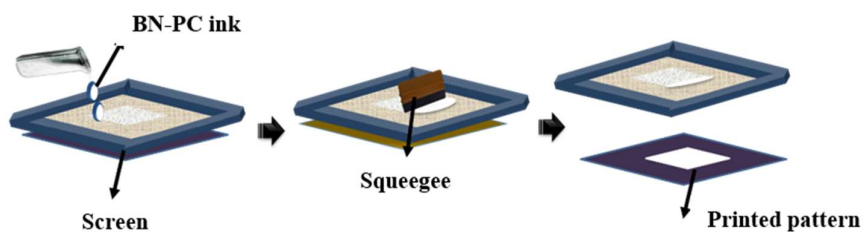
Figure 3.2: *Schematic illustration of the screen printing process using BN-PC ink*

3.2.4 Fabrication of FS-TENG device

The traditional CS mode assembly was used for the fabrication of FS-TENG device. Flexible BoPET acts as the supporting structure for TENGs while also contributing to structural stability. Substrates for contact materials were cut in square shapes of dimensions 3 cm×3 cm. The FS-TENG was prepared by printing the prepared BN-PC ink onto BoPET substrate as negative tribo-material and PVP printed on BoPET as the counter one. The conductive copper tape was used as the electrodes for FS-TENG, and thin copper leads were attached to this conductive tape as leads for taking external connections. The separation between two contact materials is maintained as 1 cm using the BoPET support structure. For developing the control FS-TENG device (without BNNS), the entire fabrication process was repeated by printing PC film and PVP films as contact materials. The schematic model and the photograph of the FS-TENG are depicted in Figures 3.3(a) and (b).
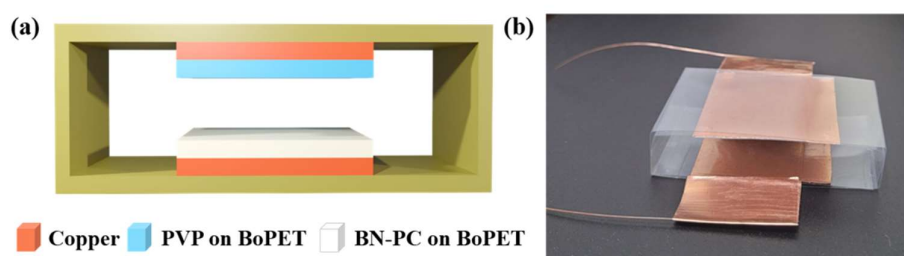
Figure 3.3: (a) Schematic model of the FS-TENG. (b) Photograph of the fabricated TENG device

3.2.5 Characterization methods

The colloidal stability and flow characteristics of the formulated ink were analyzed at 20 °C using a rheometer (Rheo plus 32, Anton Paar, Graz, Austria) equipped with a chiller. The contact angle of the formulated ink was analyzed by a contact angle measuring device (DSA 30, KRUSS GmbH, Germany). Thermal stability and gravimetry of the dried BN-PC ink and polycarbonate polymer were investigated by a thermogravimetric analyzer TA Q50, at a 10 °C/min heating rate. The FTIR spectra of the ink and polymers were carried out using Nicolet Magna 560 FTIR (Thermo Scientific, Massachusetts, USA). The surface and cross-sectional morphology of the printed patterns were viewed using a SEM (Karl Zeiss EVO 50, Oberkochen, Germany). Atomic force microscopy (AFM,

Multimode, Bruker, Germany) in tapping mode was used to evaluate the surface topology of the film on the BoPET substrate. The optical imaging of the printed films were taken using a polarizing optical microscope (Leica DM2700P, Germany) attached to a charge-coupled device camera. The electrical characteristics of the FS-TENG device were analyzed using a source measuring unit (Keithley 2450), and a current preamplifier (SR570, Stanford Research) coupled with a digital phosphor oscilloscope (Tektronix DPO2004B, USA). Using a custom-developed force impactor, a cyclic uniform mechanical force (~10 N) was applied to the FS-TENG device periodically, and the corresponding electrical outputs were recorded. An automatic force tester (AFT500, Apple Electronics) was used for measuring the force imparted. By using various load resistors, varying from 1 Ω to 1000 MΩ, the load-dependent power density of the device was calculated. Capacitor charging profiles were recorded using different values of capacitors. The cyclic stability and durability were confirmed by the continuous operation of the FS-TENG for more than10000 cycles.

3.3 Results and discussions

3.3.1. Properties of the BN-PC ink

The quality of the screen-printed films are closely related on several factors like printing parameters, substrate selection and the ink's flow characteristics. The printing parameters mainly include screen-printing speed, snap-off distance, screen mesh parameter, angle and geometry of the squeegee, etc., which can be carefully controlled for printing purposes. In addition, to maintain the proper ink adhesion on various substrates and colloidal stability of the ink, choice, concentration, and addition sequence are critical. Here, the ink rheology of the screen printable hexagonal boron nitride nanosheets based ink is customized with polycarbonate as a polymer binder and Triton X100 as an additive. Then choice of polycarbonate as a binder for BNNSs is owing to its good solution processability, low cost, and higher glass-transition temperature of around 150°C. The photograph of the prepared highly viscous ink is given in the inset of Figure 3.4(a). Further, the rheogram of the formulated ink (Figure 3.4(a)) shows a considerable decrease in viscosity with the increase in external shear rate. This pseudoplastic behavior is suitable for application in screen printing since this enables continuous extrusion of the viscous ink through the tensioned screen mesh under normal conditions.[21,25] Note that

the observed viscosity of the ink is 2 Pa.s at a shear rate of 10 s^{-1} gradually decreases and levelled to a constant lower value at higher shear. Similar rheological behavior was observable in other 2D material-based inks also and usually the required range of the ink viscosity for screen printing is 1–10 Pa.s.[26] Also the dynamic viscoelastic behavior of the ink, represented in Figure 3.4(b), indicates viscous liquid-like nature in the entire strain region where loss modulus (G'') dominates over storage modulus (G'). The storage modulus and loss modulus in the rheology analysis of the formulated ink represents the solid and liquid behaviour respectively, as a function of shear stress. Apart from this, surface wetting parameter is also an essential component in printing, and can be identified from the contact angle measurement.[27] The observed lower value of contact angle, 63° (Figure 3.4(c)), attests to its better wettability provided by the high affinity of the ink towards the BoPET substrate.[28,29]
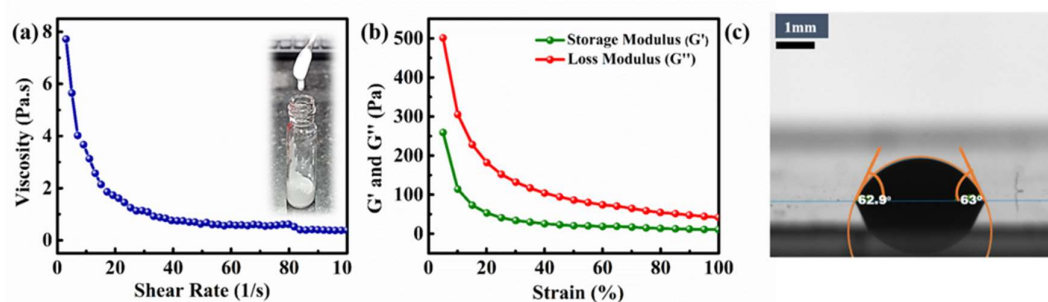
Figure 3.4: *(a) Viscosity variation of the formulated ink with shear rate. The inset of figure 3.4 (a) shows the photograph of the BN-PC ink. (b) The plot of storage modulus and loss modulus versus strain. (c) Contact angle measurement of the BN-PC ink on BoPET substrate*

In the FT-IR analysis of BN-PC ink and pristine PC polymer (Figure 3.5(a)), the characteristic peaks observed in the fingerprint region 400-1000 cm^{-1} arise from the C-C bond stretching vibrations of polymer material. Similarly, the peaks in the range 1232–1164 cm^{-1} are due to the presence of asymmetric O–C–O deformations of the carbonate group. While the observed CH$_3$ vibration peak at 1081 cm^{-1} and the additional peak near 1015 cm^{-1} is the symmetric deformation of the O–C–O carbonate group. Further, the C=C stretching vibrations appear at 1506 cm^{-1} due to the presence of aromatic ring carbon, and carbonate group C=O deformations occur near 1775 cm^{-1}. All these peaks are common to both the FT-IR spectra and it arises from the polymer material. Whereas, the two strong and sharp absorption peaks observed at 760 cm^{-1} and 1360 cm^{-1} in the BN-PC FTIR

spectrum are the characteristic peaks of h-BN. These peaks arise from broad B–N–B out-of-plane bending and B–N in-plane stretching vibrations respectively.[30,31,32] Thus the FTIR spectra establishes the formation of the composite ink as expected.
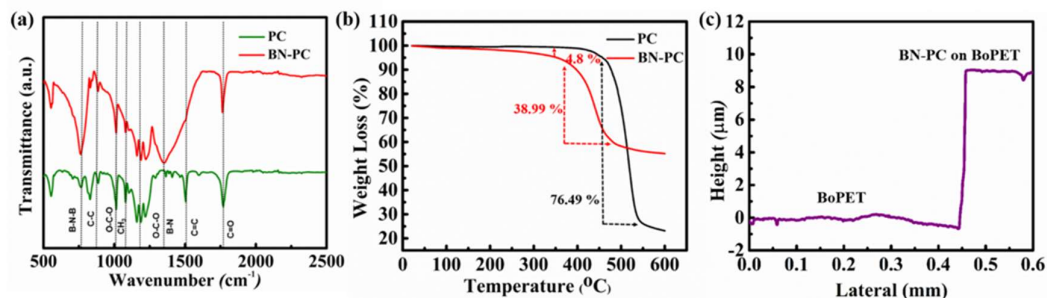
Figure 3.5: *(a) FT-IR analysis of pristine polycarbonate and ink powder. (b) Thermal degradation behavior of polymer and BN-PC ink. (c) Thickness profile of the printed ink on the BoPET substrate*

The thermal behavior of dried screen printed ink was analyzed by using thermogravimetric analysis (TGA), which is depicted in Figure 3.5(b). The weight loss observed at a temperature range of 100-350 °C in the BN-PC polymer composite was mainly attributed to the evaporation of volatile residual solvents and also the thermal degradation of the surfactant present in the ink. The main weight loss starts in both samples after a temperature of ~370 °C arises because of the cleavage of the carbonate functional groups present in the polymer material. In pure polymer PC, almost 80% of the degradation takes place after 400 °C. The observed weight loss in BN-PC sample is comparably less because of the filler loading, and the incorporation of higher thermal stability filler like BNNSs in polycarbonate-based ink enhances its thermal stability.[33,34,35] The thickness of the BN-PC film on BoPET substrate was identified from the profilometric technique, and the thickness value is found to be 8.5 ± 2 μm (see Figure 3.5(c)).

3.3.2. Morphology of PC & BN-PC ink screen printed on BoPET substrate

The surface morphological analysis of the screen-printed PC and BN-PC films were done with the aid of SEM and AFM surface imaging. The surfaces of the printed ink consist of homogenously dispersed nanosheets embedded in the polymer matrix parallel to the surface due to the leveling effect of the squeegee.[36] The microstructure of BN-PC film shows good compatibility between the filler material and polymer binder (Figure 3.6(a)). Even after continuous cycles of operation, the surface of the BN-PC film showed only minute changes compared with the films before operations as in Figure 3.6(b). Whereas

the film thickness of the printed pattern on the substrate surface for 3 strokes of printing, on average, is found to be 7.5 ± 2 μm, which was estimated using the cross-sectional SEM (see Figures 3.6(c) and (d)). This thickness value is in agreement with the value estimated using the profilometer.
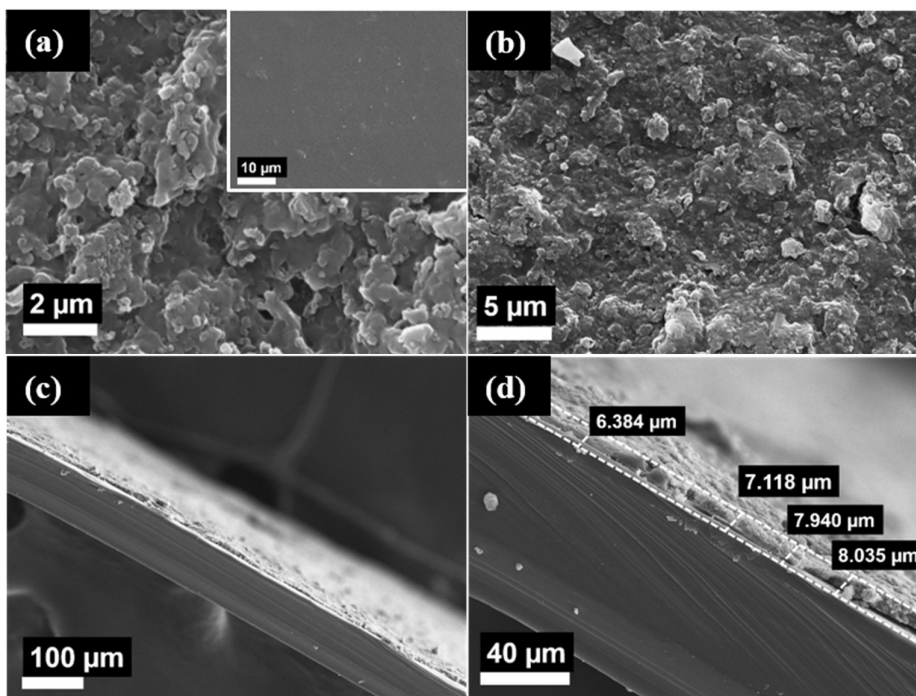
Figure 3.6: *(a) Surface morphology of the BN-PC ink screen printed on BoPET substrate via SEM analysis. Inset of 3.6 (a) PC printed on BoPET without BNNSs. (b) SEM image of BN-PC film after 10000 cycles of operation. (c) & (d) Cross-sectional view of the printed ink on BoPET*

The formulated ink screen-printed on BoPET substrate having a white translucent nature. Uniformity and homogeneity of the film is ensured by the multiple strokes of printing. Where the horizontal stacking of multiple layers is realized effectively because of the preferred low potential energy arrangements of the ink when initially it is printed on the pristine substrate and then over the printed layers. Similar behavior of printed patterns were observed in other 2D material-based screen-printed graphene inks also.[7,37]

The AFM analysis is also extensively used to make meticulous observations on surface topography and evaluate the textural characteristics of diverse film surfaces. Here, the surface morphology of the screen-printed pattern was obtained from the AFM analysis of PC and BN-PC film surfaces with different weight percentages of BNNSs. (see

Figures 3.7 (a), (b), (c) and (d)) also corroborates with the inference obtained using the SEM.
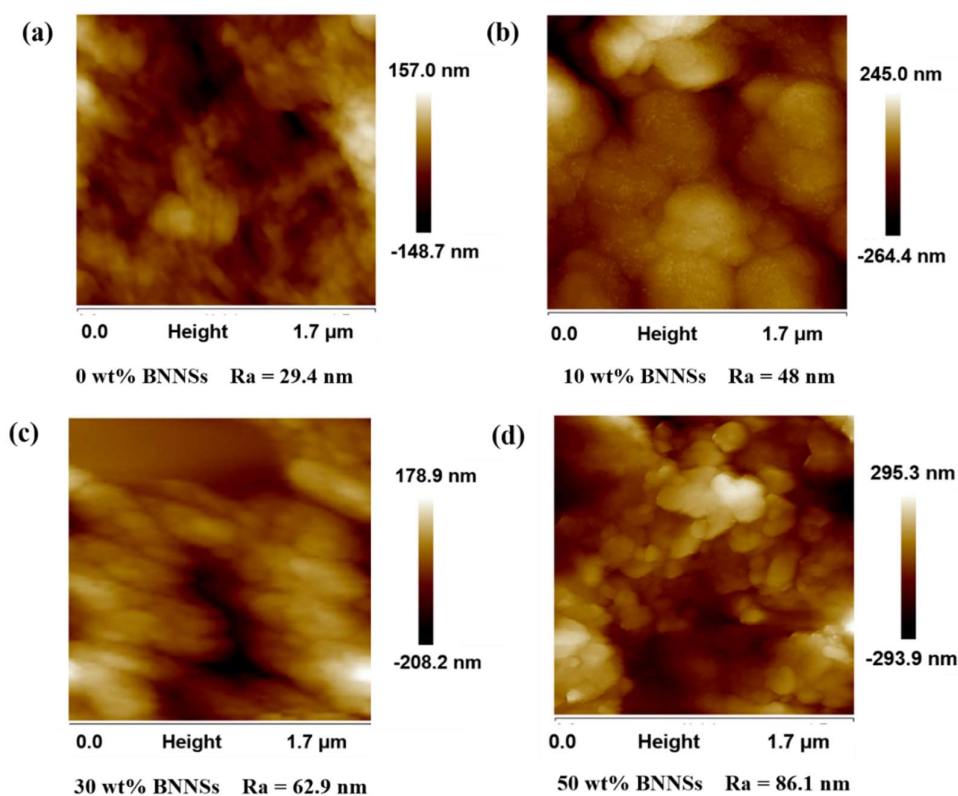
Figure 3.7: *(a) AFM images of BN-PC film with (a) 0 wt%, (b) 10 wt%, (c) 30 wt%, and (d) 50wt % of BNNSs (Ra- Average surface roughness)*

The AFM surface roughness analysis of BN-PC film with 50 wt% BNNSs shows that the film exhibited an average surface roughness value (Ra) of 86.1 nm, which is a measure of roughness and general variations over the entire scanning area. A root mean square roughness (Rq) of 107 nm represents the standard deviation in surface height profiles. Where the distribution of spikes relative to the mean line above or below is obtained from the kurtosis value and it was found to be 2.76 which represents bumpy surfaces. The positive skewness value of 0.336 also indicates the presence of bumps than valleys and shows that the surface of the printed sample has predominant height variations compared to printed pristine polycarbonate film. The surface roughness and root mean square roughness of PC film without BNNSs are similarly decreased to 29.4 and 38.5 nm, respectively (Figure 3.7(a)).[38,39] The observed significant increase in surface roughness

value in BN-PC film is attributed to the incorporation of an inorganic material having a higher surface roughness value compared to the polymer material.[40]

3.3.3. Output characteristics of FS-TENG device

When it comes to triboelectric nanogenerator, choice of contact material is the obvious first priority, and 2D BNNSs have been previously proven to be an excellent candidate.[31] Here, the formulated BNNSs based ink showed excellent thermal stability and good adhesion to the substrate, which are very crucial for the stable triboelectric application. In addition, the enhancement in the surface area resulted from the microscale roughness of the printed surface could magnify the triboelectric charge generation during the contact electrification.[41] Also, the screen printing process provides facile scalability when it is required. The designed screen-printed TENG comprises BNNSs in polycarbonate matrix printed on a BoPET as primary TENG material, while printed PVP as the second material, and they are chosen based on their position in the triboelectric series.[42] The detailed fabrication steps are depicted in the experimental section. Figure 3.8 shows the schematic representation of the working of the FS-TENG device and is explored well in the literatures.[43]

The fabricated FS-TENG has two contact layers, one BN-PC ink printed on BoPET substrate and a printed PVP layer. Copper electrodes were separately attached on bottom of these contact layers. The working of this vertical contact separation mode FS-TENG is illustrated in Figure 3.8. Here, the supporting structure not only provides the necessary separation gap but also provides recoiling for the same. When a mechanical force is imparted, layers come into contact and triboelectric charges are generated on the surfaces. Whereas in the releasing stage, electrostatic charge induction generates a potential difference between the electrodes. Consequently, flow of electrons takes place between the electrodes when they are connected. In this way, alternate pressing and releasing motion can generate alternating electrical signals in the external circuit.[44,45]
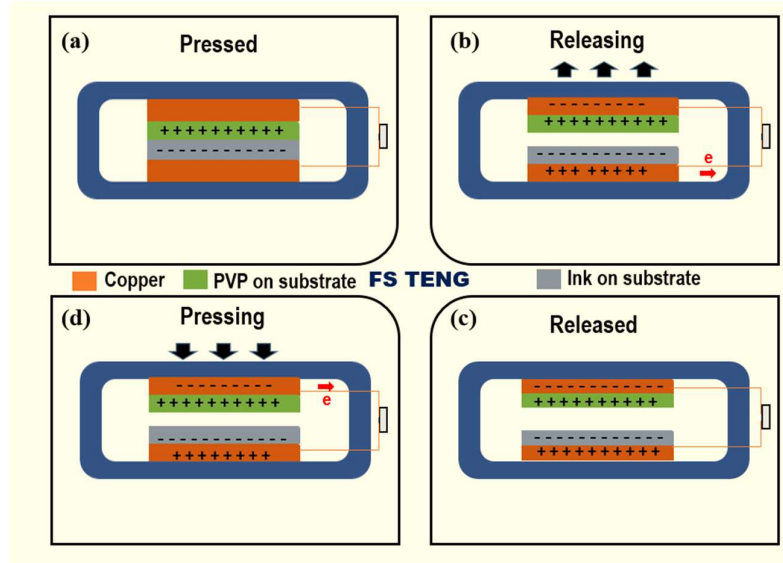
Figure 3.8: *The schematic representation of the working mechanism of FS-TENG during (a) pressed state, (b) releasing state, (c) released saturation state, and (d) further pressing state*

The output voltages (V) and short-circuit current density (J_{sc}) of the screen-printed TENGs with and without BNNSs are shown in Figures 3.9(a) and (b). For this the as-fabricated TENGs were continuously pressed and released by a custom-made force impactor test system with a vertical contact force of ~10 N at a frequency of 5 Hz, which provided stable and systematic contact between the top and bottom layers. The TENG device with BNNSs showed noticeable improvements in electrical properties compared to TENG without BNNSs. The printed polycarbonate FS-TENG against PVP exhibited an output voltage of about 400 V while the TENG with BNNSs exhibited a two-fold enhanced V of 800 V. The J_{sc} of the printed TENG with BNNSs displayed a value of 0.78 mA/m^2, which is remarkably higher than the printed TENG without BNNSs (0.55 mA/m^2). The output enhancement observed in the BNNSs ink-based TENG compared to the PC-only TENG is that the addition of a more tribo-negative and electron-trapping capable filler material contributes to the output enhancement of the fabricated device. That is, without the incorporation of BNNSs, the developed charges would be comparably less, due to the difference in tribo-polarity being small. Then the introduction of more triboelectrically negative BNNSs as a filler in the polycarbonate ink improves the triboelectric charge transfer, storage, and charge trapping ability simultaneously.[46]

The major factors influencing the contact electrification process involve the electrical polarity and charge storage capability of the materials in contact. Modulation of the electrical polarity can be achieved by either increasing the tribo-layers electro positivity or electro negativity by incorporating certain nanomaterials, and in turn improving the contact electrification. Furthermore, when BNNSs are embedded in a polymer matrix, the presence of inter-layer voids in the 2D nanomaterial sheets can capture carriers easily and then trapped them to the interior of the negative triboelectric layer and store them. This phenomenon alleviates the loss of electrons due to the air breakdown effect by reducing the surface potential.[47] The charge trapping ability of 2D layered materials also decreases the recombination of electrons with the positive ions or particles in the air, further enhancing the electrical output of TENGs. In addition, atomically thin 2D nanomaterial layers with large lateral dimensions can possess higher specific surfaces, thereby improving the contact area effectively in triboactive layers and also resulting in the efficient output performance of the device by increasing triboelectric charge density.[48,49]

To evaluate the performance of FS-TENG for practical applications, the power density of the device must be analysed critically. For this, the FS-TENG was connected to various resistors with variable values ranging from 1 Ω to 1000 MΩ. From the observed voltages corresponding to the connected loads, power density was calculated. The output power densities of the contact separation mode FS-TENG with an active contact area of 9 cm^2 without and with BNNSs are shown in Figures 3.9(c) & (d). In the power density curve, voltage increases to a maximum value as load resistance increases, meanwhile, the power density also increases and reaches a maximum, and then decreases. For the reference device, the peak power density obtained was about 0.18 W/m^2 at 200 MΩ. In comparison, the maximum peak value of power density for the FS-TENG with BNNSs is ~1.36 W/m^2, which is 7 times that of the reference that was observed at 200 MΩ.
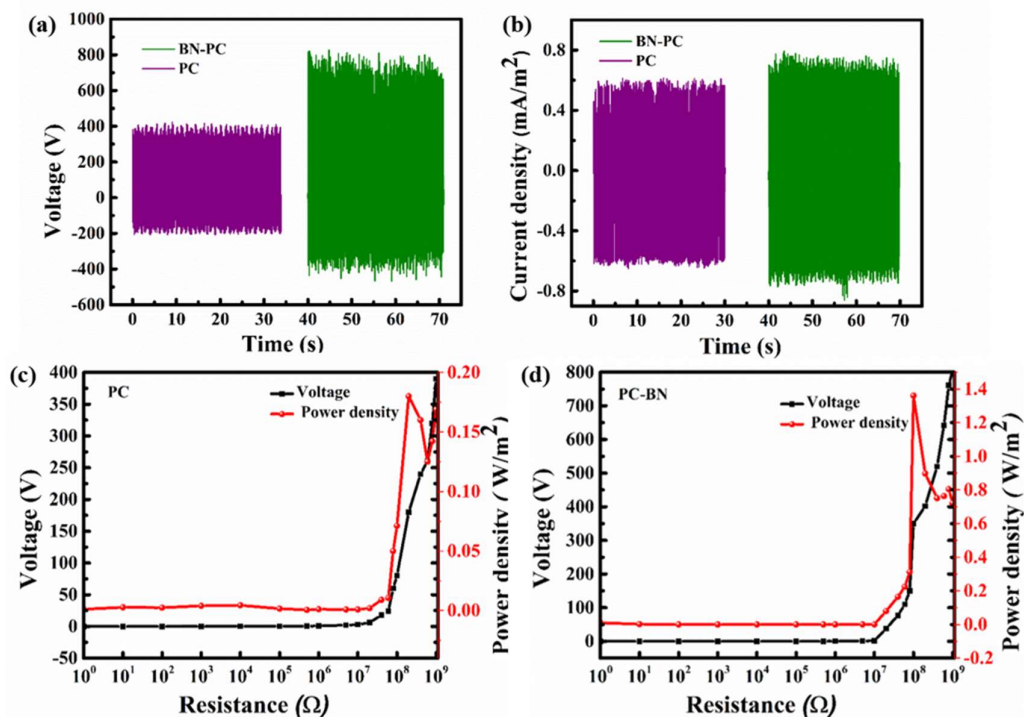
Figure 3.9: *(a) and (b) V and J_{sc} generated from the PC/PVP & BN-PC /PVP FS-TENG respectively under a mere tapping force of ~10 N at 5Hz. (c) and (d) Output power density of the PC/ PVP & BN-PC/PVP FS-TENG under various resistive loads*

For the quantitative analysis of the energy output, we connected capacitors to the FS-TENG via a rectifier circuit to identify the quantification of actual charges stored. As shown in Figure 3.10(a), a full-wave bridge rectifier was used to convert the AC output signal to DC out, and various capacitors with different capacitances (0.5 µF, 1 µF, 5 µF, 10 µF) were used for identifying the capacitor charging profile (Figure 3.10(b)). Within 180 seconds, the FS-TENG charged a 0.5 µF capacitor up to a maximum saturation voltage of 32 V. This stable electrical energy provided by the FS-TENG is sufficient for powering low-power electronic gadgets. To demonstrate this, using the TENG's output from hand tapping motion, different electronic gadgets such as digital thermometers, calculators and LEDs are successfully powered (Figure 3.10(c)). That is, the FS-TENG's output electrical performances are suitable for energy storage in capacitors and in turn power portable electronic devices.
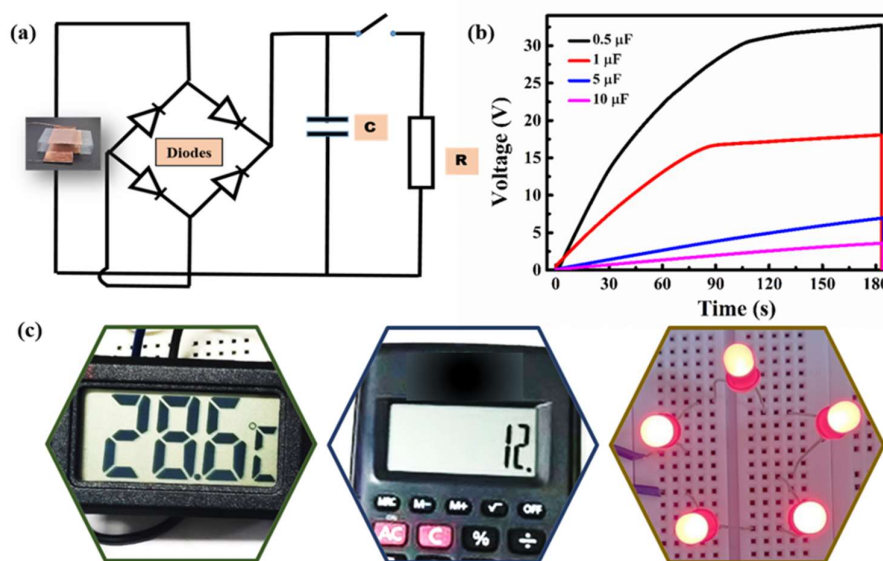
Figure 3.10: *(a) Circuit diagram of rectifying circuit for capacitor charging and powering electronic gadgets is depicted. (b) Charging profile of capacitors with capacitance values (0.5, 1, 5, and 10 μF) for the FS-TENG. (c) Photographs of using FS-TENG for powering digital thermometer, calculator, and LEDs*

To conduct a thickness-dependent investigation, BN-PC films with various printing strokes 1, 3, and 5 were done. The thickness of the film increases with the number of printing strokes. The thickness-dependent output performance of the FS-TENG device is shown in Figure 3.11 ((a) and (b)). From the observed voltage and short circuit current density, both are showing an increasing trend initially up to 3 strokes of printing and then decrease. The maximum performance was exhibited by the FS-TENG with BN-PC film with 3 strokes of printing. In comparison to the 1 and 5 strokes of printing, the generated voltage for 3 strokes printing FS-TENG is ~800 V and short-circuit current density is ~.78 mA/m^2. BN-PC films in FS-TENGs with 1 and 5 printing strokes exhibit an impressive output voltage of 715 V, and 650 V and J_{sc} of 0.72 mA/m^2, 0.70 mA/m^2, respectively. A similar trend of thickness-dependent output variations is available in literature.[50] In order to have a better understanding of how the BNNSs in composite structure affects BN-PC/PVP FS-TENG output enhancement, we have furnished TENG outputs with various weight percentages of BNNSs, which is shown in the Figure 3.11. Evidently, the output voltage 3.11(c) and current density 3.11(d) are improved significantly with increasing BNNSs concentration.
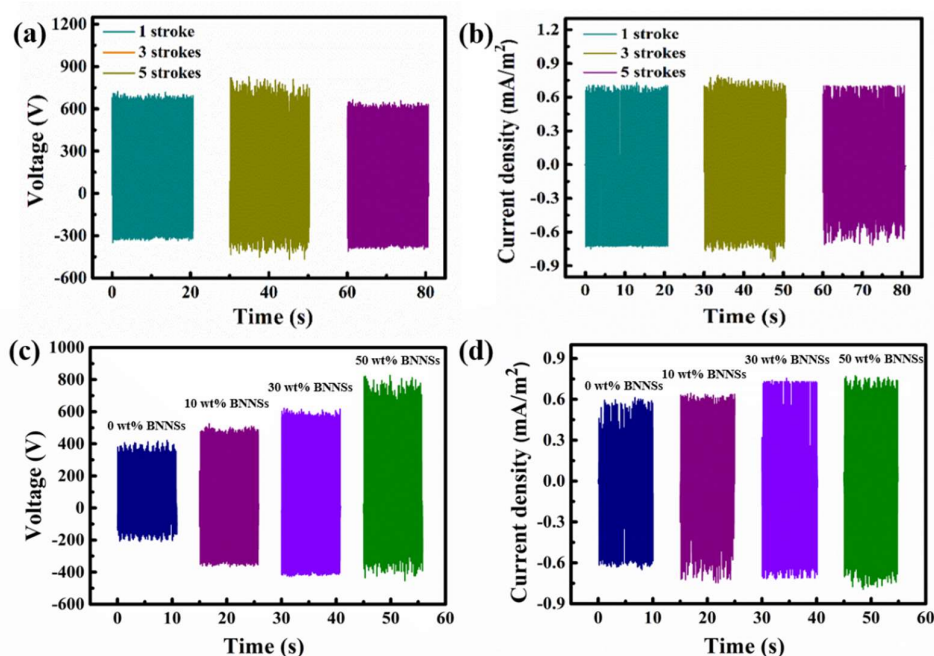
Figure 3.11: *(a) Thickness dependent V and (b) J_{sc} of BN-PC FS-TENG. (c) V and (d) J_{sc} of BN-PC/PVP FS- TENG with 0, 10, 30, and 50 wt% BNNSs*

Since the FS-TENG's practical implementation is focused on powering portable or wearable electronic gadgets, the capability of the FS-TENG to harvest bio-mechanical energy is to be investigated. For this, harvesting energy from biomechanical inputs such as the single finger, multiple fingers, and palm force are investigated and demonstrated. The output for all these are graphically represented in Figures 3.12(a) & (b). The output voltages developed from single finger tapping, multiple fingers tapping, and palm tapping was 400 V, 730 V, and 1150 V, respectively. Similarly, the corresponding short-circuit current density obtained are 0.32 mA/m^2, 1 mA/m^2, 1.5 mA/m^{2,} respectively. Here, the process where continuous tapping of the device attached to the palm generated comparably higher voltage and current than the single finger and multiple finger motions. This is primarily because the pressing force is much higher in palm tapping compared to others, which contributes to more area of contact. In addition to that, the long-term cyclic stability and adaptability of the fabricated device are very crucial for the practical environment.
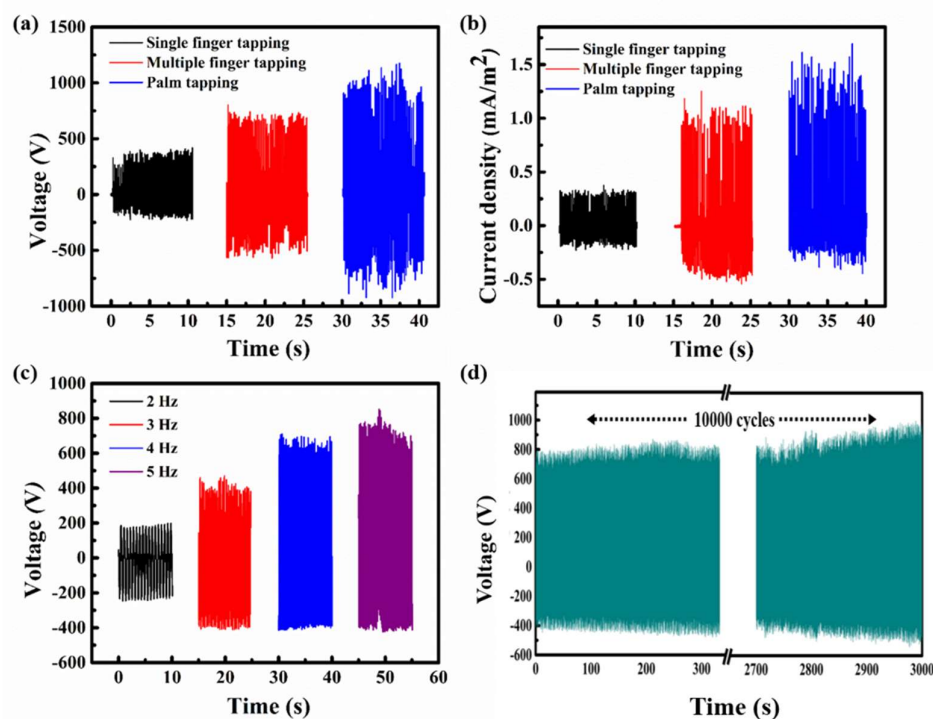
Figure 3.12: *(a) & (b) V & J$_{sc}$ from different human body movements (e.g., single finger contact, multiple fingers pressing, and palm pressing). (c) Frequency influence on the output voltage of FS-TENG. (d) Cyclic stability test for 10000 cycles*

Two confirmatory experiments, frequency-dependent output performance analysis, and a cyclic stability test have been carried out with the FS-TENG device using the force impactor. The influence of tapping frequency on the output voltage is shown in Figure 3.12(c). With increase in the working frequency of the force impactor, the output voltage linearly increases from 210 to 800 V with respect to the increase in frequency from 2 to 5 Hz. At a higher tapping frequency, external electrons in the device system can attain equilibrium in a faster way providing better performance.[51] The screen-printed BN-PC-based TENG showed good practical stability, which is verified by continuous press-release operation of 10000 cycles at 5 Hz. The generated output voltage of 800 V reproducible during the entire cycle of operation (Figure 3.12(d)).

A study of the influence of different parameters of TENG on the output performance is also systematically investigated by varying its area of contact and separation distance. Figure 3.13(a) and (b) shows the V and J$_{sc}$ values of the FS-TENG with three contact areas 1, 4, and 9 cm², constructed at a constant separation gap of 1 cm.
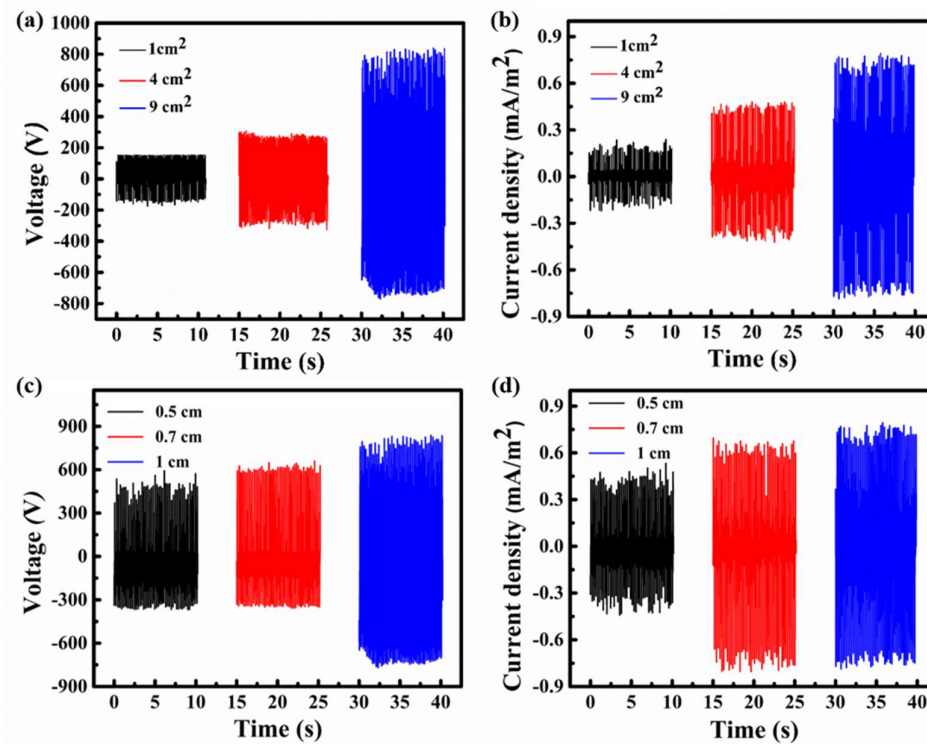
Figure 3.13: *(a) & (b) Comparison of the V and J$_{sc}$ measured from different contact areas of FS-TENG. (c) & (d) Dependence of V and J$_{sc}$ on the separation gap of TENG.*

From the figure, it can be seen that the device output increases significantly from 170 V to 800 V, with a proportionate increase in the contact area from 1 cm^2 to 9 cm^2. The increase in the output voltage can be due to the fact that more triboelectric charge accumulation occurs in large-area devices. In the same way, keeping the contact area at a constant value of 9 cm^2, dependence on separation distance was evaluated (Figures 3.13(c) and (d)). The V and J$_{sc}$ show a significant increase as a function of the separation gap. This increase in output voltage is mainly contributed from the lowering of its capacitance value. Whereas, short circuit current density directly depends on the velocity contribution which is more predominant than the inverse square dependence on the separation gap.[52] A higher speed of motion arises from the increase in the structure modulus of the supporting material, which contributes to the stress and recoiling speed of the system.[11,52,53]

3.4 Conclusions

In summary, we have demonstrated the development of a FS-TENG device, working in vertical CS mode for scavenging mechanical energy. The FS-TENG having an active surface area of 9 cm^2 and 1 cm separation distance, is fabricated using BN-PC-composite ink as tribonegative and PVP as tribopositive materials. The formulated BN-PC ink consists of BNNSs as filler, polycarbonate as binder and other thixotropy adjustment components. Under specific mechanical inputs, the electrical voltage and current density of the FS-TENG device were systematically analyzed and compared. The BN-PC-based FS-TENG can deliver an impressive voltage of ~800 V and current density of ~0.78 mA/m^2, under a mechanical force of ~10 N impacted at 5 Hz frequency. The peak value of power density was ~1.36 W/m^2, at a resistive load of 200 MΩ. These apparent results are significantly higher than the output results obtained from similar FS-TENG constructed using PC ink alone (without BNNSs filler). Interestingly, the power density of BN-PC-based FS-TENG showed ~7 times higher value than the FS-TENG without BNNSs. Charge trapping ability and higher surface contact area are the major contributing factors to the output enhancement of FS-TENG with BNNSs ink. The influence of various structural parameters like contact surface area of the tribo-active materials and separation distance on the output performance of FS-TENG were systematically studied. The output of the device showed a monotonic trend with the structural parameters, wherein the maximum output was observed for the device with a contact area of 9 cm^2 at a separation gap of 1 cm. Further, variations in the output of FS-TENG was studied using various biomechanical input forces, and additionally confirmed the cyclic stability of the device even after 10000 continuous cycles of operations. To demonstrate its practical use, the fabricated FS-TENG was utilized to power up commercial grade LEDs, digital thermometers, and calculators, where the mechanical impulse was derived from bio-mechanical movements.

3.5 References

(1) Jiao, P.; Matin Nazar, A.; Egbe, K.-J. I.; Barri, K.; Alavi, A. H. Magnetic Capsulate Triboelectric Nanogenerators. *Sci. Rep.* **2022**, *12* (1), 89.

(2) Zheng, S.; Wang, H.; Das, P.; Zhang, Y.; Cao, Y.; Ma, J.; Liu, S. F.; Wu, Z. Multitasking MXene Inks Enable High-Performance Printable Microelectrochemical Energy Storage Devices for All-Flexible Self-Powered Integrated Systems. *Adv. Mater.* **2021**, *2005449*, 1–10.

(3) B. S. Athira, Ashitha George, K. Vaishna Priya, U. S. Hareesh, E. B. G.; Kuzhichalil Peethambharan Surendran, and A. C. High-Performance Flexible Piezoelectric Nanogenerator Based on Electrospun PVDF-BaTiO3 Nanofibers for Self-Powered Vibration Sensing Applications. *ACS Appl. Mater. Interfaces* **2022**, *107339*, 39.

(4) Wu, Y.; Luo, Y.; Cuthbert, T. J.; Shokurov, A. V; Chu, P. K.; Feng, S.; Menon, C. Hydrogels as Soft Ionic Conductors in Flexible and Wearable Triboelectric Nanogenerators. *Adv. Sci.* **2022**, *2106008*, 1–24.

(5) Feng, P.; Xia, Z.; Sun, B.; Jing, X.; Li, H.; Tao, X.; Mi, H. Enhancing the Performance of Fabric-Based Triboelectric Nanogenerators by Structural and Chemical Modification. *ACS Appl. Mater. Interfaces* **2021**, *16916-16927*, 14.

(6) Wang, N.; Liu, Y.; Ye, E.; Li, Z.; Wang, D. Control Methods and Applications of Interface Contact Electrification of Triboelectric Nanogenerators : A Review. *Mater. Res. Lett* **2022**, *97-123*, 3.

(7) Joseph, A. M.; Nagendra, B.; Bhoje Gowd, E.; Surendran, K. P. Screen-Printable Electronic Ink of Ultrathin Boron Nitride Nanosheets. *Acs Omega* **2016**, *1220–1228*, 6.

(8) Lin, Y.; Chen, J.; Tavakoli, M. M.; Gao, Y.; Zhu, Y.; Zhang, D.; Kam, M.; He, Z.; Fan, Z. Printable Fabrication of a Fully Integrated and Self-Powered Sensor System on Plastic Substrates. *Adv. Mater.* **2019**, *1804285*, 1–9.

(9) Franco, M.; Motealleh, A.; Costa, C. M.; Hilliou, L.; Perinka, N.; Ribeiro, C.; Viana, J. C.; Costa, P.; Lanceros-mendez, S. Environmentally Friendly Conductive Screen-Printable Inks Based on N-Doped Graphene and Polyvinylpyrrolidone. *Adv. Eng. Mater.* **2021**, *2101258*, 1–11.

(10) A. T.; Seol, M.; Han, J.; Moon, D.; Yoon, K. J.; Hwang, C. S. Author ' s Accepted Manuscript All-Printed Triboelectric Nanogenerator. *Nano Energy* **2017**, *82-88*, 6.

(11) Salauddin, M.; Rana, S. M. S.; Sharifuzzaman, M.; Rahman, M. T.; Park, C.; Cho, H.;

Maharjan, P.; Bhatta, T.; Park, J. Y. A Novel MXene/Ecoflex Nanocomposite-Coated Fabric as a Highly Negative and Stable Friction Layer for High-Output Triboelectric Nanogenerators. *Adv. Energy Mater.* **2021**, *2002832*, 1.

(12) Xu, Y.; Schwab, M. G.; Strudwick, A. J.; Hennig, I. Screen-Printable Thin Film Supercapacitor Device Utilizing Graphene / Polyaniline Inks. *Adv. Energy Mater.* **2013**, *1035-1040*, 8.

(13) Chen, H.; Chen, S.; Zhang, Y.; Ren, H.; Hu, X.; Bai, Y. Sand-Milling Fabrication of Screen-Printable Graphene Composite Inks for High-Performance Planar Micro-Supercapacitors. *ACS Appl. Mater. Interfaces* **2020**, *56319-56329*, 50.

(14) Li, W.; Zhang, H.; Kagita, S.; Shamim, A. All Screen-Printed , Polymer-Nanowire Based Foldable Electronics for Mm-Wave Applications. *Adv. Mater. Technol.* **2021**, *2100525*, 11.

(15) Cao, R.; Pu, X.; Du, X.; Yang, W.; Wang, J.; Guo, H.; Zhao, S.; Yuan, Z.; Zhang, C.; Li, C.; Wang, Z. L. Screen-Printed Washable Electronic Textiles as Self-Powered Touch/Gesture Tribo-Sensors for Intelligent Human − Machine Interaction. *ACS Nano* **2018**, *5190-5196*, 6.

(16) Wen, D.; Liu, X.; Deng, H.; Sun, D.; Qian, H.; Brugger, J. Nano Energy Printed Silk- Fi Broin-Based Triboelectric Nanogenerators for Multi-Functional Wearable Sensing. *Nano Energy* **2019**, *104123*, 6.

(17) Zhang, D.; Xu, Z.; Yang, Z.; Song, X. High-Performance Flexible Self-Powered Tin Disulfide Nanoflowers/Reduced Graphene Oxide Nanohybrid-Based Humidity Sensor Driven by Triboelectric Nanogenerator. *Nano Energy* **2020**, *104251*, 6.

(18) Zhang, K.; Feng, Y.; Wang, F.; Yang, Z.; Wang, J. Two Dimensional Hexagonal Boron Nitride (2D-HBN): Synthesis, Properties and Applications. *J. Mater. Chem. C* **2017**, 11992–12022, 46.

(19) Wang, X.; Weng, Q.; Bando, Y.; Golberg, D. Functionalized Hexagonal Boron Nitride Nanomaterials : Emerging Properties and Applications Include the Controlled Synthesis. Chem. Soc. Rev. **2016**, *3989–4012*, 14.

(20) Chen, T.; Liu, Z.; Hu, X.; Zhao, G.; Qin, Z.; Tosin Aladejana, J.; Peng, X.; Xie, Y.; Wu, B. Fire-Resistant Plant Fiber Sponge Enabled by Highly Thermo-Conductive Hexagonal Boron Nitride Ink. *Chem. Eng. J.* **2022**, *132135*, 14.

(21) Zhu, X.; Ng, L. W. T.; Hu, G.; Wu, T.; Um, D.; Macadam, N.; Hasan, T. Hexagonal Boron Nitride Enhanced Optically Transparent Polymer Dielectric Inks for Printable Electronics.

Adv. Funct. Mater. **2020**, *2002339*, 31.

(22) Sci, J. V. Transistors with Graphene and Hexagonal Boron Nitride Inks Inkjet-Printed MoS$_2$ -Based Field-Effect Transistors with Graphene and Hexagonal Boron Nitride Inks. *J.Vac.Sci.Technol*. **2020**, *042206*, 4.

(23) Carey, T.; Cacovich, S.; Divitini, G.; Ren, J.; Mansouri, A.; Kim, J. M.; Wang, C.; Ducati, C.; Sordan, R.; Torrisi, F. Fully Inkjet-Printed Two-Dimensional Material Field-Effect Heterojunctions for Wearable and Textile Electronics. *Nat. Commun.* **2017**, *1202,* 1*.

(24) Moraes, A. C. M. De; Hyun, W. J.; Seo, J. T.; Downing, J. R.; Lim, J.; Hersam, M. C. Ion-Conductive , Viscosity-Tunable Hexagonal Boron Nitride Nanosheet Inks. *Adv. Funct. Mater.* **2019**, *1902245*, 39.

(25) Li, H.; Liu, S.; Li, X.; Wu, Z. S.; Liang, J. Screen-Printing Fabrication of High Volumetric Energy Density Micro-Supercapacitors Based on High-Resolution Thixotropic-Ternary Hybrid Interdigital Micro-Electrodes. *Mater. Chem. Front.* **2019**, *626–635*, 4.

(26) Li, H.; Li, X.; Liang, J.; Chen, Y. Hydrous RuO 2 -Decorated MXene Coordinating with Silver Nanowire Inks Enabling Fully Printed Micro-Supercapacitors with Extraordinary Volumetric Performance. *Adv. Energy Mater.* **2019**, *1803987,* 15.

(27) Sivan, A.; Chandran, A.; Kuzhichalil, S. MWCNT Ink with PEDOT : PSS as a Multifunctional Additive for Energy Efficient Flexible Heating Applications. *Appl. Mater. Today* **2021**, *100987*, 15.

(28) Marmur, A. Soft Contact : Measurement and Interpretation of Contact Angles. *Soft Matter* **2006**, *12–17*, 1.

(29) Hebbar, R. S.; Isloor, A. M.; Ismail, A. F. *Chapter 12 - Contact Angle Measurements*. *Membrane Characterization* **2017**, *219-255*, 1.

(30) Kumar, R.; Kamakshi; Kumar, M.; Awasthi, K. Functionalized Pd-Decorated and Aligned MWCNTs in Polycarbonate as a Selective Membrane for Hydrogen Separation. *Int. J. Hydrogen Energy* **2016**, *23057–23066*, 48.

(31) Bhavya, A. S.; Varghese, H.; Chandran, A.; Surendran, K. P. Massive Enhancement in Power Output of BoPET-Paper Triboelectric Nanogenerator Using 2D-Hexagonal Boron Nitride Nanosheets. *Nano Energy* **2021**, *10662*, 48.

(32) Parshin, A. M.; Gunyakov, V. A.; Zyryanov, V. Y.; Shabanov, V. F. Domain Structures in Nematic Liquid Crystals on a Polycarbonate Surface. *Int. J. Mol. Sci* **2013**, *16303-16320,* 8.

(33) Lago, E.; Toth, P.; Pugliese, G.; Solution blending preparation of

polycarbonate/graphene composite: boosting the mechanical and electrical properties *RSC Adv*. **2016**. *97931-97940,* 100.

(34) Kaleemulla, S.; Dhanumalayan, E.; Investigation of Structure , Dielectric and Thermal Properties of Hexagonal Boron Nitride Dispersed Polymer Blends. *J. Mater. Sci. Mater. Electron.* **2019**, *17459–17468*, 18.

(35) Nie, X.; Sang, X. Exfoliation of Hexagonal Boron Nitride Assisted with Hierarchical Ionic Fragments by Ball-Milling for Achieving High Thermally Conductive Polymer Nanocomposite. *Polym. Compos*. **2022**, *946–954*. 2.

(36) Hyun, W. J.; Secor, E. B.; Hersam, M. C.; Frisbie, C. D.; Francis, L. F. High-Resolution Patterning of Graphene by Screen Printing with a Silicon Stencil for Highly Flexible Printed Electronics. *Adv. Mater.* **2015**, 109–115, 1.

(37) Arapov, K.; Rubingh, E.; Abbel, R.; Laven, J.; De With, G.; Friedrich, H. Conductive Screen Printing Inks by Gelation of Graphene Dispersions. *Adv. Funct. Mater.* **2016**, *586–593*, 4.

(38) Kumar, B. R.; Rao, T. S. AFM studies on surface morphology , topography and texture of nanostructured zinc aluminum oxide thin films. *Dig. J. Nanomater. Biostructures* **2012**, *1881–1889*, 4.

(39) Qureshi, A.; Shah, S.; Pelagade, S.; Surface Modification of Polycarbonate by Plasma Treatment Surface Modification of Polycarbonate by Plasma Treatment. *J. Phys. Conf*. **2010**, *012108,* 4.

(40) Sattanathan, M.; Subramani, S.; Mohamed, K.; Devarajan, M. Synthesis and Characterization of Hexagonal Boron Nitride Coating on Polyethylene Terephthalate. *Iran. Polym. J.* **2019**, *969–976,* 11*.*

(41) Varghese, H.; Hakkeem, H. M. A.; Chauhan, K.; Thouti, E.; Pillai, S.; Chandran, A. A High-Performance Flexible Triboelectric Nanogenerator Based on Cellulose Acetate Nanofibers and Micropatterned PDMS Films as Mechanical Energy Harvester and Self-Powered Vibrational Sensor. *Nano Energy* **2022**, *107339*, 98.

(42) Garcia, C.; Trendafilova, I.; Guzman de Villoria, R.; Sanchez del Rio, J. Self-Powered Pressure Sensor Based on the Triboelectric Effect and Its Analysis Using Dynamic Mechanical Analysis. *Nano Energy* **2018**, *401–409*, 50.

(43) Varghese, H.; Chandran, A. A Facile Mechanical Energy Harvester Based on Spring Assisted Triboelectric Nanogenerators. *Sustain. Energy Fuels* **2021**. *5287-5294,* 20*.*

(44) Zhang, D.; Yu, L.; Wang, D.; Yang, Y.; Mi, Q.; Zhang, J. Multifunctional Latex/ Polytetrafluoroethylene-Based Triboelectric Nanogenerator for Self-Powered Organ-like Mxene/Metal-Organic Framework-Derived Cuo Nanohybrid Ammonia Sensor. *ACS Nano* **2021**, *2911–2919*, 2.

(45) Salauddin, M.; Rana, S. M. S.; Rahman, M. T.; Sharifuzzaman, M.; Maharjan, P.; Bhatta, T.; Cho, H.; Lee, S. H.; Park, C.; Shrestha, K.; Sharma, S.; Park, J. Y. Fabric-Assisted MXene/Silicone Nanocomposite-Based Triboelectric Nanogenerators for Self-Powered Sensors and Wearable Electronics. *Adv. Funct. Mater.* **2022**, *2107143,* 5.

(46) Kuang, H.; Li, Y.; Huang, S.; Shi, L.; Zhou, Z.; Gao, C.; Zeng, X.; Pandey, R.; Wang, X.; Dong, S. Piezoelectric Boron Nitride Nanosheets for High Performance Energy Harvesting Devices. *Nano Energy* **2021**, *105561*, 80.

(47) Liu, Y.; Ping, J.; Ying, Y. Recent Progress in 2D-Nanomaterial-Based Triboelectric Nanogenerators. *Adv. Funct. Mater.* **2021**, *2009994*, 17.

(48) Wang, N.; Liu, Y.; Ye, E.; Li, Z.; Wang, D. Control Methods and Applications of Interface Contact Electrification of Triboelectric Nanogenerators: A Review. *Mater. Res. Lett.* **2022**, *97–123*, 3.

(49) Seol, M.; Kim, S.; Cho, Y.; Byun, K.; Kim, H.; Kim, J.; Kim, S. K.; Kim, S.; Shin, H.; Park, S. Triboelectric Series of 2D Layered Materials *Adv. Mater* **2018.** *1801210,* 39*.

(50) Syamini, J.; Chandran, A. Mylar Interlayer-Mediated Performance Enhancement of a Flexible Triboelectric Nanogenerator for Self-Powered Pressure Sensing Application. **2023**.

(51) Kim, Y.; Wu, X.; Lee, C.; Oh, J. H. Characterization of PI / PVDF-TrFE Composite Nano Fi Ber-Based Triboelectric Nanogenerators Depending on the Type of the Electrospinning System. *ACS Appl. Mater. Interfaces* **2021**. *36967-36975,* 31.

(52) Varghese, H.; Chandran, A. Triboelectric Nanogenerator from Used Surgical Face Mask and Waste Mylar Materials Aiding the Circular Economy. *ACS Appl. Mater. Interfaces* **2021**. *51132-51140*, 43.

(53) Niu, S.; Liu, Y.; Wang, S.; Lin, L.; Zhou, Y. S.; Hu, Y.; Wang, Z. L. Theoretical Investigation and Structural Optimization of Single-Electrode Triboelectric Nanogenerators. *Adv. Funct. Mater.* **2014**, *3332–3340*, 22.

Chapter 4

Self-powered flexible triboelectric tactile sensor made of electrospun cellulose nanofibers and BNNS-based composite ink
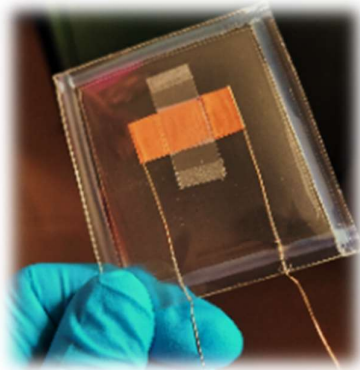
In this chapter, we developed a self–powered tactile sensor using two complimentary triboelectric materials; (i) screen-printed BNNSs composite ink on polymer substrate and (ii) electrospun cellulose acetate nanofibers. Low magnitude forces down to below 1 N could be sensed by this modified tactile sensor system.

4.1 Introduction

The power management issues of multi-dimensional sensor arrays could be resolved intelligently by assimilating the principle of alternate resources like triboelectric nanogenerators (TENGs).[1] These issues include installation, maintenance and management of these sensor networks in bleeding edge domains like intelligent sports, touch control, health care, security, and document management systems.[2] Prominent among the galaxy of sensors used to transform information from the physical world to digital format, includes capacitive sensing and other self-powered sensors. This type of sensing is highly suitable for facilitating human-machine interaction. The challenge before future electronics is to transform the capacitive touch sensors to be energy autonomous.[3]

Numerous studies have reported the application of TENG-based active sensors for human machine-interactions. For example, Pu *et al*. reported a super stretchable transparent tactile sensor system for touch or pressure sensing, which found applications in soft robotics, functional displays, electronic skins, and other areas.[4] This sensor system was developed by hybridizing two elastomers, one as electrification layer while ionic hydrogels like polyacrylamide-based hydrogel containing lithium chloride as the electrode layer. This sandwich-structured sensor system in single electrode mode could sense even a low input pressure. In 2020, Li *et al.* also reported a soft TENG-based triboelectric sensor array system that was realized *via* direct ink writing technology. In terms of voltage modulation, this array of sensors could recognize the touching outline of physical objects. Such printed arrays could find promising use in e-skin for soft robotics.[5] Yet another study has shown that instantaneous force sensing using flexible and ultrathin TENGs could sense force instantly without the need for additional power supply.[6] Such systems have profound applications including touch sensing in electronics that are sustainable and intelligent. In fact, touch sensors open up a plethora of innovative interaction methods in small-scale wearable electronics. Triboelectric nanogenerator-based touch sensors are one step toward self-powered sensors for the sustainable future.

The usability of green materials such as cellulose-based natural polymers into energy industry expands their application horizon. In addition to abundance and renewability, cellulose-based materials are lightweight, biodegradable, flexible, and mechanically strong. cellulose readily gains a positive charge by losing electrons, making

them a positive candidate for eco-friendly TENGs.[7] When positive cellulose material and a very negative triboelectric substance are combined properly in a TENG configuration, the triboelectric potential difference between the layers is found to be greatly improved.[8]

2D materials, can provide better output performance in TENGs due to their physical, chemical, and opto-electronic characteristics.[9] As seen in previous chapters, 2D h-BN can be employed in its hybrid/composite form to enhance the output performance of TENGs.[10] It is reasonable to expect that cellulose and h-BN based triboelectric pair with a sizable polarity difference, can guide to the realization of high-performance TENGs. Further, to increase the surface charge density in a contact-electrification phenomenon, triboelectric material surfaces are modified *via* suitable methods contributing to enhanced performance of the device.[11]

In the present investigation, we have introduced a novel flexible screen-printed TENG-based self-powered tactile sensor for touch detection. Screen-printed BNNSs polyvinyl pyrrolidone composite ink (BN-PVP) on BoPET substrate and surface-modified electrospun cellulose acetate (ES-CA) nanofibers, served as the two contact materials. This flexible TENG in vertical CS mode produced remarkable results of output voltage ~1200 V and short-circuit current density of 1.2 mA/m^2 respectively. Here the incorporation of 2D nanosheets in polymer matrix greatly improves the power output of the fabricated TENG. Further, a self-powered tactile sensor was fabricated for touch sensing with slight modifications on the TENG structure. Remarkably, the developed TENG-based tactile sensor was able to detect and distinguish apart ~0.05 N forces. The sensitivity achieved here is 3.98 V/N for comparably lower forces of less than 2N, whereas, for higher forces in the range of 2–10 N, it is found to be 1.843 V/N.

4.2 Experimental

4.2.1 Materials

Pristine h-BN (powder size ~1 μm and 98 % purity) is procured from Sigma-Aldrich. The binder polymer polyvinyl pyrrolidone (PVP) and cellulose acetate (CA) of average molecular weight Mn ~30,000 were also purchased from Sigma-Aldrich (India). DMF, a dispersing organic solvent, is acquired from HPLC (India). The substrate material Mylar® (BoPET) was received from DuPont, USA. Ethanol for printing was procured from

Merck Chemicals, India. All reagents and chemicals were used without further purification.

4.2.2 BN-PVP ink formulation

Liquid phase exfoliation of bulk h-BN in an organic solvent, DMF produced 2D BNNSs. These BNNSs were blended with polymer binder PVP and dispersant *via* a solution mixing process and continuous stirring, that converted the mixture to an ink (BN-PVP). Delaminated BNNSs and polymer in a 1:1 weight ratio were dispersed in 1 mL of organic solvent taken in a culture tube. Afterwards, the highly viscous dispersion was magnetically stirred for 12 hours at 700 rpm rotation speed. In this method, PVP plays a dual role; as polymer matrix for the composite as well as binder for the formulated ink. A similar procedure was also adopted for printing pure PVP without BNNSs.

4.2.3 Screen printing of triboelectric layer using BN-PVP ink

Highly viscous BN-PVP ink was screen-printed on a flexible substrate (BoPET) as shown in Figure 4.1, for casting a film suitable for the contact-separation device structure. Here a home-made nylon screen with predesigned square patterns was used for printing the composite ink. The first step in the printing process was to spread the rheology-controlled BN-PVP ink over the nylon-screen. Following this, the rubber squeegee moves horizontally over the screen surface, which pushes the ink to pass through the open pores of the screen. Consequently, the desired pattern was inscribed on the substrate surface that was placed under the screen at a specific snap-off distance.

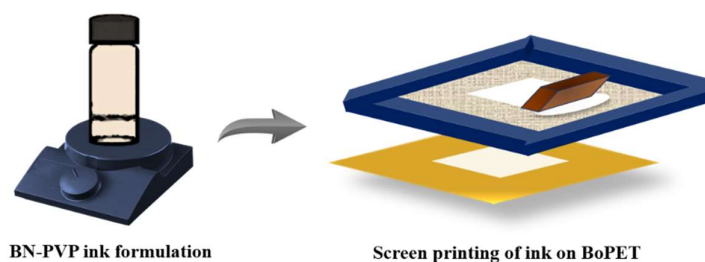BN-PVP ink formulation   Screen printing of ink on BoPET

Figure 4.1: *Schematic depicting the BN-PVP ink formulation and screen printing*

The number of strokes of printing can be varied to control the thickness of the printed film. The smooth-printed BN-PVP film on the BoPET substrate was then dried at 60 °C in an oven. This acts as the negative layer of the fabricated TENG. Through a similar

printing procedure, pure polymer PVP film (without adding BNNS filler) on BoPET substrate was also made for comparing the device outputs.

4.2.4 Preparation of electrospun-cellulose acetate (ES-CA) nanofiber mat

Fibers of CA was prepared using electrospinning technique. For this, we used a well-dispersed homogeneous solution of CA in a solvent mixture of acetone and DMF. The solution was loaded in the syringe of the spinner that has ~1 mm inner needle diameter. The CA solution's flow rate was set around 1 mL/h at a spinning voltage of 15 kV, to produce nanometer dimension fibers. During the electrospinning operation, a solution was continuously extruded towards the rotating collector drum covered with Al foil, which is kept 15 cm away from the nozzle tip. The spinning collector drum (rotation speed ~900 rpm) and needle tip were linked to the ground (negative) and positive electrodes, respectively. The CA nanofiber mat developed on the surface of Al foil, dried in a vacuum oven at 60 °C overnight.

4.2.5 BN-PVP/ES-CA TENG-based tactile sensor fabrication

The flexible BN-PVP/ES-CA TENG was designed in CS mode using a flexible BoPET substrate. BN-PVP ink printed on BoPET substrate and electrospun-cellulose acetate nanofiber mat on aluminum foil were taken as the two opposite contact materials for TENG. The polymer substrate, BoPET was employed as the support structure for assembling positive and negative TENG contact materials. The negative BN-PVP on the BoPET triboelectric layer with the back copper electrode layer and positive ES-CA layer on Al, were arranged on the rectangular flexible frame using suitable adhesives as two opposite materials. The two electrode layers, copper and Al, were arranged as sandwich layers between the rectangular framework and negative and positive triboelectric materials, respectively. Electrodes were connected to the measuring instruments through copper wires. With the help of a homemade continuous force impactor system, output performance of the fabricated device could be assessed. The BN-PVP/ES-CA TENG was converted into a tactile sensor by modifying the contact area and separation distance between the two triboelectric materials. The two contact materials of area 1 cm² were arranged with a spacing of 80 µm between them, while the spacing was maintained using a BoPET layer. The entire system was encapsulated within a protective layer using

vacuum sealing method. Figure 4.2 shows a schematic of the electrospinning procedure for creating a cellulose acetate nanofiber mat on aluminium foil and also the photograph of tactile sensor system with 1 cm x 1 cm area that employ ES-CA nanofibers and BN-PVP ink on BoPET.
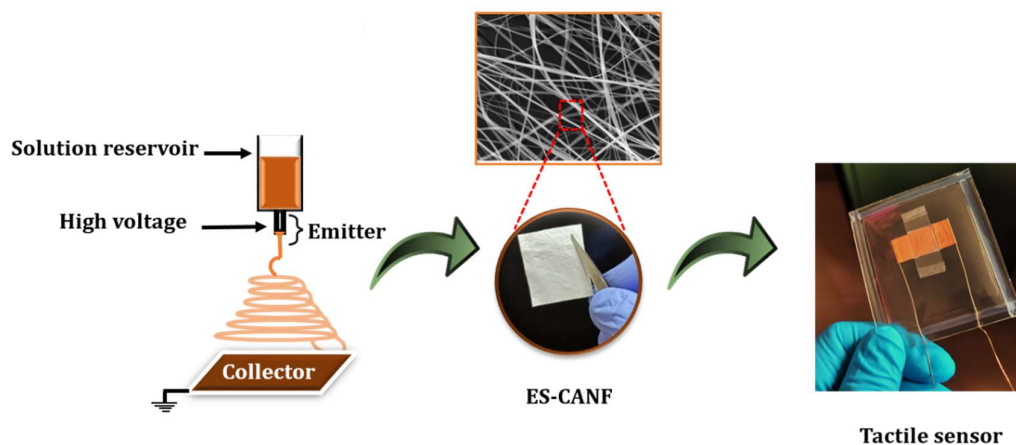
Figure 4.2: *Schematic illustration representing the electrospinning process for developing cellulose acetate nanofiber mat on an aluminum foil for fabricating a (1x1) area tactile sensor*

4.2.6 Characterization methods

Various characterization techniques were used to conduct a systematic examination of the developed BN-PVP ink, its coating on the polymer substrate, ES-CA nanofibers, BN-PVP/ES-CA TENG device, and also the BN-PVP/ES-CA TENG-based tactile sensor. The rheological characteristics like viscosity and visco-elastic properties of the BN-PVP composite inks were tested using Anton Paar Rheo plus 32 rheometer (Graz, Austria). This study examined viscosity of the inks at shear rates varying from 0 to 100 s^{-1}. The FT-IR spectra of the filler BN-PVP ink powder and pure polymer PVP were recorded using a Thermo Scientific Nicolet Magna 560 FTIR instrument (Massachusetts, USA). The contact angle measurement instrument DSA 30, KRUSS GmbH sessile drop method, Hamburg, Germany was used to investigate the wettability of ink on the substrate surface. Wide-angle X-ray diffraction (WAXD) measurements of the cellulose acetate nanofibers were performed using the Xeuss WAXS system (Xenocs, Grenoble, France). The surface of screen-printed BN-PVP films on a polymer substrate was investigated by scanning electron microscopy technique (SEM Zeiss EVO 50, Oberkochen, Germany) at the

accelerating voltage of 15 kV. A polarising optical microscope with a CCD camera was used to capture the optical images of the printed films (Leica, DM2700P, and Germany). All the electrical measurements of the fabricated PVP/ES-CA TENG with and without BNNSs were carried out using a Keithley 2450 source measurement unit system (Tektronix, USA). The device's short-circuit current was measured using a Stanford Research low-noise SR570 current preamplifier setup. A custom-made modified force impactor system that was used as the mechanical input source for the operation of TENG can impart ~10 N force with variable frequencies. Many custom-made resistors and capacitors were used to study the load-dependent output power density and charging profile of the developed TENGs. All the device characterizations were conducted at ambient conditions. A mark 10 force impactor (ESM303 stand and M5-50 gauge) was used to supply the input forces for analyzing the performance of the fabricated touch sensor.

4.3 Results and discussions

4.3.1 Rheology and structural analysis of BN-PVP ink

Precise control over the ink composition is necessary for the printing to be effective and to provide the desired qualities for the formulated inks. The even distribution of filler particles (BNNSs) in the vehicle system controls the ink's colloidal stability. The well dispersed filler in DMF solvent with suitable bio-compatible binder material PVP stabilizes the filler nanosheets in dispersion and modifies the rheology appropriate for screen printing.[12] The adherence of the ink to the substrate surface was also improved by PVP. The flow characteristics of the BN-PVP composite ink was carried out to investigate the printability of the prepared ink. As shown in Figure 4.3(a), the viscosity variation of the BN-PVP ink shows typical shear thinning behavior with the variation of shear rate from lower 1 s^{-1} to higher 100 s^{-1}. The inset Figure 4.3(a) is the photographic representation of the BN-PVP ink. This colloidal ink mixture displays an ideal pseudoplastic behaviour. In other words, the observed behavior is towards decreasing viscosity linearly as a function of shear rate. At a shear rate of 10 s^{-1}, it shows an ideal viscosity of about 3.2 Pa.s which is within the required range suitable for screen printing.[13] The viscoelastic property of the BN-PVP ink was further analyzed using the diagrams of storage modulus (G') and loss modulus (G''), as depicted in Figure 4.3(b). In the entire strain region, the storage modulus shows a decreasing trend compared to the

loss modulus values ($G'' > G'$). This implies that the BN-PVP ink possesses an ideal viscous liquid-like behaviour rather than a solid-like nature, that promotes solidification of the inks during printing.[14]

A comparison of FT-IR spectra of the pure polymer and the composite BN-PVP is displayed in Figure 4.3(c). A distinctive peak was seen at 1652 cm^{-1} in pure polymer PVP, corresponding to the C-O stretching vibrations. This recorded peak at 1652 cm^{-1} is also evident in the FT-IR spectra of the BN-PVP composite. The other peaks of pure polymer centered at 1423 cm^{-1} represent bending of the C-H bond, while the peak at 1288 cm^{-1} shows wagging vibrations of the CH$_2$.[15] These polymer peaks are absent in the BN-PVP sample because these vibrational lines and the peak for B-N in-plane stretching vibrations of the BNNSs overlap in this window. Two more peaks are seen in the BN-PVP composite in addition to the polymer peak at 1652 cm^{-1}. These peaks are located at 760 cm^{-1} and 1342 cm^{-1} representing the out of plane B–N–B bending vibration and B–N stretching vibration respectively.[16]
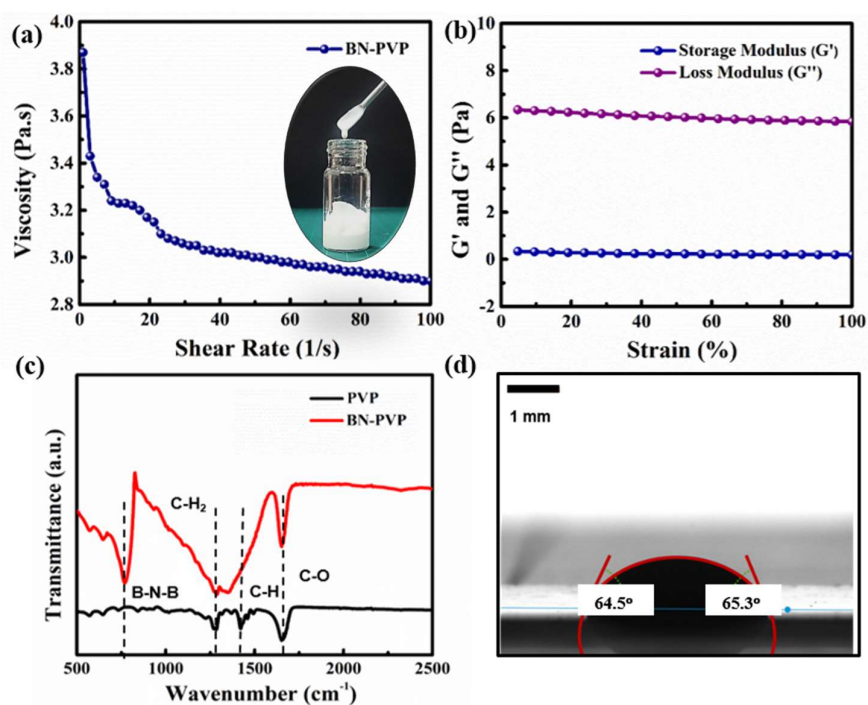

Figure 4.3: (a) Viscosity-shear rate study of the BN-PVP ink. The inset of figure 4.3(a) represents the photograph of the BN-PVP ink. (b) Storage modulus and loss modulus variation of BN-PVP ink with respect to shear strain. (c) Comparison of FTIR spectra PVP and BN-PVP and (d) the contact angle of the BN-PVP ink on BoPET substrate

The contact angle of the formulated BN-PVP ink was used to determine its wetting behaviour on the substrate surface as well as its interface characteristics. A static ink droplet on the BoPET surface with an average contact angle θ = 64.9° is shown in Figure 4.3(d). This contact angle formed on the substrate surface might provide vital information about its wetting nature. Lower contact angle values, almost equal to θ = 0°, signify more liquid spreading nature of the substrate surface. In other words, the substrate surface is more hydrophilic and has better wetting when θ is less than 90°. On the other hand, when θ is more than 90°, it is commonly referred to as hydrophobic in nature and has a poor wetting quality.[17,18] Better wettability and affinity of the BN-PVP ink on the BoPET substrate are shown by the recorded contact angle, which is 64.9°.

4.3.2 Morphology analysis of BN-PVP on BoPET

The representative SEM micrograph of the surface of screen-printed BN-PVP coating on BoPET is exhibited in Figure 4.4(a). The films produced by the screen printing process are homogeneous and have excellent ink distribution across the substrate. The PVP polymer matrix contains the exfoliated BNNSs embedded in it with minimal aggregation.
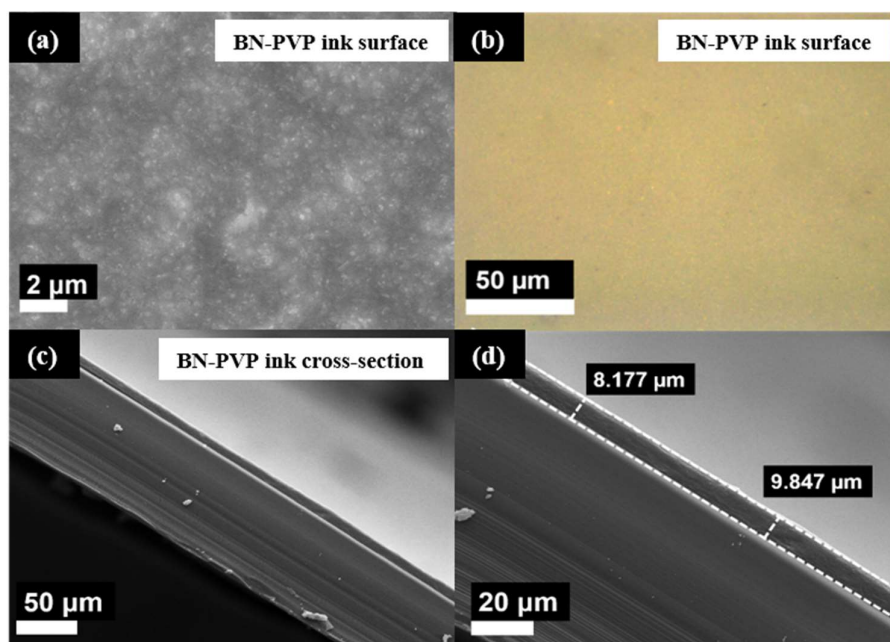
Figure 4.4: *(a) SEM image of BN-PVP ink surface on BoPET. (b) Optical image of BN-PVP ink surface on BoPET. (c) & (d) SEM cross-sectional images of BN-PVP ink on BoPET substrate showing the film's thickness*

As seen in Figure 4.4(b), the optical image of the BN-PVP ink surface is also displayed. The thickness evaluation of the BN-PVP coating on the substrate surface is shown in Figures 4.4(c) and (d). The average thickness of the films was measured to be approximately 9μm, where the film was formed after two screen printing cycles. The factors such as solid content contribution, viscosity of the ink and the number of printing strokes, determine the printed film thickness.[19,20]

4.3.3 Cellulose acetate nanofibers structure and morphology

Among the tested triboelectric materials, sustainable cellulose materials are considered triboelectrically positive.[21] The cellulose film-based triboelectric positive layer is a consequence of several procedural steps, including electrostatic spinning, laser treatment, and plasma treatment. These strategies may enhance the functionality of TENGs and operate more effectively.[22] As a positive TENG material, ES-CA nanofibers were developed in this study.

Figure 4.5: *(a) FT-IR spectra and (b) WAXD pattern of ES-CA nanofibers. Similarly, the (c) SEM micrograph showing the ES-CA nano fibers and (d) the optical image of ES-CA nanofibers on Al foil are represented*

The FT-IR spectra of ES-CA nanofibers in Figure 4.5(a) shows strong characteristic absorption peaks at 1751 cm^{-1} and 1240 cm^{-1}. These peaks arise as a result of C=O (carbonyl) stretching vibrations and acetyl C-O stretching respectively. The additional peak observed at 1052 cm^{-1} is also due to the C-O stretching vibrations.[23]

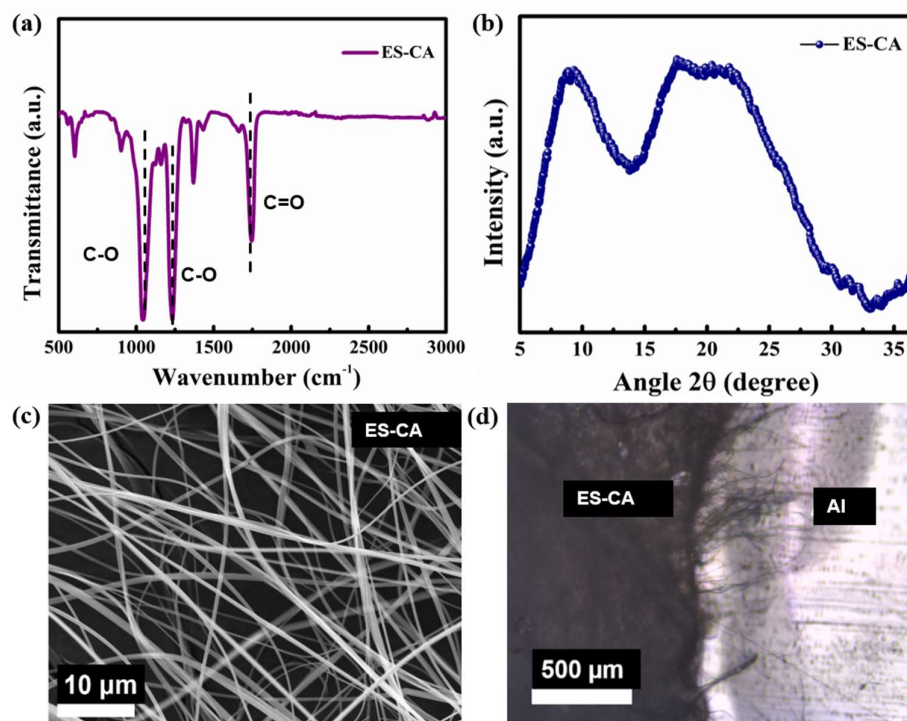The less sharp, comparatively weak intensity peaks in the WAXD pattern of ES-CA nanofibers, is seen in Figure 4.5 (b). This suggests that the structure is amorphous and lacks a regular molecular structure.[24] SEM micrograph of the prepared cellulose acetate nanofibers from the electrospinning method is included in Figure 4.5(c). From these images, it can be seen that thin nanofibers with varying widths and lengths, do not form any beads. Its smooth surfaces, which indicate the purity of the fibers generated, may be single or joined to many sections. The optical image of the ES-CA nanofibers on Al substrate is represented in Figure 4.5(d).

4.3.4 Performance of BN-PVP/ES-CA TENG

The BN-PVP/ES-CA flexible TENG was developed, using ES-CA nanofibers as the positive triboelectric layer with a very positive triboelectric polarity and correspondingly BNNSs embedded PVP polymer with a negative triboelectric polarity as the opposite contact layer. ES-CA nanofibers with higher specific surface area and porosity could provide better mechanical contact during the device operation, which enhanced the magnitude of the induced triboelectric charges.[25] In addition to that, the charge trapping nature resulted by the inclusion of BNNSs as the filler material for the polymer-based ink, further improved the TENG output by confining more generated tribocharges on the surface. The presence of 2D BNNSs in the BN-PVP composite structure also transformed the surface charge potential to a larger negative value, which resulted in a significant triboelectric potential difference between the two top and bottom contact layers.[26,27]

Figure 4.6 schematically illustrates the basic working mechanism of the BN-PVP/ES-CA TENG. This device uses an ES-CA nanofibers mat as the positive layer and BN-PVP ink on BoPET substrate as the negative layer, which are arranged in a CS mode configuration. The forced contact generates a collection of equal-dense opposite charges between the two contacting triboelectric layers. When the force is released, the separation between triboelectric layers creates an electrical potential difference, in order to maintain an equilibrium, it drives the flow of electrons from the top electrode to the bottom one

owing to electrostatic induction. As a result, an instantaneous current flow is observed in the external circuit. The external circuit allows the flow of electrons to move back and forth, resulting in an alternating electrical output, due to the sequential operation of pressing and releasing.[28]
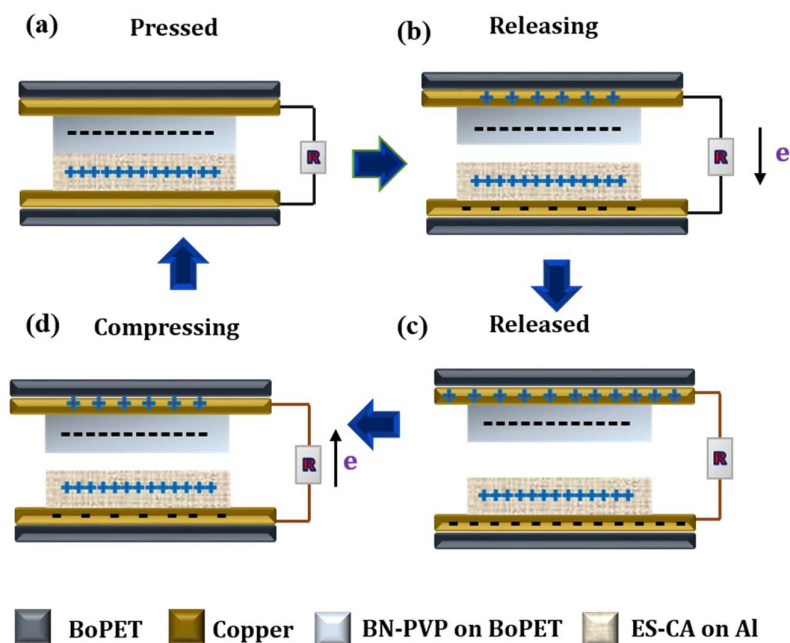
Figure 4.6: Schematic representation of the operation of flexible BN-PVP/ES-CA TENG in CS mode configuration. (a) Initial contact stage, (b) separation stage, (c) separated stage of saturation, and (d) further contacting stage

To examine the mechanical energy harvesting performance of the BN-PVP/ES-CA TENG, a specifically modified force impactor setup was used. The electrical measurements of the TENG, having a 9 cm^2 area with 10 mm gap was analyzed. The output voltage and current density comparison plots are shown in Figures 4.7 (a) & (b), which exhibit an improved triboelectric performance by the introduction of BNNSs, which may have attributed to the charge-trapping nature of 2D nanomaterials in its composite structure.[10] The flexible screen-printed TENG employing BN-PVP on BoPET and ES-CA nanofibers has generated a massive output voltage of 1200 V and a current density of 1.2 mA/m^2, respectively. This fabulous result is significantly much greater than the PVP/ES-CA TENG without BNNSs. Specifically, PVP/ES-CA TENG only yields an output voltage of 180 V and a current density of 0.23 mA/m^2 respectively.

From the impedance matching experiments, the power densities of both PVP/ES-CA TENG and BN-PVP/ES-CA TENG were investigated by using different resistors with varying resistance values, as shown in Figures 4.7(c) and (d) respectively. With increasing resistance, the BN-PVP/ES-CA TENG's output voltage progressively rises to a maximum of 1200 V. From the load-matching study, output power initially increases and then decreases. The calculated instantaneous power density of the BN-PVP/ES-CA TENG on external load reaches a maximum of 1.4 W/m2 at 200 MΩ resistance condition is shown in Figure 4.7(d). This observed power density is more than 100 times higher than the power density of 0.015 W/m2 for PVP/ES-CA TENG represented in Figure 4.7(C). It is obvious that small-scale electronic devices can be powered by this high output power.
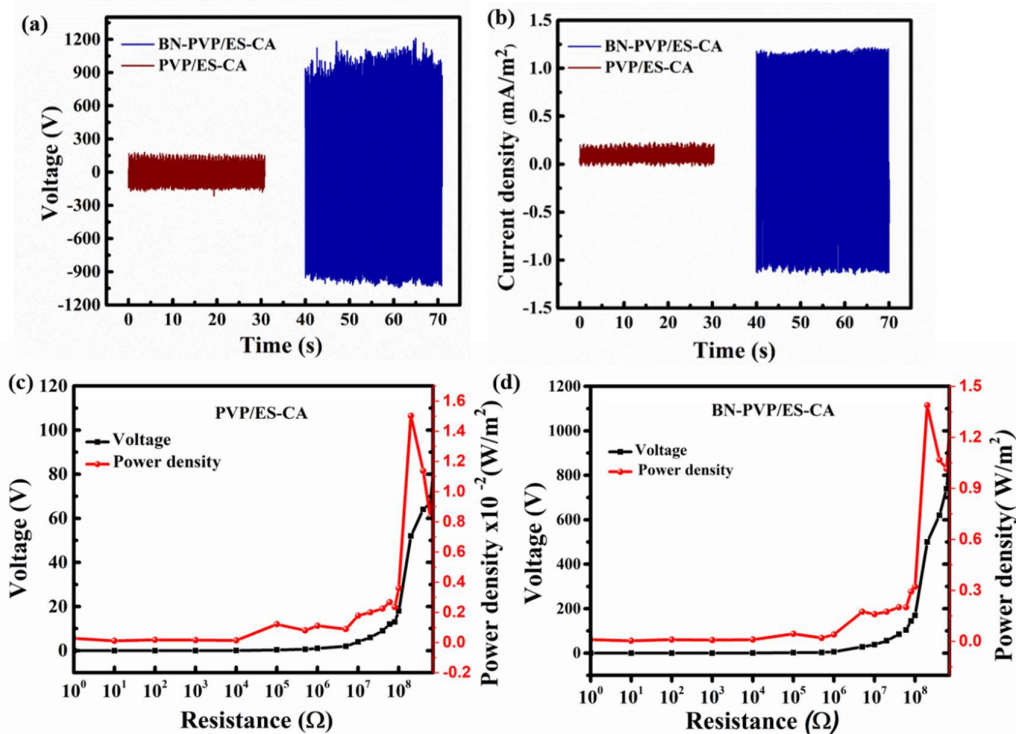
Figure 4.7: *(a) Output voltage comparison of PVP/ES-CA & BN-PVP/ES-CA TENG having device area 9 cm2. (b) Current density comparison of PVP/ES-CA & BN-PVP/ES-CA TENG. (c) Power density of PVP/ES-CA TENG without BNNSs in polymer matrix with varying load resistance. (d) Power density of BN-PVP/ES-CA TENG*

Figure 4.8(a) depicts the capacitor charging curves *via* a bridge rectifier by BN-PVP/ES-CA TENG, utilizing various capacitors with capacitance values of 0.5 µF, 1 µF, 5 µF, and 10 µF. For capacitors with higher capacitance values, longer charging times are needed. The BN-PVP/ES-CA TENG could charge the above capacitors to an adequate level which is good enough to power handheld electronic devices and sensor units. Regarding the relationship between TENG's output characteristic on the input frequency, Figure 4.8(b) illustrates how the output voltage of the fabricated TENG device varies in frequency. It shows significant enhancement as the frequency increases from a lower to higher value. Since the maximum output is recorded at 5 Hz frequency, all other subsequent measurements of the BN-PVP/ES-CA TENG were conducted under 5 Hz frequency. The durability analysis of the BN-PVP/ES-CA TENG was further conducted by elongated cycles of operation. Almost 12000 cycles of contact and separation movement produce stable output without any degradation. The durability analysis of the BN-PVP/ES-CA TENG is represented in Figure 4.8(c).
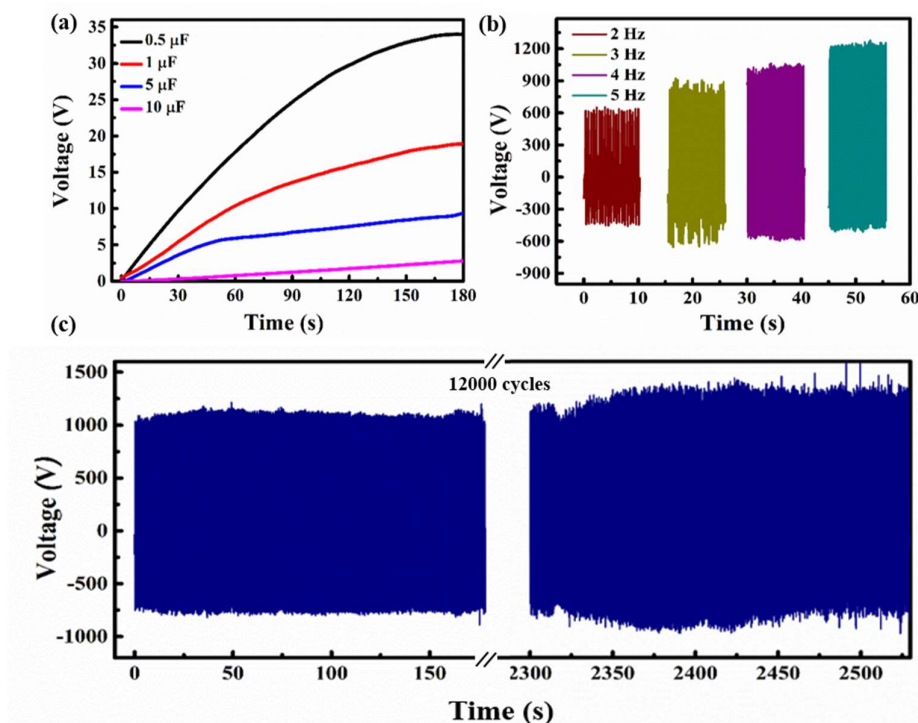
Figure 4.8: *(a) Analysis of BN-PVP/ES-CA TENG capacitor charging profile with different capacitors of varying capacitances. (b) Analysis of the output voltage of BN-PVP/ES-CA TENG with respect to frequency. (c) Durability study of BN-PVP/ES-CA TENG after 12000 cycles of device operation.*

Figures 4.9(a) and (b) represent the variation of output voltage and short-circuit current density of BN-PVP/ES-CA TENG under diverse magnitudes of biomechanical forces. These results show a significant increment in the intensity of the applied forces. The impact of force is obviously higher for palm pressing compared to single-finger tapping and multiple-finger tapping.
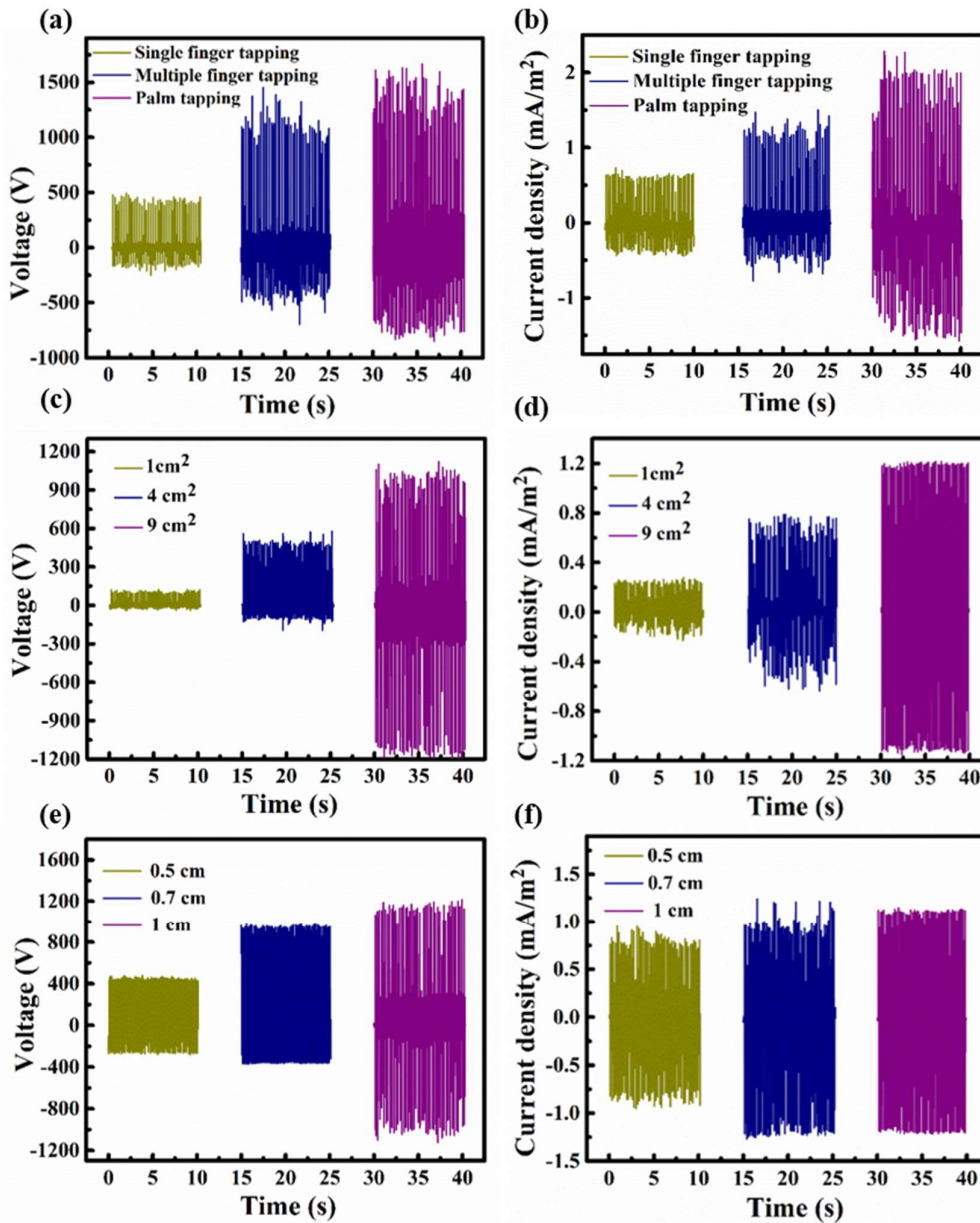
Figure 4.9: *(a) & (b) Output voltage and current density of BN-PVP/ES-CA TENG under various biomechanical pressures from pressing with a single finger, several fingers, and the palm. (c) & (d) Output voltage & current density of BN-PVP/ES-CA TENG with varying contact areas. (e) & (f) Output voltage & current density of BN-PVP/ES-CA TENG with different separation gaps*

Correspondingly, the output results are also considerably higher for palm pressing. Relatively inferior results were obtained for single-finger pressing. The higher impact force can provide better surface contact between the triboelectric materials and the output will be higher.[31] As shown, an output voltage of 1640 V and short-circuit current density of 2 mA/m^2 were obtained in the palm pressing condition which well above that for single-finger (500 V and 0.66 mA/m^2) and multiple-finger tapping (1300 V and 1.4 mA/m^2). Yet another variable is the triboelectric materials contact area that was shown to influence the output performance of BN-PVP/ES-CA TENG. This was investigated by systematically creating TENGs with triboelectric layers of constant separation gaps but varying contact areas of 1, 4, and 9 cm^2. Proportionate variations observed in output voltage and short circuit current density as a function of the device's contact area are depicted in Figures 4.9(c) and (d). As expected, enhanced charge transfer and surface charges are responsible for the observed improvement in the device performance.[32,33] For example, the voltage outputs of devices with contact areas 1, 4, and 9 cm^2 are 110 V, 520 V, and 1200 V respectively. The corresponding current densities are 0.27 mA/m^2, 0.8 mA/m^2, and 1.2 mA/m^2. In a similar way, to examine the influence of separation gap on the device output, a series of TENGs were built with a constant contact area of 9 cm^2 with various separation gaps (0.5 cm, 0.7 cm, and 1 cm). Figures 4.9(e) and (f) illustrates the fluctuation in output voltage and short-circuit current density of these BN-PVP/ES-CA TENGs with various separation gaps. Both the voltage and current density show an increasing trend with the separation gap also, and the maximum voltage of the device (~1200 V), was achieved with a 10 mm separation between the contact layers.

4.3.5 BN-PVP/ES-CA TENG as a self-powered tactile sensor

The force-sensitive study of the present BN-PVP/ES-CA TENG demonstrates its exceptional potential as a self-powered tactile sensor for touch-sensing applications. To investigate the application of the fabricated device for pressure sensing, the BN-PVP/ES-CA TENG's structural configuration was suitably modified by decreasing the contact materials area to 1 cm^2 and the separation gap to approximately 85 μm. The TENG-modified self-powered tactile sensor is displayed as the inset image of Figure 4.10(a) and the experimental setup is in Figure 4.10(b). To examine the sensitivity of the tactile sensor, a different magnitude of forces ranging from 0.05 N to 10N with slow movement

speeds, have been applied to the device. It is discovered that the BN-PVP/ES-CA tactile sensor output voltage is clearly force-sensitive. Figure 4.10(a) indicates the output voltage variation produced by the tactile sensor under different pressure conditions. These results indicate the triboelectric sensor's linear dependence on force and also its ability to detect very minute forces. This linear trend can be explained by the more effective surface contact between the triboelectric materials at higher force conditions, which improve its output results.
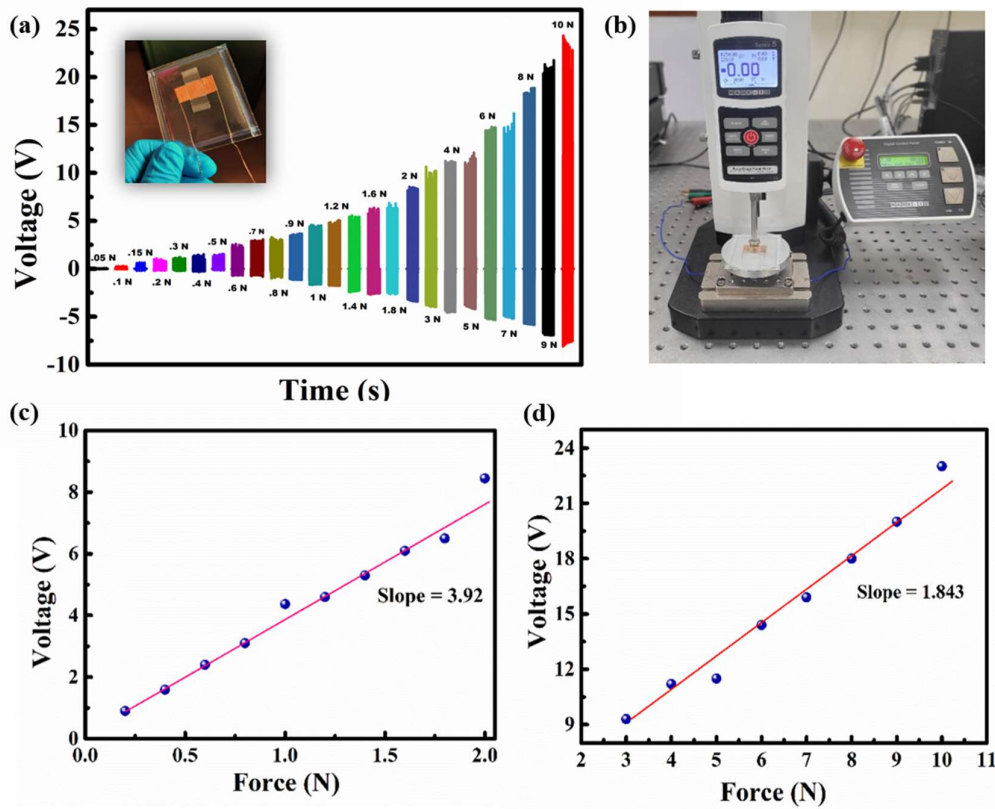
Figure 4.10: *Tactile sensing performance of the BN-PVP/ES-CA TENG based tactile sensor. (a) Output voltage variation with respect to applied pressure ranging from 0.05N to 10N. (b) Photographic image of the Mark-10 digital force gauge set-up used for studying tactile sensor performance of the device, and the sensitivity of the tactile sensor in the force ranges of (c) 0.05 N to 2N as well as from (d) 2N to 10N*

The observed resolution is ~0.05 N for the triboelectric tactile sensor in the current experimental design. As the force changes from 0.05 N to 2 N, the tactile sensor's output voltage varies linearly from millivolts to 9 V. Figure 4.10(c) illustrates the corresponding sensitivity in this lower force region, which is 3.98 V/N. In the higher force

range from 2 N to 10 N, a similar trend can be seen. At 10 N force, the maximum voltage could reach up to 23 V, and the observed sensitivity is 1.843 V/N, as shown in Figure 4.10(d). The tactile sensor's sensitivity is higher in the lower force regime because there is a greater shift in the creation of triboelectric charges in this lower force regime. As the force increases, the device reaches a saturation point and sensitivity decreases thereafter. On the contrary, in low-pressure situations, the developed BN-PVP/ES-CA tactile sensor is ideal to detect even the smallest force variations with exceptional sensitivity.[29,30]

4.4 Conclusions

In conclusion, this work package demonstrates the design and realization of a flexible TENG for biomechanical energy harvesting and also for tactile sensing. In this journey, electrospun cellulose acetate (ES-CA) nanofibers and screen-printed BNNSs composite ink (BN-PVP) on BoPET substrate were used as the positive and negative trioactive materials respectively. Ours is an improvised design with a 10 mm separation gap and 9 cm^2 contact area that yielded an impressive result of ~1200 V as the output voltage and 1.2 mA/m^2 as the short-circuit current density. The resultant peak power density could go up to 1.4 W/m^2, for a 3 cm × 3 cm area device. The device performance is comparably much higher than a similar PVP/ES-CA TENG constructed using PVP alone (without 2D nanosheets). Specifically, the power density of BN-PVP/ES-CA TENG is over 100 times better than the reference device without 2D fillers (PVP/ES-CA TENG). The new device is flexible and durable for long-term operations, making it a suitable practical choice for powering wearable and portable devices. The high power delivering capability of the TENG could be translated into a self-powered sensitive tactile sensor. For this, a BN-PVP/ES-CA based touch sensor was fabricated, for detecting input forces of very low magnitude (0.05 N). Remarkably, the low force sensitivity of the sensor is 3.98 V/N, whereas, for comparably higher forces (2–10 N), it is found to be 1.843 V/N. In brief, innovative material design and device architecture lead to the development of a flexible high energy TENG and tactile sensor, which offers a viable solution towards energy autonomous wearable devices.

4.5 References

(1) Zhou, Y.; Shen, M.; Cui, X.; Shao, Y.; Li, L.; Zhang, Y. Triboelectric Nanogenerator Based Self-Powered Sensor for Artificial Intelligence. *Nano Energy* **2021**, *84*, 105887.

(2) Zhou, Q.; Pan, J.; Deng, S.; Xia, F.; Kim, T. Triboelectric Nanogenerator-Based Sensor Systems for Chemical or Biological Detection. *Adv. Mater.* **2021**, *2008276*, 1–21.

(3) Zuk, S.; Pietrikova, A.; Vehec, I. Capacitive Touch Sensor. *Microelectron. Int.* **2018**, *3*, 153–157.

(4) Pu, X.; Liu, M.; Chen, X.; Sun, J.; Du, C.; Zhang, Y.; Zhai, J.; Hu, W.; Wang, Z. L. Ultrastretchable, Transparent Triboelectric Nanogenerator as Electronic Skin for Biomechanical Energy Harvesting and Tactile Sensing. *Sci. Adv.* **2017**, *3*, 1–11.

(5) Li, H.; Fang, X.; Li, R.; Liu, B.; Tang, H.; Ding, X.; Xie, Y. All-Printed Soft Triboelectric Nanogenerator for Energy Harvesting and Tactile Sensing. *Nano Energy* **2020**, *78*, 105288.

(6) Chen, S. W.; Cao, X.; Wang, N.; Ma, L.; Zhu, H. R.; Willander, M.; Jie, Y.; Wang, Z. L. An Ultrathin Flexible Single-Electrode Triboelectric- Nanogenerator for Mechanical Energy Harvesting and Instantaneous Force Sensing. *Adv. Energy Mater.* **2016**, *7,* 1601255.

(7) Niu, Z.; Cheng, W.; Cao, M.; Wang, D.; Wang, Q.; Han, J.; Long, Y.; Han, G. Recent Advances in Cellulose-Based Flexible Triboelectric Nanogenerators. *Nano Energy* **2021**, *87*, 106175.

(8) Shi, K.; Zou, H.; Sun, B.; Jiang, P.; He, J.; Huang, X. Dielectric Modulated Cellulose Paper/PDMS-based Triboelectric Nanogenerators for Wireless Transmission and Electropolymerization Applications. *Adv. Funct. Mater.* **2020**, *30* (4), 1904536.

(9) Liu, Y.; Ping, J.; Ying, Y. Recent Progress in 2D-Nanomaterial-Based Triboelectric Nanogenerators. *Adv. Funct. Mater.* **2021**, *2009994*, 1–16.

(10) Khandelwal, G.; Maria Joseph Raj, N. P.; Kim, S. J. Materials Beyond Conventional Triboelectric Series for Fabrication and Applications of Triboelectric Nanogenerators. *Adv. Energy Mater.* **2021**, *11* (33), 1–32.

(11) Kim, D. W.; Lee, J. H.; Kim, J. K.; Jeong, U. Material Aspects of Triboelectric Energy Generation and Sensors. *NPG Asia Mater.* **2020**.*12* (1), 6.

(12) Joseph, N.; Varghese, J.; Sebastian, M. T. Curable Polyaniline Nanofiber Based Inks. *J. Mater. Chem. C* **2016**, *4*, 999–1008.

(13) Tang, X.; Wu, K.; Qi, X.; Kwon, H.; Wang, R.; Li, Z.; Ye, H.; Hong, J.; Choi, H. H.; Kong, H.; Lee, N.; Lim, S.; Jeong, Y. J.; Kim, S. Screen Printing of Silver and Carbon Nanotube Composite Inks for Flexible and Reliable Organic Integrated Devices. *ACS Appl. Nano*

Mater. **2022**. *5* (4), 4801-4811.

(14) Li, H.; Li, X.; Liang, J.; Chen, Y. Hydrous RuO2- Decorated MXene Coordinating with Silver Nanowire Inks Enabling Fully Printed Micro-Supercapacitors with Extraordinary Volumetric Performance. *Adv. Energy Mater.* **2019**, *1803987*, 1–13.

(15) Samuel, E. J. J.; Sathiyaraj, P.; Deminskii, M. A.; Konina, K. M. Synthesis of Polyvinylpyrrolidone (PVP)- Green Tea Extract Composite Nanostructures Using Electrohydrodynamic Spraying Technique. *Mater. Sci. Eng.* **2017,** *1*, 012043.

(16) Hassan, M. I. J.; Haider, M. I. J.; Hamid, A. U.; Ikram, I. S. M.; Qumar, A. R. U. 2D Chemically Exfoliated Hexagonal Boron Nitride (HBN) Nanosheets Doped with Ni : Synthesis, Properties and Catalytic Application for the Treatment of Industrial Wastewater. *Appl. Nanosci.* **2020**. *10*, 3525-3528.

(17) Gru, M.; Waugh, D. G.; Lawrence, J.; Langer, N.; Scholz, D. On the Droplet Size and Application of Wettability Analysis for the Development of Ink and Printing Substrates. *Langmuir* **2019**. *35* (38), 12356-12365.

(18) Luca, G. De; Amendola, E.; National, I. Surface Modification and Adhesion Improvement of Polyester Films. *Open Chem. J.* **2012**. *11* (1), 35-45.

(19) Franco, M.; Motealleh, A.; Costa, C. M.; Hilliou, L.; Perinka, N.; Ribeiro, C.; Viana, J. C.; Costa, P.; Lanceros-mendez, S. Environmentally Friendly Conductive Screen-Printable Inks Based on N-Doped Graphene and Polyvinylpyrrolidone. *Adv. Eng. Mater.* **2022**, *2101258*, 1–11.

(20) Ju, J.; Zhao, Z.; Du, X.; Sun, X.; Liu, J.; Li, W. Thermally Conductive and Anti-Corrosive Epoxy Composite Coatings by Synchronously Incorporating Boron Nitride/Graphene Fillers and Polyvinyl Pyrrolidone. *Ceram. Int.* **2023**, *49* (17), 28854–28863.

(21) Song, Y.; Shi, Z.; Hu, G.H.; Xiong, C.; Isogai, A.; Yang, Q.; Recent advances in cellulose-based piezoelectric and triboelectric nanogenerators for energy harvesting: a review. *J. Mater. Chem. A* **2021**. *9* (4), 1910-1937.

(22) Zhou, J.; Wang, H.; Du, C.; Zhang, D.; Lin, H.; Chen, Y.; Xiong, J. Cellulose for Sustainable Triboelectric Nanogenerators. *Adv. Energy Sustainability Res.* **2022**. *3* (5), 2100161.

(23) Rahmawati, F.; Fadillah, I.; Mudjijono, M. Composite of Nano-TiO2 with Cellulose Acetate Membrane from Nata de Coco (Nano-TiO2/CA (NDC)) for Methyl Orange Degradation. *J. Mater. Environ. Sci* **2017**, *8* (1), 289–297.

(24) Varghese, H.; Hakkeem, H. M. A.; Chauhan, K.; Thouti, E.; Pillai, S.; Chandran, A. A High-Performance Flexible Triboelectric Nanogenerator Based on Cellulose Acetate Nanofibers and Micropatterned PDMS Films as Mechanical Energy Harvester and Self-Powered Vibrational Sensor. *Nano Energy* **2022**, *98*, 107339.

(25) Cheon, S.; Kang, H.; Kim, H.; Son, Y.; Lee, J. Y.; Shin, H.; Kim, S.; Cho, J. H. High-Performance Triboelectric Nanogenerators Based on Electrospun Polyvinylidene Fluoride–Silver Nanowire Composite Nanofibers. *Adv. Funct. Mater.* **2018**, *1703778*, 1–7.

(26) Bhavya, A. S.; Varghese, H.; Chandran, A.; Surendran, K. P. Massive Enhancement in Power Output of BoPET-Paper Triboelectric Nanogenerator Using 2D-Hexagonal Boron Nitride Nanosheets. *Nano Energy* **2021**, *90*, 106628.

(27) Zheng, Y.; Cheng, L.; Yuan, M.; Wang, Z.; Zhang, L. An Electrospun Nanowire-Based Triboelectric Nanogenerator and Its Application in a Fully Self-Powered UV Detector. *Nanoscale* **2014**, *6* (14), 7842–7846.

(28) Bera, B.; Wang, K.; Bera, B. Literature Review on Triboelectric Nanogenerator Related Papers Literature Review on Triboelectric Nanogenerator. *Imperial Journal of Interdisciplinary Research* **2016***, 2* (10)*, 1263-1271.*

(29) Varghese, H.; Abdul, H. M.; Farman, M.; Thouti, E.; Pillai, S.; Chandran, A. Self-Powered Flexible Triboelectric Touch Sensor Based on Micro-Pyramidal PDMS Films and Cellulose Acetate Nanofibers. *Results Eng.* **2022**, *16*, 100550.

(30) Syamini, J.; Chandran, A. Mylar Interlayer-Mediated Performance Enhancement of a Flexible Triboelectric Nanogenerator for Self-Powered Pressure Sensing Application. *ACS Appl. Electron. Mater* **2023**. *5* (2), 1002-1012.

(31) Ko, Y. H.; Nagaraju, G.; Lee, S. H.; Yu, J. S. PDMS-Based Triboelectric and Transparent Nanogenerators with ZnO Nanorod Arrays. *ACS Appl. Mater. Interfaces.* **2014** *6* (9), 6631-6637.

(32) Varghese, H.; Chandran, A. Triboelectric Nanogenerator from Used Surgical Face Mask and Waste Mylar Materials Aiding the Circular Economy. *ACS Appl. Mater. Interfaces.* **2021**. *13* (43), 51132-51140.(33) Gomes, A.; Rodrigues, C.; Pereira, A. M.; Ventura, J. Influence of Thickness and Contact Area on the Performance of PDMS-Based Triboelectric Nanogenerators. *arXiv preprint arXiv* **2018** , 2, 1–7.

Chapter 5

Flexible TENG using hexagonal boron nitride aerogel and ethyl cellulose on ITO-PET substrate
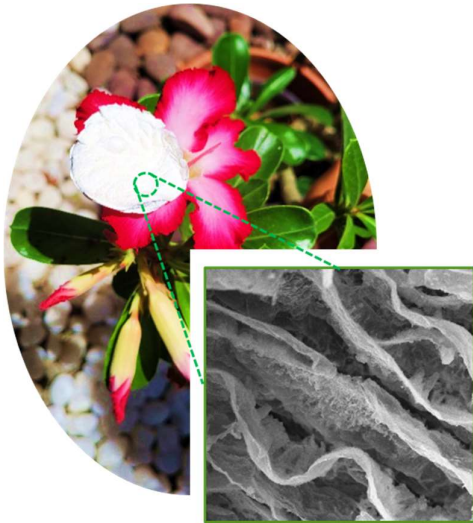
Porous structures as triboelectric layer is believed to perform better than the dense films of the same material, when subjected to external force of same magnitude. In chapter 5, we employed a functionalized and porous h-BN based 3D structure as triboelectric negative layer against a spin coated positive material like ethyl-cellulose film on ITO-PET. The ability to successfully power a number of commercial LEDs

5.1 Introduction

The prospective development of sensor systems for emerging technological needs, as discussed in previous chapters, requires technologies that can scavenge power from surrounding stray energy resources. TENGs can provide viable self-sustaining energy solutions for the associated electronics and sensor networks.[1] Even though remarkable improvements in the output performance of TENGs have been observed in these recent years, they are still being hampered by several challenges that need to be prevailed over.[2] Numerous studies are continuing to develop novel functional materials as well as innovative structures for efficient TENG devices. One strategy is to enhance the surface charges of the TENG by increasing the frictional material's overall contact surface area. To accomplish high contact area and improved relative capacitance, various materials are explored.[3]

In accordance with that, the lightest solid materials-aerogels, with extraordinary porosity, flexibility, 3D mesh-like structure, and high specific surface area, have shown impressive performance when used in TENGs.[4,5] Additional charges are accumulated on the surface of the porous materials as a result of high surface area and electrostatic induction. Tiny deformations on porous structures contribute to efficient capturing of the mechanical energy. In this way, nanogenerators built based on aerogels can be considered to form an innovative and creative way to address the current global energy dilemma.[6]

Aerogels are made through umpteen methods using both organic and inorganic components. Specifically, 2D material-based aerogels seem to be ideal choices for practical applications due to their high mechanical robustness, extremely lightweight, and ability to withstand harsh environmental conditions in their operations.[7,8] As shown in previous chapters, layered BNNSs or "white graphene" with superior thermal, mechanical, and electrical properties, have stimulated research interest in diverse areas.[9] Aerogels based on BNNSs are more resistant to oxidation and intercalation. Further, they have good thermal conductivity and stability, and are even stable at temperatures up to 1000°C.[10]

Numerous reports discuss the use of BNNSs in polymer composite architectures, both in film and nanofibers form, for energy harvesting applications. For example, Pang *et al*. reported a polyimide based sandwich-structured TENG, PI/BNNS/PI in which the

film of BNNS interlayer was utilized as a negative frictional layer for output enhancement.[11] In another work, Mahapatra *et al*. developed a BNNS-embedded flexible cotton hybrid device for health monitoring.[12] In addition to these strategies, several effective surface modification methods involving BNNSs also shown to considerably improve their energy scavenging characteristics.[13] So far as mechanical energy harvesting with BNNSs is concerned, two strategies are most effective; (a) functionalization and (b) 3D porous structure formation.[14,15] Both strategies are used in the present investigation.

Accordingly, we have utilized functionalized BNNS-based 3D porous structure to fabricate a high-performance TENG. The BNNSs incorporated macroscopic porous structure was developed via an in-situ scalable freeze-drying method. In this protocol, oxygen functionalization and chemical cross-linking of liquid-phase-exfoliated BNNSs with polyvinyl alcohol (PVA) molecules were carried out. These lightweight free-standing BNNSs/PVA porous structures have improved mechanical stability that are contributed by the developed interconnections between the nanosheets, compared to the other pristine BN-based porous structures. Here, PVA molecules act as a bridge between the nanosheets that hold the individual layers together through the intermolecular hydrogen bonding interaction, leading to the formation of a network structure. Resultant is the functionalized porous aerogel (P-BN) with BNNSs and PVA molecules as tribo-negative layer against the ethyl cellulose layer coated on ITO-PET as positive material that provides better performance for powering handheld electronic devices.

5.2 Experimental

5.2.1 Materials

Bulk h-BN, was used as the starting material that was commercially procured from Sigma Aldrich (powder size ~1μm). Potassium permanganate ($KMnO_4$), borax (sodium tetraborate), and hydrogen peroxide (H_2O_2) were received from Merck Chemicals, India. Sulphuric acid (H_2SO_4), phosphoric acid (H_3PO_4), resorcinol, and glutaraldehyde solution were also received from Merck Chemicals. Ethyl cellulose (EC) and polyvinyl alcohol (PVA) were supplied by Sigma Aldrich. Deionized water (DI) was used as the solvent for exfoliation. The substrate for spin coating was ITO-PET (indium tin oxide coated polyethylene terephthalate) from Shilpent. All reagents and materials were used as received.

5.2.2 Functionalization of h-BN

Oxidized h-BN (O-BN) was synthesized by adopting a modified process similar to that used to prepare graphene oxide.[16] In this procedure, initially, a dispersion of h-BN was prepared in 200 ml acid mixture of H_2SO_4 and H_3PO_4 in the ratio 9:1, which was then continuously stirred for 2h at 50° C. Following the addition of KMnO4 as oxidizing agent, the dispersion was then stirred again for overnight. Afterwards, the resulting solution mixture was added to an ice-filled beaker. Later, H_2O_2 was gradually added in drops to dissolve any leftover $KMnO_4$ in the solution generating a white solution with effervescence. Stirring continued for additional period of 1h, and then allowed to cool. The functionalized product was collected and then washed several times with DI water, followed by washing with 30 wt% aqueous solution of HCl and ethanol. The residual powder was dried subsequently in an oven at 50°C overnight.

5.2.3 Conversion of functionalized O-BN to 3D porous aerogel (P-BN)

The porous structure of BNNSs was developed via a covalent polymerisation process using cross-linking agents externally.[17] For that, O-BN powder was dispersed in 10 mL DI water for continuous sonication, and stirring for 15 h aided the exfoliation of the material into well-separated individual nanosheets. Then very small quantities of resorcinol (5 mg), glutaraldehyde solution (40 μL), and sodium tetraborate were added and then stirred again for 2h. Afterward, 1 wt% PVA solution in DI water was further added to the above solution and then sonicated for 2h. The final step was to transfer the solution mixture to a mold for liquid nitrogen treatment and then freeze-dried. The functionalization of bulk h-BN and its 3D porous structure formation via the chemical cross-linking method, is schematically represented in Figure 5.1. This schematic also contains the photographic image of the light-weight aerogel.

5.2.4 Preparation of spin-coated EC film on ITO-PET

The positive triboelectric material employed in the current investigation was spin-coated EC film on the PET side of ITO-coated PET. A 10 wt% solution of EC in a 1:4 mixture of ethanol and toluene solvents provided a highly viscous solution after continuous magnetic stirring at 60° C for 6h. After cooling, the resultant clear solution was spin-coated on the surface of ITO-PET substrate of area 2 cm x 2 cm, using a spin coating

equipment SpinNXG-P1, Apex Instruments, India. The rotation speed of the instrument was set to 2000 rpm for uniform films. Finally, the spin-coated EC film was dried overnight in an oven with a temperature set at 60 °C.

5.2.5 Fabrication of porous aerogel based TENG (P-TENG)

In the present investigation also, a conventional CS mode TENG device was employed for energy harvesting. A BoPET substrate was used to build a flexible support for TENG that was bent into the shape of a rectangular cage that serve as the support structure. The synthesized porous aerogel was served as the negative layer, while the EC film developed on ITO-PET served as the tribo-positive layer. These two triboelectric materials were arranged as two opposing materials in flexible TENG.
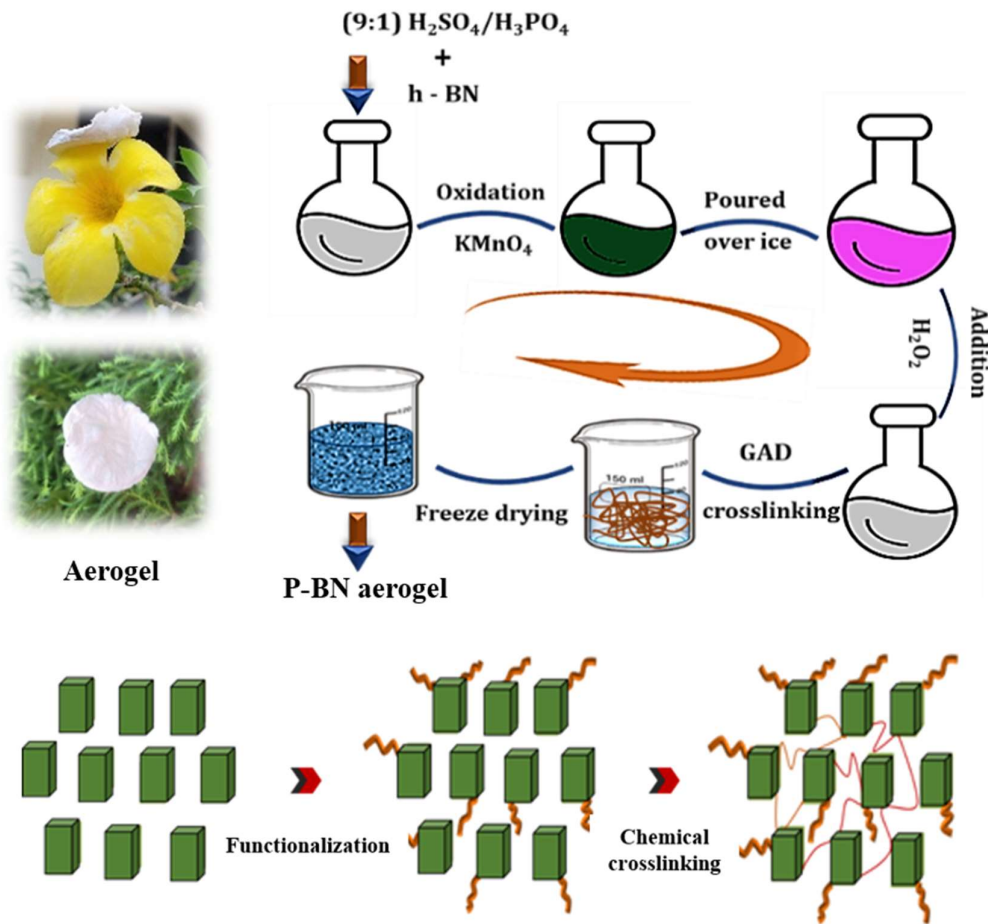

Figure 5.1: A Schematic presenting the functionalization of h-BN followed by chemical cross-linking to form BNNS based porous monolithic solid

A double-sided conducting copper tape was used as the conducting electrode layer attached to the back side of both the triboelectric materials. An adhesive tape was used to attach the two materials with electrodes to the supporting structure. Two copper leads were drawn from the back electrodes for providing electrical connection to the fabricated P-TENG device for measurements. To examine the output performance of P-TENG systematically, a specially designed homemade force impactor was developed for converting mechanical energy to readable electric power.

5.2.6 Characterization methods

Oxygen functionalization and elemental composition analysis of O-BN was identified from an X-ray photoelectron spectroscopic (XPS) study using PHI 5000 Versa Probe II, Focus X-ray photo-electron spectroscope, purchased from ULVAC-PHI, Inc. USA, equipped with microfocused (200μm, 15 kV) monochromatic Al K$_\alpha$ X-ray source (hν= 1486.6 eV). Multipack software was used for peak fitting purposes. The binding energy reference was considered to be the C 1s line. The background was taken as the Shirley background for curve fitting. Fourier transform infrared (FT-IR) spectroscopic analysis was performed using Nicolet Magna 560 FTIR (Thermo Scientific, Massachusetts, USA), to identify the characteristic bonds in the analyzed material under the study as well as to compare the chemical structure of pristine h-BN with the derived porous material. The BET (Brunauer–Emmett–Teller) surface area of the bulk h-BN and synthesized porous aerogels were analyzed from nitrogen adsorption-desorption isotherms recorded using the instrument Gemini 2375, Micromeritics, Norcross, USA. The samples were previously degassed before measurement at 200 °C for 5 hours. A thermal stability study of the BNNSs/PVA aerogel was carried out using a TGA TA Q50 working under inert atmosphere of continuous argon flow. The temperature ramp for the samples was set from room temperature to 800°C at a heating rate of 5°C/min. The highly porous network structure of the aerogel after functionalization and freeze-drying was revealed from the surface morphological analysis carried out via Zeiss EVO 50, scanning electron microscope Oberkochen, Germany. Optical images of the aerogel were recorded using a Leica DM2700P Polarizing Optical Microscope, Germany with a CCD (charge-coupled device) camera. Voltage and current measurements of the developed aerogel-based P-TENG were measured using a source measurement unit (Keithley 2450, Tektronix USA) and a low-

noise current preamplifier setup (SR570, Stanford Research, USA). The power density calculation and capacitor charging profile of the fabricated P-TENG were conducted with the use of resistive banks and various capacitors. A modified electric sewing machine can act as a force impactor system that can deliver a constant force of ~10 N for measuring the device's performance. The cyclic stability of the device was assessed by performing the operations over 15,000 continuous cycles.

5.3 Results and discussions

5.3.1. Structural analysis of functionalized O-BN

Highly porous BNNS-based aerogel was developed using a functionalization followed by chemical crosslinking and subsequent freeze-drying process. The initial stage of porous structure formation is the oxidation that will introduce some hydroxyl groups over the surface and edges of pristine h-BN. An efficient and simple oxygen functionalization method using a mixture of acids was confirmed from XPS analysis.
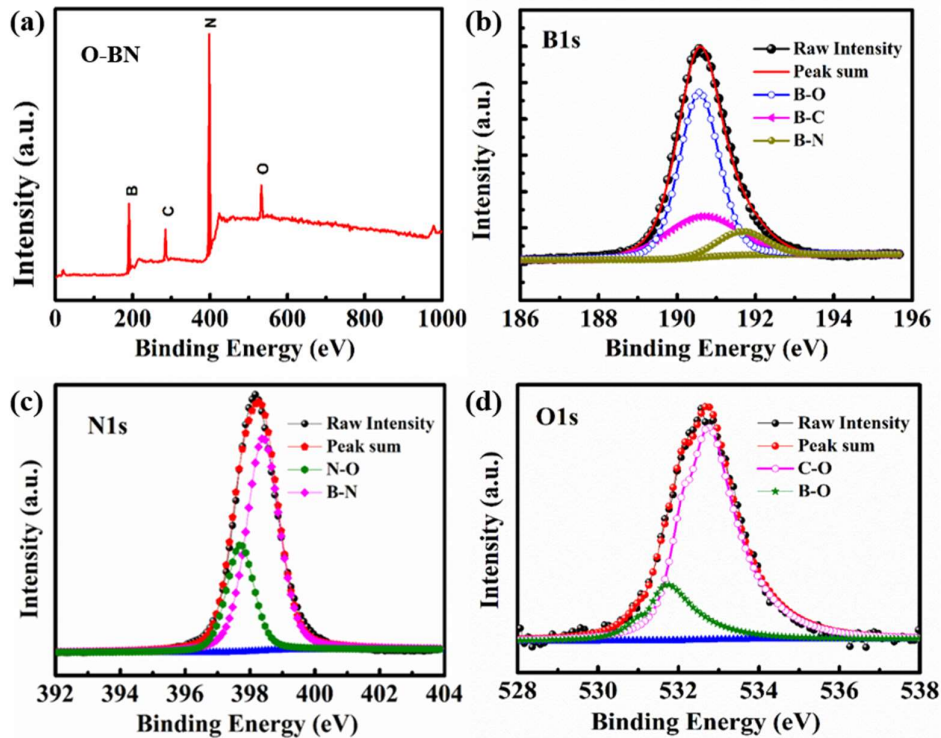

Figure 5.2: (a) XPS survey spectra of O-BN. De-convoluted XPS spectra of O-BN (b) B 1s (c) N 1s and (d) O 1s

This oxygen functionalization promotes the exfoliation of stacked layered structures into separate individual layers. After functionalization, the presence of additional oxygen-containing functional groups are evident from the XPS survey spectrum depicted in Figure 5.2(a).

It shows the presence of oxygen in addition to the B and N elements. Further, a detailed analysis on the de-convoluted XPS spectra of individual elements is shown in Figures 5.2(b), (c), and (d), that confirms oxygen functionalization. An observed peak at 192.5 eV in the de-convoluted B 1s spectra indicates the presence of B-O bonding. Similarly, the shoulder peaks observed in N 1s and O 1s spectra indicate the presence of N-O and C-O bonding respectively.[18]

In order to dig deep into the oxygen functionalized porous aerogel structure, the presence of developed hydroxyl groups as a result of oxidation on the edges or surfaces of P-BN was identified from FT-IR analysis. A comparative analysis of FT-IR spectra of bulk h-BN and P-BN aerogel is shown in Figure 5.3(a). The highly intense prominent bands observed at 817 cm^{-1} and 1370 cm^{-1} are the characteristic B-N-B out-of-plane bending vibrations and B-N in-plane stretching vibrations of h-BN respectively that are observed in both samples.[19,20] Other than the major peaks, a broad peak observed near the spectral range 3300 cm^{-1} in the P-BN aerogel structure represents the presence of –OH groups on the boron sites. Additional characteristic bands developed at the peak positions of 1100 cm^{-1} and 959 cm^{-1} after porous structure formation indicate the in-plane bending of B-O-H and B–N–O bonds respectively, that confirms the attachment of hydroxyl groups on the edges or surfaces of h-BN.[21] These hydroxyl groups as a result of oxidation, act as an anchoring point for further hydrogen bond formation with PVA molecules that connect the individual BN layers via a cross-linking chemistry that improves its mechanical stability too. A peak appeared after aerogel formation at 2900 cm^{-1}, representing the C-H stretching vibrations for covalent hemiacetal linkages.[22]

A thermal stability comparison of the h-BN and P-BN structure was conducted. The represented thermogram in Figure 5.3(b) shows the thermal behavior of samples in the inert atmosphere of argon gas. According to the apparent TGA results, pure h-BN is thermally stable up to a higher temperature of 750° C, but the P-BN begins to disintegrate when the temperature rises from lower to higher. Initial weight loss observed below 100° C in the TGA analysis of P-BN may be attributed to the presence of water molecules

adsorbed on the surface of P-BN. Above 230° C, almost 60% weight loss was observed by 500° C. The thermal decomposition in this temperature window is due to the elimination of various oxygen-containing functional groups present in the porous material, that were induced as a result of the cross-linking process.[23]

To explore the surface area and pore structure of the as-developed porous material were studied using N_2 adsorption–desorption isotherms. These isotherms exhibit a kind of type II isotherm curve in analysis with the IUPAC classifications.[24,25] The hysteresis loops of H3 type were observed at higher pressure regions (P/Po >0.80).
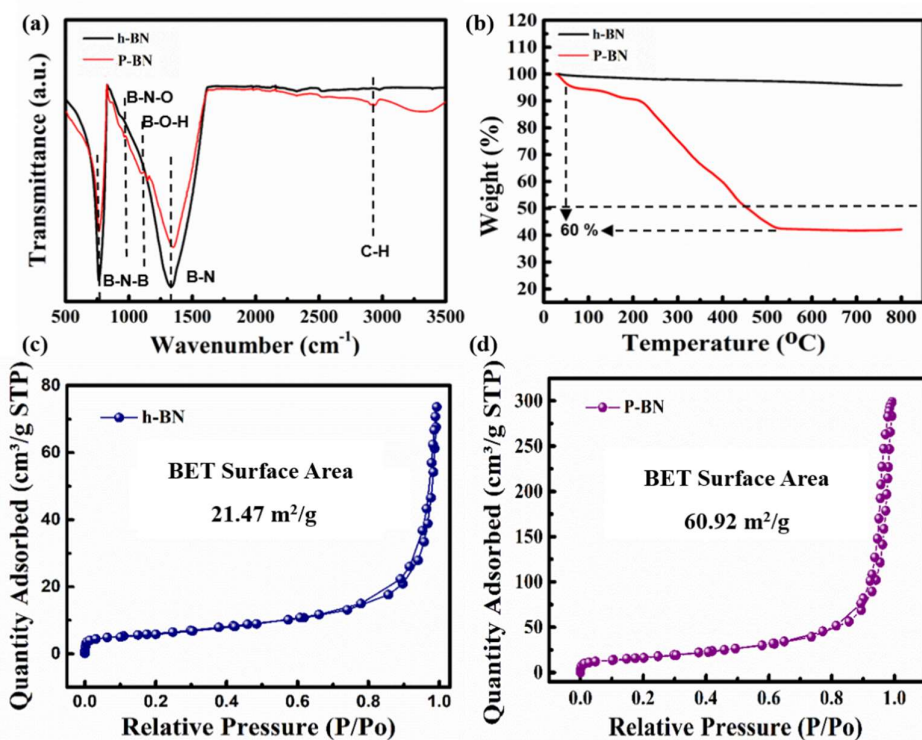
Figure 5.3: *(a) FT-IR spectra of pristine h-BN and P-BN (b) TGA analysis of pristine h-BN and P-BN. BET surface area of (c) bulk h-BN and (d) P-BN from N_2 adsorption-desorption isotherm analysis*

From the isotherm curves of pure h-BN and P-BN, BET (Brunauer–Emmett–Teller) specific surface area of the porous structure is comparably higher than the pristine material. Porous h-BN has a BET surface area of ~60.9 m^2/g with mesoporous structure whereas for pristine material surface area is a lower value of around 21.74 m^2/g.

5.3.2. Morphology analysis

Surface morphology analysis and energy dispersive X-ray (EDX) study of h-BN and O-BN samples before and after functionalization are illustrated in the SEM images shown in Figures 5.4(a) and (b) respectively. A more stacked thick structure is observed for pristine h-BN compared to the oxidized product. Fewer stacks and a smaller lateral dimension suggest that the oxidation process causes exfoliation of the material.[26] The distribution of various elements in pristine h-BN and its functionalized products were identified from the EDX mapping of samples along with their corresponding SEM images. The elemental atomic weight percentage is also incorporated as an inset table along with the EDX mapping.

Element	Atomic %
Boron	43.65
Carbon	9.95
Nitrogen	46.40

Element	Atomic %
Boron	41.32
Carbon	12.5
Nitrogen	43.76
Oxygen	2.42
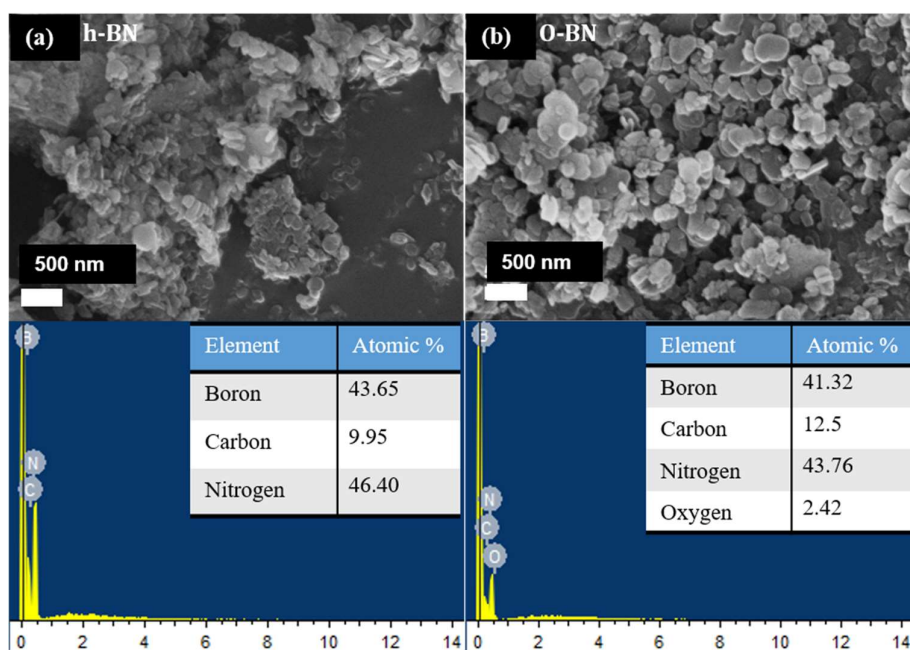
Figure 5.4: (a) SEM image of the pristine h-BN before oxygen functionalization with EDX analysis showing the elemental composition, and (b) SEM image of the O-BN with EDX analysis

Based on this quantitative analysis, major atomic percent by weight in samples are demonstrated by boron and nitrogen elements. After functionalization, small amounts of additional oxygen are present in the oxidized sample that could have resulted from the surface oxidation process.[27]

The development of extended solids with multifunctional properties from 2D materials using a solution mixing based self-assembly process can build covalently

interconnected nanosheets with improved mechanical properties. The structure and surface morphology of the synthesized aerogels of multi-layered structures in different magnifications were further investigated to gain a better understanding of the critical role of layered BNNSs in producing such porous lightweight and low-density aerogels. The aerogel structure was developed from BNNSs to create a distinctive, well-organized three-dimensional structure.
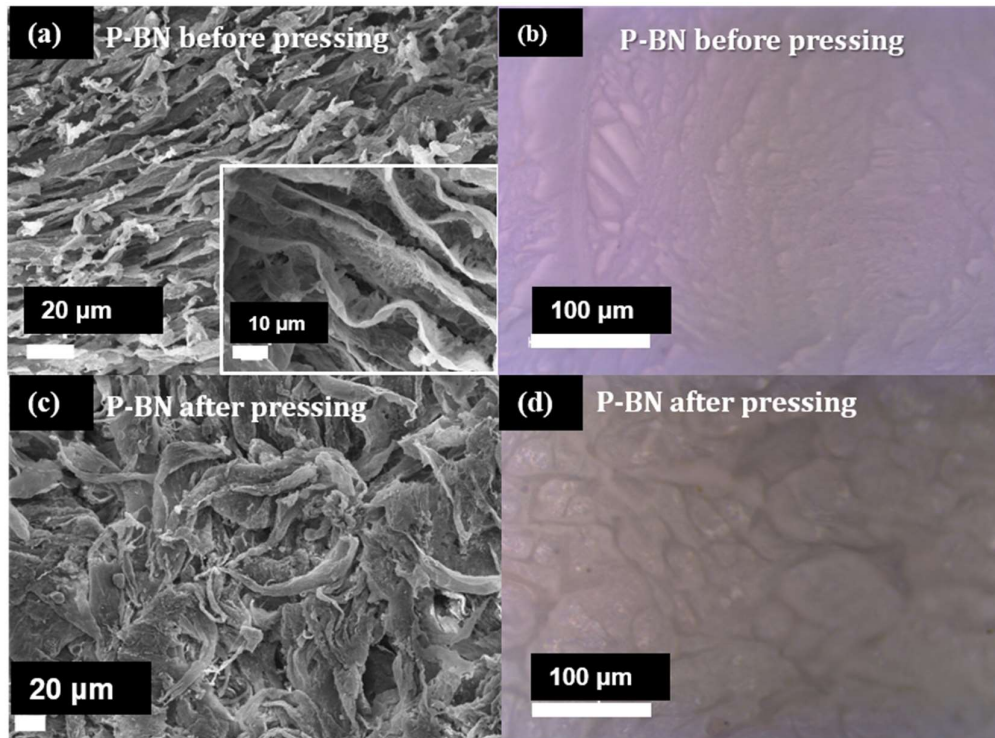
Figure 5.5: (a) Low magnification SEM image of the P-BN. Inset figure higher magnification SEM image of the P-BN aerogel. (b) Optical photograph depicting the P-BN aerogel before pressing. (c) SEM image of the P-BN aerogel after pressing. (d) Optical image showing the P-BN aerogel after pressing

The cross-linked interconnected BNNS layers are shown in the SEM images of Figure 5.5(a). The inset of Figure 5.5(a) represents the high-magnification SEM image of the aerogel and indicates the uniform network porous structure with layered connections.[10,28] The optical image of the porous aerogel is shown in Figure 5.5(b). The SEM microstructure of aerogel in a pressed state after several cycles of device operation is shown in figure 5.5(c) with the corresponding optical image after pressing represented in Figure 5.5(d).

5.3.3. P-BN aerogel based TENG (P-TENG): device performance

In this work, a novel class of high-performance triboelectric nanogenerator based on P-BN aerogel is demonstrated. The developed P-TENG is made up of a thin, porous aerogel film that acts as the negative triboelectric material and a positive EC polymer film that is spin-coated on the ITO-PET surface. Remarkably, the aerogel-based TENG with an active contact area of 4 cm^2 and a 5 mm separation gap between the layers, could yield excellent outcomes. This shows that, incorporating a porous structure into the TENG can significantly improve its output performance which may be associated with the comparably higher surface area of the porous films can produce more output power than its dense films with the same mechanical force.[5]

When compressing a porous structure, the increased contact area results in the development of more charges, and electrostatic induction also adds some additional charges to the pore surfaces. Moreover, higher deformation of the porous films under a compressive force will significantly improve the relative capacitance. Furthermore, an interlayer PET between the EC film and the ITO electrode in a multilayer hetero-structure way definitely enhance the P-TENG's capacity for charge retention. The generated charges will be effectively preserved by this method inhibits interfacial charge recombination on the electrodes. In these ways, enhanced electrical performance of the device could be expected.[29,30]

The power generation mechanism in P-TENG is shown in Figure 5.6. When mechanical stress is acting on the two triboelectric materials, charge transfer between the material surfaces takes place. This process generates positive charges to form on the surface of ethyl cellulose and negative charges on the P-BN layer surfaces. In addition to the surface contact between the triboelectric materials, the electrostatic effects resulting from the compression of pores also contribute to the produced charges. In the releasing stage of P-TENG, a voltage differential is established between the two copper electrodes. This causes electrons to move through external circuit producing an output electrical signal. In the subsequent cycle of applying stress on the P-TENG, the reverse flow of electrons in the external circuit occurs, generating an electrical signal in the opposite direction.[30,31]
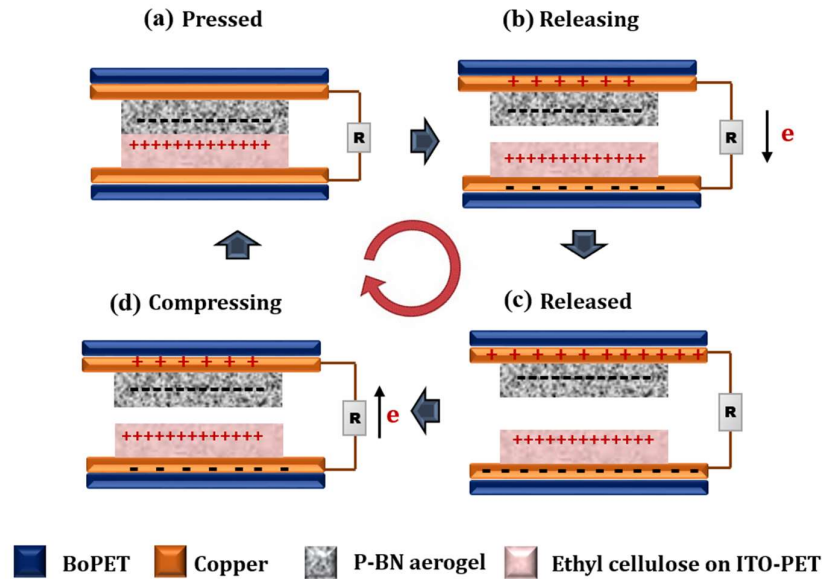
Figure 5.6: *Schematic depicting the working mechanism of P-TENG with EC film on ITO-PET (a) Pressed state (b) Releasing state (c) released state of saturation (d) further pressing cycle*

The P-TENG is markedly effective in producing improved output results with EC coating, whose working mechanism is briefly displayed in Figure 5.6. When a mechanical impulse of magnitude 10 N acts at a frequency of 5 Hz, the P-TENG generates an output voltage of 720 V and current density (J_{sc}) of 10 mA/m^2, respectively (Figures 7(a) & (c)). In comparison with the performance of P-TENG without an EC coating on ITO-PET, the presently observed result is significantly better. The recorded output voltage and current density for P-TENG without EC coating are only 190 V and 0.875 mA/m^2 respectively (Figure 5.7(a) & 5.7(c)).

Additionally, the following studies were also performed to analyze the power density parameter of P-TENGs. To evaluate their power density performance, the P-BN aerogel nanogenerator with and without EC film on ITO-PET was connected to various load resistors. The output voltage exhibits an increasing trend at an operating frequency of 5 Hz for both P-TENGs with and without EC coating on ITO-PET. When the load resistance rises from lower 1 Ω to higher 1000 MΩ, P-TENG without EC film exhibits an observed maximum output power density of 0.12 W/m^2 at 100 MΩ load resistance, as shown in Figure 5.7(b). The peak instantaneous power density of P-TENG with EC film on ITO-PET reaches 1.7 W/m^2 at 100 MΩ load resistance, as shown in Figure 7(d).
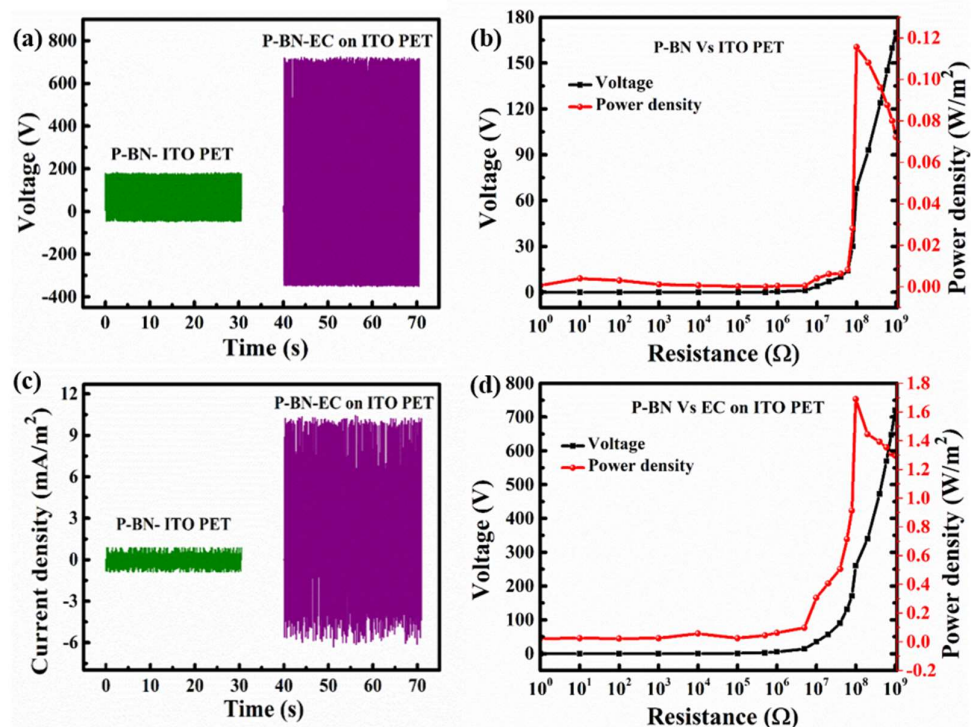
Figure 5.7: *(a) Output voltage of P-TENG with and without EC film on ITO-PET having an area of 4 cm^2 under a mechanical force of 10 N & 5Hz frequency. (b) Power density of P-TENG without EC on ITO-PET obtained as a function of different load resistance. (c) Current density generated from P-TENG with and without EC film. (d) Power density of P-TENG with EC on ITO-PET*

It is worthwhile to note that the output power density of nanogenerator has been improved massively (14 times) with EC coating on ITO-PET, compared to the P-TENG without EC film. The highly tribo-positive EC coating on ITO-PET combined with P-BN aerogel increases the charge transfer between the material surfaces, and the charge storage PET interlayer effectively stores the produced charges.. This generated power is good enough to power numerous small-scale electrical gadgets and energy storage devices.

The capacitor charging profiles of P-TENG with EC film using several capacitors with different capacitance values were examined to analyze the energy harvesting capability of the device for practical use. Figure 5.8(a) illustrates the P-TENGs capacitor charging performance, demonstrating that a 0.5 μF capacitor can be charged more quickly than other capacitors with higher capacitance values. The capacitor charging profile for a 0.5 μF capacitor attains a voltage of 27 V within 3 minutes. To demonstrate the P-TENG's

practical usefulness, it was connected to electronic devices like calculator, digital thermometer and 15 green LEDs placed in series through a bridge rectifier. The mechanical stress on the P-TENG caused the LEDs to ignite instantly as shown in Figure 8(d) also useful for powering other devices too Figure 8(b) & (c). This certifies that low power electronic gadgets could be easily powered using the P-TENG. These experiments suggest that P-BN aerogel-based TENG may be used as a cheap, sustainable and environmentally friendly power source.
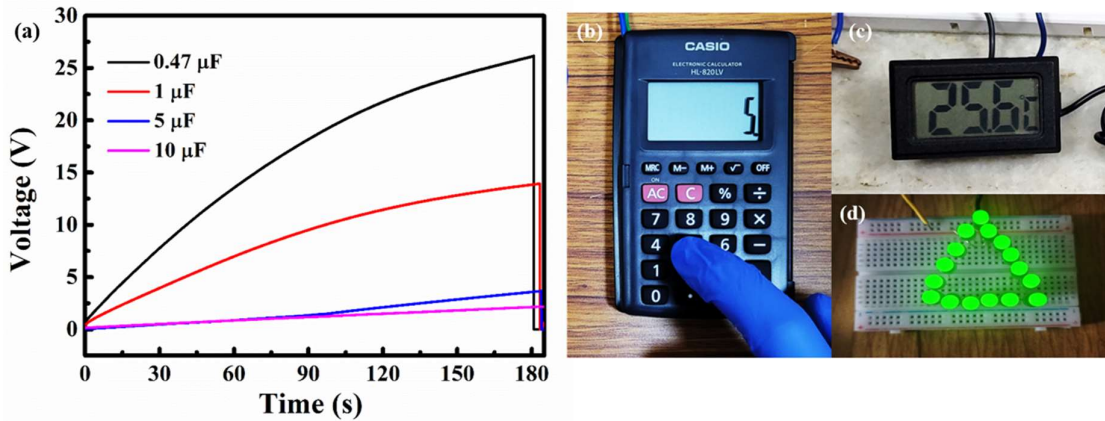

Figure 5.8: *(a) Capacitor charging curve of P-TENG with EC film using different capacitors with capacitances 0.5 µF, 1 µF, 5 µF, and 10 µF. (b) Lighting of 15 LEDs using P-TENG with EC coating on ITO-PET*

The force-dependent output performance of the P-TENG with EC film was recorded by applying different biomechanical forces of varying magnitudes such as single-finger force, multiple-finger force, and palm pressing to portray the biomechanical energy harvesting capability of the P-TENG. Figures 5.9(a) and (b) display the output voltage and current density produced by the applied biomechanical forces respectively. The output voltage and current density show an increasing trend as a function of the magnitude of the force exerted on P-TENG. For example, palm pressing could exert comparably higher force than single-finger force as well as multiple-finger tapping forces, where the former contributes to the efficient contact between the trioactive layers during the operation. The voltage and current density generated by the P-TENG are 1030 V and 12.5 mA/m^2 due to palm pressing state. This result is obviously better than the single-finger pressing force (300 V and 2.6 mA/m^2) and multiple-finger force (820 V and 9.5mA/m^2).
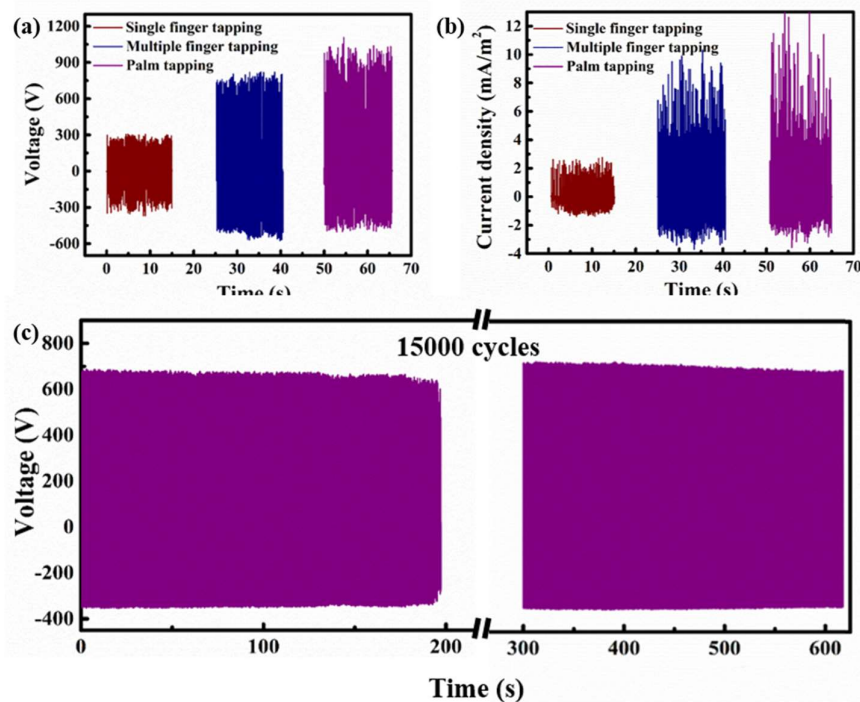
Figure 5.9: *(a) Output voltage and (b) current density of P-TENG with EC film on ITO-PET under different biomechanical forces of single finger pressing, multiple finger pressing, and palm pressing. (c) Durability analysis of the P-TENG with EC coating over 15,000 cycles of operation.*

The durability of the energy harvesting device is a critical parameter that needs to be evaluated for the prepared porous energy harvestor, P-TENG. The continuous testing of the device with 15,000 cycles of pressing and releasing events at a frequency of 5 Hz is represented in Figure 5.9(c). After this many cycles, the developed voltage remains almost the same with only minute changes. These experimental results indicate the reliability and robustness of the P-TENG.[32] Dimensions of the P-BN aerogel layer was shown to have an intuitive influence on the electrical output performance of P-TENG with EC coating. By changing the contact area of aerogel film, an investigation of output performance was conducted to study how this parameter affects the performance of the device. Figure 5.10(a) and (b) represent the output voltage and current density of P-TENG with EC film having three contact areas, 1, 4, and 9 cm². The recorded results of output voltage (190 V, 720 V, 1290 V) and current density (6.4 mA/m², 10 mA/m², 12.1 mA/m²) for respective areas 1, 4 and 9 cm² indicate considerable enhancement in its voltage and current performance as the contact area changes from lower to higher values at a constant separation gap of 5 mm. Obviously, this indicates the scalability of the P-TENG and the

development of more triboelectric charges in higher contact area improves the performance of the device.

Finally, the output performance is also significantly influenced by another parameter; TENG's separation gap. To study the influence of the separation gap, output voltage, and current density were systematically analyzed by varying the separation gap from 3 mm to 7 mm, while the contact area remains constant (4 cm^2). Figures 5.10(c) and (d)) display the output voltage and current density dependence with the TENG's separation gap. The observed results for 3, 5, and 7 mm separation are 520 V, 720 V, and 830 V output voltages while 6.5 mA/m^2, 10 mA/m^2, and 11.7 mA/m^2 are the current densities, respectively.
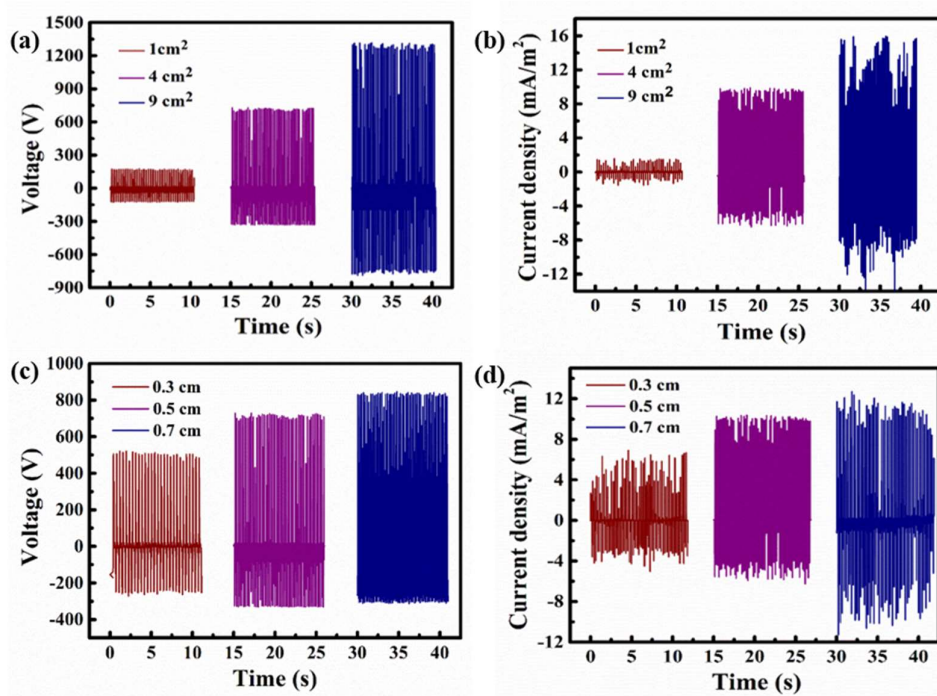

Figure 5.10: (a) Output voltage and (b) current density of P-TENG with EC film on ITO-PET having different contact areas. (c) Output voltage and (b) current density of P-TENG with EC film on ITO-PET with varying device separation gaps.

5.4 Conclusions

In conclusion, this work package accomplishes the development of a unique porous aerogel structure based on h-BN that serves as a tribo-active negative layer for mechanical energy harvesting. These aerogels were developed via oxygen functionalization followed by chemical cross-linking and porous structure formation. In this study, oxygen-functionalized h-BN was cross-linked covalently using glutaraldehyde-resorcinol chemistry, resulting in the generation of a porous monolithic solid with 3D interconnected network. The as-prepared h-BN-based aerogel shows layered and porous structure with a comparably higher surface area than its bulk counterpart. This porous aerogel was employed to enhance the output of TENGs. To demonstrate the output performance P-TENG, highly viscous EC solution spin-coated on the surface of ITO PET as positive material, was paired with P-BN aerogel as a negative triboactive material. The assembled P- TENG exhibited an output voltage of ~720 V and a short-circuit current density of ~10 mA/m^2 for a 2 cm x 2 cm device, under 10 N external force applied at 5 Hz frequency. Power density reached the highest ever value of this doctoral investigation (~1.7 W/m^2). This high power nanogenerator was employed to successfully power a series of commercial LEDs, which is a testimony to its suitability for future potential applications. Further, the developed P-TENG possesses excellent electrical output performance as well as superior mechanical stability even after continuous several thousand cycles of operations.

5.5 References

(1) Wang, R.; Mu, L.; Bao, Y.; Lin, H.; Ji, T.; Shi, Y.; Zhu, J.; Wu, W. Holistically Engineered Polymer – Polymer and Polymer – Ion Interactions in Biocompatible Polyvinyl Alcohol Blends for High-Performance Triboelectric Devices in Self-Powered Wearable Cardiovascular Monitorings. *Adv. Mater.* **2020**, *2002878*, 1–10.

(2) Liu, Y.; Mo, J.; Fu, Q.; Lu, Y.; Zhang, N.; Wang, S.; Nie, S. Enhancement of Triboelectric Charge Density by Chemical Functionalization. *Adv. Funct. Mater.* **2020**, *2004714*, 1–33.

(3) Khandelwal, G.; Maria, N. P.; Kim, S. J. Materials Beyond Conventional Triboelectric Series for Fabrication and Applications of Triboelectric Nanogenerators. *Adv. Energy Mater.* **2021**, *11* (33), 1–32.

(4) Korkmaz, S; Kariper, I. A. Aerogel Based Nanogenerators : Production Methods, Characterizations and Applications. *Int. J. Energy Res.* **2020**, *44* (14), 11088–11110.

(5) Zheng, Q.; Fang, L.; Guo, H.; Yang, K.; Cai, Z.; Meador, M. A. B.; Gong, S. Highly Porous Polymer Aerogel Film-Based Triboelectric Nanogenerators. *Adv. Funct. Mater.* **2018**, *1706365*, 1–9.

(6) Luo, C.; Yu, H.; Zhang, Y.; Shao, Y.; Yin, B.; Ke, K.; Zhou, L.; Zhang, K.; Yang, M. Enhanced Triboelectric Nanogenerator Based on a Hybrid Cellulose Aerogel for Energy Harvesting and Self-Powered Sensing. *ACS Sustain. Chem. Eng.* **2023**, *11* (25), 9424-9432.

(7) Androulidakis, C.; Kotsidi, M.; Gorgolis, G.; Pavlou, C.; Sygellou, L.; Paterakis, G.; Koutroumanis, N.; Galiotis, C. Multi-Functional 2D Hybrid Aerogels for Gas Absorption Applications. *Sci. Rep.* **2021**, *11* (1). 13548.

(8) Feng, L.; Wei, P.; Song, Q.; Zhang, J.; Fu, Q.; Jia, X.; Yang, J.; Shao, D.; Li, Y.; Wang, S.; Qiang, X.; Song, H. Lei Feng, Peng Wei, Qiang Song, Jiaxu Zhang, Qiangang Fu, Xiaohua Jia, Jin Yang, Dan Shao, Yong Li, Sizhe Wang, Xinfa Qiang, and Haojie Song. Superelastic, Highly Conductive, Super hydrophobic, and Powerful Electromagnetic Shielding Hybrid Aerogels Built From Orthogonal Graphene and Boron Nitride Nanoribbons *ACS Nano*, **2022**, *16* (10), 17049-17061.

(9) Yang, Z.; Zhang, X.; Xiang, G. 2D Boron Nitride Nanosheets in Polymer Nanofibers for Triboelectric Nanogenerators with Enhanced Performance and Flexibility. *ACS Appl. Nano Mater. 2022, 5 (11),* 16906-16911.

(10) Vinod, S.; Tiwary, C. S.; Alves, P.; Taha-tijerina, J.; Ozden, S.; Chipara, A. C.; Vajtai, R.;

Galvao, D. S.; Narayanan, T. N.; Ajayan, P. M. Low-density Three-dimensional Foam Using Self-reinforced Hybrid Two-Dimensional Atomic Layers. *Nat. Commun.* **2014**, *5* (1), 4541.

(11) Pang, L.; Li, Z.; Zhao, Y.; Zhang, X.; Du, W.; Chen, L.; Yu, A.; Zhai, J. Triboelectric Nanogenerator Based on Polyimide/Boron Nitride Nanosheets/Polyimide Nanocomposite Film with Enhanced Electrical Performance. *ACS Appl. Electron. Mater.* **2022**, *4* (6), 3027-3035.

(12) Mahapatra, P. L.; Singh, A. K.; Lahiri, B.; Kundu, T. K.; Roy, A. K.; Kumbhakar, P.; Tiwary, C. S. Energy Harvesting Using Cotton Fabric Embedded with 2D Hexagonal Boron Nitride. *ACS Appl. Mater. Interfaces*, **2022,** *14* (26), 30343-30351.

(13) Tan, X.; Wang, S.; You, Z.; Zheng, J.; Liu, Y. Xueqiang Tan, Shuting Wang, Zhongyuan You, Jimin Zheng, and Ying Liu. High Performance Porous Triboelectric Nanogenerator Based on Silk Fibroin@ MXene Composite Aerogel and PDMS Sponge**.** *ACS Mater. Lett.* **2023**, *5*, 1929-1937.

(14) Zhou, Q.; Wang, W.; He, Y.; Li, Z.; Zhao, R.; Tao, G.; Hu, B.; Hou, C. High-Performance Polyimide Aerogel Film-Based Triboelectric Nanogenerator for Trace Liquid Analyzing. *ACS Appl. Polym. Mater.* **2023,** *5* (7)**,** 5466-5473.

(15) Saadatnia, Z.; Mosanenzadeh, S. G.; Esmailzadeh, E.; Naguib, H. E.   A High-Performance Triboelectric Nanogenerator Using Porous Polyimide Aerogel Film. *Sci. Rep.* **2019**, *9* (1), 1379

(16) Marcano, D. C.; Kosynkin, D. V; Berlin, J. M.; Sinitskii, A.; Sun, Z.; Slesarev, A.; Alemany, L. B.; Lu, W.; Tour, J. M. Improved Synthesis of Graphene Oxide. *ACS Nano*, **2010**, *4* (8), 4806-4814.

(17) Owuor, P. S.; Park, O.; Woellner, C. F.; Jalilov, A. S.; Susarla, S.; Joyner, J.; Ozden, S.; Duy, L.; Salvatierra, R. V.; Vajtai, R.; Tour, J. M.; Lou, J.; Soares, D. Lightweight Hexagonal Boron Nitride Foam for CO_2 Absorption. *ACS Nano*, **2017**, *11* (9), 8944-8952.

(18) Bhimanapati, G. R.; Robinson, J. A. Large-scale Synthesis and Functionalization of Hexagonal Boron Nitride Nanosheets. *Nanoscale*, **2014**, *6* (20), 11671–11675.

(19) Hou, J.; Li, G.; Yang, N.; Qin, L.; Grami, M. E.; Zhang, Q. Preparation and Characterization of Surface Modified Boron Nitride Epoxy Composites With Enhanced Thermal Conductivity. *RSC Adv.* **2014**, *4* (83), 44282–44290.

(20) Zeng, X.; Lei, Y.; Shuhui, Y.; Hao, L.; Rong, S.; Jianbin, X.; and Ching, W. Artificial Nacre-Like Papers Based on Noncovalent Functionalized Boron Nitride Nanosheets with

Excellent Mechanical and Thermally Conductive Properties. *Nanoscale*, **2015**, *7* (15), 6774-6781.

(21) Sudeep P.M.; Odzen, S.; Radhakrishnan, S.; Kukovecz, A.; Konya, Z.; Vajtai, R.; Ajayan, P. M.; Narayanan, N. T. Functionalized Boron Nitride Porous Solids *RSC Advances.* **2015**. *5* (114), 93964-93968.

(22) Qi, X.; Yang, L.; Zhu, J.; Hou, Y.; Yang, M. Stiffer but More Healable Exponential Layered Assemblies with Boron Nitride Nanoplatelets. *ACS Nano*, **2016**, *10* (10), 9434-9445.

(23) Sudeep P.M.; Odzen, S.; Radhakrishnan, S.; Kukovecz, A.; Konya, Z.; Vajtai, R.; Ajayan, P. M.; Narayanan, N. T. Functionalized Boron Nitride Porous Solids *RSC Advances.* **2015**. *5* (114), 93964-93968.

 (24) Liu, Q.; Cheng, C.; Ren, C. Porous Hexagonal Boron Nitride Sheets: Effect of Hydroxyl and Secondary Amino Groups on Photocatalytic Hydrogen Evolution. *ACS Appl. Nano Mater,* **2018**, *1* (9), 4566-4575.

(25) Guan, M.; Hao, L.; Chen, L.; Gao, F.; Qiu, S.; Zhou, H.; Chen, H. Facile Mechanical-Induced Functionalization of Hexagonal Boron Nitride and Its Application as Vehicles for Antibacterial Essential Oil. *ACS Sustain. Chem. Eng.* **2020***, 8* (40)*,* 15120-15133.

(26) Siburian, R.; Sihotang, H.; Simanjuntak, C. New Route to Synthesize of Graphene Nano Sheets. *Orient. J. Chem.* **2018**, *34* (1), 182-187.

(27) Jin, H.; Li, Y.; Li, X.; Shi, Z.; Xia, H.; Xu, Z.; Qiao, G. Functionalization of Hexagonal Boron Nitride in Large Scale by a Low-Temperature Oxidation Route, *Mater. Lett.* **2016**, 175, 244-247.

 (28) Yin, J.; Li, X.; Zhou, J.; Guo, W. Ultralight Three-Dimensional Boron Nitride Foam with Ultralow Permittivity and Superelasticity. *Nano Lett. 13* (7), **2013**. 3232-3236.

(29) Syamini, J.; Chandran, A. Mylar Interlayer-Mediated Performance Enhancement of a Flexible Triboelectric Nanogenerator for Self-Powered Pressure Sensing Application. *ACS Appl. Electron. Mater.* **2023**. *5* (2), 1002-1012.

(30) Zhang, L.; Liao, Y.; Wang, Y.; Zhang, S.; Yang, W.; Pan, X.; Wang, Z. L. Cellulose II Aerogel-Based Triboelectric Nanogenerator. *Adv. Funct. Mater.* **2020**, *2001763*, 1–9.

(31) Saadatnia, Z.; Ghaffari, S.; Li, T.; Esmailzadeh, E.; Naguib, H. E. Polyurethane Aerogel-Based Triboelectric Nanogenerator. *Nano Energy* **2019**, *65*, 104019.

(32) Varghese, H.; Chandran, A. A Facile Mechanical Energy Harvester Based on Spring Assisted Triboelectric Nanogenerators. *Sustain. Energy Fuels* **2021**. *5* (20), 5287-5294.

Chapter 6

Summary and scope for future work

Power density (W/m²)
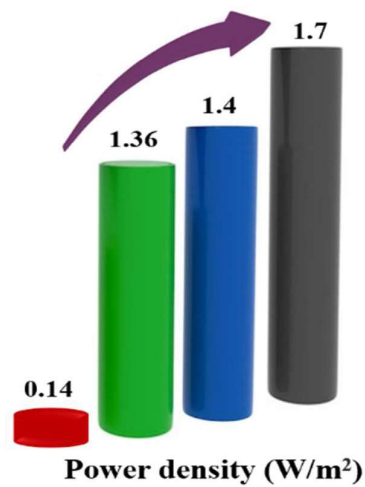
This chapter provides a brief overview of the current doctoral investigation and its potential future scopes. The present research illustrates how an energy harvesting device (TENG) functions to power handheld electronic devices. An organized study for enhancing the power density of the device was also highlighted.

6.1 Summary

Throughout human history, there has always been an increasing need for efficient, sustainable, and clean energy sources. A new class of vibrational NGs have emerged that can harvest energy from the working environment. Since the availability of traditional energy sources are dwindling day by day, many modifications in vibrational energy scavengers have been extensively explored during the last few decades. Among them, TENGs have proven to be a promising technology due to their high efficiency, low cost, and ease of harvesting kinetic energy from the surroundings to effective electricity. The present thesis is organized as a detailed investigation on how to improve the power efficiency of TENGs by way of design and material innovation.

In order to ameliorate the performance of TENGs, researchers are continuously searching for novel materials and innovative designs. For example, the development of high-surface-area nano/microstructures is one approach, while the use of composite materials with charge trapping sites is another approach. Fabrication of tribo-active composite materials containing charge-trapping 2D materials is a promising way to enhance the surface charge density of TENGs. The atomistically thin layered structure of 2D materials is ideal for the creation of incredibly thin, transparent and flexible electronics. Further, the 2D material-incorporated TENGs are believed to be advantageous in addressing the device's sensitivity concerns to harsh conditions like bending, crumbling etc.

BNNS, is a structural analog of graphene having a hexagonal planar structure with alternate boron and nitrogen atoms. This 2D layered material has attracted ever-growing research interest in the past few years, due to its superior mechanical, electrical, and thermal properties. As elaborated in 4 working chapters of this doctoral thesis, we have developed a series of composite architectures and chemically modified porous structures based on 2D BNNSs for constructing extremely versatile and flexible TENGs. The major findings of the present study are outlined below.

Initially, BNNSs was developed from bulk h-BN using a liquid-phase exfoliation technique aided by ultrasonication and was employed as an efficient triboelectric electron acceptor material in rigid BoPET-paper TENG. This BNNSs incorporated polymer assembly paired with conventional paper in contact separation mode, showed excellent

electrical output performance. Here, a current density value of ~0.48 mA/m² and a peak power density of 0.14 W/m² were achieved. We could demonstrate that this device generates sufficient energy to power consumer electronic gadgets. On scaling up, the presently reported strategy has the potential to power up more energy-demanding devices.

In comparison with traditional manufacturing methods, ink-based printing techniques could also be suitably employed to manufacture flexible TENGs owing to low cost, superior fabrication accuracy, high versatility and satisfactory production efficiency, etc. Against this background, a high-performance flexible screen printed TENG was developed using BNNS composite ink. Remarkably, the flexible screen printed TENG fabricated using BNNSs composite ink exhibited a short-circuit current density of ~0.78 mA/m² and a maximum output power density of 1.36 W/m². One may notice that the power generation is drastically improved in printed flexible BNNSs TENG. We believe that with the further improvement in the TENG design, their application horizon can be further extended towards building self-powered sensing systems, and also for soft/flexible electronics.

With this objective, a flexible TENG fabricated using screen-printed BNNSs composite ink and electrospun cellulose acetate nanofibers yield an impressive power density of 1.4 W/m². This TENG design was suitably modified into a self-powered tactile sensor for haptic detection. Interestingly, even extremely low magnitude (0.05 N) input forces could be detected by this device. It was estimated that the developed touch sensor's sensitivity is 1.843 V/N for higher forces in the range of 2–10 N, while 3.98 V/N for extremely small forces less than 2 N.

Finally, a porous monolithic solid with a 3D interconnected network was developed using chemical functionalization and covalent cross-linking of BNNSs, intended to further improve TENG's output. For this, oxygen-functionalized BNNSs were cross-linked covalently using glutaraldehyde-resorcinol chemistry. Surprisingly, the recorded output performance of the porous TENG with spin-coated ethyl cellulose film on the surface of ITO PET exhibited an impressively high short-circuit current density of ~10 mA/m² and power density ~1.7 W/m² were achieved. This power density is the highest outcome of this doctoral investigation.

In summary, the innovatively designed TENGs with 2D BNNSs outperformed those without the 2D nanofillers in terms of power output. This power (>1.5 W/m^2) is sufficient to power small-scale electronic devices and also good enough to support highly sensitive self-powered tactile sensor based on TENG principles. The results obtained in the present research are quite important from a scientific point of view and can inspire innovative device concepts towards the IoT goal of energy autonomous devices and thin film sensors.

6.2. Scope for future work

The findings in the present thesis provide an excellent scope for future research as briefed below.

o   The output performance of TENGs can be further enhanced by functionalizing the surface of 2D materials with different functional groups such as F and –OH.

o   To increase the surface charge density and to produce better output, different kinds of surface modification techniques that alter the effective area of triboelectrification can be adopted.

o   An array of sensors achieved by the assembly of individual triboelectric devices could produce better outcomes in sensing operations.

o   To address the power concerns related to wearable and portable electronic devices, a hybrid system that makes use of the synergetic effects of triboelectricity and piezoelectricity called piezo–tribo hybrid nanogenerator would enhance the energy harvesting efficiencies. Further, hybrid or coupled energy harvesters based on electromagnetic, thermoelectric, pyroelectric and photovoltaic can be investigated.
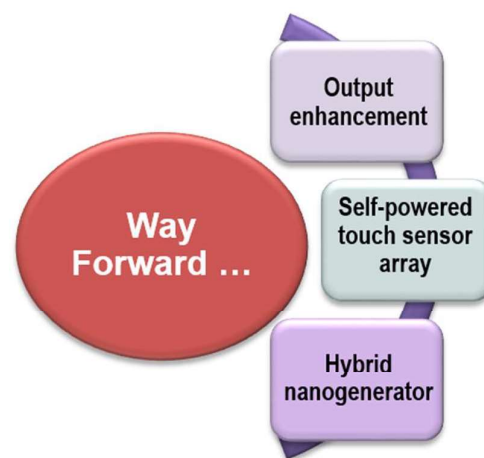
ABSTRACT

Name of the Student: **Bhavya A. S.**	Registration No.: **10CC18A39012**
Faculty of Study: **Chemical Sciences**	Year of Submission: **2024**
AcSIR academic centre/CSIR Lab: **CSIR-National Institute for Interdisciplinary Science and Technology (CSIR-NIIST)**	
Name of the Supervisor: **Dr. K. P. Surendran**	
Title of the thesis: **2D- Hexagonal Boron Nitride Heterostructures based Triboelectric Nanogenerator for Mechanical Energy Harvesting and Tactile Sensing Applications**	

This doctoral thesis mainly describes the design and fabrication of 2D material incorporated triboelectric nanogenerators (TENGs) for energy harvesting and tactile sensing applications. These devices are truly critical solutions for a maintainable future energy needs. Chapter 1 gives a brief overview about the importance of this sustainable energy harvesting technology for the current era, its mechanism, theory and the output enhancement strategies are also included. In addition to that the importance of 2D materials in TENG developments are also visited. Chapter 2 of this research investigation provides an efficient method for enhancing the overall harvested mechanical energy of a polymer-paper TENG via the incorporation of exfoliated BNNSs for powering self-powered electronic systems and portable low-power devices. We have successfully demonstrated that the liquid-phase exfoliated BNNSs can act as efficient triboelectric electron acceptors in the lab-scale demonstration of the TENG device. In the third chapter, we have formulated a viscosity tunable ultra-thin BNNSs filler based screen printable ink for realizing an all printable ink. This successful demonstration of a contact separation mode flexible TENG using a screen printable ink portrays a novel scalable strategy for green power generation. In Chapter 4, a self-powered printed tactile sensor is actualised with screen printed BNNSs composite ink and cellulose acetate nanofibers for haptic feedback. Which can be readily implemented in a multitude of application fields, such as robotics and prosthetics, for achieving tactile perceptions precisely. In chapter 5, a chemically functionalized BNNS based porous structure (aerogel) was used as a negative material for TENG fabrication with a central aim to improve the TENG's output for the purpose of powering small-scale electronic devices and also for energy autonomous sensor development while being structurally lightweight.

List of Publications

Publications emanated from the thesis

[1]   Bhavya, A. S.; Varghese, H.; Chandran, A.; Surendran, K. P. Massive Enhancement in Power Output of BoPET-Paper Triboelectric Nanogenerator Using 2D-Hexagonal Boron Nitride Nanosheets. Nano Energy 2021, 10662, 48. (IF–19.069)

[2]   Bhavya, A. S.; Varghese, H.; Chandran, A.; Surendran, K. P. Two-dimensional Hexagonal Boron Nitride Nanosheet–Polycarbonate Composite Ink-Based Printed Flexible Triboelectric Nanogenerator for Scavenging Mechanical Energy. ACS Appl. Electron. Mater. 2023, 5483–5493, 5.

[3]   Bhavya, A. S.; Hakkeem, H. M.; Pillai, S.; Chandran, A.; Surendran, K. P. Development of Self-powered Flexible Triboelectric Tactile Sensor Made of Electrospun Cellulose Nanofibers and BNNS-based Composite Ink (Manuscript under preparation)

[4]   Bhavya, A. S.; Chandran, A.; Surendran, K. P. Realization of a Flexible TENG with Triboelectric Layer Made of Functionalized Hexagonal Boron Nitride Porous 3D Structure and Ethyl Cellulose on ITO PET Substrate (Manuscript under preparation)

Other Publications

[1]   Bhavya, A. S.; Nair, A. A.; Surendran, K. P. Fluorinated Hexagonal Boron Nitride as Multiferroic Magneto-electric Material (Manuscript under preparation)

[2]   Bhavya, A. S.; Surendran, K. P. "Exfoliation Methods and Functionalization Techniques of Hexagonal Boron Nitride" (Book chapter communicated)

List of Conference Proceedings

[1] Bhavya, A. S.; Surendran, K. P. Band gap tuning of hexagonal boron nitride for microelectronic device applications, 3rd International Conference on Advanced Functional Materials (ICAFM 2019), held on 9 December, 2019 CSIR NIIST, Thiruvananthapuram, India (Poster presentation)

Abstract: Two dimensional hexagonal boron nitride (h-BN) is an isomorph of graphene with a very similar layered structure. This 2D material exhibits high mechanical strength, thermal stability and chemical inertness which qualify them suitable for application in the field of transistors, nergystorage and photoelectric devices. The insulator characteristic of hexagonal boron nitride delimits its applications in microelectronics. Its poor electron mobility is stemmed from its wide optical bandgap 5.6 eV, which can be tuned by a number of strategies such as by doping, substitution, functionalization and hybridization. For microelectronic applications, hBN can be used only if one can bring about its band gap to semiconducting ranges, where band gap plays a central role that governs the electron transport and light-matter interactions in 2D materials. Chemical modification of h-BN by functionalizing its surface with various dopants, is a convenient strategy to tailor the bandgap of 2D materials. In the present research, the layered structure of h-BN is presented as an ideal platform for band gap engineering. With this objective, fluorinated hexagonal boron nitride nanosheets were prepared by using simple chemical functionalization method in which fluorine doped into the mechanically exfoliated boron nitride in isopropyl alcohol (IPA). Our initial results suggest that an impressive reduction in bandgap occurred from 5.6 eV to below 3 eV. These experiments were repeated several times to test the consistency of results. Various spectroscopic and surface morphological characterizations were done and assessing the applicability of bandgap tuned h-BN in electronic devices are currently underway.

[2] Bhavya, A. S.; Surendran, K. P. Acid Mediated Synthesis of Fluorinated Hexagonal Boron Nitride for Magnetic Semiconductor applications, International conference on Physics of Materials and Nanotechnology (ICPN 2021), held on 28-29 October, 2021 Mangalore University, through MS Teams online platform (Poster presentation)

Abstract: Two dimensional hexagonal boron nitride (2D-hBN), one of the most promising inorganic nanomaterial, is isostructrural to graphene due to its very similar layered structure. Owing to its exotic opto-electrical properties, mechanical robustness, thermal stability and chemical inertness, this material has been extensively studied for application in field effect

transistors (FETs), tunneling devices, energy storage devices, photoelectric devices and nanofillers. Through properly designed functionalization, it is expected that many exotic and novel properties can emerge in 2D materials. 2D-hBN being an insulator with optical bandgap ~5.5 eV, its band structure can be engineered by a number of strategies such as doping, substitution, functionalization and hybridization, thereby making it a truly versatile functional material. Electrical transport measurements done on 2D-hBN reveal that its wide band gap delimits its applications in microelectronics. They can be qualified to use in electronic devices, only if one can reduce its band gap to semiconducting range (close to those of conventional semiconductors such as Si, GaAs etc). Chemical modification of h-BN by functionalizing its surface with various dopants, provide a platform for reducing its bandgap. The present work reports that meticulously controlled fluorination in hexagonal boron nitride nanosheets could be achieved through a simple acid-mediated chemical functionalization method. In this process, fluorine is doped into the mechanically exfoliated BNNSs, and as a consequence, its bandgap is reduced from 5.6 eV to below 3 eV. More importantly, the acid mediated fluorination can induce magnetism in the diamagnetic h-BN system. As a result of this combined effect, this material can be utilized as a magnetic semiconductor for device level applications.

[3] Bhavya, A. S.; Varghese, H.; Chandran, A.; Surendran, K. P. 2D-Hexagonal Boron Nitride Nanosheets/BoPET Assembly based Triboelectric Nanogenerator for Mechanical Energy Harvesting Applications, International Conference on Technologies for Smart Green Connected Societies (ICTSGS-1), held on November 29-30, 2021 through MS Teams online platform (Oral presentation)

Abstract: Boron nitride nanosheets (BNNSs), a structural analog of graphene having a hexagonal planar structure with alternate Boron and Nitrogen atoms. This 2D layered material has attracted ever-growing research interest in the past few years, due to its superior mechanical, electrical, and thermal properties. All along the history of mankind, there exists an ever growing demand for clean, sustainable, and efficient sources of energy. Since conventional energy sources are dwindling, new class of energy harvesting nanogenerators (NGs) have been extensively investigated during the last few decades which are capable of harvesting energy from the working environment such as heat, light, and mechanical vibrations. Among them, triboelectric nanogenerators (TENGs) have proven to be a promising technology due to their high efficiency, low cost, and ease of harvesting from the natural environments. Search for new materials along with cutting-edge designs are going on, aimed to enhance the output performances of triboelectric nanogenerators (TENGs). Single layered 2D materials are rarely being tested in TENG devices. Transparency, flexibility, and very high surface-to-volume are the basic characteristics of 2D materials. Along with these properties, the atomic layer thickness also contributes to the possibility to obtain very thin devices, even if stacking structures are used in the fabrication process.

In the present research, we have successfully fabricated a contact separation mode TENG using a liquid-phase exfoliated 2D material, hexagonal boron nitride (h-BN) which is employed as an efficient triboelectric electron acceptor material. In contact-separation mode TENGs, the fundamental mechanism of electricity generation depends on the contact electrification and electrostatic induction process occurring in the triboelectric materials which should lie far apart in the triboelectric series. Ultra-sonication assisted liquid-phase exfoliation method in DMF solvent is used for the exfoliation of bulk h-BN. Subsequently, an energy-efficient contact separation mode TENG (CS-TENG) prototype was fabricated using exfoliated boron nitride nanosheets (BNNSs). The exfoliated BNNSs were spin-coated on the surface of BoPET utilizing polyvinyl butyral as a binder for the thin film, where the 2D material can act as the triboelectric negative material, against the paper as the counter positive material with glass as rigid structural support for the device. In order to provide the necessary recoil during contact separation, two sponges were docked between the tribo-layers that maintain a separation distance of 3 mm. The new BNNSs based CS-TENG device, paired with ordinary paper as counter material, yielded excellent results. Even under moderate finger tapping, the fabricated device could generate an output voltage of ~200 V and a current density value of ~0.48 mA/m^2. The highest value of power density for the BNNSs incorporated TENG device reached 0.14 W/m^2, which is much higher than that of the TENG device without the BNNSs. Small electronic gadgets such as LCD clocks, digital thermometers, and LEDs can be successfully powered using BNNSs/BoPET-paper TENG. The present concept of incorporating 2D materials in TENG design, opens door to new horizons of application to 2D materials, as an efficient booster of the output power density of TENGs. Thus, this method has been proven to be a promising alternative for satisfying the demands of distributed energy for the Internet of Things (IoTs) and sensor networks. With the further improvement in the output performance of h-BN incorporated TENGs, their application can be extended for powering small electronic gadgets for micro or nano power sources, building self-powered systems, and also for soft/flexible electronics.

[4]   Bhavya, A. S.; Varghese, H.; Chandran, A.; Surendran, K. P. High Power Output Generation in PET-paper based Contact-Separation Mode TENG Using Hexagonal Boron Nitride Nanosheets as Triboelectric Negative Material, International Conference on Chemistry and Applications of Soft Materials (CASM 2022), held on July 25-27, 2022 CSIR- NIIST, Thiruvananthapuram (Poster presentation)

Abstract: Incorporation of new materials through innovative designs is actively pursued in triboelectric nanogenerators (TENGs), with the central aim to enhance their output performance. Single layered 2D materials are rarely being tested in TENG devices. Transparency, flexibility, and very high surface-to-volume are the basic characteristics of 2D materials. Along with these properties, the atomic layer thickness also contributes to the possibility to obtain very thin

devices, even if stacking structures are used in the fabrication process

   In the present research, we have successfully fabricated a contact separation mode TENG using a liquid-phase exfoliated 2D material, hexagonal boron nitride (h-BN). Ultra-sonication assisted liquid-phase exfoliation method in DMF solvent is used for the exfoliation of bulk h-BN. The exfoliated BNNSs was spin-coated on the surface of BoPET using polyvinyl butyral as the binder for the thin film. Here the 2D material can act as the triboelectric negative material, against the paper as the counter positive material, and the innovative design yielded excellent results.

   Even under moderate finger tapping, the fabricated device could generate an impressive output voltage of ~200 V and a current density value of ~0.48 mA/m². The highest value of power density for the BNNSs incorporated TENG device reached 0.14 W/m², which is much higher than that of the TENG device without the BNNSs. Small electronic gadgets such as LCD clocks, digital thermometers, and LEDs can be successfully powered using BNNSs/BoPET-paper TENG

[5] Bhavya, A. S.; Varghese, H.; Chandran, A.; Surendran, K. P. 2D Hexagonal Boron Nitride Nanosheets-Polycarbonate Screen Printable Ink for Flexible Triboelectric Nanogenerator Applications, National Conference on Advanced Materials and Manufacturing Technologies (AMMT 2023), held on February 23, 2023 CSIR-NIIST, Thiruvananthapuram (Poster presentation)

Abstract: Boron nitride nanosheets (BNNSs), an isomorph of graphene with a very similar layered hexagonal planar structure. This 2D material offers extremely high mechanical strength, unique electronic properties, flexibility and transparency, that has attracted tremendous research interest worldwide. Growing demands for Boron nitride nanosheets (BNNSs), an isomorph of graphene with a very similar layered hexagonal planar structure. This 2D material offers extremely high mechanical strength, unique electronic properties, flexibility and transparency, that has attracted tremendous research interest worldwide. Growing demands for clean and sustainable sources of energy harvesting techniques brings rapid progress in the development of triboelectric nanogenerators (TENGs). These devices can energize small scale portable devices scavenging available mechanical energy and converting it into electricity. In comparison with traditional manufacturing methods, ink-based printing techniques can be suitably employed to manufacture TENGs owing to low cost, superior fabrication accuracy, highly versatile and satisfactory production efficiency etc. Against this background, a high-performance flexible screen printed TENG was developed here using 2D-hexagonal boron nitride nanosheets (BNNSs) composite ink, which was screen-printed on BoPET substrate as a triboelectric contact layer in TENG design. Remarkably, the flexible screen printed TENG fabricated using BNNSs based ink as tribo-negative material, paired with the printed positive polyvinyl pyrrolidone (PVP) on Mylar as tribo-positive material, exhibited an impressively high voltage of ~810 V and a short-circuit current density of ~0.77 mA/m² respectively under an external force of ~10 N with 5 Hz

frequency. Our research results suggest that these devices are useful for powering handheld electronic devices.

SCI PUBLICATIONS
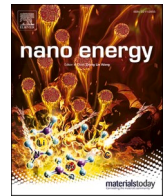
Massive enhancement in power output of BoPET-paper triboelectric nanogenerator using 2D-hexagonal boron nitride nanosheets

Ainikulangara Sundaran Bhavya [a,b], Harris Varghese [a,b], Achu Chandran [a,b,*], Kuzhichalil Peethambharan Surendran [a,b,*]

[a] Materials Science and Technology Division, CSIR, National Institute for Interdisciplinary Science and Technology (CSIR-NIIST), Industrial Estate P.O., Thiruvananthapuram 695019, India
[b] Academy of Scientific and Innovative Research (AcSIR), Ghaziabad 201002, India

ARTICLE INFO

ABSTRACT

In the present era of the Internet of Things (IoT) and sensor networks, clean and sustainable power sources are in huge demand, and triboelectric nanogenerators (TENGs) are a hot cake in green energy production. Here, we have developed a contact-separation mode TENG using liquid-phase exfoliated 2D-hexagonal boron nitride nanosheets (BNNSs) coated on biaxially-oriented polyethylene terephthalate (BoPET) and paper as counter triboelectric materials, which showed an impressive 70 times higher power output than simple BoPET-paper TENG assembly. Even under a moderate finger tapping force ($\sim$3 N), the developed BNNSs/BoPET-paper TENG device could generate an open circuit output voltage of $\sim$200 V and a short circuit current density of $\sim$0.48 mA/m^2. While under load testing, the peak value of electric power density for the BNNSs/BoPET-paper TENG device reached $\sim$0.14 W/m^2 at 200 MΩ resistive load. The incorporation of BNNSs has significantly enhanced the electron-accepting capabilities of the BoPET film which is evident from the enhanced dielectric permittivity of the BNNSs/BoPET assembly, and thus resulted in the enhanced electrical output of TENG. Additionally, the fabricated BNNSs-TENG was successfully demonstrated for powering electronic gadgets such as LCD clock, digital thermometer, and LEDs through cyclic finger tapping force.

1. Introduction

Smart cities of future demand power generation from multiple sustainable sources which can efficiently power up various energy-autonomous Internet of Things (IoT) based sensors. Within the past decade, intense research has been done in this domain to develop sustainable techniques that can harness mechanical motion into useful electrical energy [1]. Triboelectric nanogenerator (TENG) is suggested as the most promising among green energy harvesters, since it can directly convert ambient mechanical energy into electricity, without leaving any carbon footprint. Physical movements [2], mechanical vibrations [3], water waves [4], and wind power are the various forms of mechanical energy sources [5]. TENGs can harvest electrical energy from these abundant mechanical energy sources where the energy generation is based on the combined effect of two phenomena; triboelectric effect and electrostatic induction [6]. In a typical triboelectric nanogenerator operating in contact separation mode, the flow of

electrons is triggered when two dissimilar surfaces touch each other and then separates. To improve its efficiency, several strategies have been adopted such as the optimal selection of triboelectric materials and their combinations [7], surface modification of the materials by utilizing doping with nanoparticles or chemical treatments [8], designing novel device configurations [9], and also the method of polarization or corona charging which can inject charge into the triboelectric materials [10]. The power requirement for the working of small electronic devices like sensors, actuators, and wireless transmitters requires a micro- to milli-Watt power range[11]. Making use of batteries for this purpose has to address challenges such as limited life span, recycling, and other environmental-related issues [12].

2D layered materials, due to their rich spectrum of properties and atomic level thickness, offer an ocean of properties like transparency, flexibility, and together with bandgap engineering, it opens up new horizons of applications in wearable electronics, photonics, and healthcare sector [13–15]. 2D layered materials are attractive
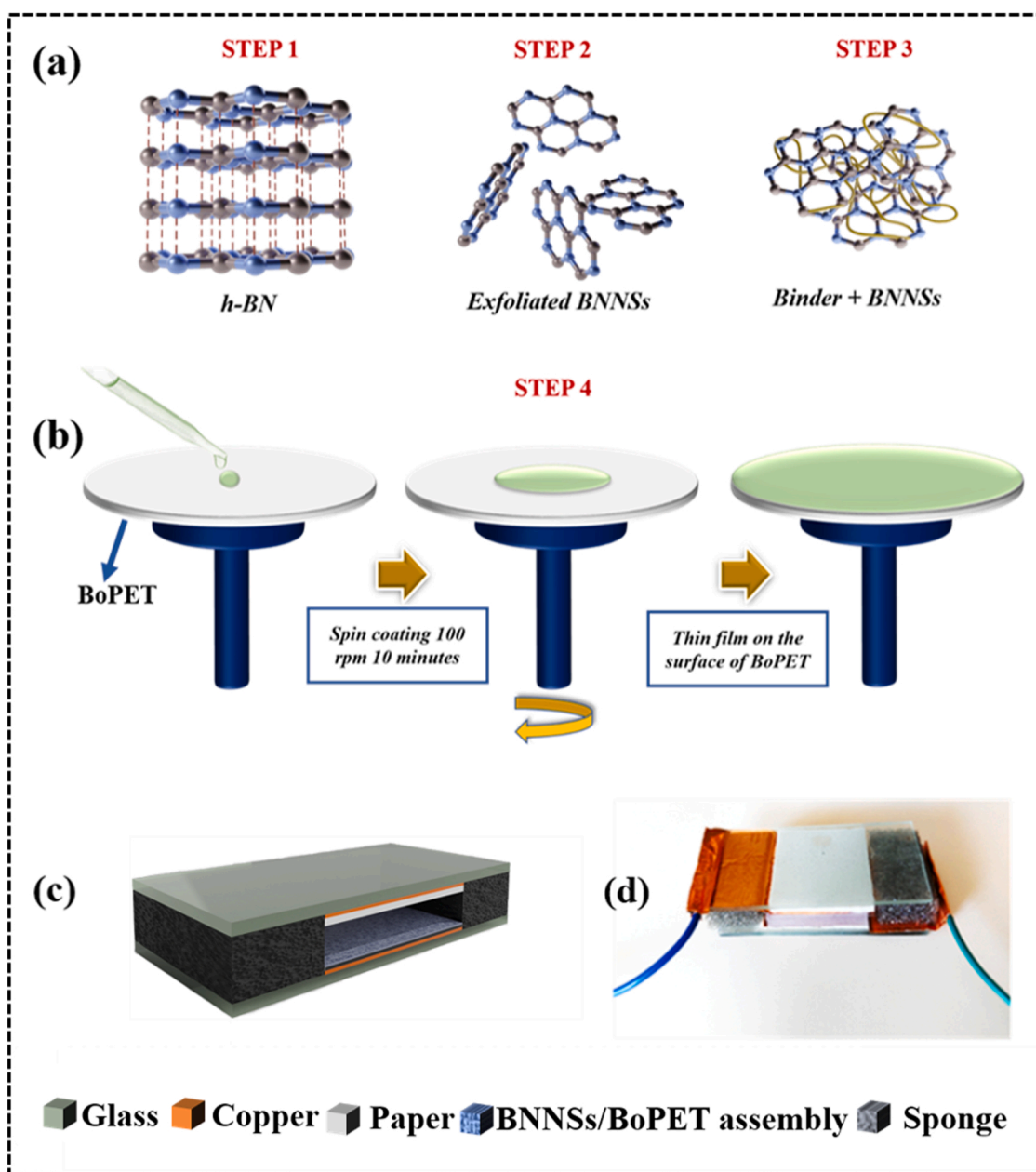

Fig. 1. (a) and (b) Schematic illustration of the exfoliation process and preparation of thin-film BNNSs on BoPET substrate through various process steps. (c) 3D model of the BNNSs/BoPET-paper TENG rendered using blender software. (d) Photograph of actual device.

candidates for TENGs since they have a high transverse area with the maximum amount of surface atoms, which qualify them suitable for applications in the fields of wearable and body insertable electronic devices [16]. However, the triboelectrification mechanism of 2D materials is not profoundly understood. In 2014, Kim et al. reported the first graphene-based transparent, flexible TENG in which large-scale graphene was grown through CVD layer-by-layer transfer technique on copper and nickel foils [17]. Recently, Seol et al. revealed the triboelectric charging behaviour of a series of 2D materials, including transition metal dichalcogenides (TMDCs). They exfoliated 2D materials chemically from their bulk flake in the liquid medium which was subsequently used for the fabrication of various materials combinations in TENGs. Finally, a modified triboelectric series was developed after including these 2D materials, by systematically analysing the output signals from various TENGs combinations [13]. Later, Dong et al. reported MXene based high-performance TENG capable of generating power from simple muscle movements [18].

Hexagonal boron nitride (h-BN), a popular 2D material isostructural to graphene, has individual layers made up of covalently bonded boron and nitrogen atoms held together by weak van der Waals force of attraction [19]. For microelectronic applications, 2D h-BN can be well integrated with other materials, such as graphene, transition metal dichalcogenides, and various polymers. Its exotic optoelectrical properties combined with high mechanical robustness, thermal stability, and chemical inertness qualify them as suitable materials for future electronic device applications [20,21]. In short, the research on single-layered materials for TENG energy harvesting is still in its rudimentary stage, with the need for improved fabrication techniques and a better understanding of electrostatic phenomenon happening in 2D materials during triboelectrification.

Against this background, we developed a boron nitride nanosheets based TENG in which the mechanically exfoliated BNNSs in a liquid medium of comparable surface energy, which was spin-coated onto BoPET substrate, after adding polyvinyl butyral (Butvar) as a binder.

This BNNSs/BoPET assembly was used as a negative triboelectric material paired with paper as the counter positive material for the fabricated TENG. In this device combination, the copper foil was used as electrodes, which are supported on the glass substrate. The fabricated BNNSs/BoPET-paper TENG device showed impressive electrical output performance with an open circuit voltage of ~200 V, a current density of ~0.48 mA/m^2, and a peak power of 0.14 W/m^2, which is ~70 times higher than simple BoPET-paper TENG.

Improving the output performance of the TENG is desirable for its real-world applications. Suitable material combinations and optimized conditions are vital elements for the output performance and the mechanical stability of the fabricated device. Here, we obtained a tremendous power enhancement in the triboelectric output performance of a BoPET-paper TENG by introducing 2D hexagonal boron nitride (h-BN) material into the negative friction layer. Our research revealed that the introduction of 2D h-BN not only enhanced the output of the triboelectric device massively but also supplemented the flexibility, lightness, and superior mechanical strength, which qualifies this material as a suitable candidate in wearable, flexible energy harvesting and storage devices.

2. Experimental

2.1. Materials

Boron nitride powder (98% purity, 1 μm size) was used as the starting material (Sigma Aldrich, USA). Dimethylformamide (DMF) was used as the solvent for exfoliation while polyvinyl butyral (Butvar-B-98) was used as a binder for spin coating (Sigma Aldrich, USA). All chemicals were used as received, without any further purification. The substrate used here is the commercially available biaxially oriented polyethylene terephthalate (BoPET, Mylar®) and a double side conducting copper foil tape (3 M Co.) was used as electrodes. Glass slides of proper dimension act as mechanical support for the device.

2.2. Exfoliation of bulk h-BN to 2D h-BNNSs

For the liquid phase exfoliation process, bulk hexagonal boron nitride powder of about 1 g was added to 100 ml of DMF solvent contained in a 250 ml beaker, and the resulting solution was subjected to a temperature-controlled ultrasonication process for 48 h at a controlled temperature of 50 °C, with the aid of low power bath sonicator. The unexfoliated layers were allowed to settle, by keeping the solution undisturbed overnight. The supernatant solution containing the exfoliated nanosheets was separated by centrifugation at 10,000 rpm for 10 min and the top 20 ml solution of the exfoliated nanosheets was collected. The exfoliation process is pictorially represented in figure1 (a) as step 2. The exfoliated BNNSs solution in DMF was mixed with 0.1 g polyvinyl butyral as a binder for making good dispersion. Then this was again sonicated for 3 h using an ultrasonic bath for making a well-dispersed solution of BNNSs. The resultant milky white-colored dispersion of exfoliated nanosheets was used for thin-film fabrication (which is depicted as step 3 in Fig. 1(a)).

2.3. Preparation of thin-film BNNSs

A well-dispersed solution of exfoliated BNNSs in DMF was then cast as thin films using the spin coating technique. The spin coating (using SpinNXG-P1, Apex Instruments, India) was done on BoPET substrate in tailor-made dimensions (2.5 cm × 2.5 cm). The rotation speed was set at 100 rpm, which was optimized to have a thickness < 25 μm, where better adhesion to the substrate was provided by the binder. The spin coating process continued for 10 min at 100 rpm speed, forming a uniform film of BNNSs dispersion on the BoPET substrate. Finally, the films were dried in an oven at a set temperature of 80 °C for 12 h for complete solvent evaporation. The thin-film formulation process is pictorially

represented as step 4 in Fig. 1(b).

2.4. Fabrication of TENG device

The BNNSs based TENG fabrication process is in the following manner. Initially, two glass slides of 5 cm × 2.5 cm dimension, as supporting substrates, were chosen. In practical scenarios, the uniform distribution of force throughout the contact surface could not be guaranteed. This would hinder the TENG to perform in its peak efficiency, thus providing rigid support such as glass which allows the force to be evenly distributed throughout the material surface ((fig. S1, Supporting Information). The open-circuit voltage (V_{oc}) value of the flexible TENG is 150 V, and the short-circuit current density (J_{sc}) of (0.2 mA/m^2). The voltage and current density values show that the observed output is comparably lower than the TENG device with glass support). In all devices, double side conductive copper foils (3 M) were pasted over glass support as electrodes, using adhesive tapes. The active area of the copper electrode is set to be 6.25 cm^2 (2.5 cm × 2.5 cm). On top of the adhesive side of the first copper electrode, BoPET which is having the BNNSs thin films was placed. Thereafter, for the second glass slide with copper, a piece of paper with proper dimension (2.5 cm × 2.5 cm) was pasted as the counter triboelectric material. Subsequently, two sponges were docked between the substrates in the vacant spaces to maintain a separation distance of 3 mm in between the tribo-layers and to provide the recoiling force. The overall structure of the fabricated TENG is schematically represented in Fig. 1(c). Finally, two copper leads were attached to the electrodes for the ease of connecting them to the measuring instruments. The photograph of the final BNNSs/BoPET-paper TENG is also depicted in Fig. 1(d).

2.5. Characterization methods

Atomic force microscopy in tapping mode (AFM, Multimode, Bruker, Germany) was used to investigate the morphology and related information regarding the layered structure of the exfoliated BNNSs sample. The sample preparation was done by drop-casting the diluted sample solution of BNNSs on a thin mica sheet. In addition, the surface roughness of the thin film structure on the BoPET substrate was also analysed by this technique. The translucent, but layered structure of the nanosheets was further confirmed using high-resolution transmission electron microscopy (HRTEM) (FEI Tecnai G2 30S-TWIN, FEI Co., Hillsboro, OR, USA), by drop-casting the diluted BNNSs sample solution sonicated in a suitable solvent onto a copper carbon-coated grid. The phase purity of the BNNSs was analysed by XRD (Cu Kα radiation, PANalytical X′Pert PRO diffractometer, the Netherlands). Raman spectra of the exfoliated nanosheets and the material without exfoliation were examined using RAM HR Evolution Raman Spectrometer equipped with 532 nm DPSS laser (Horiba Scientific Lab, Tokyo, Japan). The surface morphological analysis and thickness of the prepared BNNSs thin film were carried out using scanning electron microscopy (Zeiss EVO 50, Oberkochen, Germany). The optical micrographic images of the sample were analysed using a polarizing optical microscope (Leica DM2700P, Germany) fitted with a charge-coupled device (CCD) camera. To study the characteristic bonds in BNNSs and to compare the chemical structure with and without the incorporation of 2D materials onto the substrate, the Fourier transform infrared (FTIR) analysis of the samples was carried out, using Nicolet Magna 560 FTIR (Thermo Scientific, Massachusetts, USA). The dielectric spectroscopic studies of the thin film structure BNNSs were performed using the impedance analyser (Solartron Impedance/Gain-Phase Analyser 1260 A, USA). The electrical output characteristics of TENG devices are recorded using a source measuring unit (Keithley 2450) and a current preamplifier (SR570, Stanford Research) integrated with a digital phosphor oscilloscope (Tektronix DPO2004B, USA). By moderate finger tapping, a cyclic mechanical force (~3 N) was applied to the device systematically and the generated electrical output of the TENG device was recorded. The load-dependent power density and
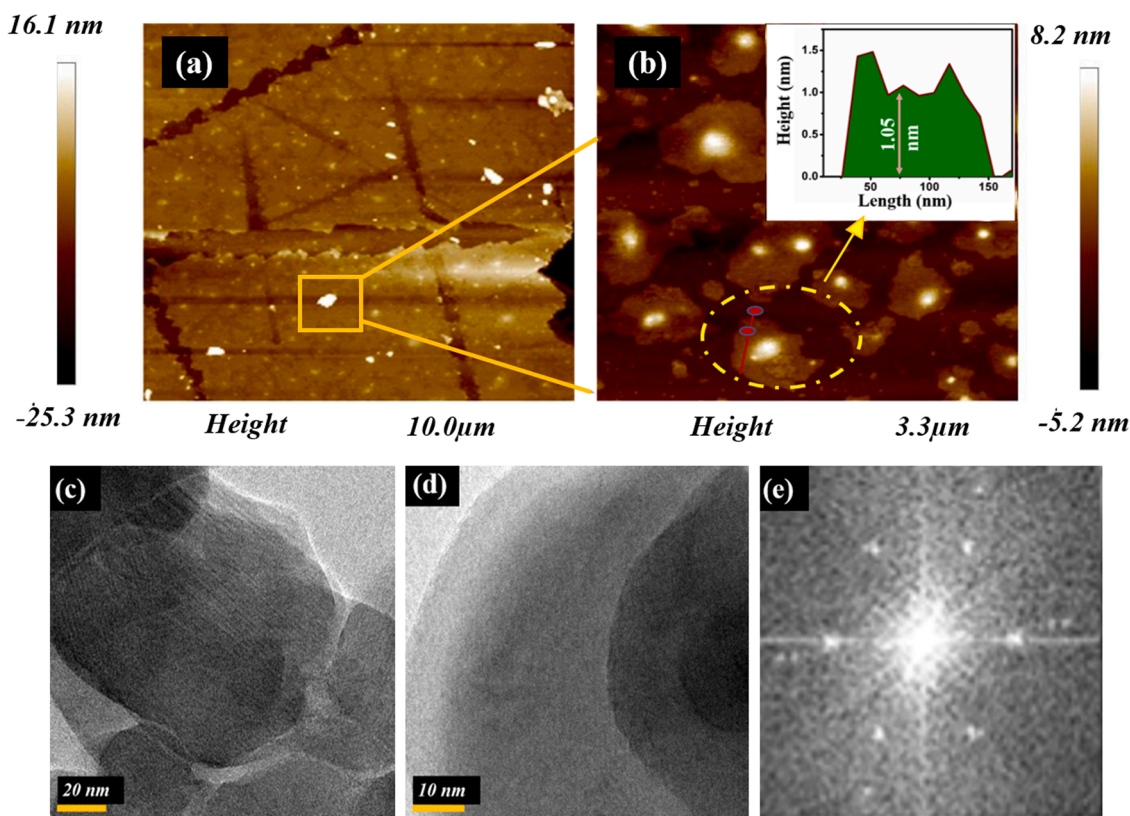
Fig. 2. (a) and (b) 2D AFM images of the exfoliated BNNSs in the tapping mode. Inset to (b) height profile of the exfoliated nanosheets. (c) and (d) TEM images of exfoliated BNNSs with a well-separated layered structure. (e) FFT pattern provides the typical six-fold symmetry and hexagonal view of the BNNSs.

capacitor charging profiles of the TENG were obtained with the help of different values of resistors and capacitors. To assess the versatility, the output performance of the TENG device was tested at various biomechanical forces like single finger tapping, simultaneous multiple finger tapping, and palm tapping, which all differ in the magnitude of force exertion. Further, the same TENG was tested under various frequencies of the applied load and also up to 10000 continuous operation cycles, to assess its durability.

3. Results and discussions

3.1. Structural and surface morphological characteristics of exfoliated BNNSs

Ultrasonication-assisted solvent exfoliation is one of the simplest and efficient ways for the exfoliation of layered materials, wherein the solvent should possess surface energy compared to the energy per unit area of the layered material. Here DMF was proved to be ideal to exfoliate the bulk material effectively, which was confirmed with the help of the following techniques.

Atomic force microscopy is traditionally used for collecting surface information as well as the lateral size (edge-to-edge) and thickness of
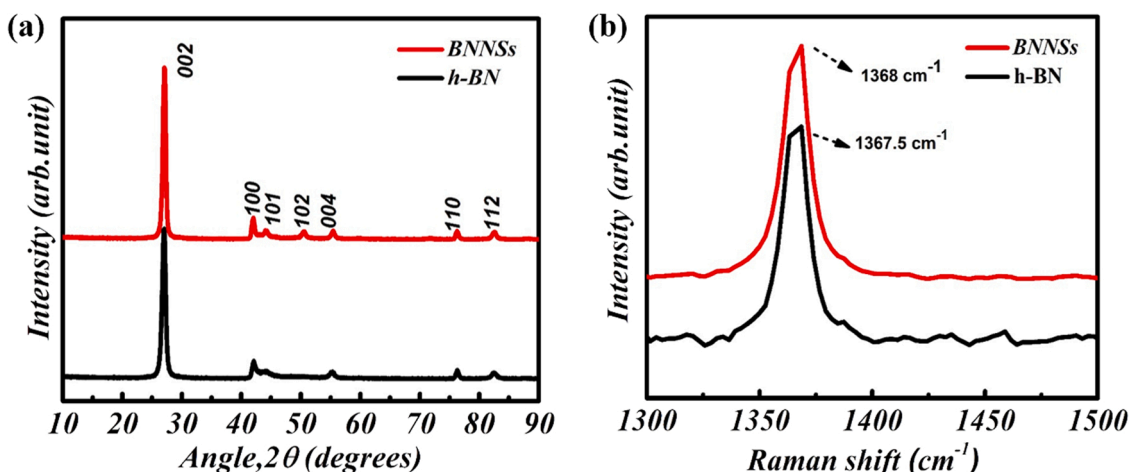

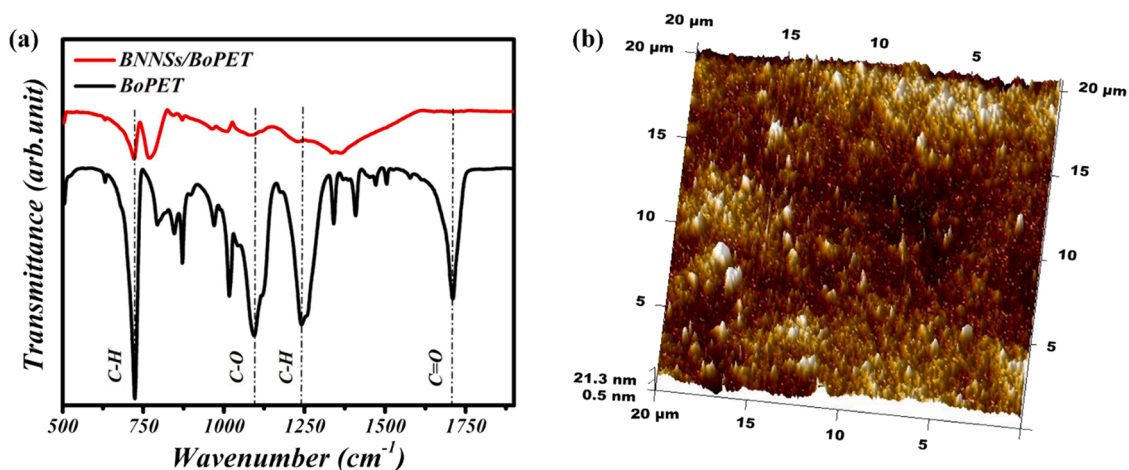**Fig. 3.** (a) XRD pattern of bulk h-BN and BNNSs. (b) Raman spectra of bulk h-BN and BNNSs.

Fig. 4. (a) FTIR spectra of uncoated BoPET film and spin-coated BoPET film with BNNSs. (b) Atomic force micrographic 3D image of BNNSs/BoPET thin-film structure.

layered materials. The AFM images in the tapping mode (see Fig. (2)(a) and (b)) confirm the exfoliation of hexagonal boron nitride which were recorded after drop-casting them onto a clean mica sheet. The height profile in the inset of Fig. 2(b) shows that the typical lateral size of the nanosheet is around 130 nm which indicates the reduction of the lateral dimension of the exfoliated material compared to its bulk counterpart of 1 μm size common in the liquid phase exfoliation process[22]. The height from the same holder substrate (mica) to the exfoliated layer provides the sheet thickness value, which is of the order of 1.05 nm. This value is in agreement with the reported values of 0.85 nm for one or two

layers. These results indicate that effective delamination of the bulk material down to one or two layers, which is an indirect testimony to the efficiency of the exfoliation method used[23,24].

Fig. 2(c) and (d) show the TEM images of the exfoliated BNNSs. The continuous solvent-assisted ultrasonication gives rise to continuous dense and sparse waves, forming an enormous number of microbubbles that implode violently, thereby creating high-speed liquid jets with high pressure and temperature [25]. These instantaneous high-pressure fronts of cavitation render constant but high pressure on bulk boron nitride, forcing them to slide apart, after releasing an enormous amount
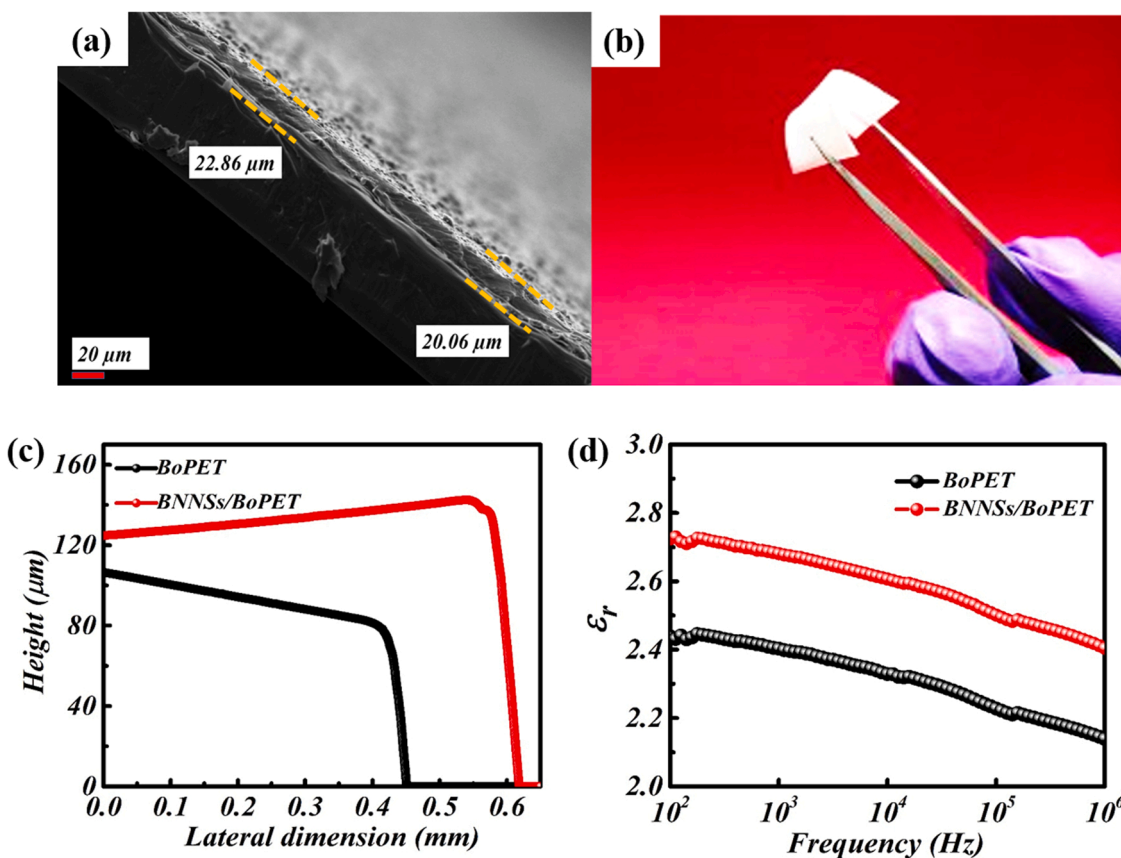

Fig. 5. (a) Magnified cross-sectional SEM micrograph showing the thickness of the BNNSs thin film on BoPET substrate. (b) Photographic image of the flexible exfoliated BNNSs spin-coated on the surface of BoPET substrate. (c) The profilometric thickness of BoPET and BNNSs/BoPET films. (d) Dielectric dispersion spectrum of BoPET and BNNSs/BoPET.

of energy to overcome the interlayer van der Waals force [26,27]. The right choice of solvent supplements this process by providing the necessary shear force to delaminate the individual h-BN layers. The so derived exfoliated sheets have lateral dimensions in the nanometer range, compared to the bulk material ($\sim$1 μm), indicating a reduction in size [28]. The seemingly translucent nature of the sheets in the present research indicates that the exfoliated sheets are thin and well-separated. The typical six-fold symmetry or honeycomb-like hexagonal planar structure is revealed from the fast Fourier transformation (FFT) pattern, which is included as Fig. 2(e). Further, the TEM micrographs indicate that there is no damage to the sheets during the synthesis and the formed thin sheets are well crystallized in nature without any defects or dislocations [29].

The crystal phase structure of the as-prepared BNNSs sample and its delamination from h-BN can be identified by analyzing the powder X-ray diffraction (XRD) patterns. From Fig. 3(a), it is evident that BNNSs are completely phase-pure which is indexed based on JCPDS file card no (00–034–0421), belonging to P6$_3$/mmc space group. The observed diffraction peaks correspond to (002), (100), (101), (102), (004), (110), and (112) are the crystallographic planes of the hexagonal phase of BN. The efficient exfoliation of bulk h-BN is confirmed from the increased intensity of the XRD peak for the crystal plane (002) in BNNSs. The increased intensity value suggests that the more exposed nature of the (002) crystal planes of BNNSs and the exfoliation takes place along this plane without any crystalline structure destruction[30]. Fig. 3(b) illustrates Raman spectra of the BNNSs along with their bulk counterpart. The observed Raman peak of BNNSs occurs at 1368 cm^{-1}, which is due to the E$_{2g}$ phonon mode. After exfoliation, the E$_{2g}$ phonon mode is slightly blue-shifted compared to the bulk h-BN, even though this shift is within the experimental error limit. The blue-shift can be explained by phonons softening phenomena by the interlayer interactions. This interaction between layers causes the elongation of B–N bonds in bulk h-BN[31,32].

3.2. Properties of Thin Film BNNSs on BoPET Substrate

The presence of BNNSs in the thin film structure of BNNSs/BoPET was examined by FTIR spectra (see Fig. 4(a)). Two core peaks of the material h-BN were identified at 786 cm^{-1} and 1342 cm^{-1}, which are associated with the broad B–N–B out-of-plane bending vibrations as well as in-plane B–N stretching vibrations respectively[33,34]. The peak observed at 1730 cm^{-1} can be attributed to the presence of C=O stretching of the ester groups present in the polymer BoPET. The peak centered at 1409 cm^{-1} is attributed to the presence of an aromatic ring in the polymeric structure. Characteristic peak around 1235.6 cm^{-1} due to the aliphatic C-H bending vibrations. The band observed at 1143 cm^{-1} attributed to the stretching vibrations of C-O and C-H skeletons. The characteristic peak centered at 730 cm^{-1} can be assigned to the out-of-plane C-H bending vibration of the polymer BoPET. Some of these characteristic peaks of the polymer BoPET are also observable in the BNNSs incorporated polymer film with the characteristic peaks of h-BN[35,36]. A typical AFM micrograph of the thin film, after spin coating on the surface of BoPET, is depicted in Fig. 4(b). A more apparent microstructure of the developed thin film on the substrate surface is clear from the three-dimensional AFM images. The average surface roughness (Ra) of the spin-coated BNNSs layer is about 7.9 nm and the root mean square roughness (Rq) value is nearly 10.2 nm which represents the standard deviation in surface heights. The extent of surface height variations can be available from these parameter values. Skewness indicates the measure of surface asymmetry or variation of the sample surface. For ideal planar surfaces, the skewness value should be zero. The lower positive value for skewness (0.55) indicates the smoothness of the thin film on the substrate. The kurtosis of the topography height distribution is the distribution of spikes from the mean position, where a normal distribution planar surface is having a kurtosis value of 3 nm. The spin-coated thin film on the BoPET substrate has a kurtosis value of 3.88 nm hence its surface is leptokurtoic[37,38].

The representative magnified cross-sectional SEM image of the BNNSs thin-film on BoPET substrate is given in Fig. 5(a). Characteristics like morphology, thickness, film packing, etc. of the thin-film structure viewed in the sectional image, reveal the quality of films. The flexibility of the spin-coated film could be seen in Fig. 5(b). Moreover, the optical micrographs of the BNNSs film (figure S2, Supporting Information) represent a uniform distribution over the substrate. To understand the surface morphology of these films further the representative SEM images of the BNNSs thin-film on BoPET are shown in (figure S3, Supporting Information). The thin-film structure of BNNSs spin-coated on the surface of BoPET supports the claim that the surface of thin-film is fairly uniform, and the presence of macropores is not observed. But on a closer look, some minor pores are visible, which is expected in the first place as a consequence of the solvent evaporation, and secondly, no post-printing sintering procedures were employed in the present protocol. From this observation, we can conclude that the presently adopted strategy is adequate to develop films with minimal aggregation of particles, discontinuity, and cracks when coated on BoPET substrate[39]. Further, the SEM surface morphology confirms the homogeneous distribution of polymer blends. Normally, hexagonal boron nitride needs functionalization to improve its interfacial adhesion. However, we used a simple sonication-assisted mixing of BNNSs directly, which provides better blending with polymer[40]. From the cross-sectional SEM images, the film's thickness is estimated to be approximately 20 μm. The thickness of the thin film was further measured by the profilometric technique (included in Fig. 5(c)). From surface profiling, the thickness of BoPET is nearly 106 μm and 125 μm for BNNSs spin-coated on the surface of BoPET. This difference in thickness value is nearly identical to the thickness obtained from cross-sectional SEM micrographs. The frequency-dependent dielectric variation of the thin film triboelectric friction material BNNSs/BoPET and BoPET only in the range of frequency 10^2–10^6 Hz is shown in Fig. 5(d). The incorporation of BNNSs results in a distinct dielectric permittivity increase of the normal BoPET substrate. The dielectric permittivity reaches 2.7 at 10^3 Hz for BNNSs/BoPET, whereas this parameter is nearly 2.4 only for the pure BoPET film. The dielectric properties of the triboelectric friction materials are closely related to the electric output performance of a TENG. The enhancement in the value of dielectric permittivity can also improve the charge trapping capability of the system[41], which further decreases the surface charge dissipation rate and also creates a visible enhancement in the surface charge density of the BNNSs/BoPET. The cumulative effect of these phenomena is expected to result in better electrical output performance of the TENG[42].

3.3. Properties of BNNSs/BoPET Triboelectric Nanogenerator

A vertical contact-separation mode TENG (CS-TENG) [43] arrangement with BNNSs/BoPET assembly, with paper as counter contact electrification material, was employed in the present research. The popularity of CS-TENG is due to its simple structural design, high instantaneous power density, and great device robustness compared with the other three fundamental working modes of the TENG [44]. This configuration is widely used to convert mechanical energy from finger typing [45], human walking [46], engine vibration [47], and also in biomedical systems [48]. As hinted before, spin-coating and subsequent heat treatment were employed for the BNNSs film development, which yielded thin and uniform BNNSs layers on the surface of BoPET, suitable for the fabrication of the TENG device. To assess the role of BNNSs on the output performance of the nanogenerator, a TENG device with bare BoPET was also fabricated with paper as the counter material. Both the devices bear the same positive contact layer (paper), and the detailed fabrication procedure is already given in the experimental section. The bottom stacked layer of BNNSs/BoPET in the friction layer acts as the negative friction material that can capture electrons from the top friction layer during the process of triboelectrification [7,49].
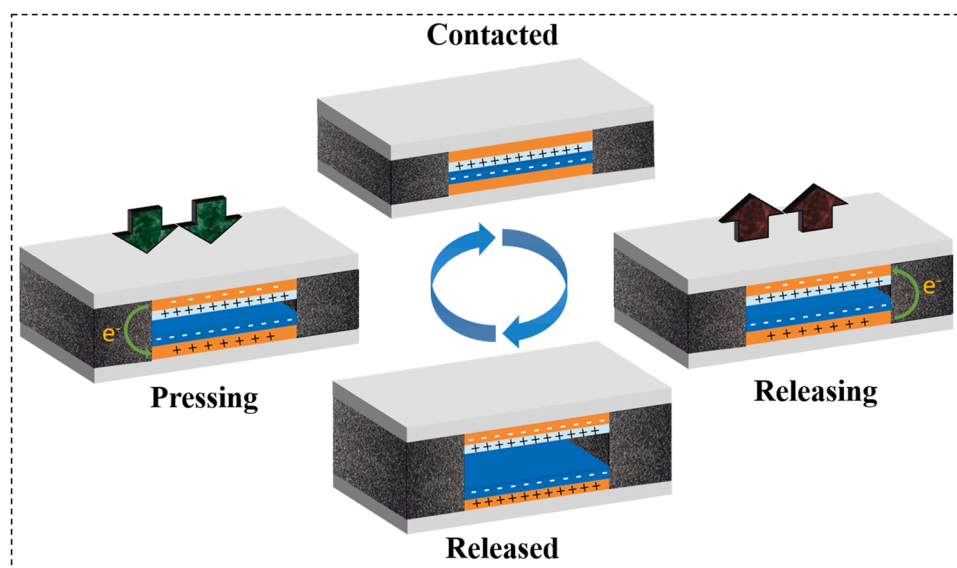
Fig. 6. Working mechanism of BNNSs/BoPET-paper TENG.
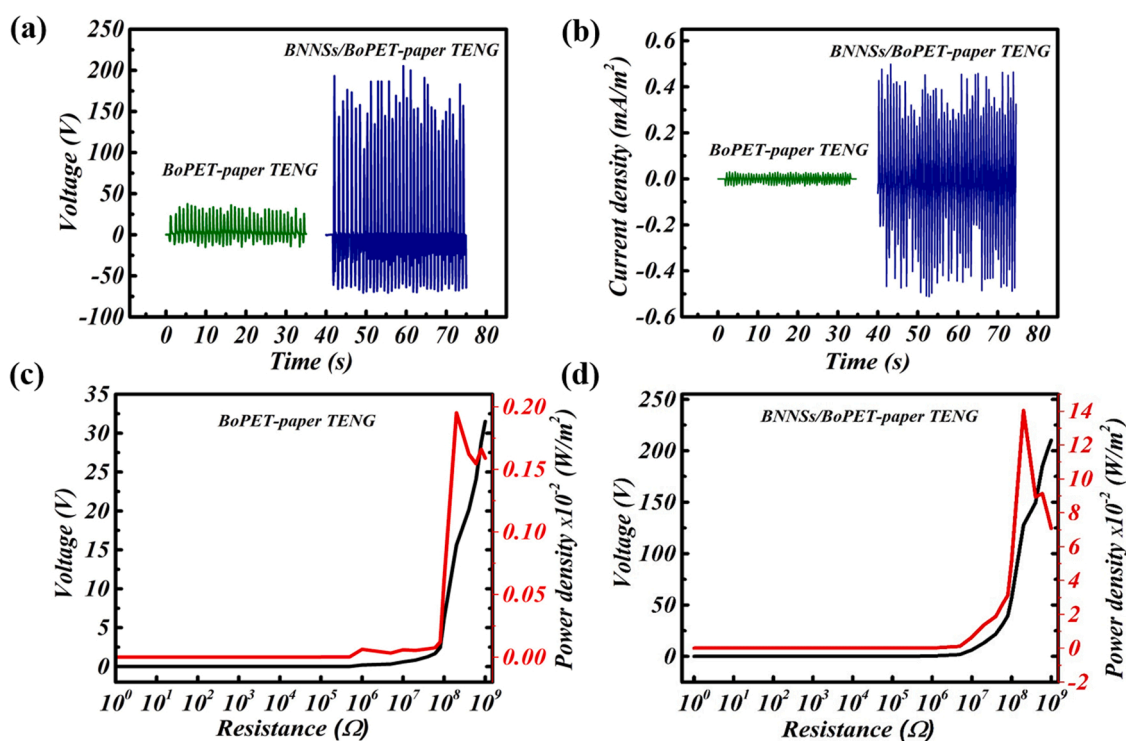

Fig. 7. (a) and (b) Open-circuit voltage & short-circuit current density generated from the BoPET-paper & BNNSs/BoPET-paper TENG respectively under single finger tapping force of ~3 N. (c) and (d) Output power density of the BoPET-paper TENG & BNNSs/BoPET-paper TENG under resistive load testing.

In contact-separation mode, the fundamental mechanism of electricity generation depends on the contact electrification and electrostatic induction process occurring in the triboelectric materials which should lie far apart in the triboelectric series [50]. Under an external force, physical contact is initiated between the two materials, having different electron affinity values, thereby generating opposite charges on surfaces, as schematically represented in Fig. 6. Once the contact is lost by releasing the external force, the generated triboelectric charges are separated, which induces charges on the electrodes. These free electrons will flow from one electrode to the other to maintain the electrostatic charge balance. As a result, an electrical potential

difference is created between the two planar electrodes placed on the top and bottom sides. On subsequent contact pressing, the electrostatic potential difference generated by the triboelectric charges diminishes, and the induced electrons will pump back [43,51]. The entire working mechanism is schematically represented in Fig. 6. Therefore, continuous pressing and releasing of the triboelectrically active structures drive the electrons to flow through the external circuit periodically [42]. In the present BNNSs incorporated TENG, the external force was provided by a moderate finger tapping (~3 N). The BNNSs/BoPET layer acts as an electron acceptor because the embedded BNNSs having the ability to trap electrons and behave as more triboelectrically negative similar to
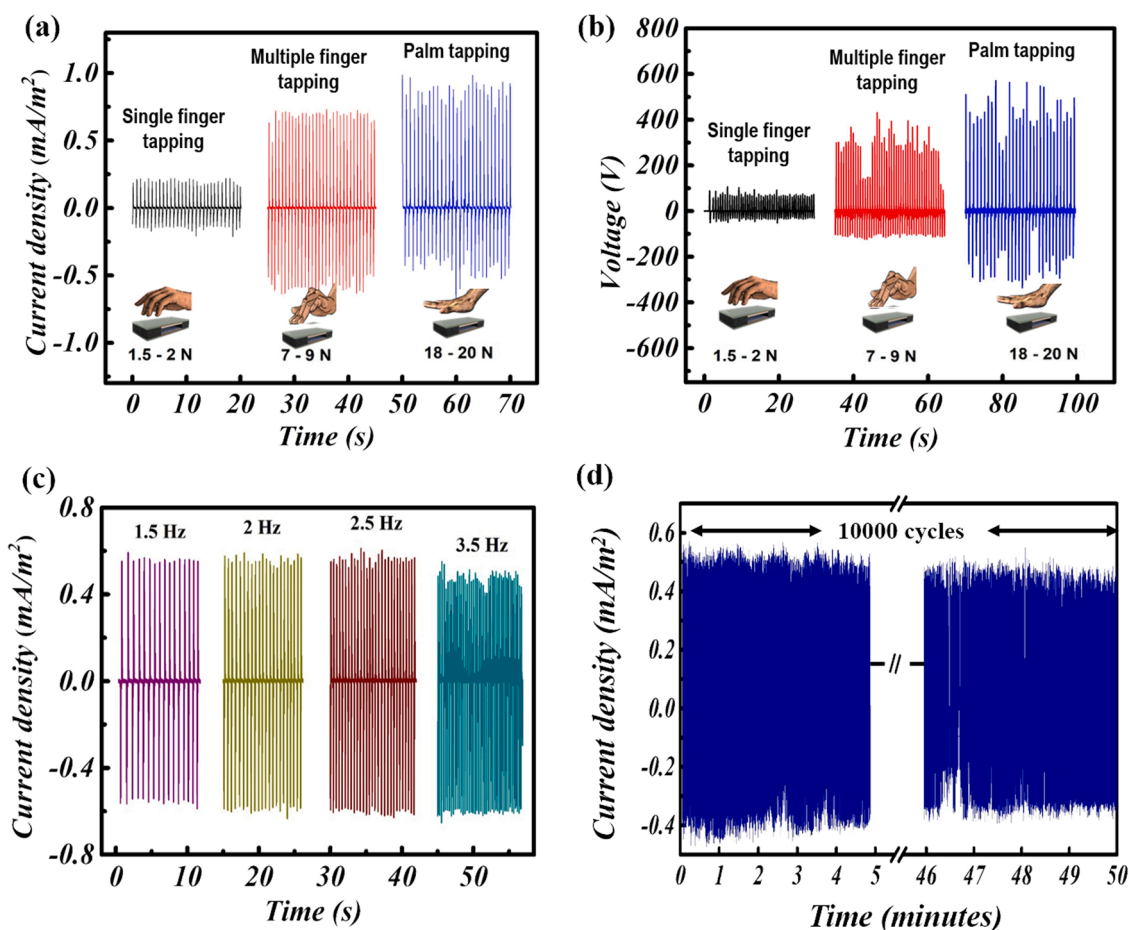
Fig. 8. (a) and (b) Short-circuit current density and open-circuit voltage generated from BNNSs/BoPET-paper TENG under various biomechanical forces such as single finger tapping, tapping with multiple fingers simultaneously, and tapping using palm. (c) Frequency dependence of generated current signals from the TENG device. (d) Durability test of the device BNNSs/BoPET-paper TENG over 10000 cycles.

other 2D materials [7].

The observed open-circuit voltage and current density of the fabricated TENG device with and without BNNSs are shown in Fig. 7(a) and (b) respectively. The open-circuit voltage (V_{oc}) of the BoPET against paper TENG (without BNNSs film) is about 36 V (figure S5, Supporting Information), whereas the open-circuit voltage value of the TENG with BNNSs film is as high as 200 V. Furthermore, it is seen from Fig. 7(b) that, the short-circuit current density (J_{sc}) of the TENG with BNNSs (0.48 mA/m^2) is comparably higher than that of the TENG without BNNSs (0.016 mA/m^2) (figure S5, Supporting Information). The output performance of the fabricated TENG devices was analysed under resistive loads ranging from 1 Ω to 1 G Ω. These experiments were carried out under ambient environmental conditions of relative humidity ~50%, and temperature ~ 27 °C.

As depicted in Fig. 7(c) and (d), the value of output voltage increases to 200 V with loading for BNNSs incorporated TENG as compared to the 36 V increment in TENG without BNNSs with the increase in load resistance. In addition, the electric power density (P_d) generated by the TENG can be calculated using the equation,

$$P_d = V^2/R \bullet A \tag{1}$$

where V is the voltage and R is the load resistance and A is the area of contact. From Fig. 7(c) and (d), it can be seen that the observed output power density initially increases to a sufficiently high value as resistance increases, and then it decreases as the resistance become too high. As per Eq. (1), the specific resistance at which maximum output power is delivered to the load is governed by the 'matching resistance' or

'impedance matching' phenomenon[52]. Here both the fabricated devices show impedance matching around a resistance value of ~200 MΩ. BoPET-paper TENG and BNNSs/BoPET-paper TENG devices exhibit a peak power density of 0.002 and 0.14 W/m^2 respectively, which shows a whopping 70 times power enhancement for the TENG, after the incorporation of an exfoliated BNNSs material.

To analyse the force-dependent output performance of the fabricated CS-TENG, different kinds of biomechanical forces such as single finger tapping (1.5–2 N), simultaneous tapping with multiple fingers (four, usually) (7–9 N), and tapping using palm (18–20 N), were carried out on the device and the corresponding current density and voltage generated were systematically analysed, as shown in Fig. 8(a) and (b). It should be noted that the average force exerted during single finger tapping is slightly inferior to moderate finger tapping (~3 N). The current density and voltage generated by the BNNSs /BoPET-paper TENG under various biomechanical forces mentioned above show that the palm tapping can generate an appreciable current density of ~1.0 mA/m^2 which is much higher than the other motions like single finger tapping (~0.25 mA/m^2) and simultaneous multiple finger tapping (~0.7 mA/m^2). The voltage curves under various forces (measured by using a voltage divider) follow the same trend as the current density curve, with a maximum value of voltage for palm tapping, which proportionately decreases with decreasing biomechanical force. Frequency-dependent current density is also depicted in Fig. 8(c), wherein the device was tested at 1.5 Hz, 2.0 Hz, 2.5 Hz, and 3.5 Hz. The BNNSs/BoPET-paper TENG shows almost the same output in the lower frequency ranges and as the frequency increases the output starts to decrease. The frequency dependency analysis showed that the BNNSs/BoPET-paper TENG is very
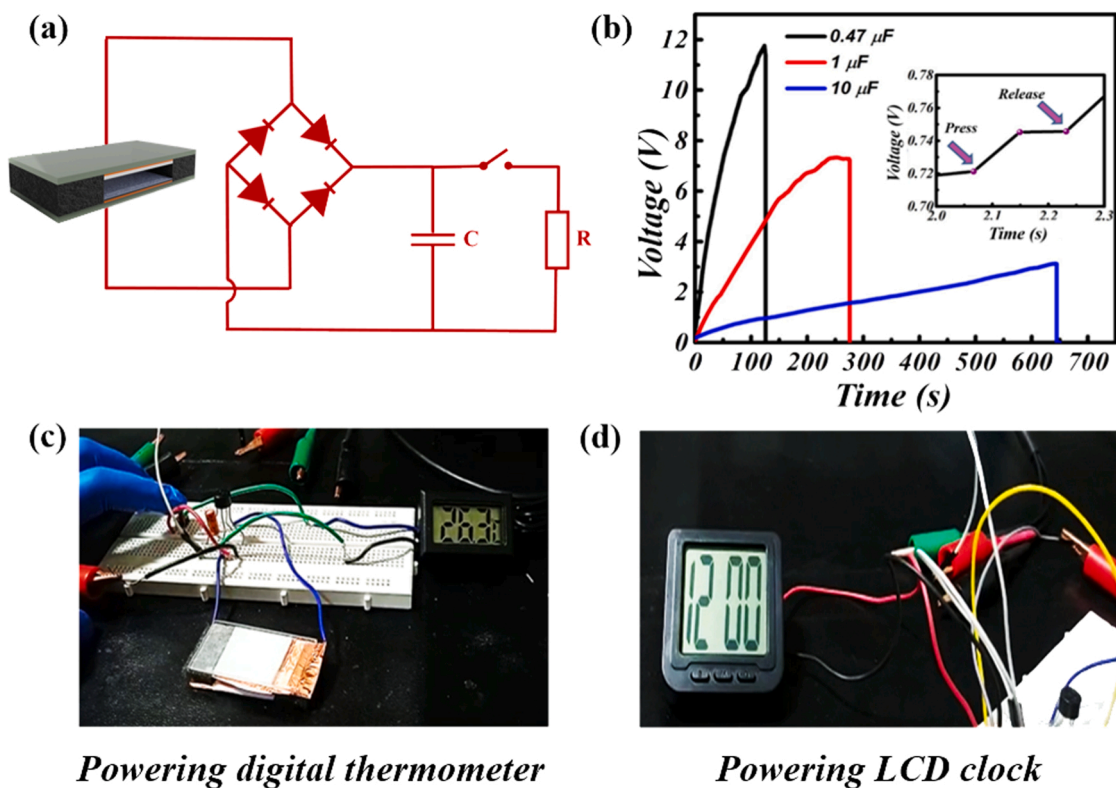
Fig. 9. (a) Pictorial representation of the circuit diagram for capacitor charging. (b) Capacitor charging process showing the voltage profile of different capacitors 0.47 μF, 1 μF, and 10 μF by using the BNNSs/BoPET-paper TENG. The Inset of figure (b) shows the enlarged detailed view of the capacitor charging event. The photographic image shows the circuit diagram for powering (c) a digital thermometer and (d) an LCD clock using the BNNSs/BoPET-paper TENG.

suitable for scavenging low-frequency biomechanical motions. Similarly, the apparent degradation of output power for long-term practical application was carried out with the help of an in-house developed force impactor that can deliver a constant force of 3 N per impact. Here, BNNSs/BoPET-paper TENG was evaluated up to 10000 cycles. This investigation showed that the short circuit current density of (~0.5 mA/m^2) has no considerable fluctuations even after the 10000 press-release cycles, indirectly certifies the practical stability of the present design of BNNSs /BoPET-paper TENG[53].

As seen before, the BNNSs based TENG generates electricity in alternating currents. However, most small-scale electronic gadgets require a DC power supply rather than an AC source which would make the devices dysfunctional [54]. Hence the generated signals of the prepared BNNSs/BoPET-paper TENG were rectified by introducing a full-wave bridge rectifier circuit (see Fig. 9(a)). These rectified output signals during the pressing and releasing motion of the TENG can charge a capacitor [49]. Fig. 9(b) shows the capacitor charging behaviour of BNNSs/BoPET-paper TENG, examined using different capacitors values (0.47, 1.0, and 10.0 μF) for charging. The saturation voltage of 0.47 μF capacitor could reach up to 12 V within a couple of minutes. As expected, the saturation voltage decreases with the increase in the capacitance values. The inset of Fig. 9(b) shows the enlarged view of the capacitor charging process, which portrays the voltage increase during the pressing and releasing of the capacitor by the TENG. The utilization of electrical energy from BNNSs/BoPET-paper TENG could be used to power small electronic devices attached parallel to the capacitor, as shown in photographic images 9(c) and (d). Accordingly, with the help of a suitable rectifier circuit, the BNNSs based TENG was able to power an LCD clock, a digital thermometer, and LEDs (see fig. S4 and supplementary videos 1 and 2 given in Supporting Information).

Supplementary material related to this article can be found online at doi:10.1016/j.nanoen.2021.106628.

4. Conclusions

Cost-effectiveness, lightweight, and sustainability are the vital elements for the materials chosen as power sources for small electronics. In this work, we have successfully demonstrated that the liquid-phase exfoliated BNNSs can act as efficient triboelectric electron acceptors in the lab-scale demonstration of a TENG device. Sonication-assisted liquid-phase exfoliation method in a suitable solvent is used for the exfoliation. Subsequently, an energy-efficient CS-TENG prototype was fabricated using exfoliated BNNSs, employing a sponge to provide the recoiling force between electrode pairs and glass as a structural support that allows the force to be evenly distributed throughout the material surface. For the film development, polyvinyl butyral was used as a binder while BoPET was used as the substrate. The new BNNSs based CS-TENG device, paired with ordinary paper as counter material, yielded excellent results. Even under moderate finger tapping, the TENG could generate an output voltage of ~200 V and a current density of ~0.48 mA/m^2. The peak value of power density for the BNNSs incorporated TENG device reached 0.14 W/m^2, which is 70 times higher than that of the TENG device without the BNNSs. Small electronic gadgets such as LCD clocks, digital thermometers, and LEDs were successfully demonstrated to power using the newly designed BNNSs/BoPET-paper TENG. Further, the versatility and durability of the TENG was tested under various frequencies of the applied load and also up to 10000 continuous operation cycles. In this way, the present protocol of harvesting mechanical energy using exfoliated BNNSs incorporated BoPET-paper TENG is proven to be advantageous, due to its simplicity in fabrication and efficiency to power energy-autonomous electronic systems and portable low-power devices.

CRediT authorship contribution statement

Ainikulangara Sundaran Bhavya: Conceptualization,

Methodology, Formal analysis, Investigation, Data curation, Writing – original draft, Writing– review & editing, Visualization. **Harris Varghese:** Conceptualization, Methodology, Formal analysis, Investigation, Data curation, Writing – original draft, Writing– review & editing, Visualization. **Achu Chandran:** Conceptualization, Methodology, Validation, Formal analysis, Investigation, Data curation, Writing – original draft, Writing– review & editing, Visualization, Supervision, Project administration, Funding acquisition. **Kuzhichalil Peethambharan Surendran:** Conceptualization, Methodology, Validation, Formal analysis, Investigation, Data curation, Writing – original draft, Writing– review & editing, Visualization, Supervision, Project administration, Funding acquisition.

Declaration of Competing Interest

The authors declare that they have no known competing financial interests or personal relationships that could have appeared to influence the work reported in this paper.

Acknowledgments

Appendix A. Supporting information

Supplementary data associated with this article can be found in the online version at doi:10.1016/j.nanoen.2021.106628.

References

[1] S.A. Han, J. Lee, J. Lin, S.-W. Kim, J.H. Kim, Piezo/triboelectric nanogenerators based on 2-dimensional layered structure materials, Nano Energy 57 (2019) 680–691.

[2] H. Zhou, D. Li, X. He, X. Hui, H. Guo, C. Hu, X. Mu, Z.L. Wang, Bionic ultra-sensitive self-powered electromechanical sensor for muscle-triggered communication application, Adv. Sci. 8 (2021), 2101020, https://doi.org/10.1002/advs.202101020.

[3] C. Wu, R. Liu, J. Wang, Y. Zi, L. Lin, Z.L. Wang, A spring-based resonance coupling for hugely enhancing the performance of triboelectric nanogenerators for harvesting low-frequency vibration energy, Nano Energy 32 (2017) 287–293, https://doi.org/10.1016/j.nanoen.2016.12.061.

[4] M. Ma, Z. Kang, Q. Liao, Q. Zhang, F. Gao, X. Zhao, Z. Zhang, Y. Zhang, Development, applications, and future directions of triboelectric nanogenerators, Nano Res. 11 (2018) 2951–2969, https://doi.org/10.1007/s12274-018-1997-9.

[5] L. Long, W. Liu, Z. Wang, W. He, G. Li, Q. Tang, H. Guo, X. Pu, Y. Liu, C. Hu, High performance floating self-excited sliding triboelectric nanogenerator for micro mechanical energy harvesting, Nat. Commun. 12 (2021) 1–10, https://doi.org/10.1038/s41467-021-25047-y.

[6] Z.L. Wang, Triboelectric nanogenerators as new energy technology for self-powered systems and as active mechanical and chemical sensors, ACS Nano 7 (2013) 9533–9557.

[7] H. Kuang, Y. Li, S. Huang, L. Shi, Z. Zhou, C. Gao, X. Zeng, R. Pandey, X. Wang, S. Dong, Piezoelectric boron nitride nanosheets for high performance energy harvesting devices, Nano Energy 80 (2021), 105561.

[8] B.D. Chen, W. Tang, C. Zhang, L. Xu, L.P. Zhu, L.J. Yang, C. He, J. Chen, L. Liu, T. Zhou, Z.L. Wang, Au nanocomposite enhanced electret film for triboelectric nanogenerator, Nano Res 11 (2018) 3096–3105, https://doi.org/10.1007/s12274-017-1716-y.

[9] Y. Hu, Z. Zheng, Progress in textile-based triboelectric nanogenerators for smart fabrics, Nano Energy 56 (2019) 16–24, https://doi.org/10.1016/j.nanoen.2018.11.025.

[10] S. Wang, Y. Zi, Y.S. Zhou, S. Li, F. Fan, L. Lin, Z.L. Wang, Molecular surface functionalization to enhance the power output of triboelectric nanogenerators, J. Mater. Chem. A. 4 (2016) 3728–3734, https://doi.org/10.1039/c5ta10239a.

[11] Z.L. Wang, Self-powered nanotech, Sci. Am. 298 (2008) 82–87.

[12] T. Cheng, Q. Gao, Z.L. Wang, The current development and future outlook of triboelectric nanogenerators: a survey of literature, Adv. Mater. Technol. 4 (2019), 1800588.

[13] M. Seol, S. Kim, Y. Cho, K. Byun, H. Kim, J. Kim, S.K. Kim, S. Kim, H. Shin, S. Park, Triboelectric series of 2D layered materials, Adv. Mater. 30 (2018), 1801210.

[14] B. Radisavljevic, A. Radenovic, J. Brivio, V. Giacometti, A. Kis, Single-layer MoS 2 transistors, Nat. Nanotechnol. 6 (2011) 147–150.

[15] F. Bonaccorso, L. Colombo, G. Yu, M. Stoller, V. Tozzini, A.C. Ferrari, R.S. Ruoff, V. Pellegrini, Graphene, related two-dimensional crystals, and hybrid systems for energy conversion and storage, Sci. (80-.) 347 (2015), 1246501.

[16] M.A.M. Hasan, Y. Wang, C.R. Bowen, Y. Yang, 2D nanomaterials for effective energy scavenging, Nano-Micro Lett. 13 (2021) 1–41.

[17] S. Kim, M.K. Gupta, K.Y. Lee, A. Sohn, T.Y. Kim, K. Shin, D. Kim, S.K. Kim, K. H. Lee, H. Shin, Transparent flexible graphene triboelectric nanogenerators, Adv. Mater. 26 (2014) 3918–3925.

[18] Y. Dong, S.S.K. Mallineni, K. Maleski, H. Behlow, V.N. Mochalin, A.M. Rao, Y. Gogotsi, R. Podila, Metallic MXenes: a new family of materials for flexible triboelectric nanogenerators, Nano Energy 44 (2018) 103–110.

[19] T.S. Sreeprasad, V. Berry, How do the electrical properties of graphene change with its functionalization? Small 9 (2013) 341–350.

[20] K. Zhang, Y. Feng, F. Wang, Z. Yang, J. Wang, Two dimensional hexagonal boron nitride (2D-hBN): synthesis, properties and applications, J. Mater. Chem. C 5 (2017) 11992–12022.

[21] Q. Weng, X. Wang, X. Wang, Y. Bando, D. Golberg, Functionalized hexagonal boron nitride nanomaterials: emerging properties and applications, Chem. Soc. Rev. 45 (2016) 3989–4012.

[22] Y. Lin, T.V. Williams, T.B. Xu, W. Cao, H.E. Elsayed-Ali, J.W. Connell, Aqueous dispersions of few-layered and monolayered hexagonal boron nitride nanosheets from sonication-assisted hydrolysis: Critical role of water, J. Phys. Chem. C 115 (2011) 2679–2685, https://doi.org/10.1021/jp110985w.

[23] A.M. Joseph, B. Nagendra, E. Bhoje Gowd, K.P. Surendran, Screen-printable electronic ink of ultrathin boron nitride nanosheets, ACS Omega 1 (2016) 1220–1228.

[24] M. Du, Y. Wu, X. Hao, A facile chemical exfoliation method to obtain large size boron nitride nanosheets, CrystEngComm 15 (2013) 1782–1786.

[25] X. Gu, Y. Zhao, K. Sun, C.L.Z. Vieira, Z. Jia, C. Cui, Z. Wang, A. Walsh, S. Huang, Method of ultrasound-assisted liquid-phase exfoliation to prepare graphene, Ultrason. Sonochem. 58 (2019), 104630, https://doi.org/10.1016/j.ultsonch.2019.104630.

[26] G. Cunningham, M. Lotya, C.S. Cucinotta, S. Sanvito, S.D. Bergin, R. Menzel, M.S. P. Shaffer, J.N. Coleman, Solvent exfoliation of transition metal dichalcogenides: dispersibility of exfoliated nanosheets varies only weakly between compounds, ACS Nano 6 (2012) 3468–3480.

[27] V. Nicolosi, M. Chhowalla, M.G. Kanatzidis, M.S. Strano, J.N. Coleman, Liquid exfoliation of layered materials (-), Science 340 (80) (2013).

[28] C. Zhi, Y. Bando, C. Tang, H. Kuwahara, D. Golberg, Large-scale fabrication of boron nitride nanosheets and their utilization in polymeric composites with improved thermal and mechanical properties, Adv. Mater. 21 (2009) 2889–2893.

[29] L. Ci, L. Song, C. Jin, D. Jariwala, D. Wu, Y. Li, A. Srivastava, Z.F. Wang, K. Storr, L. Balicas, Atomic layers of hybridized boron nitride and graphene domains, Nat. Mater. 9 (2010) 430–435.

[30] Z. Kuang, Y. Chen, Y. Lu, L. Liu, S. Hu, S. Wen, Y. Mao, L. Zhang, Fabrication of highly oriented hexagonal boron nitride nanosheet/elastomer nanocomposites with high thermal conductivity, Small 11 (2015) 1655–1659.

[31] D. Lee, S.H. Song, Ultra-thin ultraviolet cathodoluminescent device based on exfoliated hexagonal boron nitride, RSC Adv. 7 (2017) 7831–7835.

[32] K. Ba, W. Jiang, J. Cheng, J. Bao, N. Xuan, Y. Sun, B. Liu, A. Xie, S. Wu, Z. Sun, Chemical and bandgap engineering in monolayer hexagonal boron nitride, Sci. Rep. 7 (2017) 1–8.

[33] M. Ikram, J. Hassan, M. Imran, J. Haider, A. Ul-Hamid, I. Shahzadi, M. Ikram, A. Raza, U. Qumar, S. Ali, 2D chemically exfoliated hexagonal boron nitride (hBN) nanosheets doped with Ni: synthesis, properties and catalytic application for the treatment of industrial wastewater, Appl. Nanosci. 10 (2020) 3525–3528.

[34] S. Radhakrishnan, D. Das, A. Samanta, A. Carlos, L. Deng, L.B. Alemany, T. K. Weldeghiorghis, V.N. Khabashesku, V. Kochat, Z. Jin, Fluorinated h-BN as a magnetic semiconductor, Sci. Adv. 3 (2017), e1700842.

[35] A. Akpınar Borazan, D. Gökdai, Pine cone and boron compounds effect as reinforcement on mechanical and flammability properties of polyester, Composites (2018).

[36] A. Cammarano, G. Luca, E. Amendola, Surface modification and adhesion improvement of polyester films, Open Chem. 11 (2013) 35–45.

[37] A. Pullanchiyodan, K.P. Surendran, Formulation of sol–gel derived bismuth silicate dielectric ink for flexible electronics applications, Ind. Eng. Chem. Res. 55 (2016) 7108–7115.

[38] J. Varghese, K.P. Surendran, M.T. Sebastian, Room temperature curable silica ink, RSC Adv. 4 (2014) 47701–47707.

[39] A.S. Pillai, A. Chandran, S.K. Peethambharan, MWCNT Ink with PEDOT: PSS as a multifunctional additive for energy efficient flexible heating applications, Appl, Mater. Today 23 (2021), 100987.

[40] M.S. Tutgun, D. Sinirlioglu, S.U. Celik, A. Bozkurt, Preparation and characterization of hexagonal boron nitride and PAMPS-NMPA-based thin composite films and investigation of their membrane properties, Ion. (Kiel.) 21 (2015) 2871–2878.

[41] J.W. Lee, H.J. Cho, J. Chun, K.N. Kim, S. Kim, C.W. Ahn, I.W. Kim, J.-Y. Kim, S.-W. Kim, C. Yang, Robust nanogenerators based on graft copolymers via control of

dielectrics for remarkable output power enhancement, Sci. Adv. 3 (2017), e1602902.

[42] K. Shi, H. Zou, B. Sun, P. Jiang, J. He, X. Huang, Dielectric modulated cellulose paper/PDMS-based triboelectric nanogenerators for wireless transmission and electropolymerization applications, Adv. Funct. Mater. 30 (2020), 1904536.

[43] Z.L. Wang, J. Chen, L. Lin, Progress in triboelectric nanogenerators as a new energy technology and self-powered sensors, Energy Environ. Sci. 8 (2015) 2250–2282.

[44] G. Zhu, C. Pan, W. Guo, C.-Y. Chen, Y. Zhou, R. Yu, Z.L. Wang, Triboelectric-generator-driven pulse electrodeposition for micropatterning, Nano Lett. 12 (2012) 4960–4965.

[45] J. Zhong, Q. Zhong, F. Fan, Y. Zhang, S. Wang, B. Hu, Z.L. Wang, J. Zhou, Finger typing driven triboelectric nanogenerator and its use for instantaneously lighting up LEDs, Nano Energy 2 (2013) 491–497, https://doi.org/10.1016/j.nanoen.2012.11.015.

[46] G. Zhu, P. Bai, J. Chen, Z. Lin Wang, Power-generating shoe insole based on triboelectric nanogenerators for self-powered consumer electronics, Nano Energy 2 (2013) 688–692, https://doi.org/10.1016/j.nanoen.2013.08.002.

[47] J. Chen, G. Zhu, W. Yang, Q. Jing, P. Bai, Y. Yang, T. Hou, Z.L. Wang, Harmonic-resonator-based triboelectric nanogenerator as a sustainable power source and a self-powered active vibration sensor, Adv. Mater. 25 (2013) 6094–6099.

[48] X.-S. Zhang, M.-D. Han, R.-X. Wang, F.-Y. Zhu, Z.-H. Li, W. Wang, H.-X. Zhang, Frequency-multiplication high-output triboelectric nanogenerator for sustainably powering biomedical microsystems, Nano Lett. 13 (2013) 1168–1172.

[49] C. Wu, T.W. Kim, J.H. Park, H. An, J. Shao, X. Chen, Z.L. Wang, Enhanced triboelectric nanogenerators based on MoS2 monolayer nanocomposites acting as electron-acceptor layers, ACS Nano 11 (2017) 8356–8363.

[50] H. Zou, Y. Zhang, L. Guo, P. Wang, X. He, G. Dai, H. Zheng, C. Chen, A.C. Wang, C. Xu, Z.L. Wang, Quantifying the triboelectric series, Nat. Commun. 10 (2019) 1–9, https://doi.org/10.1038/s41467-019-09461-x.

[51] F.-R. Fan, L. Lin, G. Zhu, W. Wu, R. Zhang, Z.L. Wang, Transparent triboelectric nanogenerators and self-powered pressure sensors based on micropatterned plastic films, Nano Lett. 12 (2012) 3109–3114.

[52] S. Park, J. Park, Y. Kim, S. Bae, T.-W. Kim, K.-I. Park, B.H. Hong, C.K. Jeong, S.-K. Lee, Laser-directed synthesis of strain-induced crumpled MoS2 structure for enhanced triboelectrification toward haptic sensors, Nano Energy 78 (2020), 105266.

[53] H. Varghese, A. Chandran, A facile mechanical energy harvester based on spring assisted triboelectric nanogenerators, Sustain. Energy Fuels (2021), https://doi.org/10.1039/D1SE00788B.

[54] D. Wang, D. Zhang, Y. Yang, Q. Mi, J. Zhang, L. Yu, Multifunctional latex/polytetrafluoroethylene-based triboelectric nanogenerator for self-powered organ-like MXene/metal–organic framework-derived CuO nanohybrid ammonia sensor, ACS Nano 15 (2021) 2911–2919.

Harris Varghese is presently working as a junior research fellow at Materials Science and Technology Division of CSIR-NIIST, Thiruvananthapuram, India. He has received his master's degree in Physics from Cochin University of Science and Technology in 2017. His current research interest includes triboelectric nanogenerators and energy harvesting. He has authored two publications in reputed international journals and filed one patent.

Achu Chandran is currently working as scientist at CSIR-NIIST, Thiruvananthapuram, India. He has completed his Ph. D. in Engineering from AcSIR, CSIR-NPL Campus, New Delhi and subsequently joined CSIR-CEERI, Pilani as scientist in 2016. Dr. Chandran's research interest is in the area of electronic materials and devices, specifically; piezoelectric and triboelectric nanogenerators, flexible tactile sensors, printed wearable heaters, soft memory devices and MEMS packaging. He has authored more than 25 publications in reputed international journals and filed one patent. Dr. Chandran is awarded with prestigious CSIR-Young Scientist Award (2021), SERB-Early Career Research Award (2019), DAAD fellowship (2015) etc.

Kuzhichalil Peethambharan Surendran is a Principal Scientist and Associate Professor in Materials Science and Technology Division of CSIR-NIIST, Thiruvananthapuram, India. In 2005, he received his doctorate in Physics from Kerala University, India. After post-doctoral stints at Indian Institute of Science, Bengaluru, Aveiro and Coimbra Universities in Portugal, he joined IFW Dresden as Alexander von Humboldt fellow. From 2012 onwards he is a scientist in CSIR-NIIST. His current research interests include functional inks for printed electronics, 2D materials, lead free piezoelectric nanogenerators, EMI shielding materials, low temperature cofired ceramics and printed antennas. He has authored 85 papers and 3 patents.

Ainikulangara Sundaran Bhavya is working as a senior research fellow under the supervision of Dr. K. P. Surendran in Materials Science and Technology Division of CSIR-NIIST, Thiruvananthapuram, India. She completed her master's degree in chemistry from Calicut University, Kerala, India in 2014. Her current research areas include two dimensional materials for electronic device applications especially mechanical energy harvesting by triboelectric nanogenerators and magnetic semiconductors.

Article

Two-dimensional Hexagonal Boron Nitride Nanosheet−Polycarbonate Composite Ink-Based Printed Flexible Triboelectric Nanogenerator for Scavenging Mechanical Energy

Ainikulangara Sundaran Bhavya, Harris Varghese, Achu Chandran,* and Kuzhichalil Peethambharan Surendran*

Read Online

ACCESS | 📊 Metrics & More | 📰 Article Recommendations | 🆂🅸 Supporting Information

ABSTRACT: In the modern world, the rapid depletion of conventional energy sources demands urgent exploration of materials and methods for clean, efficient, and sustainable energy production. As a mechanical energy harvester, triboelectric nanogenerators (TENGs) have been investigated extensively in recent years due to their high power output, superior energy conversion efficiency, low cost, and ease of manufacturing. Herein, a high-performance flexible TENG is developed based on 2D-hexagonal boron nitride nanosheet (BNNS) ink printed on Mylar substrates as a triboelectric contact layer. The thixotropy of the BNNS dispersion was controlled by polycarbonate (PC) and other suitable organic additives. Further, the formulation was modified into a versatile ink (BN-PC ink) suited for screen printing. Remarkably, the flexible screen-printed TENG (FS-TENG) fabricated using BN-PC ink as a tribonegative material, paired with the printed polyvinylpyrrolidone (PVP) on Mylar as a tribopositive material, demonstrated a very high voltage of ∼800 V and a short-circuit current density of ∼0.78 mA/m², respectively, under an actuating force of ∼10 N with 5 Hz frequency. The FS-TENG has shown an impressive power density of ∼1.36 W m⁻² at 200 MΩ resistive load, which is ∼7 times higher than that of the TENG without BNNSs. Further, the fabricated FS-TENG device is demonstrated for powering electronic gadgets such as digital thermometers, calculators, and light-emitting diodes (LEDs) with a mere finger-tapping force of ∼5 N.

KEYWORDS: flexible triboelectric nanogenerator, functional ink, hexagonal boron nitride, printed nanogenerator, polycarbonate
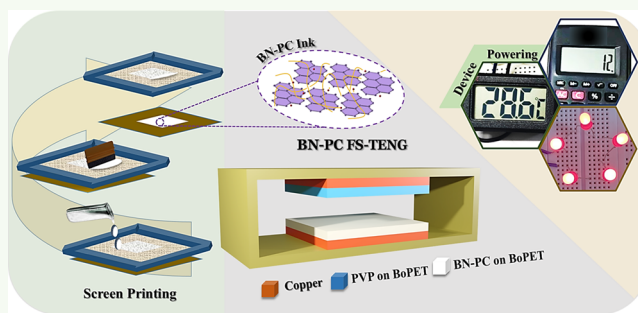
■ INTRODUCTION

The future of mankind is going to be anchored on innovations like the Internet of Things which is a critical concept in creating an elite class of autonomous and mobile gadgets that need to operate for a longer duration without any battery changes.[1,2] For this to happen, imperative efforts have to be made to harvest energy from ambient green resources for powering a multitude of portable devices. That is, energy harvesting is a key element in IoT-enabled systems that bring intelligence to the edge. Vibrational energy-harvesting techniques including triboelectric nanogenerators (TENGs) can harness energy from human motions such as dancing, walking, computer key tapping, and so forth to drive portable sensors, mobile gadgets, or even high-voltage applications.[3] As long as there is friction between triboelectrically different materials by any means, there exists a finite amount of power that can be trapped using TENG by virtue of contact electrification and electrostatic induction.[4] An intuitive approach to enhance the process of triboelectrification is the improvement of contact charges developed between the surfaces of triboelectrically dissimilar materials, where it can be done by several means.[5] To improve the output performance of TENG, either the choice of materials should lie far from each other in a triboelectric series or the modification of the active surface layer to increase the contact area, which may eventually improve the surface charge density. In addition, the contact electrification property of the triboelectric materials is strongly influenced by the charge-trapping capability of the contact materials. It is seen that the incorporation of nanomaterials with lamellar structure enhances the charge-trapping ability of frictional layers.[6]

Nowadays, developing cost-effective and scalable TENGs is getting priority. Modern printing technology promises rapid
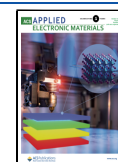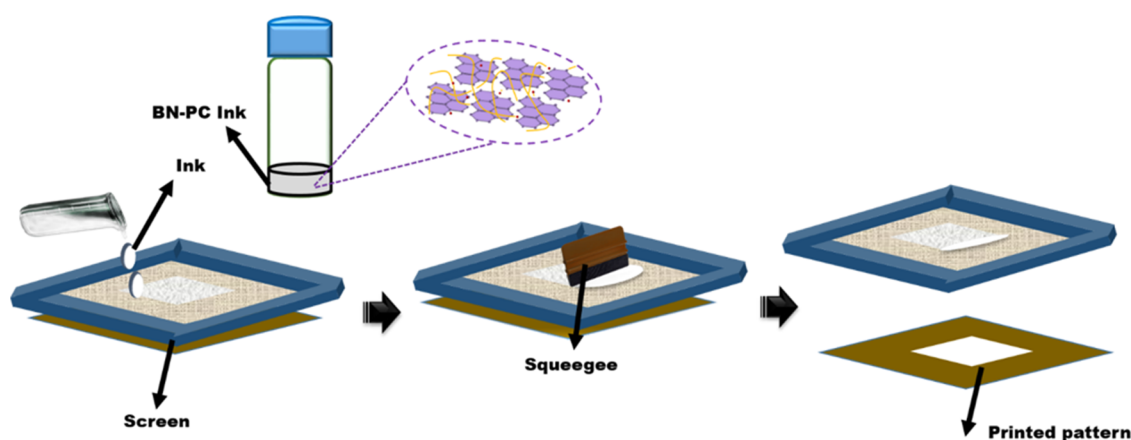
Figure 1. Schematic illustration of the screen-printing process using BN-PC ink.

advances in terms of its manufacturing efficiency and applicability in various fields. On another hand, power sources of modern times should possess features such as ultrathinness, cost effectiveness, flexibility, and sustainability. Printed electronics can meet these goals and are considered an emerging revolutionary technology aiming at relatively large-area electronic devices and components. In conventional flexible electronics, printed inks are used for various applications such as energy-harvesting, smart packaging, radiofrequency (RF) communication, and flexible display applications.[7] Even though printing is a popular scalable additive manufacturing tool, it is not much explored for fabricating flexible TENGs.[8,9] Seol and co-workers developed an all-printed TENG in which the core—shell structural frame was fabricated by using a 3D printing method, in which the printing material was polylactic acid. Two-dimensional printing was also performed to form the functional contact layer poly(methyl methacrylate) (PMMA) with a grating pattern on the nanocellulose substrate.[10] Salauddin et al. designed an MXene/Ecoflex nanocomposite-based flexible fabric TENG, which utilizes a 3D printing method for its contact material fabrication.[11] Of the available printing methods, screen printing is an inexpensive method capable of rapid mass production and also provides good control over the printing area over a wide choice of substrates like polymers, papers, fabrics, and so forth.[12] In this technique, specific patterns are deposited on various substrates using screen masks for creating large-area high-resolution 2D patterns having thicknesses down to a few microns.[13,14] There are several available reports on screen-printed TENGs. Cao et al. reported a screen-printable carbon nanotube (CNT) ink-based flexible washable electronic textile that serves as a touch or gesture sensor for intelligent human—machine interactions.[15] Similarly, Wen et al. proposed a silk fibroin-based printed TENG for wearable multifunctional sensing, which utilizes a screen-printing process to prepare the graphite interdigital electrodes on top of a soft PDMS substrate.[16] A two-dimensional material-based TENG-driven flexible self-powered humidity sensor was proposed by Zhang et al., in which a tin disulfide nanoflower/reduced graphene oxide (SnS_2/RGO) nanohybrid has been used. This SnS_2/RGO hybrid film was fabricated using the screen-printing method.[17]

Hexagonal boron nitride (h-BN) is a well-known 2D-layered material, isostructural with graphene, which is useful for a variety of stretchable and flexible applications. Exfoliated 2D materials are attractive for future energy-harvesting technology as potential active materials.[18,19] Traditionally, liquid-phase exfoliation is a scalable method for the production of layered 2D nanostructures. The well-exfoliated nanosheet dispersion combined with suitable solvents and stabilizing polymers is ideal for a wide range of printing applications.[20] In printed films, the deposited BNNSs form a porous structure, compromising their mechanical integrity, susceptibility to moisture, and also substrate adhesion. A solution-processable h-BN ink specially formulated for screen printing can yield thermally and chemically stable printed components for device applications.[21] There are several reports on h-BN nanosheet ink for use in printed electronic devices and components.[22] In 2007, Carey et al. demonstrated inkjet-printed h-BN-based ink as a gate dielectric layer in an all-printed field effect transistor.[23] Similarly, highly viscous screen-printed polymer-based BNNS inks were also developed for wearable and flexible electronics.[24] A printed 2D BNNS-based flexible triboelectric nanogenerator is a novel concept for power generation.

Herein, a successful demonstration of a contact separation mode FS-TENG using BNNS ink screen printed on a polymer substrate for powering electronic devices is reported. The formulated viscosity-tunable ink, for screen-printing purposes, incorporates ultrathin boron nitride nanosheets (BNNSs) as a filler material, with polycarbonate as a polymer binder and other organic additives suitable for printing and rheology adjustments. A printed flexible TENG device is developed with the formulated screen-printed ink as a negative material against the printed polyvinylpyrrolidone as the positive tribomaterial. Notably, the embedded layered 2D material boosts the output performance of FS-TENG by ∼7 times. The FS-TENG was further able to power small electronic devices such as thermometers, calculators, and LEDs.

■ EXPERIMENTAL METHODS

Materials. High-purity boron nitride powder (1 μm size), as well as the polymers polyvinylpyrrolidone (PVP) and polycarbonate (PC), was procured from Sigma-Aldrich, USA. The dispersant solvent dimethylformamide (DMF) was purchased from HPLC Lab Reagents in India. Commercially available Mylar (BoPET) (DuPont, USA) with 80 μm thickness was used as the substrate for screen printing as well as the structural framework for FS-TENG. Ethanol (Merck Chemicals) was used for printing purposes as a substrate cleaning agent. A conducting copper tape (3 M Co.) with adhesive on both sides was used as the electrode for FS-TENG. All chemicals were used without any further modification or purification.

Formulation of BN-PC Ink. BNNS—polycarbonate composite ink was formulated by simple solution mixing, followed by sonication and magnetic stirring. Initially, exfoliated BNNSs for screen-printable ink were produced by a liquid-phase-assisted exfoliation method. For that bulk, h-BN of 1 g was added to 100 mL of DMF, and then sonication was continued 48 h for effective delamination, from which the exfoliated sheets were collected from the supernatant solution after centrifugation (detailed characterization is shown in Supporting Information Figures S1 and S2). The unexfoliated layers that settled down in the bottom of the solution were discarded. These collected exfoliated BNNSs were dried in an oven set temperature of 60 °C. Thereafter, polycarbonate and BNNSs in the weight ratio of 1:1 (0.5 g) were added to 1 mL of DMF solvent in a culture tube, followed by the addition of 50 μL of Triton X100 as a thixotropy-controlling additive. The so-derived ink suspension was mechanically stirred vigorously for 12 h with 700 rpm speed to ensure homogeneous mixing for stable dispersion. The entire process was repeated without using BNNSs for printing a pure polymer (PC) film.

Preparation of the Printed Triboelectric Layer. The rheology-optimized screen-printable ink of exfoliated BNNSs was made into a flexible composite film by using the screen-printing technique. Here, a custom-made silk screen with a desired square pattern of active area of 9 cm^2 (3 cm × 3 cm), fabricated by photoresistive masking, was used as the screen for the printing of BN-PC ink on the BoPET (Mylar) substrate. The screen-printing process using the BN-PC ink is schematically represented in Figure 1. Initially, the prepared viscous ink is placed over the screen with the substrate under it at a fixed snap-off distance. Then, with the help of a rubber squeegee, the ink was cast as films onto the substrate through the screen in desired patterns. With repeated printing strokes, the thickness and quality of the film can be controlled. Here, the interparticle cohesion and adhesion of the BNNSs on the BoPET substrate were made possible by the polycarbonate binder. Finally, it was dried in an oven at 60 °C to obtain polycarbonate BNNS films on BoPET. Similarly, 20 wt % PVP in DMF was screen-printed on BoPET and dried in the oven for use as the counter contact layer for the FS-TENG device.

Fabrication of the FS-TENG Device. The traditional contact separation mode assembly was used for the fabrication of the FS-TENG device. Flexible BoPET acts as the supporting structure for TENGs while also contributing to the structural stability. Substrates for contact materials were cut in square shapes of dimensions 3 cm × 3 cm. The FS-TENG was prepared by printing the prepared BN-PC ink onto the BoPET substrate as a negative tribomaterial and polyvinylpyrrolidone (PVP) printed on BoPET as the counter one. The conductive copper tape was used as the electrode for FS-TENG., Thin copper leads were attached to this conductive tape as leads for taking external connections. The separation between two contact materials is maintained at 1 cm using the BoPET support structure. For developing the control FS-TENG device (without BNNS), the entire fabrication process was repeated by printing a PC film and PVP films as contact materials. The schematic model and the photograph of the FS-TENG is depicted in Figure 2a,b.

Characterization. The colloidal stability and flow characteristics of the synthesized ink with a polymer binder were analyzed at 20 °C by using a rheometer (Rheo plus 32, Anton Paar, Graz, Austria) equipped with a chiller. The contact angle of the formulated ink was analyzed by a sessile drop test utilizing a contact angle measuring device (DSA 30, KRÜSS GmbH, Hamburg, Germany). Thermal

stability and gravimetry of the dried BN-PC ink and polycarbonate polymer were investigated by a TA Q50 thermogravimetric analyzer at a 10 °C/min heating rate under a nitrogen gas atmosphere. The Fourier transform infrared (FTIR) spectra of the ink and polymers were obtained using a Nicolet Magna 560 FTIR system (Thermo Scientific, Massachusetts, USA). The surface and cross-sectional morphologies of the printed patterns were viewed using a scanning electron microscope (Karl Zeiss EVO 50, Oberkochen, Germany). An atomic force microscope (Multimode, Bruker, Germany) in tapping mode was used to evaluate the surface topology of the film on the BoPET substrate. The optical images of the printed films were taken using a polarizing optical microscope (Leica DM2700P, Germany) attached to a charge-coupled device camera. The electrical characteristics of the FS-TENG device were analyzed using a source-measuring unit (Keithley 2450) and a current preamplifier (SR570, Stanford Research) coupled with a digital phosphor oscilloscope (Tektronix DPO2004B, USA). Using a custom-developed force impactor, a cyclic uniform mechanical force (~10 N) was periodically applied to the FS-TENG device, and the corresponding electrical outputs were recorded. An automatic force tester (AFT500, Apple Electronics) was used for measuring the force imparted. By using various load resistors, varying from 1 Ω to 1000 MΩ, the load-dependent power density of the device was calculated. Capacitor charging profiles were recorded using different values of capacitors. The cyclic stability and durability were confirmed by the continuous operation of the FS-TENG for more than 10,000 cycles.

■ RESULTS AND DISCUSSION

Properties of the BN-PC Ink. The quality of the screen-printed films is closely related to several factors like screen-printing parameters, substrate selection, and the ink rheology. The printing parameters mainly include screen-printing speed, snap-off distance, screen mesh parameter, angle, geometry of the squeegee, and so forth, which can be carefully controlled for printing purposes. In addition, to maintain the proper ink adhesion on various substrates and colloidal stability of the ink, the choice, concentration, and addition sequence are critical. Here, the ink rheology of the screen-printable hexagonal boron nitride nanosheet-based ink is customized with polycarbonate as a polymer binder and Triton X100 as an additive. Then, the choice of polycarbonate as a binder for BNNSs is made owing to its good solution processability, low cost, and higher glass-transition temperature of around 150 °C. The photograph of the prepared highly viscous ink is given in the inset of Figure 3a. Further, the rheogram of the formulated ink (Figure 3a) shows a considerable decrease in viscosity with the increase in the external shear rate. This pseudoplastic behavior is suitable for application in screen printing since this enables continuous extrusion of the viscous ink through the tensioned screen mesh under normal conditions.[21,25] Note that the observed viscosity of the ink is 2 Pa s at a shear rate of 10 s^{-1} which gradually decreases and levels to a constant lower value at higher shear values. A similar rheological behavior is observable in other 2D material-based inks also,[26] and usually, the required range of the ink viscosity for screen printing is 1−10 Pa s.[26] Also, the dynamic viscoelastic behavior of the ink, represented in Figure 3b, indicates a viscous liquid-like nature in the entire strain region where the loss modulus (G'') dominates over storage modulus (G'). The storage modulus and loss modulus in the rheology analysis of the formulated ink represent the solid and liquid behaviors, respectively, as a function of shear stress. Apart from this, the surface wetting parameter is also an essential component in printing and can be identified from the contact angle measurement.[27] The observed lower value of contact angle, 63° (Figure 3c), attests to its better wettability
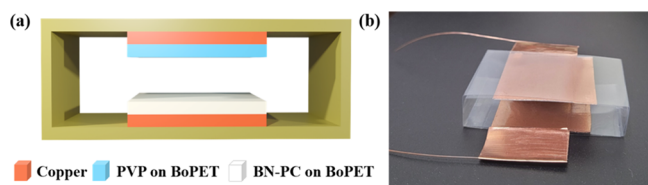

Figure 2. (a) Schematic model of the FS-TENG. (b) Photograph of the fabricated TENG device.
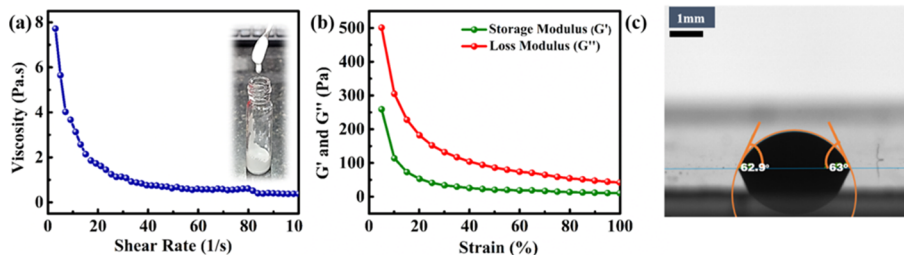
Copper   PVP on BoPET   BN-PC on BoPET

Figure 3. (a) Viscosity variation of the formulated ink with the shear rate. The inset of Figure 3a shows the photograph of the BN-PC ink. (b) Plot of storage modulus and loss modulus vs strain. (c) Contact angle measurement of the BN-PC ink on the BoPET substrate.
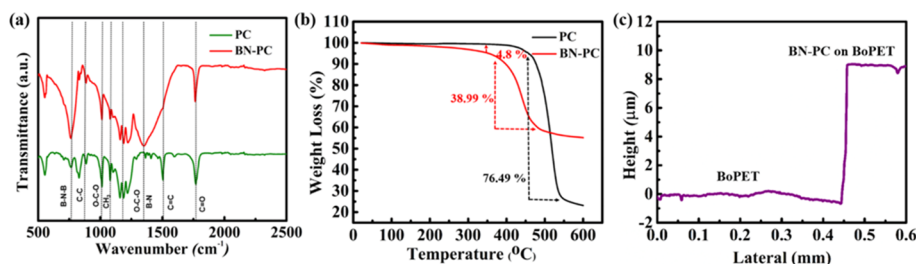

Figure 4. (a) FT-IR analysis of pristine polycarbonate and ink powder. (b) Thermal degradation behavior of the polymer and BN-PC ink. (c) Thickness profile of the printed ink on the BoPET substrate.
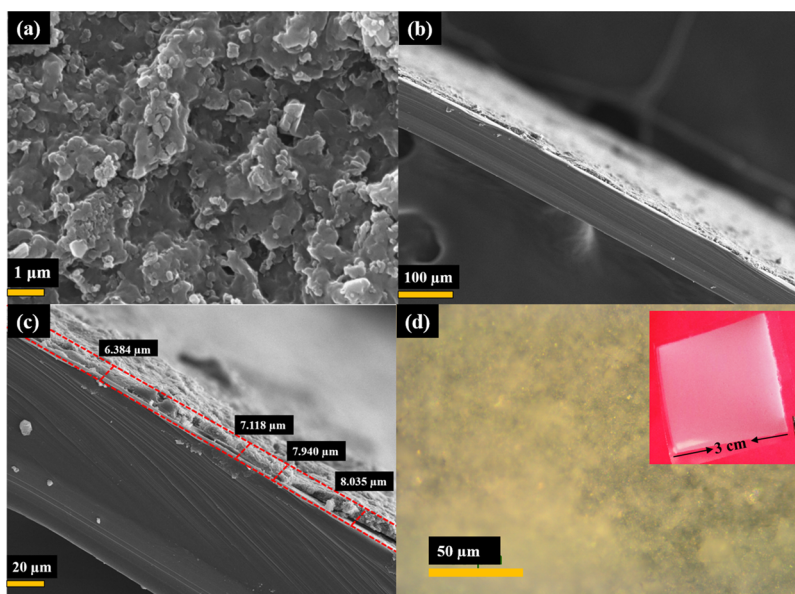

Figure 5. (a) Surface morphology of the BN-PC ink screen-printed on the BoPET substrate via SEM analysis. (b,c) Similarly, cross-sectional analysis of the printed ink on the BoPET substrate is also done. (d) Additionally, optical image of the printed ink with the photograph of the printed film with an area of 9 cm² as the inset is represented.

provided by the high affinity of the ink toward the BoPET substrate.[28,29]

In the FT-IR analysis of the BN-PC ink and pristine polycarbonate polymer (Figure 4a), the characteristic peaks observed in the fingerprint region of 400−1000 cm^{-1} arise from the C−C bond stretching vibrations of the polymer material. Similarly, the peaks in the range 1232−1164 cm^{-1} are due to the presence of asymmetric O−C−O deformations of the carbonate group. However, the observed CH_3 vibration peak at 1081 cm^{-1} and the additional peak near 1015 cm^{-1} are the symmetric deformations of the O−C−O carbonate group. Further, the C=C stretching vibrations appear at 1506 cm^{-1} due to the presence of aromatic ring carbon, and the carbonate group C=O deformations occur near 1775 cm^{-1}. All these

peaks are common to both the FT-IR spectra, and they arise from the polymer material. However, the two strong and sharp absorption peaks observed at 760 and 1360 cm^{-1} in the BN-PC FTIR spectrum are the characteristic peaks of h-BN. These peaks arise from the broad B−N−B out-of-plane bending and B−N in-plane stretching vibrations, respectively.[30−32] Thus, the FTIR spectra establish the formation of the composite ink as expected. The thermal behavior of the dried screen-printed ink was analyzed by using thermogravimetric analysis (TGA), which is depicted in Figure 4b. The weight loss observed in the temperature range of 100−350 °C in the BN−PC polymer composite was mainly attributed to the evaporation of volatile residual solvents and also the thermal degradation of the surfactant present in the ink. The main weight loss in both
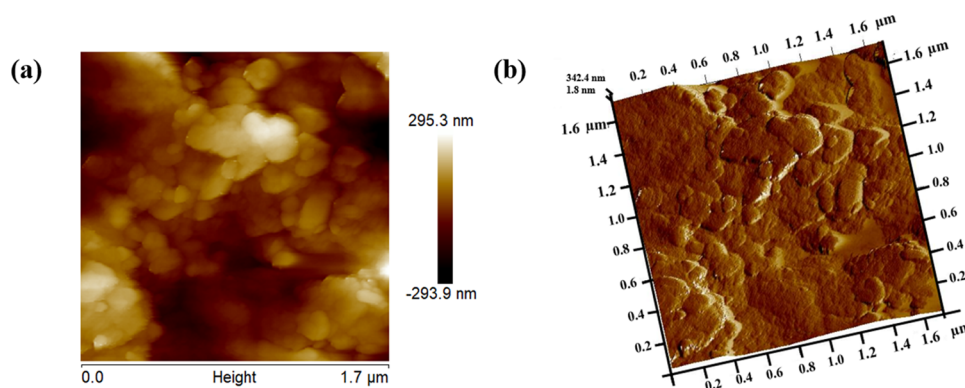
Figure 6. (a) Two-dimensional and (b) 3D AFM images of BN-PC ink on a BoPET substrate.

samples after a temperature of ∼370 °C arises because of the cleavage of the carbonate functional groups present in the polymer material. In pure polymer PC, almost 80% of degradation takes place after 400 °C. The observed weight loss in the BN-PC sample is comparably less because of the filler loading, and the incorporation of higher thermal stability fillers like BNNSs in polycarbonate-based inks enhances its thermal stability.[33−35]

Morphology of BN-PC Ink Screen-Printed on BoPET Substrate. The surface morphological analysis of the screen-printed PC (Supporting Information Figure S7a) and BN-PC films was done with the aid of SEM and AFM surface imaging. The surfaces of the printed ink consist of homogeneously dispersed nanosheets embedded in the polymer matrix parallel to the surface due to the leveling effect of the squeegee.[36] The microstructure of the BN-PC film shows good compatibility between the filler material and the polymer binder (Figure 5a). However, the film thickness of the printed pattern on the substrate surface for three strokes of printing, on average, is found to be 7.5 ± 2 μm, which was estimated using the cross-sectional SEM (see Figure 5b,c). This thickness value is in agreement with the value from the profilometer, which is also found to be 8.5 ± 2 μm (Figure 4c). The optical image of the printed surface is shown in Figure 5d whose inset bears a clear photographic image of the formulated ink screen-printed on a BoPET substrate having a white translucent nature. Uniformity and homogeneity of the film are ensured by the multiple strokes of printing, and the horizontal stacking of multiple layers is realized effectively because of the preferred low potential energy arrangements of the ink when initially it is printed on the pristine substrate and then over the printed layers. A similar behavior of printed patterns is observable in other 2D material-based screen-printed graphene inks.[7,37]

The AFM analysis is also extensively used to make meticulous observations on the surface topography and evaluate the textural characteristics of diverse film surfaces. Here, the surface morphology of the screen-printed pattern obtained from the AFM analysis of the BN-PC film surface (see Figure 6a,b) also corroborates with the inference obtained using SEM. AFM shows that the film exhibited an average surface roughness value (R_a) of 86.1 nm, which is a measure of roughness and general variations over the entire scanning area. A root-mean-square roughness (R_q) of 107 nm represents the standard deviation of the surface height profiles. However, the distribution of spikes relative to the mean line above or below is obtained from the kurtosis value, and it was found to be 2.76, which represents bumpy surfaces. The positive skewness value

of 0.336 also indicates the presence of bumps compared to valleys and shows that the surface of the printed sample has predominant height variations compared to the printed pristine polycarbonate film. The surface roughness and root-mean-square roughness of the PC film without BNNSs are similarly decreased to 29.4 and 38.5 nm, respectively (Supporting Information Figure S7b,c).[38,39] The observed significant increase in surface roughness value in the BN-PC film is attributed to the incorporation of an inorganic material having a higher surface roughness value compared to the polymer material.[40]

Output Characteristics of the FS-TENG Device. In a triboelectric nanogenerator, the choice of contact material is the obvious first priority, and 2D BNNSs have been previously proven to be an excellent candidate.[31] Here, the formulated BNNS-based ink showed excellent thermal stability and good adhesion to the substrate, which are very crucial for stable triboelectric application. In addition, the enhancement in the surface area that resulted from the microscale roughness of the printed surface could magnify the triboelectric charge generation during the contact electrification.[41] Also, the screen-printing process provides facile scalability if it is required. The designed screen-printed TENG comprises hexagonal boron nitride in the polycarbonate matrix printed on a BoPET substrate as a primary TENG material, while printed PVP as the second material, and they are chosen based on their position in the triboelectric series.[42] The detailed fabrication steps are depicted in Experimental Methods. Figure 7 shows the schematic representation of the working of the FS-TENG device and is explored well in the literature.[43]

The fabricated FS-TENG has two contact layers, one BN-PC ink printed on the BoPET substrate and a printed PVP layer. Copper electrodes were separately attached on the bottom of these contact layers. The working of this vertical contact separation mode FS-TENG is illustrated in Figure 7. Here, the supporting structure not only provides the necessary separation gap but also provides recoiling for the same. When a mechanical force is imparted, layers come into contact, and triboelectric charges are generated on the surfaces. However, in the releasing stage, electrostatic charge induction generates a potential difference between the electrodes. Consequently, the flow of electrons takes place between the electrodes when they are connected. In this way, alternate pressing and releasing motion can generate alternating electrical signals in the external circuit.[44,45] The output voltages and current density of the screen-printed TENGs with and without boron nitride nanosheets are shown in Figure 8a,b. For this, the as-fabricated
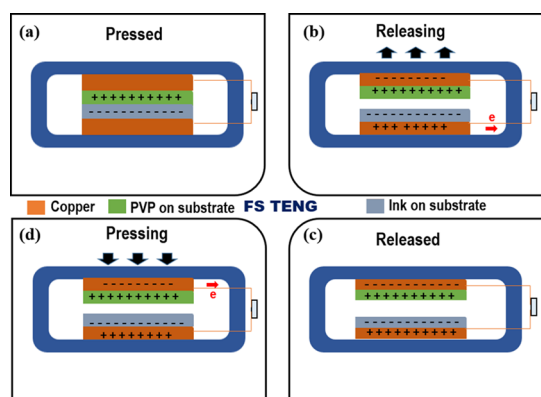
Figure 7. Schematic representation of the working mechanism of FS-TENG. (a) Pressed state, (b) releasing state, (c) released saturation state, and (d) further pressing state.

TENGs were continuously pressed and released by a custom-made force impactor test system, with a vertical contact force of ~10 N at a frequency of 5 Hz, which provided a stable and systematic contact between the top and bottom layers. The TENG device with boron nitride nanosheets showed noticeable improvements in electrical properties compared to the TENG without BNNSs. The printed polycarbonate FS-TENG against polyvinylpyrrolidone exhibited an output voltage of about 400 V, while the TENG with BNNSs exhibited a two-fold enhanced output voltage of 800 V. The short-circuit current density (J_{sc}) of the printed TENG with BNNSs displayed a value of 0.78 mA/m^2, which is remarkably higher than the printed TENG without BNNSs (0.55 mA/m^2). The output enhancement observed in the BNNS ink-based TENG compared to the PC-only TENG is that the addition of a more tribonegative and electron-trapping-capable filler material contributes to the output enhancement of the fabricated device. That is, without the incorporation of BNNSs, the developed charges would be comparably less,

due to the difference in tribopolarity being small. Then, the introduction of more triboelectrically negative BNNSs as a filler in the polycarbonate ink improves the triboelectric charge transfer, storage, and charge-trapping ability simultaneously.[46]

The major factors influencing the contact electrification process involve the electrical polarity and charge storage capability of the materials in contact. Modulation of the electrical polarity can be achieved by increasing either the tribolayers' electropositivity or electronegativity by incorporating certain nanomaterials and in turn improving the contact electrification. Furthermore, when BNNSs are embedded in a polymer matrix, the presence of interlayer voids in the 2D nanomaterial sheets can capture carriers easily and then trap them in the interior of the negative triboelectric layer and store them. This phenomenon alleviates the loss of electrons due to the air breakdown effect by reducing the surface potential.[47] The charge-trapping ability of 2D-layered materials also decreases the recombination of electrons with positive ions or particles in the air, further enhancing the electrical output of TENGs. In addition, atomically thin 2D nanomaterial layers with large lateral dimensions can possess higher specific surfaces, thereby improving the contact area effectively in trioactive layers and also resulting in the efficient output performance of the device by increasing triboelectric charge density.[48,49]

To evaluate the performance of FS-TENG for practical applications, the power density of the device must be analyzed critically. For this, the FS-TENG was connected to various resistors with variable values ranging from 1 Ω to 1000 MΩ. From the observed voltages corresponding to the connected loads, power density was calculated using the formula $P = V^2/RA$, where V is the voltage, R is the resistance, and A is the contact area. The output power densities of the contact separation mode FS-TENG with an active contact area of 9 cm^2 without and with BNNSs are shown in Figure 8c,d. In the power density curve, voltage increases to a maximum value as load resistance increases; meanwhile, the power density also
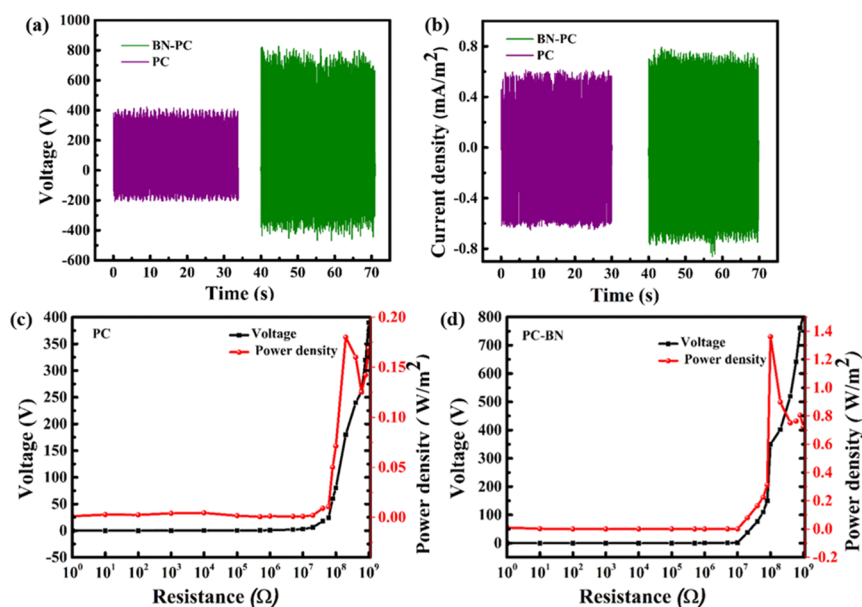

Figure 8. (a,b) Output voltage and short-circuit current density generated from the PC/PVP and BN-PC/PVP FS-TENG, respectively, under a mere tapping force of ~10 N at 5 Hz. (c,d) Output power density of the PC/PVP and BN-PC/PVP FS-TENG under various resistive loads from 1 Ω to 1000 MΩ.
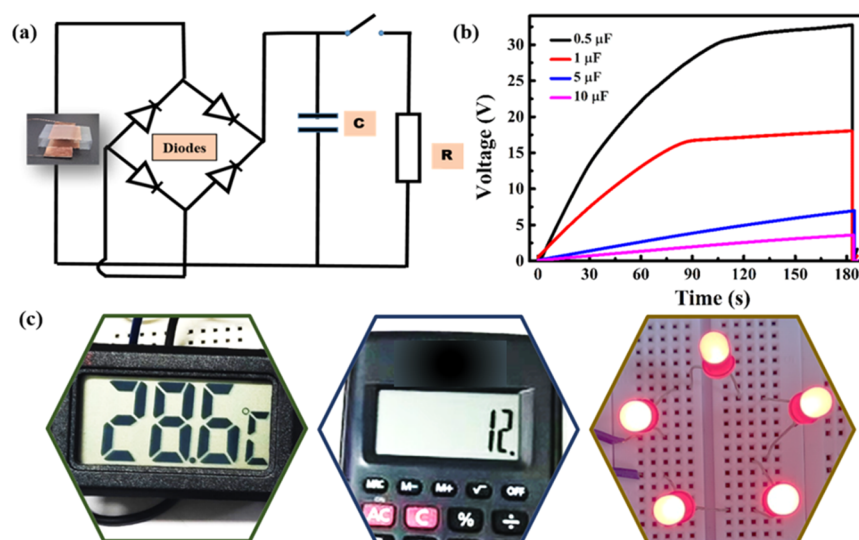
Figure 9. (a) Circuit diagram of rectifying circuit for capacitor charging and powering electronic gadgets. (b) Obtained charging profile of capacitors with capacitance values (0.5, 1, 5, and 10 μF) for the FS-TENG. (c) Photographs of using FS-TENG for powering digital thermometers, calculators, and LEDs.
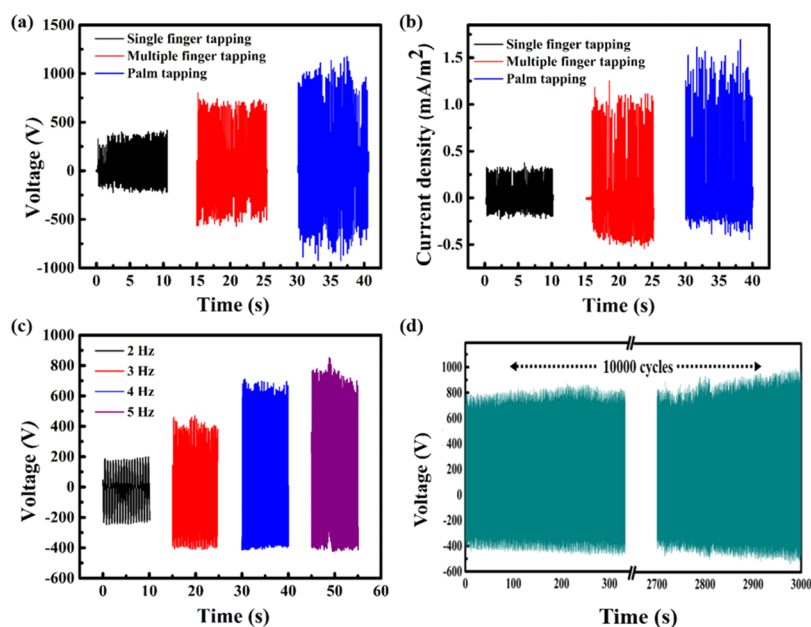

Figure 10. (a,b) Output voltage and current density measured from different human body movements (e.g., single finger-tapping, multiple finger-tapping, and palm-tapping). (c) Frequency dependence on the output voltage of FS-TENG. (d) Cyclic stability test for 10,000 cycles at a frequency of 5 Hz and a force of 10 N.

increases and reaches a maximum and then decreases. For the reference device, the peak power density obtained was about 0.18 W m^{-2} and was observed at 200 MΩ. In comparison, the maximum peak value of power density for the FS-TENG with BNNSs is ~1.36 W m^{-2}, which is 7 times that of the reference and was observed at 200 MΩ. Then, for the quantitative analysis of the energy output, we connected capacitors to the FS-TENG via a rectifier circuit to identify the quantification of actual charges stored. As shown in Figure 9a, a full-wave bridge rectifier was used to convert the AC output signal to DC output, and various capacitors with different capacitances (0.5, 1, 5, and 10 μF) were used for identifying the capacitor charging profile (Figure 9b). Within 180 s, the FS-TENG charged a 0.5 μF capacitor up to a maximum saturation voltage of 32 V. This stable electrical energy provided by the FS-

TENG is sufficient for powering low-power electronic gadgets. To demonstrate this, using the TENG's output from the hand-tapping motion, different electronic gadgets such as digital thermometers, calculators, and LEDs are successfully powered (Figure 9c). That is, the FS-TENG's output electrical performance is suitable for energy storage in capacitors which in turn power portable electronic devices.

Since the FS-TENG's practical implementation is focused on powering portable or wearable electronic gadgets, the capability of the FS-TENG to harvest biomechanical energy from biomechanical inputs such as the single finger, multiple fingers, and palm force is also demonstrated. The output for all these is graphically represented in Figure 10a,b. The output voltages developed from single finger-tapping, multiple finger-tapping, and palm-tapping were 400, 730, and 1150 V,
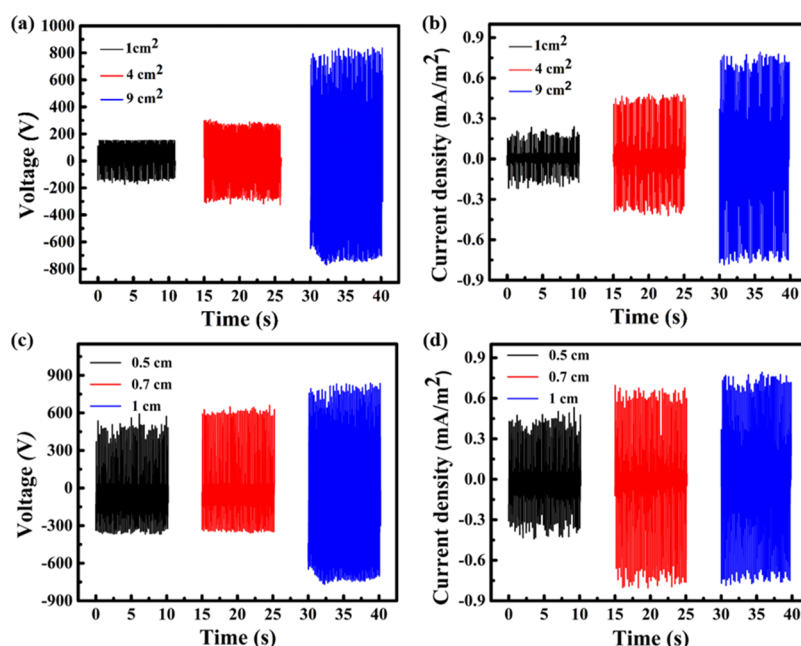
Figure 11. (a,b) Comparison of V and J_{sc} measured from different contact areas of FS-TENG. (c,d) Dependance of V and J_{sc} on the separation gap between contact materials in the TENG device.

respectively. Similarly, the corresponding short-circuit current densities obtained are 0.32, 1, and 1.5 mA/m². In this process, continuous tapping of the device attached to the palm generated comparably higher voltage and current than the single finger motion and multiple finger motion. This is primarily because the pressing force is much higher in palm tapping compared to that in other hand tappings, which contributes to more area of contact. In addition to this, the long-term cyclic stability and adaptability of the fabricated device are crucial for practical environment. Two confirmatory experiments, frequency-dependent output performance analysis and a cyclic stability test, have been carried out with the FS-TENG device using the force impactor. The influence of tapping frequency on the output voltage is shown in Figure 10c. With an increase in the working frequency of the force impactor, the output voltage linearly increases from 210 to 800 V with respect to the increase in frequency from 2 to 5 Hz. At a higher tapping frequency, external electrons in the device system can attain equilibrium in a faster way, providing better performance.[50] The screen-printed BN-PC-based TENG showed good practical stability, which is verified by a continuous press-release operation of 10,000 cycles at 5 Hz. The generated output voltage of 800 V was reproducible during the entire cycle of operation. Even after continuous cycles of operation, the surface of the BN-PC film showed only minute changes compared with the films before operations (Supporting Information Figure S6).

A study of the influence of different parameters of TENG on the output performance is also systematically investigated by varying its contact area and separation gap. Figure 11a,b shows the V (voltage) and J_{sc} (short circuit current density) values of the FS-TENG with three different contact areas, 1, 4, and 9 cm², constructed at a constant separation gap of 1 cm. From the figure, it can be seen that the device output increases from 170 to 800 V, with the increase in contact area from 1 to 9 cm². The increase in the output voltage can be understood since more triboelectric charge accumulation occurs in large-

area devices. In the same way, keeping the contact area at a constant value of 9 cm², dependence on the separation distance is evaluated (Figure 11c,d). The output voltage and current density show significant increases as a function of the separation gap. This increase in output voltage is mainly caused by the lowering of its capacitance value. However, short-circuit current density directly depends on the velocity contribution, which is more predominant than the inverse square dependence on the separation gap.[51] A higher speed of motion arises from the increase in the structure modulus of the supporting material, which contributes to the stress and recoiling speed of the system.[11,51−59]

■ CONCLUSIONS

In summary, we have demonstrated the development of a FS-TENG device working in a vertical contact separation mode for scavenging mechanical energy. The FS-TENG having an active surface area of 9 cm² and 1 cm separation distance is fabricated using the BN-PC-composite ink as tribonegative and PVP as tribopositive materials. The formulated BN-PC ink consists of hexagonal boron nitride nanosheets as fillers, polycarbonate as the binder, and other thixotropy adjustment components. Under specific mechanical inputs, the electrical output voltage and current density of the FS-TENG device were systematically analyzed and compared. The BN-PC-based FS-TENG can deliver an impressive output voltage of ∼800 V and a short-circuit current density of ∼0.78 mA/m², under a compressive force of ∼10 N impacted at 5 Hz frequency. The peak value of the power density was ∼1.36 W m⁻² at a resistive load of 200 MΩ. These exhibited results are significantly higher than the output results obtained from similar FS-TENGs constructed using PC ink alone (without BNNS fillers). Interestingly, the power density of the BN-PC-based FS-TENG showed ∼7 times higher value than the FS-TENG without BNNSs. Charge-trapping ability and higher surface contact area are the major factors contributing to the output enhancement of FS-TENG with BNNS ink. The influence of

various structural parameters like contact surface area of the trioactive materials and separation distance on the output performance of FS-TENG was systematically studied. The output performance of the device showed a monotonic trend with the structural parameters, wherein the maximum output was observed for the device with a contact area of 9 cm^2 and a separation gap of 1 cm. Further, variations in the output of FS-TENG were studied using various biomechanical input forces, and the cyclic stability of the device was additionally confirmed even after 10,000 continuous cycles of operations. To demonstrate its practical use, the fabricated FS-TENG was utilized to power up commercial LEDs, digital thermometers, and calculators, where the mechanical impulse was derived from biomechanical movements.

■ ASSOCIATED CONTENT

ⓢ Supporting Information

The Supporting Information is available free of charge at https://pubs.acs.org/doi/10.1021/acsaelm.3c00712.

> Powering of digital thermometer using the screen-printed BN-PC/PVP FS-TENG (AVI)
>
> Powering of calculator using the screen-printed BN-PC/PVP FS-TENG (AVI)
>
> TEM images of bulk and exfoliated h-BN, structural analysis of bulk and exfoliated h-BN, charge calculation of FS-TENG using an enlarged short-circuit current profile, output performance of FS-TENG with bulk h-BN, thickness-dependent output performance of BN-PC/PVP FS-TENG, SEM image of the BN-PC film after 10,000 cycles of operation, AFM images and SEM image of the screen-printed PC film (PDF)

■ AUTHOR INFORMATION

Corresponding Authors

　Achu Chandran − *Materials Science and Technology Division, CSIR-National Institute for Interdisciplinary Science and Technology (CSIR-NIIST), Thiruvananthapuram 695019, India; Academy of Scientific and Innovative Research (AcSIR), Ghaziabad 201002, India;* Email: achuchandran@niist.res.in

　Kuzhichalil Peethambharan Surendran − *Materials Science and Technology Division, CSIR-National Institute for Interdisciplinary Science and Technology (CSIR-NIIST), Thiruvananthapuram 695019, India; Academy of Scientific and Innovative Research (AcSIR), Ghaziabad 201002, India;* ⓞ orcid.org/0000-0001-5269-1489; Email: kpsurendran@niist.res.in

Authors

　Ainikulangara Sundaran Bhavya − *Materials Science and Technology Division, CSIR-National Institute for Interdisciplinary Science and Technology (CSIR-NIIST), Thiruvananthapuram 695019, India; Academy of Scientific and Innovative Research (AcSIR), Ghaziabad 201002, India*

　Harris Varghese − *Materials Science and Technology Division, CSIR-National Institute for Interdisciplinary Science and Technology (CSIR-NIIST), Thiruvananthapuram 695019, India; Academy of Scientific and Innovative Research (AcSIR), Ghaziabad 201002, India*

Complete contact information is available at:
https://pubs.acs.org/10.1021/acsaelm.3c00712

■ REFERENCES

(1) Jiao, P.; Matin Nazar, A.; Egbe, K.-J. I.; Barri, K.; Alavi, A. H. Magnetic Capsulate Triboelectric Nanogenerators. *Sci. Rep.* **2022**, *12* (1), 89 DOI: 10.1038/s41598-021-04100-2.

(2) Zheng, S.; Wang, H.; Das, P.; Zhang, Y.; Cao, Y.; Ma, J.; Liu, S. F.; Wu, Z. Multitasking MXene Inks Enable High-Performance Printable Microelectrochemical Energy Storage Devices for All-Flexible Self-Powered Integrated Systems. *Adv. Mater.* **2021**, *33*, No. e2005449, DOI: 10.1002/adma.202005449.

(3) Athira, B. S.; George, A.; Vaishna Priya, K.; Hareesh, U. S.; Bhoje Gowd, E.; Surendran, K. P.; Chandran, A. High-Performance Flexible Piezoelectric Nanogenerator Based on Electrospun PVDF-BaTiO3 Nanofibers for Self-Powered Vibration Sensing Applications. *ACS Appl. Mater. Interfaces* **2022**, *14*, 44239−44250, DOI: 10.1021/acsami.2c07911.

(4) Wu, Y.; Luo, Y.; Cuthbert, T. J.; Shokurov, A. V.; Chu, P. K.; Feng, S.; Menon, C. Hydrogels as Soft Ionic Conductors in Flexible and Wearable Triboelectric Nanogenerators. *Adv. Sci.* **2022**, *9*, No. e2106008, DOI: 10.1002/advs.202106008.

(5) Feng, P.; Xia, Z.; Sun, B.; Jing, X.; Li, H.; Tao, X.; Mi, H. Enhancing the Performance of Fabric-Based Triboelectric Nanogenerators by Structural and Chemical Modification. *ACS Appl. Mater. Interfaces* **2021**, *13* (14), 16916−16927, DOI: 10.1021/acsami.1c02815.

(6) Wang, N.; Liu, Y.; Ye, E.; Li, Z.; Wang, D. Control Methods and Applications of Interface Contact Electrification of Triboelectric Nanogenerators: A Review. *Mater. Res. Lett* **2022**, *10* (3), 97−123, DOI: 10.1080/21663831.2022.2026513.

(7) Joseph, A. M.; Nagendra, B.; Bhoje Gowd, E.; Surendran, K. P. Screen-Printable Electronic Ink of Ultrathin Boron Nitride Nanosheets. *ACS Omega* **2016**, *1* (6), 1220−1228, DOI: 10.1021/acsomega.6b00242.

(8) Lin, Y.; Chen, J.; Tavakoli, M. M.; Gao, Y.; Zhu, Y.; Zhang, D.; Kam, M.; He, Z.; Fan, Z. Printable Fabrication of a Fully Integrated and Self-Powered Sensor System on Plastic Substrates. *Adv. Mater.* **2019**, *31* (5), No. 1804285, DOI: 10.1002/adma.201804285.

(9) Franco, M.; Motealleh, A.; Costa, C. M.; Hilliou, L.; Perinka, N.; Ribeiro, C.; Viana, J. C.; Costa, P.; Lanceros-mendez, S. Environmentally Friendly Conductive Screen-Printable Inks Based on N-Doped Graphene and Polyvinylpyrrolidone. *Adv. Eng. Mater.* **2021**, *24* (6), No. 2101258, DOI: 10.1002/adem.202101258.

(10) Nanogenerator, A. T.; Seol, M.; Han, J.; Moon, D.; Yoon, K. J.; Hwang, C. S. All-Printed Triboelectric Nanogenerator. *Nano Energy* **2017**, *44*, 82−88, DOI: 10.1016/j.nanoen.2017.11.067.

(11) Salauddin, M.; Rana, S. M. S.; Sharifuzzaman, M.; Rahman, M. T.; Park, C.; Cho, H.; Maharjan, P.; Bhatta, T.; Park, J. Y. A Novel MXene/Ecoflex Nanocomposite-Coated Fabric as a Highly Negative and Stable Friction Layer for High-Output Triboelectric Nano-

generators. *Adv. Energy Mater.* **2021**, *11* (1), No. 2002832, DOI: 10.1002/aenm.202002832.

(12) Xu, Y.; Schwab, M. G.; Strudwick, A. J.; Hennig, I. Screen-Printable Thin Film Supercapacitor Device Utilizing Graphene / Polyaniline Inks. *Adv. Energy Mater.* **2013**, *3* (8), 1035−1040, DOI: 10.1002/aenm.201300184.

(13) Chen, H.; Chen, S.; Zhang, Y.; Ren, H.; Hu, X.; Bai, Y. Sand-Milling Fabrication of Screen-Printable Graphene Composite Inks for High-Performance Planar Micro-Supercapacitors. *ACS Appl. Mater. Interfaces* **2020**, *12* (50), 56319−56329, DOI: 10.1021/acsami.0c16976.

(14) Li, W.; Zhang, H.; Kagita, S.; Shamim, A. All Screen-Printed, Polymer-Nanowire Based Foldable Electronics for Mm-Wave Applications. *Adv. Mater. Technol.* **2021**, *6* (11), No. 2100525, DOI: 10.1002/admt.202100525.

(15) Cao, R.; Pu, X.; Du, X.; Yang, W.; Wang, J.; Guo, H.; Zhao, S.; Yuan, Z.; Zhang, C.; Li, C.; Wang, Z. L. Screen-Printed Washable Electronic Textiles as Self-Powered Touch/Gesture Tribo-Sensors for Intelligent Human − Machine Interaction. *ACS Nano* **2018**, *12* (6), 5190−5196, DOI: 10.1021/acsnano.8b02477.

(16) Wen, D.; Liu, X.; Deng, H.; Sun, D.; Qian, H.; Brugger, J. Printed Silk- Fi Broin-Based Triboelectric Nanogenerators for Multi-Functional Wearable Sensing. *Nano Energy* **2019**, *66*, No. 104123, DOI: 10.1016/j.nanoen.2019.104123.

(17) Zhang, D.; Xu, Z.; Yang, Z.; Song, X. High-Performance Flexible Self-Powered Tin Disulfide Nanoflowers/Reduced Graphene Oxide Nanohybrid-Based Humidity Sensor Driven by Triboelectric Nanogenerator. *Nano Energy* **2020**, *67*, No. 104251, DOI: 10.1016/j.nanoen.2019.104251.

(18) Zhang, K.; Feng, Y.; Wang, F.; Yang, Z.; Wang, J. Two Dimensional Hexagonal Boron Nitride (2D-HBN): Synthesis, Properties and Applications. *J. Mater. Chem. C* **2017**, *5*, 11992−12022, DOI: 10.1039/C7TC04300G.

(19) Wang, X.; Weng, Q.; Bando, Y.; Golberg, D. Functionalized Hexagonal Boron Nitride Nanomaterials: Emerging Properties and Applications Include the Controlled Synthesis. *Chem. Soc. Rev.* **2016**, *45*, 3989−4012, DOI: 10.1039/c5cs00869g.

(20) Chen, T.; Liu, Z.; Hu, X.; Zhao, G.; Qin, Z.; Tosin Aladejana, J.; Peng, X.; Xie, Y.; Wu, B. Fire-Resistant Plant Fiber Sponge Enabled by Highly Thermo-Conductive Hexagonal Boron Nitride Ink. *Chem. Eng. J.* **2022**, *429*, No. 132135, DOI: 10.1016/j.cej.2021.132135.

(21) Zhu, X.; Ng, L. W. T.; Hu, G.; Wu, T.; Um, D.; Macadam, N.; Hasan, T. Hexagonal Boron Nitride − Enhanced Optically Transparent Polymer Dielectric Inks for Printable Electronics. *Adv. Funct. Mater.* **2020**, *30* (31), No. 2002339, DOI: 10.1002/adfm.202002339.

(22) Sci, J. V. Transistors with Graphene and Hexagonal Boron Nitride Inks Inkjet-Printed MoS 2 -Based Field-Effect Transistors with Graphene and Hexagonal Boron Nitride Inks. *J. Vac. Sci. Technol.* **2020**, *4*, No. 042206, DOI: 10.1116/6.0000082.

(23) Carey, T.; Cacovich, S.; Divitini, G.; Ren, J.; Mansouri, A.; Kim, J. M.; Wang, C.; Ducati, C.; Sordan, R.; Torrisi, F. Fully Inkjet-Printed Two-Dimensional Material Field-Effect Heterojunctions for Wearable and Textile Electronics. *Nat. Commun.* **2017**, *8*, 1202 DOI: 10.1038/s41467-017-01210-2.

(24) De Moraes, A. C. M.; Hyun, W. J.; Seo, J. T.; Downing, J. R.; Lim, J.; Hersam, M. C. Ion-Conductive, Viscosity-Tunable Hexagonal Boron Nitride Nanosheet Inks. *Adv. Funct. Mater.* **2019**, *29* (39), No. 1902245, DOI: 10.1002/adfm.201902245.

(25) Li, H.; Liu, S.; Li, X.; Wu, Z. S.; Liang, J. Screen-Printing Fabrication of High Volumetric Energy Density Micro-Supercapacitors Based on High-Resolution Thixotropic-Ternary Hybrid Interdigital Micro-Electrodes. *Mater. Chem. Front.* **2019**, *3*, 626−635, DOI: 10.1039/c8qm00639c.

(26) Li, H.; Li, X.; Liang, J.; Chen, Y. Hydrous RuO$_2$-Decorated MXene Coordinating with Silver Nanowire Inks Enabling Fully Printed Micro-Supercapacitors with Extraordinary Volumetric Performance. *Adv. Energy Mater.* **2019**, *9* (15), No. 1803987, DOI: 10.1002/aenm.201803987.

(27) Sivan, A.; Chandran, A.; Kuzhichalil, S. MWCNT Ink with PEDOT: PSS as a Multifunctional Additive for Energy Efficient Flexible Heating Applications. *Appl. Mater. Today* **2021**, *23*, No. 100987, DOI: 10.1016/j.apmt.2021.100987.

(28) Marmur, A. Soft Contact: Measurement and Interpretation of Contact Angles. *Soft Matter* **2006**, *2*, 12−17, DOI: 10.1039/b514811c.

(29) Hebbar, R. S.; Isloor, A. M.; Ismail, A. F. Chapter 12 - Contact Angle Measurements. *Membrane Characterization* **2017**, *1*, 219−255.

(30) Kumar, R.; Kamakshi; Kumar, M.; Awasthi, K. Functionalized Pd-Decorated and Aligned MWCNTs in Polycarbonate as a Selective Membrane for Hydrogen Separation. *Int. J. Hydrogen Energy* **2016**, *41* (48), 23057−23066, DOI: 10.1016/j.ijhydene.2016.09.008.

(31) Bhavya, A. S.; Varghese, H.; Chandran, A.; Surendran, K. P. Massive Enhancement in Power Output of BoPET-Paper Tribo-electric Nanogenerator Using 2D-Hexagonal Boron Nitride Nanosheets. *Nano Energy* **2021**, *90* (PartB), 10662 DOI: 10.1016/j.nanoen.2021.106628.

(32) Parshin, A. M.; Gunyakov, V. A.; Zyryanov, V. Y.; Shabanov, V. F. Domain Structures in Nematic Liquid Crystals on a Polycarbonate Surface. *Int. J. Mol. Sci.* **2013**, *14* (8), 16303−16320, DOI: 10.3390/ijms140816303.

(33) Lago, E.; Toth, P.; Pugliese, G. Solution blending preparation of polycarbonate/graphene composite: boosting the mechanical and electrical properties. *RSC Adv.* **2016**, *6*, 97931−97940, DOI: 10.1039/C6RA21962D.

(34) Kaleemulla, S.; Dhanumalayan, E. Investigation of Structure, Dielectric and Thermal Properties of Hexagonal Boron Nitride Dispersed Polymer Blends. *J. Mater. Sci.: Mater. Electron.* **2019**, *30*, 17459−17468, DOI: 10.1007/s10854-019-02096-0.

(35) Nie, X.; Sang, X. Exfoliation of Hexagonal Boron Nitride Assisted with Hierarchical Ionic Fragments by Ball-Milling for Achieving High Thermally Conductive Polymer Nanocomposite. *Polym. Compos.* **2022**, *43* (2), 946−954, DOI: 10.1002/pc.26424.

(36) Hyun, W. J.; Secor, E. B.; Hersam, M. C.; Frisbie, C. D.; Francis, L. F. High-Resolution Patterning of Graphene by Screen Printing with a Silicon Stencil for Highly Flexible Printed Electronics. *Adv. Mater.* **2015**, *27* (1), 109−115, DOI: 10.1002/adma.201404133.

(37) Arapov, K.; Rubingh, E.; Abbel, R.; Laven, J.; De With, G.; Friedrich, H. Conductive Screen Printing Inks by Gelation of Graphene Dispersions. *Adv. Funct. Mater.* **2016**, *26* (4), 586−593, DOI: 10.1002/adfm.201504030.

(38) Kumar, B. R.; Rao, T. S. AFM studies on surface morphology, topography and texture of nanostructured zinc aluminum oxide thin films. *Dig. J. Nanomater. Biostruct.* **2012**, *7* (4), 1881−1889.

(39) Qureshi, A.; Shah, S.; Pelagade, S. Surface Modification of Polycarbonate by Plasma Treatment. *J. Phys.: Conf. Ser.* **2010**, *208*, No. 012108, DOI: 10.1088/1742-6596/208/1/012108.

(40) Sattanathan, M.; Subramani, S.; Mohamed, K.; Devarajan, M. Synthesis and Characterization of Hexagonal Boron Nitride Coating on Polyethylene Terephthalate. *Iran. Polym. J.* **2019**, *28*, 969−976, DOI: 10.1007/s13726-019-00757-9.

(41) Varghese, H.; Hakkeem, H. M. A.; Chauhan, K.; Thouti, E.; Pillai, S.; Chandran, A. A High-Performance Flexible Triboelectric Nanogenerator Based on Cellulose Acetate Nanofibers and Micro-patterned PDMS Films as Mechanical Energy Harvester and Self-Powered Vibrational Sensor. *Nano Energy* **2022**, *98*, No. 107339, DOI: 10.1016/j.nanoen.2022.107339.

(42) Garcia, C.; Trendafilova, I.; Guzman de Villoria, R.; Sanchez del Rio, J. Self-Powered Pressure Sensor Based on the Triboelectric Effect and Its Analysis Using Dynamic Mechanical Analysis. *Nano Energy* **2018**, *50*, 401−409, DOI: 10.1016/j.nanoen.2018.05.046.

(43) Varghese, H.; Chandran, A. A Facile Mechanical Energy Harvester Based on Spring Assisted Triboelectric Nanogenerators. *Sustain. Energy Fuels* **2021**, *5*, 5287−5294, DOI: 10.1039/D1SE00788B.

(44) Zhang, D.; Yu, L.; Wang, D.; Yang, Y.; Mi, Q.; Zhang, J. Multifunctional Latex/ Polytetrafluoroethylene-Based Triboelectric Nanogenerator for Self-Powered Organ-like Mxene/Metal-Organic

Framework-Derived Cuo Nanohybrid Ammonia Sensor. *ACS Nano* **2021**, *15* (2), 2911−2919, DOI: 10.1021/acsnano.0c09015.

(45) Salauddin, M.; Rana, S. M. S.; Rahman, M. T.; Sharifuzzaman, M.; Maharjan, P.; Bhatta, T.; Cho, H.; Lee, S. H.; Park, C.; Shrestha, K.; Sharma, S.; Park, J. Y. Fabric-Assisted MXene/Silicone Nano-composite-Based Triboelectric Nanogenerators for Self-Powered Sensors and Wearable Electronics. *Adv. Funct. Mater.* **2022**, *32* (5), No. 2107143, DOI: 10.1002/adfm.202107143.

(46) Kuang, H.; Li, Y.; Huang, S.; Shi, L.; Zhou, Z.; Gao, C.; Zeng, X.; Pandey, R.; Wang, X.; Dong, S. Piezoelectric Boron Nitride Nanosheets for High Performance Energy Harvesting Devices. *Nano Energy* **2021**, *80*, No. 105561, DOI: 10.1016/j.nanoen.2020.105561.

(47) Liu, Y.; Ping, J.; Ying, Y. Recent Progress in 2D-Nanomaterial-Based Triboelectric Nanogenerators. *Adv. Funct. Mater.* **2021**, *31* (17), No. 2009994, DOI: 10.1002/adfm.202009994.

(48) Wang, N.; Liu, Y.; Ye, E.; Li, Z.; Wang, D. Control Methods and Applications of Interface Contact Electrification of Triboelectric Nanogenerators: A Review. *Mater. Res. Lett.* **2022**, *10* (3), 97−123, DOI: 10.1080/21663831.2022.2026513.

(49) Seol, M.; Kim, S.; Cho, Y.; Byun, K.; Kim, H.; Kim, J.; Kim, S. K.; Kim, S.; Shin, H.; Park, S. Triboelectric Series of 2D Layered Materials. *Adv. Mater* **2018**, *30* (39), No. 1801210, DOI: 10.1002/adma.201801210.

(50) Kim, Y.; Wu, X.; Lee, C.; Oh, J. H. Characterization of PI / PVDF-TrFE Composite Nano Fi Ber-Based Triboelectric Nano-generators Depending on the Type of the Electrospinning System. *ACS Appl. Mater. Interfaces* **2021**, *13* (31), 36967−36975, DOI: 10.1021/acsami.1c04450.

(51) Varghese, H.; Chandran, A. Triboelectric Nanogenerator from Used Surgical Face Mask and Waste Mylar Materials Aiding the Circular Economy. *ACS Appl. Mater. Interfaces* **2021**, *13* (43), 51132−51140, DOI: 10.1021/acsami.1c16557.

(52) Niu, S.; Liu, Y.; Wang, S.; Lin, L.; Zhou, Y. S.; Hu, Y.; Wang, Z. L. Theoretical Investigation and Structural Optimization of Single-Electrode Triboelectric Nanogenerators. *Adv. Funct. Mater.* **2014**, *24* (22), 3332−3340, DOI: 10.1002/adfm.201303799.

(53) Guo, R.; Zhang, H.; Pei, Z.; Yang, S.; Ge, C.; Sang, S.; Hao, R. A Voiceprint Recognition Sensor Based on a Fully 3D-Printed Triboelectric Nanogenerator via a One-Step Molding Route. *Adv. Eng. Mater.* **2020**, *22* (5), No. 1901560, DOI: 10.1002/adem.201901560.

(54) Li, H.; Fang, X.; Li, R.; Liu, B.; Tang, H.; Ding, X.; Xie, Y. All-Printed Soft Triboelectric Nanogenerator for Energy Harvesting and Tactile Sensing. *Nano Energy* **2020**, *78*, No. 105288, DOI: 10.1016/j.nanoen.2020.105288.

(55) Hedau, B.; Kang, B.-C.; Ha, T.-J. Enhanced Triboelectric Effects of Self-Poled MoS2-Embedded PVDF Hybrid Nanocomposite Films for Bar-Printed Wearable Triboelectric Nanogenerators. *ACS Nano* **2022**, *16* (11), 18355−18365, DOI: 10.1021/acsnano.2c06257.

(56) Qian, C.; Li, L.; Gao, M.; Yang, H.; Cai, Z.; Chen, B.; Xiang, Z.; Zhang, Z.; Song, Y. All-Printed 3D Hierarchically Structured Cellulose Aerogel Based Triboelectric Nanogenerator for Multi-Functional Sensors. *Nano Energy* **2019**, *63*, No. 103885, DOI: 10.1016/j.nanoen.2019.103885.

(57) Yoon, H.; Kim, D.; Seung, W.; Khan, U.; Kim, T. Y.; Kim, T.; Kim, S. 3D-Printed Biomimetic-Villus Structure with Maximized Surface Area for Triboelectric Nanogenerator and Dust Fi Lter. *Nano Energy* **2019**, *63*, No. 103857, DOI: 10.1016/j.nanoen.2019.103857.

(58) Liu, G.; Xu, C. One-Stop Fabrication of Triboelectric Nanogenerator Based on 3D Printing. *EcoMat* **2021**, *3* (5), 12130 DOI: 10.1002/eom2.12130.

(59) Li, H.; Li, R.; Fang, X.; Jiang, H.; Ding, X.; Tang, B. 3D Printed Flexible Triboelectric Nanogenerator with Viscoelastic Inks for Mechanical Energy Harvesting. *Nano Energy* **2019**, *58*, 447−454, DOI: 10.1016/j.nanoen.2019.01.066.